



**Politecnico
di Torino**

Master's Degree in Mechatronic engineering.

Master's Degree Thesis

**Statistical analysis and digital filtering of data
derived from a human cardiac impedance
measurement instrument.**

Supervisors

Andrea Manuello Bertetto.

Alberto Concu

Candidate

Pietro Roberto Bianco.

AY 2021/2022.

Acknowledgement.

I owe eternal gratitude to my parents and my family: I truly cannot imagine the day of my graduation without their efforts and help.

The present work would not be possible without the contribution of colleagues, teachers of Politecnico, and friends.

My supervisors guided me in this journey, and I am grateful for all the knowledge they shared with me, in mechatronics, medical science, but also in common sense and simplicity.

Special thanks go to Andrea Fois, whose technical support and experience were decisive, and captain Pietro Gaviati, who donated his precious time for the realization of this and many other scientific works.

I owe my gratitude to Professor Elvio Bonisoli and Ph.D. Simone Venturini of DIMEAS, who dedicated their time and competence for the realization of this master thesis.

Last but not least, a well-earned mention to Andrea Cadeddu. He knows the reason.

Abstract.

The analysis of sampled data represents the most important feature in analysis systems in many fields of research.

While a wide variety of physical phenomena can be used to collect information on the state of a general process, in practice stochastic random noise, due to different reasons, reduces the efficiency of data detection and acquisition systems, prompting researchers to develop statistical estimation techniques, conceived, if needed, for the specific problem under investigation.

Mechatronic engineers are often requested to provide researchers with a full range of information on a specific phenomenon under investigation, better if recorded among a span time of days or even weeks, implying the implementation of remote acting devices or remote data acquisition systems. The whole process can also include the modelling and trend predictions of expected data series.

This is especially true in Biomedical applications, not only in signal detection of biological parameters, but also in the developing of mathematical models of energy consumption, aimed to reduce the usage of invasive techniques that can stress or even harm the subject.

Among the others, cardiac impedance technique challenges researchers in developing of non-invasive techniques for heart-rate detection and systolic blood volume, allowing the prediction of Stroke Volume (SV) variation on time, a methodology that can allow to study the adaptation of human body to the variation of environmental conditions, for example during navigation. On the other hand, further information on the metabolic

Keywords: Spectral analysis, FIR, Machine learning, Cardioimpedance, modelling, digital filtering.

Table of Contents

Abstract.....	3
Introduction.....	7
Digital signal processing. Issues and applications.	8
Physical meaning of signals.	8
Time series. Periodic signals and harmonic analysis	8
Digital filtering: basics.	9
Fourier Analysis.....	10
Statistics fundamentals.....	12
Reconstruction of the spectrum of a signal.	14
Windowing and wavelets.....	17
Deep learning and machine learning.	23
MATLAB tools.....	25
Biomedical applications and estimation techniques.....	26
Instrumentation.....	27
Electronic sensors and devices.....	27
Spirometer.	27
Lead electrodes.....	28
MEMS devices.....	29
Mechanical sensors, electromechanical sensors.....	29
Accelerometers.	29
Chemical sensors.....	31
Metabolic measurements.....	31
Oxygen sensors. Concentration.	31
Magneto-mechanical oxygen sensor.	31

Magnetopneumatic oxygen sensor.....	32
Carbon Dioxide sensors.....	33
Metabolimeter VO2000 MedGraphics.	34
STEVAL-MKI 121V1.....	34
INEMO-M1.	34
WT901SDCL accelerometer from Wit Motion.....	36
Armband SenseWear Pro3.	37
Use of Disposable electrodes.	39
Detection of cardiac impedance.....	39
Mechatronics in biomedical engineering.	42
Bioelectromagnetism.	42
Electrophysiology of biological tissues.....	44
Transcranial Magnetic Stimulation (TMS).....	45
Electrophysiology of the heart.....	45
Electrophysiology of equilibrium and locomotion.....	45
Energetic consideration. Metabolism.....	47
Mechanical energy.	48
Chemical energy and metabolism.	49
Efficiency of locomotion.	49
Correlation between mechanical energy and metabolic energy.	50
Indirect calorimetry.....	50
The human gait.	50
Transthoracic electrical bioimpedance cardiography.	52
Adaptation of human body during navigation.....	61
Experimental data.	62
Data treatment.	69
Identification of main frequencies of the spectrum in ICG.....	73
Identification of impedance features.....	74
Accelerometer on the boat.	77
Stroke volume graphs.....	81

Relation between accelerations and Stroke Volume.	81
Tests on human gait.	88
Discussion of Results.	94
Conclusions.	102
Appendix A: MATLAB code for the computation of Stroke volume.	111
Appendix B: ARMA models of the filtered data.	114
Appendic C: Stroke Volume graphs.	133
Appendix D: regression model concerning the correlation between Stroke Volume and acceleration for test subjects.	173

Introduction.

Working in signal analysis means often to manipulate data obtained from measurements. Contrary to common sense, engineers rarely deal with magic boxes or similar devices, capable of digesting random a set of complex data and easily provide the ready-made solution for every problem.

Instead, data interpretation can be a long and costly process, that starts from the assumptions on the very same object of study, and not rarely involves a trial-and-error procedure. A rough understanding of the phenomenon itself, basic knowledge of employed sensors (their working principles, characteristics, bias, drift etc.) used during measurements, is always the starting point for any analysis: the quest for an algorithm good for any occurrence must be regarded as just another fruitless attempt to invent a magic box, not less than the *motus perpetuus*.

Accordingly, the present work starts with the description of the main tools used in signal analysis: the basic math behind it, filtering, modelling and statistical reliability of such forecasting. Then, a description of the sensors used during the test is introduced.

Eventually, the latter part deals with the subject to which all these concepts are applied, with all the conclusion that can be drawn from all the evidences collected.

Digital signal processing. Issues and applications.

Physical meaning of signals.

A signal can be seen as the measurement of the variation among the time of a physical value. Signals are usually continuous but sampled and recorded by specific devices. This allows to study a signal in digital environment[6,8,33].

Digital signal processing has a wide field of applications, starting from control technology to biomedical applications, geophysics (e.g., earthquake prediction and analysis), sound and image analysis, meteorologic forecasting, and many others. Generally speaking, the techniques introduced in the present work represent a ubiquitous tool in the study of the mechanics of vibrations.

Time series. Periodic signals and harmonic analysis.

Since we work in digital environment, a signal is usually represented by a time series, that is, a collection of data on a certain time and identified by a time sampling step[12]. In many cases a periodicity of the original signal can be detected or observed, or it is known that the signal is periodic. The main interest is to detect the frequencies related to the original problem and investigate the composition of the amplitude of the signal. The investigation of this property of a random (often periodic signals). One of the main issues in signal analysing is related to analog to digital conversion. As it will be widely explained in the following sections, the frequency of a signal has great influence. For example, in the present work in order to avoid aliasing the acquisition system has a samples frequency is 2kHz. This sampling frequency was chosen considering a cardiac frequency (at rest) of 65-70 beats-per-minute. The raw data provided by instruments are affected by random noise due to different causes. The purpose of the process is to provide filtering, rectifying and smoothing of the original data. As any human activity, data collection can be influenced by many sources of noise or errors. Errors can be divided in avoidable errors (due to sampling methodology) and unavoidable totally random errors.

For instance, electromagnetic interference can be sometimes diminished using proper hardware design and correction of cross talking and other interference phenomena. In a world totally interconnected by wireless technologies, the first source of noise can be appointed to the electromagnetic pollution. The designer of data collector instrumentation must consider shielding techniques.

The study of the fundamental frequencies of a signal (or time series) is the harmonic analysis. Thermal phenomena, moisture variation of the testing environment can also affect both DAQ and probe systems, since are correlated to temperature drift and thermal bias of the circuitry.

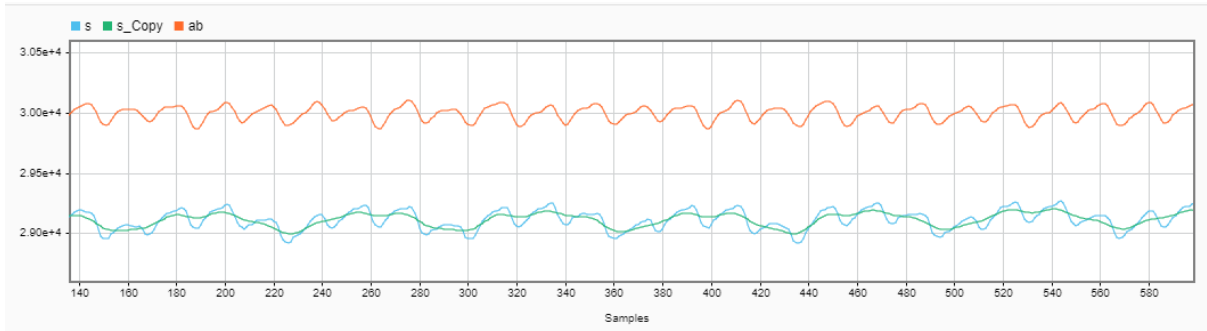


Figure 1-Example of noise: Breathing activity and its influence on Impedance Cardiogram(ICG). The red signal is obtained filtering the original signal, while the green line represents the oscillation due to breathing activity. The composition of the two signals is the original signal represented in blue.

Breathing activity introduces a further oscillation pole in the Bode diagram of the detected impedance.

Digital filtering: basics.

Digital filtering requires performing algebraic manipulation of the data that can cancel or minimize random noise and detect the tendency of the real signal [16].

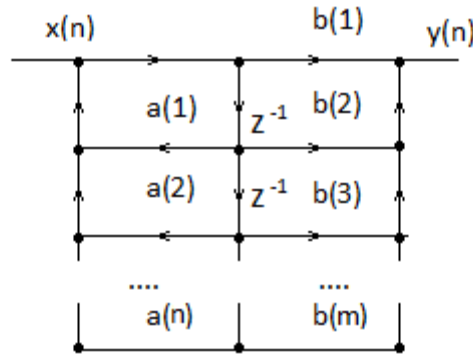


Figure 2- A digital filter structure using the z-transform notation.

The filter equation can be represented by the equation:

$$H(z) = \frac{B(z)}{A(z)} = \frac{\sum_{n=0}^M b_n z^{-n}}{1 + \sum_{n=1}^N a_n z^{-n}}$$

That can also graphically represented by a scheme, as depicted in figure.

The basic concept behind digital filter consists of analyse the spectrum of the signal and detect the most important frequencies and filter with specific filters the original signal, excluding noise or undesired signals that can hinder the identification of the process of interest.

Classical filtering.

A simple filter classification can be[16]:

- low pass filter.
- high pass filter.
- band pass filter.
- stop band filter or notch filter.

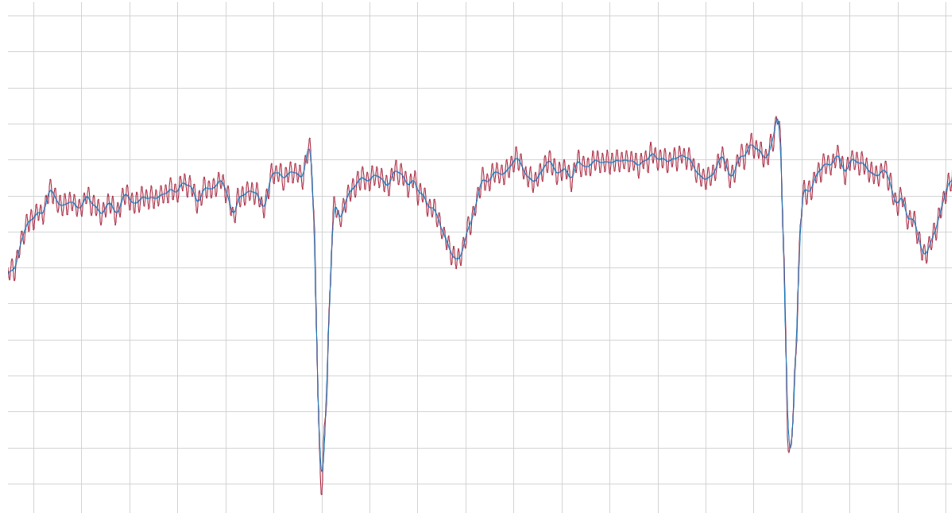


Figure 3- filtering of ECG signal from noise at high frequencies.

Classical filtering applies both to digital and analogic field and basically exploits the same method, that is, the derivation of a set of coefficients of an algebraic manipulation of the system that can reduce the influence of the undesired frequency. For analogic systems, the filter is represented by a differential equation and a Laplace transform, for discrete systems the filter is represented by a difference equation and the Z-transform. Typical technique for the design of a filter are Chebyshev, Bessel and Elliptic filters. As previously stated, usually noise sources with high frequencies are to be considered as caused by electromagnetic interference, whereas noise sources at low frequencies are related to mechanical, thermal noise. In any case, some assumptions on the nature of an unknown signal must be made and validated in a second moment.

Fourier Analysis.

Fourier analysis is the main tool used in signal analysis[36,38,39].

A periodic signal can always be represented by means of Fourier Series that is ideally represented by an infinite number of members, but in reality a good approximation of the original signal can be obtained with a set of members, that is, by a truncated Fourier series of desired precision.

$$f(t) = \frac{a_0}{2} + \sum_{1}^{\infty} a_m \cos\left(\frac{m\pi x}{L}\right) + b_m \sin\left(\frac{m\pi x}{L}\right)$$

A Fourier series with a finite number of elements is identified by its frequencies and its coefficients.

The Fourier integral and the Fourier transform.

The Fourier integral is a powerful mathematical tool that allow to translate a differential problem into an algebraic problem. Roughly speaking, a generic equation in the time space is translated in the corresponding problem in the frequency space. For random periodic signals, the Fourier transform results can be graphically represented by the diagrams of phase amplitude, in a logarithmic scale.

Main components of a periodic signal.

The Fourier transform allow to identify the main frequencies and the magnitude of the fundamental harmonics of the sampled signal[9,11].

Dynamical system modelling.

It is possible to describe a dynamical system using a set of linear differential equations. When it is not possible to define a linear system, a non linear system can be approximated by a linear system using linearization techniques[7,14].

Dynamical systems can be either represented by means of a continuous model or a discretized model. At the present moment, discrete representation is almost uniquely used in system modelling practice, due to digital technology, but it is still possible to obtain continuous systems using analogic electronics, mechanical or fluidic computing machines. A classical text concerning mechanical analogic computers was written by A. Svoboda[14].

Discrete Fourier Transform. Fast Fourier Transform.

The Fourier Transform applies to continuous systems. But usually sampled data are detected and elaborated by digital devices. This means that the data are always expressed as a time series with a certain sampling time. It is necessary to develop discrete signal analysis.

The first step is to transform the differential equations of a dynamic model into difference equation. In a difference equation, the future value of a dynamic model are obtained considering the past values, but, contrary to difference equations, this is done on discrete time intervals.

The transform form time series to frequency domain can be performed using the discrete transfer function.

$$X(e^{j\omega}) = \sum_{n=-\infty}^{\infty} x(n) e^{-jn\omega}$$

The computability of the Fourier discrete transfer function can be costly and in fact it is not used. Instead, the Fast Fourier Transform represents an easier algorithm and it is usually preferred in computation.

Spectrum analysis.

Fourier analysis is a power tool, signals affected by random noise, however, require more sophisticated tools. Statistical analysis is requested in order to detect the true signal frequency, since this is greatly affected by signal noise. The result of the discrete Fourier transform is a set of complex numbers. In order to obtain the spectrum of the signal, the norm of the signal must be computed.

$$|F(f)| = w$$

A simple technique consists of analysing a set of cycles of the periodic signal of interest. This technique allows to derive the standard deviation and the mean value of the spectrum, helping to identify the spectrum of the signal and the noise frequency.

Noise and statistical analysis.

Usually, in scientific and engineering, detected signals are periodic signals or signals where a trend can be found. The deviation from the regular behaviour is usually due to undesired influence on the output. Once the general trend or expected behaviour is identified, variation from a regular output of the series must be regarded as disturbance and are filtered. Usually, noise at high frequencies can be modelled as random noise with a Gaussian distribution, whereas noise at low frequencies is due to physical behaviour of the components.

The energy of a signal.

The starting point in statistical analysis of signals is the definition of energy [6,10,12] of a signal. Thanks to Parseval's theorem, it is possible to relate the energy of a signal in the time-domain to the frequency-domain function: these two integrals have the same value.

$$\int_0^{\infty} |f(t)|^2 dt = \int_0^{\infty} |H(\omega)| d\omega$$

This equation is of paramount importance, since it states that the area determined by the graph of the signal representation in time domain must be equal to the area computed in the frequency domain considering the Fourier transfer function.

Statistics fundamentals.

Random signals are studied using the probability distribution function. A random signal is usually represented

A totally random signal can be represented by the white noise signal. However, usually it is possible to identify the main components of the signal, or, said differently, the main frequencies and amplitudes that can approximate the signal. According to this approach, a random signal can be seen as the composition of different simple signals.

The white noise.

White noise is a condition of totally random signal and its spectrum ideally represented by a rectangle where no main oscillation frequency is to be found[13,15,17].

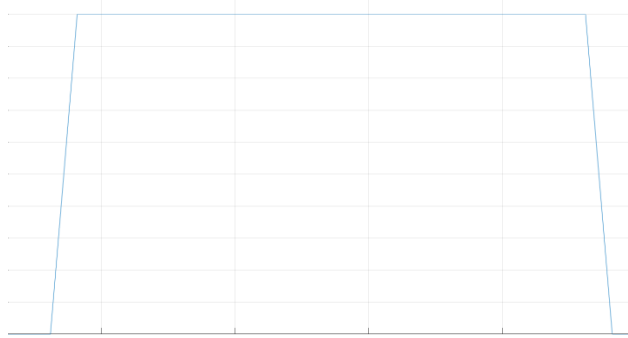


Figure 4 - Spectrum of white noise signal, represented by a continuous frequency band.

Ergodicity.

Ergodicity is the property of a random signal to be follow a certain regularity. In ergodic systems, the variation of the observed time series is likely to repeat itself[33].

Variance and correlation of a time series.

The variance and covariance are generally determined both for continuous an the discrete signals.

The variance of two time series can be defined as:

$$r_{xy} = \sum_n^{n+l} xy$$

The autocovariance is computed on the elements of the same time series, considering a lag l:

$$r_{kl} = \sum_1^n x[k]x[k + l]$$

For example, considering the time series expressed by a sinusoidal function:

$$f(n) = A \sin(n\omega + \phi)$$

The autocorrelation can be written as:

$$r_{kl} = \frac{A^2}{2} \cos[(k - l)\omega]$$

When the value used in computation refers to a single signal, they are called autocorrelation and auto variance. Autocorrelation and autocovariance values are widely used in the estimation of statistical models, as widely explained in the following paragraphs. Statistical methods applies both to time series and to their spectrum. The result can be immediately applied in the prediction of the time series itself, or in the determination of the main components of the signal.

Power spectral density of a generic signal.

Different techniques are exploited in statistical analysis of generic signal. The main frequencies and the spectral decomposition of the signal are unknown, but with specific mathematical tools it is possible to derive at least the most likely representation of the signal. The process of “system identification”, provides a model that can represent the trend of phenomenon, economic, physics or social that can be. The estimation of a signal is of paramount interest in the study of casual connections. The power spectral density(PSD) is obtained from the discrete time Fourier transform of the autocorrelation sequence.

$$P_x(e^{j\omega}) = \sum_{k=-\infty}^{\infty} r_x(k)e^{-jk\omega}$$

Where the autocorrelation function is derived from the spectrum of the time series, that is, the Fast Fourier Transform.

Reconstruction of the spectrum of a signal.

Autoregressive Moving average method.

In economic analysis and forecasting, predictive models are realized using the known time series of a certain event[12,17,18,24]. This approach can be used both directly on time series of interest or on the estimation of the spectrum of such time series, as in the present work.

Autoregressive method

$$y[n] = - \sum_{i=0}^m a_i y[n-i] + e[n]$$

Autoregressive method identify a series of coefficients that better represent the coefficients of the difference equation of the signal.

Moving average

The moving average is aimed for the definition of coefficients b_i that identify the variation of the average of a Gaussian noise function.

$$y[n] = \sum_{i=0}^m b_i e[n-i]$$

Autoregressive-moving average

The ARMA method is described by the equation:

$$y[n] = \sum_{i=1}^L b_i[n-i] - \sum_{i=1}^L a_i y[n-i]$$

Where the signal is decomposed into a Gaussian noise with zero mean and computable variance. The methods mentioned above are based on matrix computation of covariance and autocovariance matrix.

Computation of models. Autocovariance and Autocorrelation matrices.

The previous models are obtained using matrix computation [12,13,34],. Matrices and linear algebra are of paramount importance for the computation are the autocovariance and autocorrelation matrix.

For a generic vector:

$$x = [x(0), x(1), \dots, x(n)]^T$$

The autocorrelation can be obtained as matrix of autocorrelation matrix.

$$R_x = E[xx^H] = \sum_{j=1}^n \sum_{i=1}^p x(i)x(j) e(i)$$

Where e is the base vector,

Design of optimal filtering.

In optimal filtering it is necessary to define a cost function for the validation of the suggested model. Classical optimal filtering is based on Chebyshev and Bessel polynomials.

Optimization algorithms.

Optimization and optimization algorithms are involved in the problem defined so far.

The fundamental tool for optimization is the calculus of variation in the continuous domain, but the optimization techniques can be applied to the discrete time domain.

Spectral estimation, ARMA models, deep learning techniques: all of these tools require the definition of optimization techniques, aimed to find the best model or minimize the error in modelling, for example, of a scattered dataset detected from a generic time signal. The fundamental optimization technique is the Least Square Algorithm, that rely on a particular inversion matrix called pseudoinverse matrix, that is widely used in many other applications in system estimation. This matrix is obtained as:

$$A^\dagger = A^t (AA^T)^{-1}$$

That is the generalization of the inverse of a matrix, since it applies to rectangular matrices as well.

Using the Pseudo inverse of a matrix, it is possible to derive the coefficient of the polynomial of the Least Square or generally speaking, an interpolating polynomial, setting the degree of

the polynomial (that determines the number of columns). Optimization algorithms are used for the estimation of statistical parameters that can be used to create a model. Maximum Likelihood estimator is widely used in the definition of the best model, considering the best estimation procedure. Using this method, the approximation of a time series can be made with polynomials.

Taylor series expansion.

One tool that can be used in modelling is the Taylor series expansion. This series is used in the determination of a simple model, considering the simplicity of computation and manipulation.

Hessian matrix.

A special use of approximation method is devoted to the Hessian matrix, that is derived from the equation of the model and it is used to detect a maximum or a minimum of a function. This methods can be applied to Taylor series representing an approximation of a time series.

Convergence condition.

The main feature in approximation is the use of numerical methods with convergence condition where the computation is interrupted:

$$|x_{n+1} - x_n| < \epsilon$$

The algorithm is repeated until the desired precision is obtained. This procedure does not allow, however, to ensure that the found solution is also the absolute minimal solution. Further assumptions must be made, for example, regarding the convexity of the domain.

Smoothing of the data.

Sometimes, smoothing techniques can be used. The original data can be treated with many smoothing algorithms. Among the others, Savitzky Golay algorithm[20] can be easily used for this purpose. Savitzky-Golay algorithm allows to obtain a smoother curve representing a dataset. The algorithm is implemented in Matlab and available using the the “smooth” routine, adding ‘sgolay’ in the parameters . Specific tools are available to perform numerical computation.

Decimation.

Decimation of the original data is often necessary in order to obtain a better approximation of the spectrum[19,20].

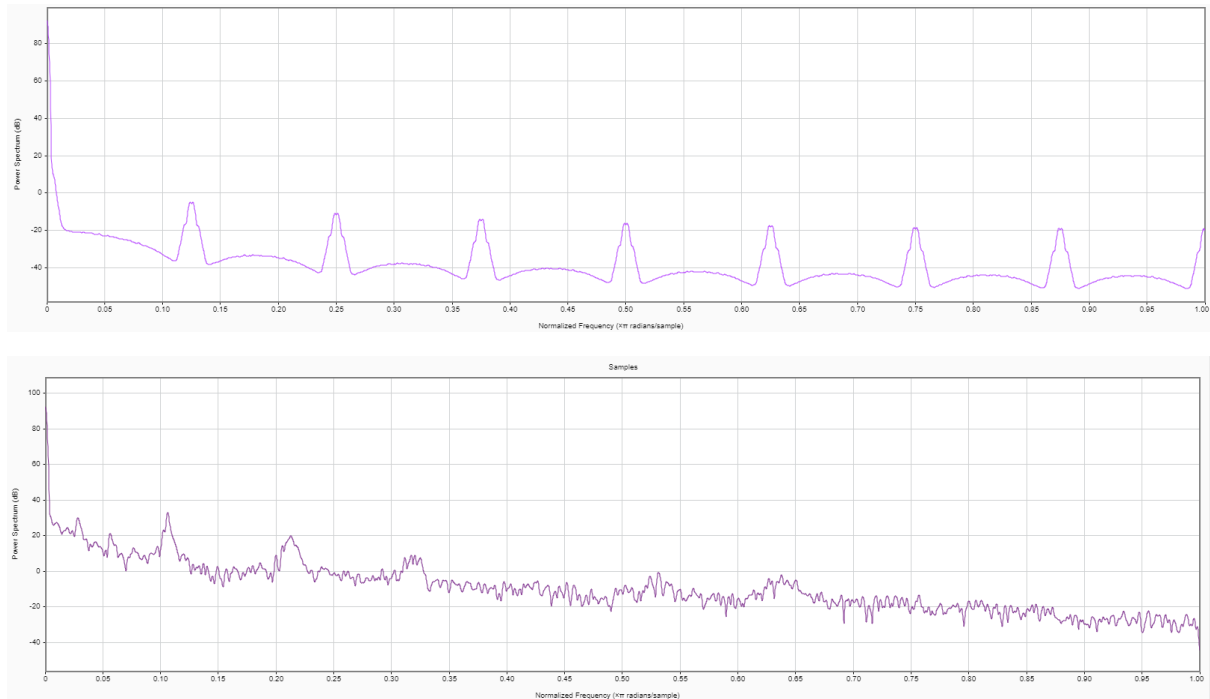


Figure 5-The spectrum of a signal and the spectrum of the decimated signal. On the spectrum of the decimated time series it is possible to identify the frequency components of the time series.

Windowing and wavelets.

The Fourier transform applied to the impulse response produces a distortion of the spectrum the so called sidelobes.

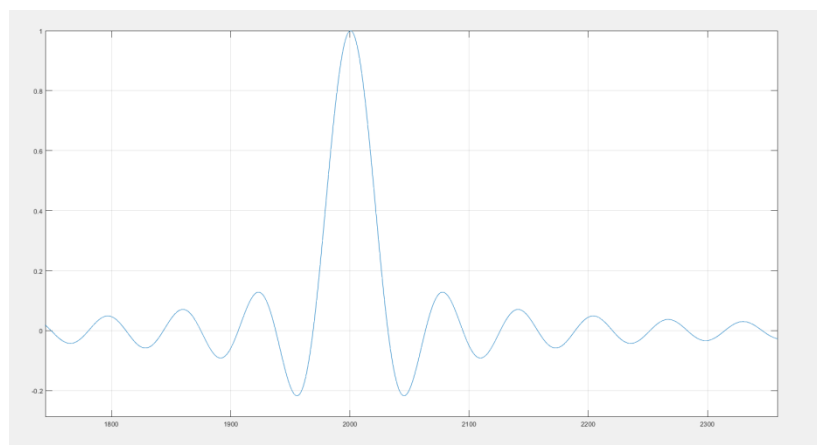


Figure. distortion due to Fourier transform of impulsive signal.

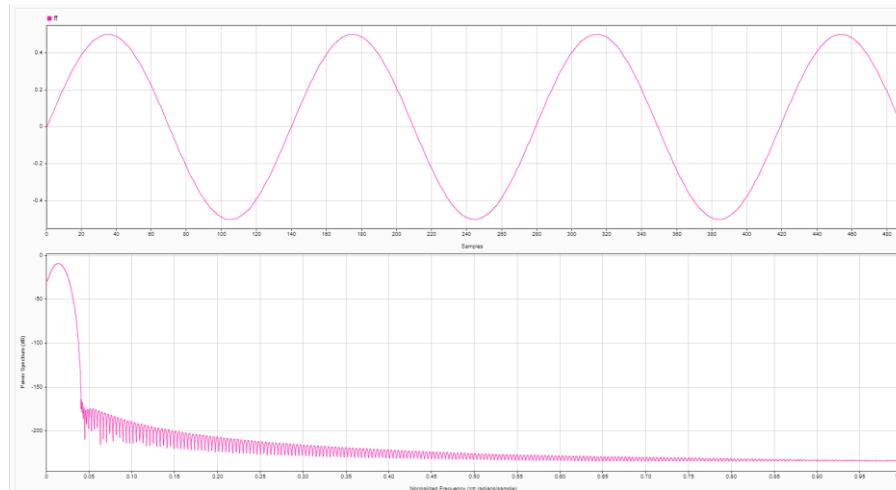


Figure7 - Sidelobes in the spectrum of the signal $f(n) = 0.5 \sin(5n)$. It is worth notice that every sampled point is represented by a sidelobe in the Bode diagram of the spectrum.

The of the signal and sidelobes can be seen for the spectrum of the signal $f(n) = 0.5\sin(5n)$.

For simple signals it is still possible to determine the most important components, but for complex signals it is often necessary to resort to more complex mathematical tools.

Leakage is the distortion of the space

Using a filter, a number of samples is set and with algebraic manipulations the sidelobe effect can be limited. The new graph allows to identify the components of the periodic signals. This technique is called windowing.

Gibbs phenomenon.

In presence of discontinuity, an oscillatory behaviour is observed. This is due to the variation of the expected behaviour. As a result, the plotted graph is affected by undesired oscillations that can influence further data treatment.

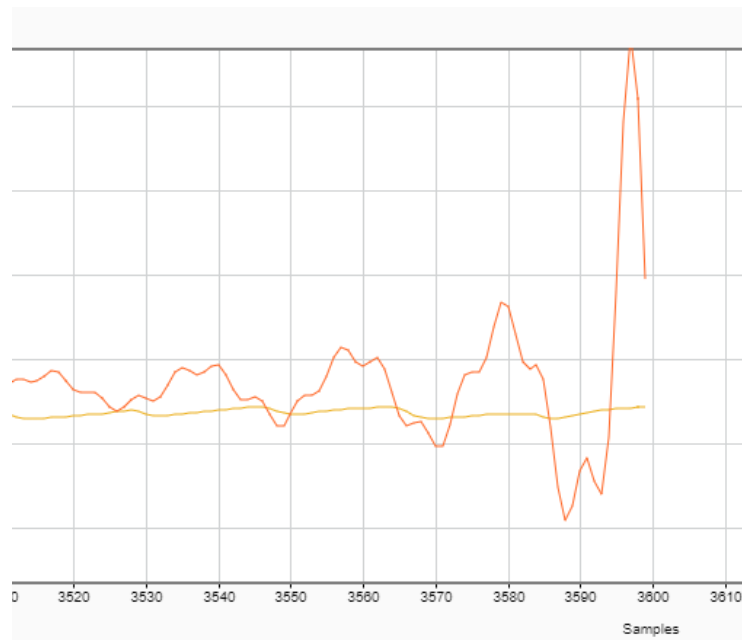


Figure 8-Gibbs phenomenon approximating a time series with a m

Windowing.

A particular set of filter are the Window filter[12,40]. Among the most common we have:

- Kaiser window.
- Hanning window.
- Hamming window.

Windows are used to control sidelobes in the frequency plot of a signal. Sidelobes are usually due to the leakage effect. Roughly speaking, windowing consists of algebraic manipulations of a specific subset of the original data, in order to maximize the influence of the central elements and minimize the effect of the initial and final elements of the time series.

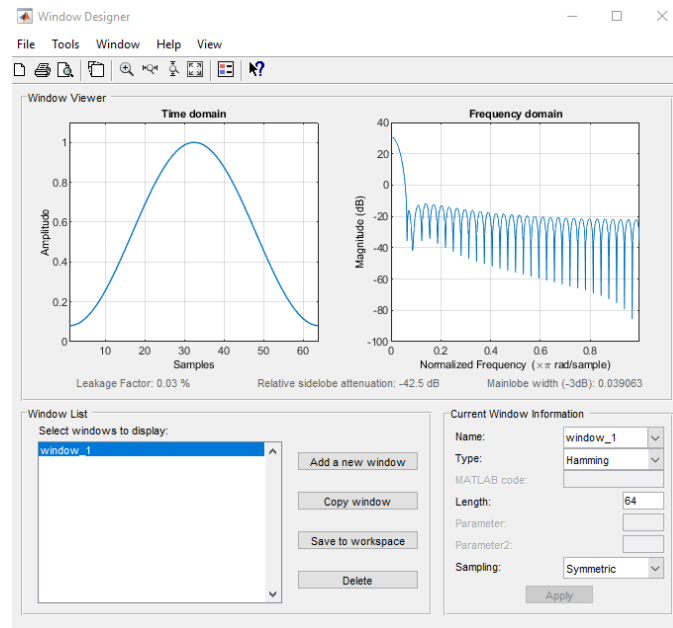


Figure 9- MATLAB windowing tool representing the Hamming windows.

Wavelet transform.

The above mentioned techniques apply for stationary periodic signals. However, it is also possible to use the wavelet theory, that allows to perform the analysis of a class of more general signals.

The continuous wavelet transform is defined by the equation:

$$C(a, \tau) = \int \frac{1}{\sqrt{a}} \Psi^* \left(\frac{t - \tau}{a} \right) x(t) dt.$$

As already seen in digital filtering, Fourier transform can be also applied to the wavelet analysis, and the continuous and in the discrete case. The transform is in this case called short Fourier transform and can be regarded as a two dimension integration. In the wavelet approach, it is a generalization of windowing and filtering methods, where, roughly speaking, a set of filters and windows evolves during the sample time, in order to detect the spectrum of a limited interval.

The method is iterated changing the band pass filters and the scaling coefficients. The scaling of the signal allows to detect which frequency can be used and which must be ignored.

Spectrogram.

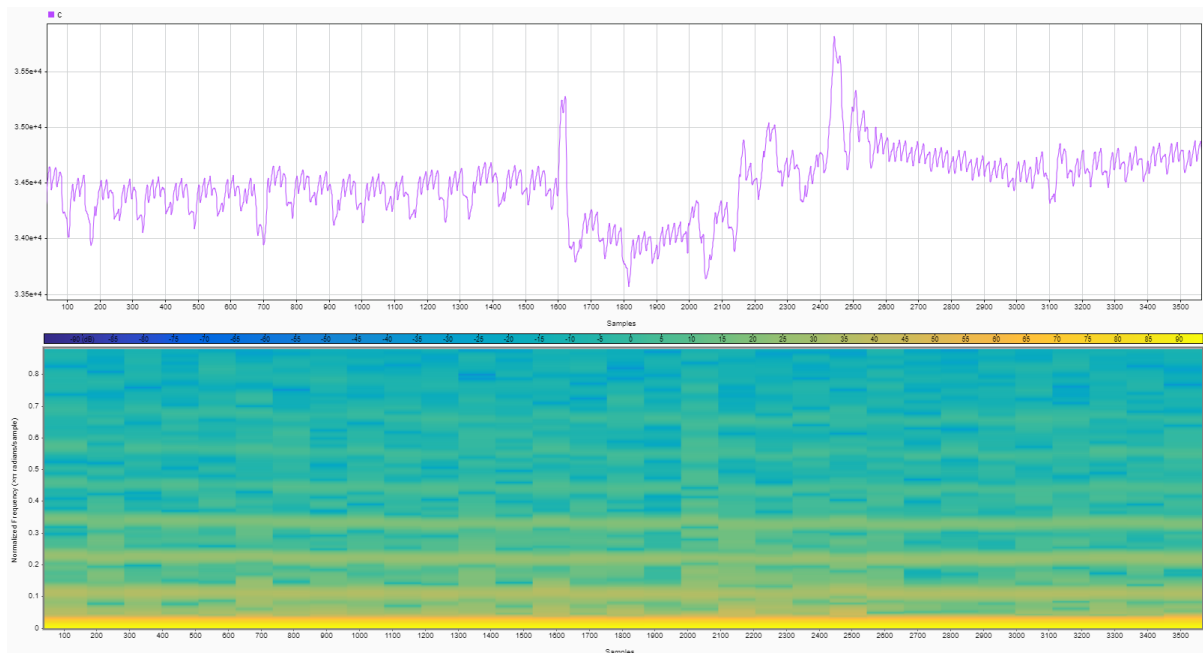


Figure 10 - Spectrogram of an ICG signal, containing random noise and disturbances.

The spectrogram is obtained with wavelet techniques and represents the variation of the frequencies during the sampling time. Similar to spectrogram, a scalogram provides the same information, but considering the variation of the scale that is used in computation. A wavelet analysis allows to reconstruct the coefficients of the signal and its frequencies and the approximation.

As it can be seen, a spectrogram is in reality 3 dimensional geometric entity. It is either possible to represent a scalogram by a 3D graph, or using a coloured map to identify the gradients.

Persistence spectrum.

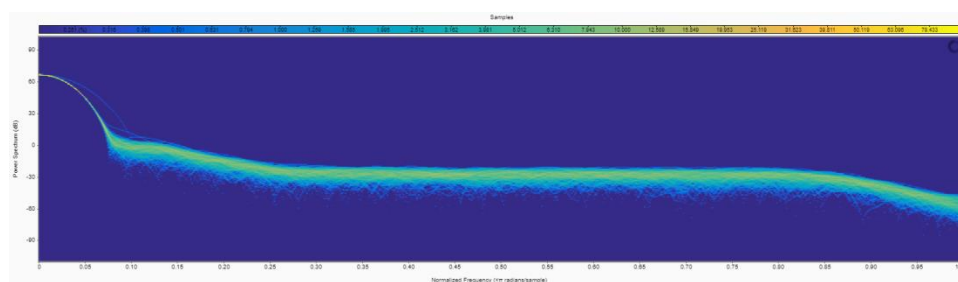


Figure 11-Persistence spectrum obtained by MATLAB signal analyser tool.

Persistence spectrum is a histogram that can be plotted by Matlab automatic library and represents the spectrogram of a signal during time. This means that a signal is sampled over a limited data and the spectrogram is plotted only for this interval. The output of a persistence spectrum is

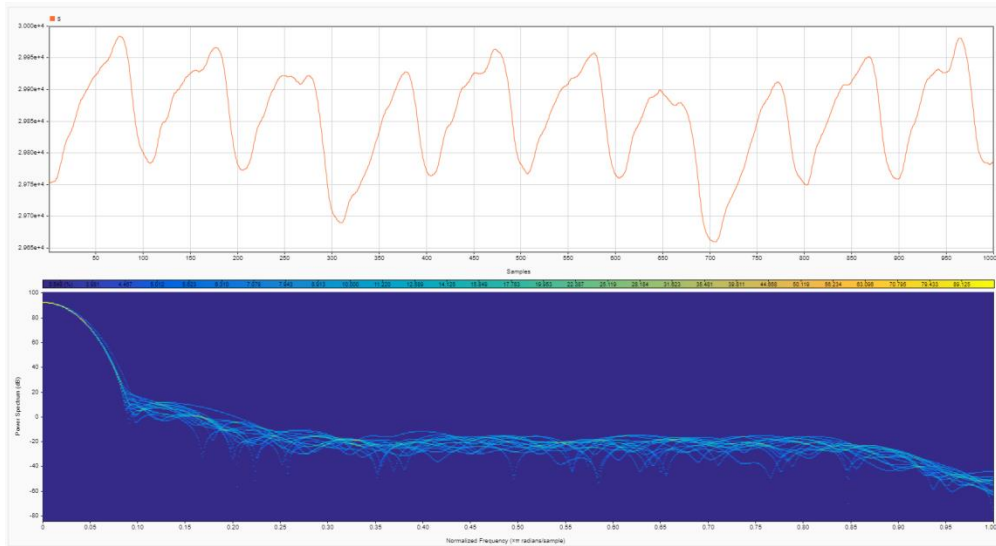


Figure 12- Persistence spectrum of an ICG signal.

a family of curves that allow to understand the occurrence of the same amplitude among the whole sampling.

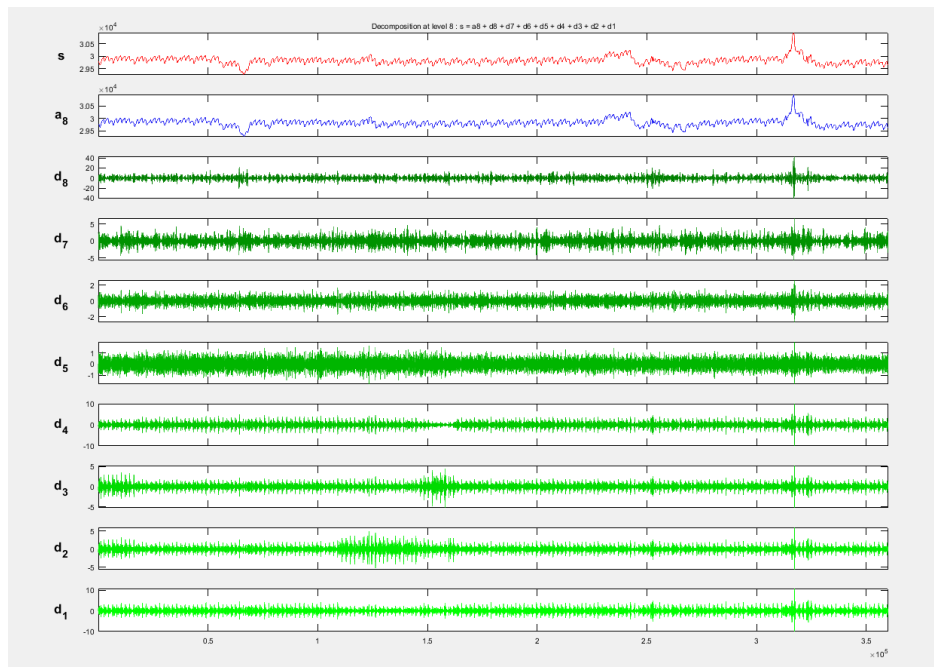


Figure 13 - Wavelet transform of an ICG time series obtained from Wavelet MATLAB tool.

MATLAB Wavelet tool.

MATLAB provides a wide variety of libraries for the analysis of wavelet methods. The wavelet function tool was used, but also other commands, such as mowt are useful to derive the data signal. In fact, wavelet analysis can be seen as a set of filters that are applied to a signal. The filtration is repeated iteratively, changing the coefficients of the filter.

Considering j steps in the algorithm flow, it is possible to identify the j^{th} wavelet using the equation:

$$\frac{1}{N} \sum_{k=0}^{N-1} H_{j,k} e^{\frac{j2\pi kn}{N}}$$

Where the original signal is scaled according to:

$$H_{jk} = H_{2^{j-1}k \bmod N} \prod_{m=0}^{j-2} G_{2^m k \bmod N}$$

The wavelet scaling filter is provided by:

$$G_{jk} = \prod_{m=0}^{j-1} G_{2^m k \bmod N}$$

The result is a set of filtered data obtained from the original time series that is represented by:

- a scaling factor;
- a pass band filter.

In this algorithm, the difference between two values is identified by a factor 2^j .

Short time Fourier Transform.

The short time Fourier transform is used in Wavelet analysis and simply represents a generalization of the concept of the Fourier analysis. The goal is to apply the discrete Fourier transform to a single interval of the whole sampling.

The reconstruction of the system is expressed by the coefficients chosen in the analysis that either represent the amplitude of the wave(scale) and the frequencies.

Deep learning and machine learning.

Convolutional neural networks.

Convolutional neural networks are used in many fields for data analysis and image recognition[42,44]. The main goal is to develop a set of neural cells that can be used on a network and on different layers, in order to perform an automatic task, as image recognition. Image recognition is here used to identify desired shape waves and features of the signals and perform the computation that are required to study physiological trends. Neural network can be used to derive the coefficients necessary to perform wavelet filtering. Every node represents a convolution operation. The goal is to use a certain number of inputs, that are usually a subset of bits from a converted file(a digital picture, for example)[43]. In convolutional network, the coefficients are computed considering the desired output.

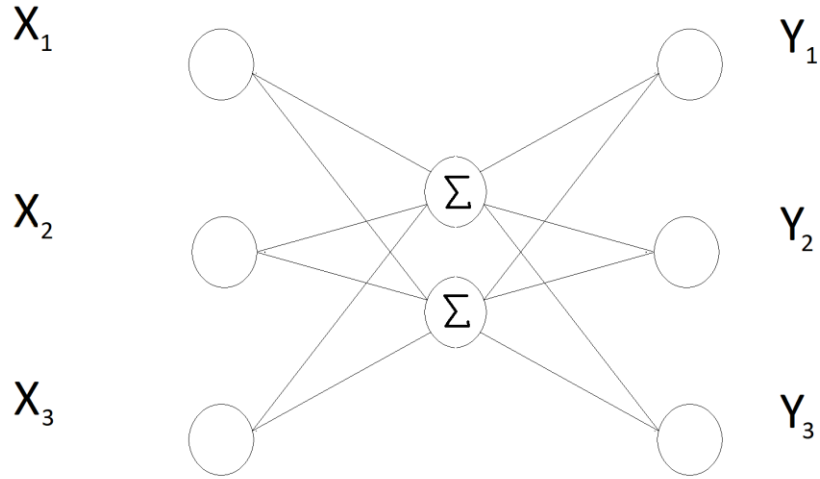


Figure 14-A convolutional neural network is a complex system of convolution operation on a certain input set, that can be used to provide a desired output. A typical application of neural network is image recognition, where to the digital input is associated a set of output(“dog”, ”car”, ”hand” etc.).

In machine learning, the model is derived manually using the initial data and the adjusting is performed by trial-and-error procedure, whereas in Deep learning the neural network synthesis can be performed automatically[41,45].

Both techniques can be used to derive the best estimation of the spectrum of a signal. But can be also used in feature extraction and identification. Learning activity in this case depends on a wide set of data where the extraction of equations or other model is time consuming. In this case, deep learning allows to derive a complex model starting only from data. The main feature used in deep learning is the identification is the detection of edges in the data set. The detection of the edges is identified by a probability distribution function.

Deep learning is also used in feature extraction. Let it be the time series provided by an accelerometer wore by an athlete. Let the time series be available on the whole time. One might be interested in the determination of the activities of the athlete. It is obvious that if the athlete is sleeping or resting, the acceleration must be zero, whereas must reach a maximum when the athlete is training.

Peak of acceleration detected	Activity
0-0.05g	Sleeping/resting/leisure time
0.3-0.7g	Climbing
1-1.2g	running
1.2-1.5	Jump/obstacle running.

Table 1- An attempt to identify the activity of an athlete starting from the measured accelerations.

Obviously, only from acceleration time series it is not possible to determine all the activities of the athlete. Instead, it is necessary to provide at least some hints about the activity of the athlete.

The previous estimation can be done by a simple threshold system. What with machine learning and deep learning can be done, though, is to study the shape of the acceleration data

series, to specifically identify the activity performed by the athlete. The output can be used to perform the caloric consumption of the athlete.

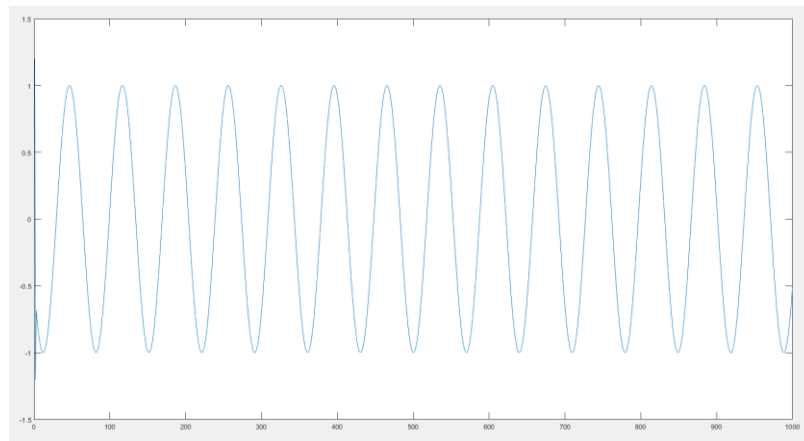


Figure 15- A sinusoidal is the ideal approximation of a person walking.

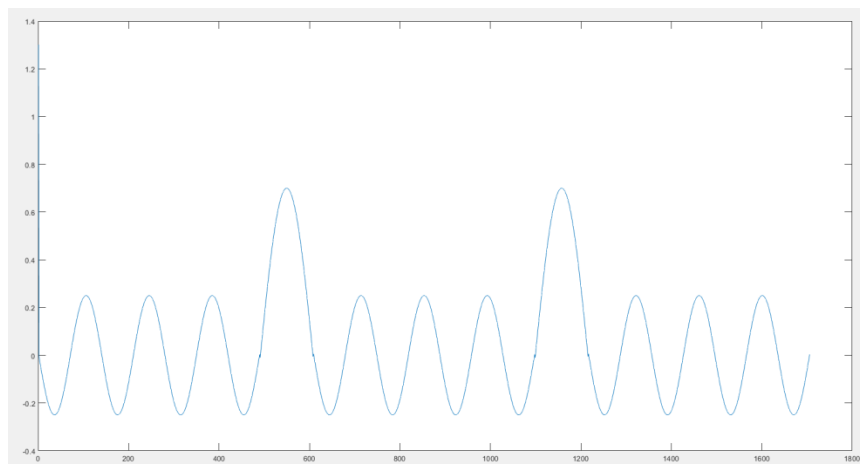


Figure 16- An athlete competing in obstacle course racing.

Another application of deep learning can be the detection of arrhythmia.

MATLAB tools.

MATLAB software already provides to users a wide variety of libraries that can be used to perform harmonic analysis and statistical analysis of signals and time series.

Fast Fourier transform and inverse Fast Fourier transform are standard library. The most common filters are available as well. Not only functions: MATLAB provides standard applications, such as signal analysis and spectral estimation. Wavelet toolbox and Econometric toolbox, with the respective libraries and functions, can be downloaded and installed and represent other useful tools in system analysis. Machine learning and Deep learning can be performed using classification learner, deep network designer, neural network pattern recognition, and so on.

However, even with a such variety of instruments, it is often necessary to develop customized functions in order to perform specific tasks.

Matlab differentiation.

The Matlab differentiation routine was used during the analysis, however, if the saving rate is not synchronized with the sampling rate of the device, meaning that the sampled data repeat their values on many cells of saved array the during sampling time, Matlab derivative routine fails to compute the real derivative. For example, in the data used in the present work, it was noted that the data was repeated for averagely 10-15 cells of the data vector. The repetition was not even observed on constant sampling time. This required the development of a specific routine for the derivation with an “if” condition: when the same value was observed, a counter took a record of the occurrence of this value and when a new value was detected, the difference of the two values was divided by the number of occurrence and the counter reset. This was first noted when the derivative of the impedance was found equal to 60-70Ohm/s, whereas the expected value, computed graphically, should be around 0.4-0.6Ohm/s.

Biomedical applications and estimation techniques.

All the techniques mentioned in the previous chapters can be applied in the study of biomedical systems and phenomena, but let it is worth noticing that great attention must be paid in the applying of the used methods[47]. Many of these models were developed for economic systems in econometrics. This means that the models are devised to find the trend of a certain time series, for example, the prediction of the value of stocks or cryptocurrencies. This means that the oscillations on small periods, for example of days or weeks, can be ignored. This is not true in biomedical practice. For example, an ECG can be certainly used to provide a rough estimation of cardiac output; but, on the other hand, it is often important to see the details of the temporal variation, in order to detect arrhythmia or other clinical conditions. In this sense, not only is important to analyse a long timeframe, but also small periods of time. Moreover, the detected signal can be influenced by other biological processes, and it might be necessary to eliminate the corresponding harmonics. For this reason, it is not possible to define a mere mathematical method valid for all seasons. Instead, some assumptions must be made in advance, and validated or rejected during the modelling procedure. For this reason, collaboration with physicians and medics is vital in this discipline.

Instrumentation.

Biomedical engineering requires a wide variety of sensors and data loggers. A sensor can be seen as a two port system, where the input is the value to be measured and the output is the reading value, according to a user-friendly interface[62,98,99].

Biomedical instrumentation can be classified according to different criteria. For example, considering the physical working principle, it is possible to identify:

- mechanical sensors;
- electromagnetic sensors;
- hydraulic, pneumatic, fluidic sensors;
- chemical sensors.

Electronic sensors and devices.

Electronic and electromagnetic sensors are of paramount importance in biomedical measurements, due to their cost, the almost infinite possibility of interfaces they can be connected to, and availability[47]. Of course, in many cases electronic devices are but an interface between the phenomenon and the researcher, whereas at the bottom layer another kind of physical principle is used for measuring.

- resistive sensors.
- capacitive sensors.
- inductive sensors(including transformers).
- photoelectric and optoelectronic transducers.

Different geometries can also identify different type of sensors (for example, linear capacitive sensors vs cylindrical capacitive sensors).

Among the chemical sensors, a wide range of sensors is devoted to the investigation of oxygen consumption and the derivation of information about metabolism. The detection of the signal is usually performed by means of DAQ systems, that must collect the data avoiding electromagnetic disturbance.

An obvious characteristic of the realization material must be the inertance of the material to biological tissues.

Spirometer.

Spirometry techniques are used to examine the breath of a subject. Spirometers are basically flowmeters aimed to measure air exchange in animals and man.

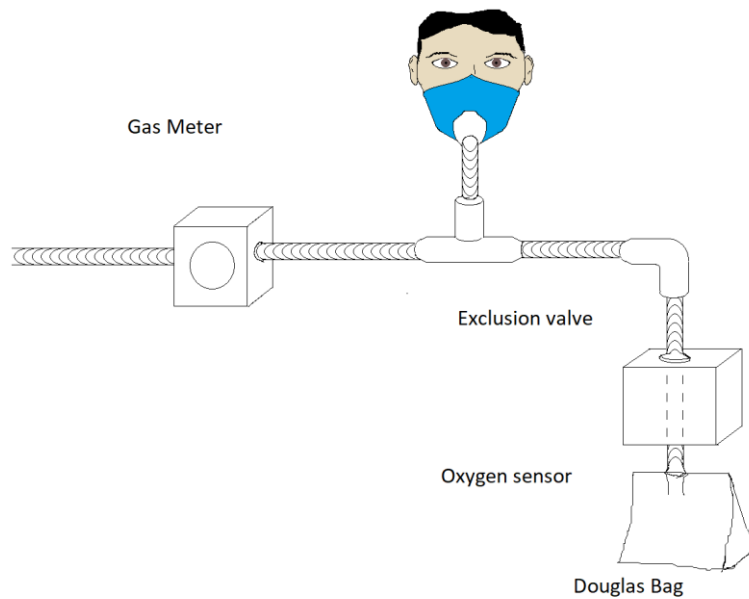


Figure 17- Layout of the Douglas bag.

One of the first set ups used in spirometry was the Douglas bag [8], either applied on animals or human subjects. The gas released during expiration was collected into a vessel or control volume, that is a bag, where the concentration was measured with one of the methods above mentioned. Taking into account the respiratory cycle and atmospheric oxygen concentration, the consumed oxygen can be computed relying on the different concentration measured inside the bag.

Lead electrodes.

As previously said, it is sometimes necessary to measure a current or, better said, the impedance of a certain tissue. Electrodes are placed between two points and both current and voltage are measured, in order to obtain the impedance on the path between the two electrodes[46]. Usually, alternate currents are used, since the penetration inside the tissue is deeper, due to corresponding alternating magnetic fields generated into the tissue itself.

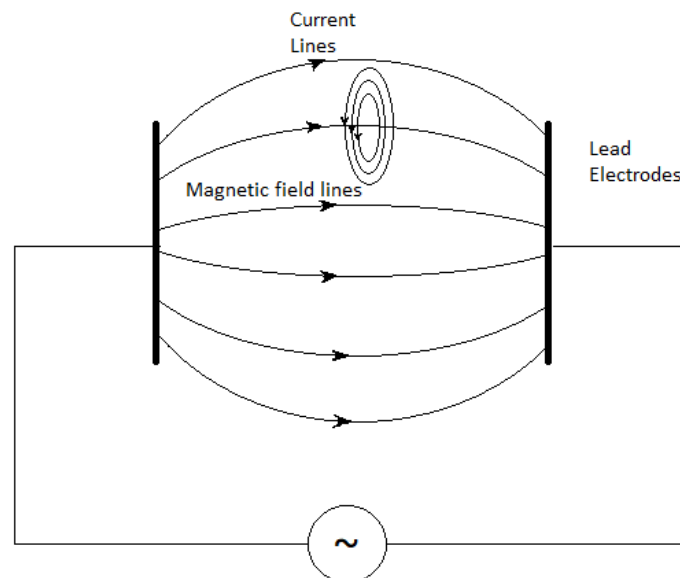


Figure 18- Current lines between two electrodes.

MEMS devices.

Micro electro-mechanical systems are presently used in measurement applications and have a wide variety of applications. MEMS technology allows to realize both mechanical and electrical parts, integrated on a single chip. Miniaturization is allowed by means of specific lens and lithographic technologies, where a shape can be reproduced changing the scale of reduction, just by changing the distance of the emitting source from the worked surface [97,101].

Mechanical sensors, electromechanical sensors.

Accelerometers.

Accelerometers are used to measure the mechanical activity of the human body and a direct estimation of calories spent in mechanical work[95].

The simplest accelerometer is realized using an electromagnet in a magnetic field generated by a coil or, said differently, it can be devised with a permanent magnet and an coil circuit, where the magnet is allowed to oscillate among one direction.

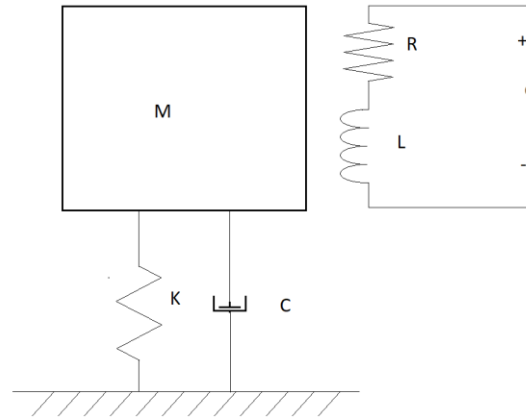


Figure 19- Equivalent model of accelerometer coupled with a coil.

An equivalent design of the accelerometer takes into account the mass of the accelerometer, the internal friction of the spring, the equivalent stiffness of the spring, the equivalent resistance of the coil, the equivalent impedance of the coil. The output measure must be the current or, equivalently, the voltage.

$$m \ddot{z} + c \dot{z} + kz = F(t),$$

If the direction of motion is parallel to gravity vector, we have:

$$m \ddot{z} + c \dot{z} + kz = mg,$$

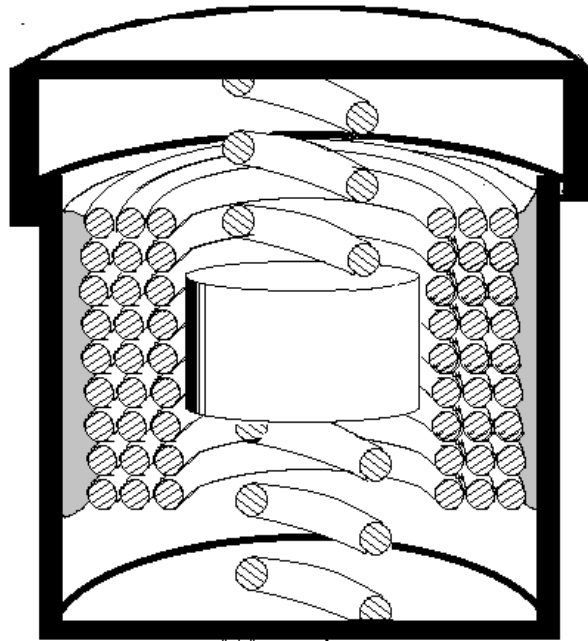


Figure 20 – a simple accelerometer.

Other accelerometers are realized using piezoelectric materials, exploiting either longitudinal displacement or bending.

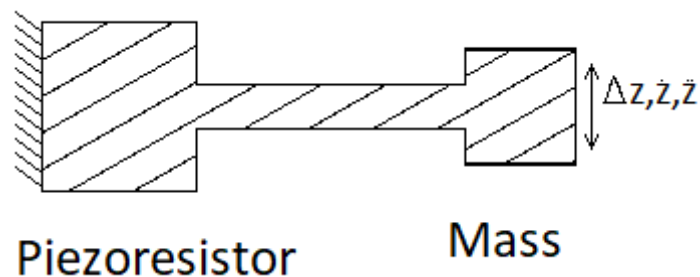


Figure 21 - A flexural accelerometer.

A typical example is provided by cantilever accelerometers. The material is piezoelectric and this allows a wide miniaturization of the device, that can be exploited, for example in smartphones.

The equation describing the model is similar to linear accelerometer, but must be derived considering flexural behaviour of the forces acting.

The Lagrange equation. Generalized coordinates.

But how is it possible to derive the equation for a mechanical system? A procedure is possible using the Lagrange equation. The Lagrange equation states that: the mechanical equation of motion of a mechanical system can be derived using the kinetic energy and the potential energy of the system. In particular, it is possible to write:

$$L = T - U$$

$$\frac{d}{dt} \left(\frac{\partial L}{\partial \dot{q}} \right) - \frac{\partial U}{\partial q} = 0$$

This equation is valid for conservative systems. For non conservative systems, the Rayleigh dissipation function can be used to model internal damping in the accelerometer or in a generic vibrating system.

$$F = \frac{1}{2} C \dot{z}^2.$$

More complex models requires a multy-body approach.

Monoaxial accelerometers and triaxial accelerometers.

All the previous considerations apply to monoaxial accelerometers, however, in biomedical engineering it is often required the usage of triaxial accelerometers, that, most of the time, can be realized using three monoaxial accelerometers.

Chemical sensors.

Metabolic measurements.

The instrument detects the volume of oxygen and carbon dioxide thanks to specific probes. The aim is to identify the gases exchanges and variation of oxygen and carbon dioxide concentration during breathing activity.

Oxygen sensors. Concentration.

In order to detect the concentration of oxygen, two main techniques can be used:

- It is possible to use a flowmeter and detect the concentration in the flow, or
- it is possible to isolate a control volume where the concentration can be measured.

In both cases, the concentration is measured relying on three main physical aspects:

- spectroscopy;
- magnetic properties of the matter;
- chromatographic behavior.

Magneto-mechanical oxygen sensor.

Magneto-mechanical oxygen sensor exploits the torque produced by a magnetic field, the intensity of which changes accordingly to the atmosphere.

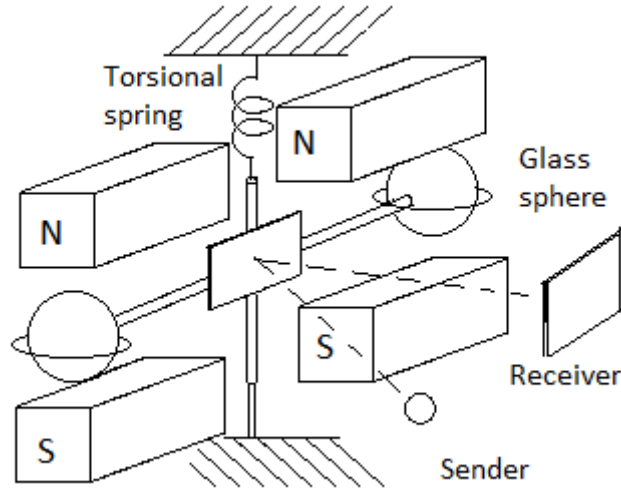


Figure 22-Oxygen magneto-mechanic sensor with optical displacement sensor.

The intensity of the force acting on the glass sphere is obtained using the equation:

$$F = (\kappa_{atm} - \kappa_g)V\mu_0 H \frac{\partial H}{\partial s}$$

Where κ_{atm} , κ_g are the magnetic susceptibility of respectively the gas and the glass, V is the volume of one sphere, μ_0 is the magnetic field constant, H is the vector of the magnetic field and the remanent term is the gradient of the vector. The two forces acting on the two sphere generate a torque that, in this case, it is balanced by a torsional spring. The output of the measurement is the angular displacement that can be read with many devices, for example an encoder on the pin axis, or, as in the illustration, using optical methods.

Magneto-pneumatic oxygen sensor.

A magneto-pneumatic oxygen sensor exploits the influence of a magnetic field on a gas flow.

The difference is usually detected using a pressure sensor, for example a bellows or membrane sensor, where the mechanical input must be converted into an electronic signal, for example, using a capacitor or a micro current sensor.

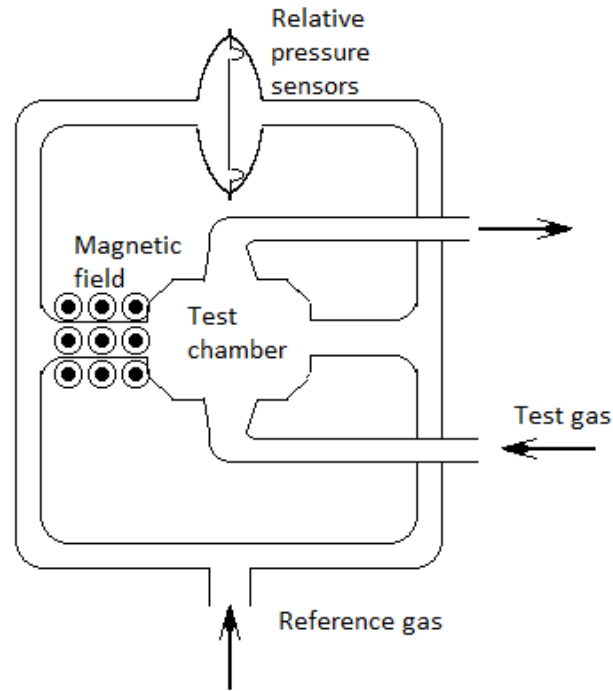


Figure 23- Magneto-pneumatic oxygen sensor.

The relative pressure can be estimated using the equation:

$$\Delta P = a(\kappa_g - \kappa_{atm})\mu_0 H^2$$

Where a is an experimental constant to be detected, κ_g, κ_{atm} are the magnetic susceptibility

Hot wire sensor.

Hot wire sensor is used as flowmeter, but special models allow to study concentrations of different gases.

Carbon Dioxide sensors.

Carbon Dioxide sensors are used to compute the volume of Carbon dioxide. Physical principles are related to the previously stated phenomena.

DAQ systems.

Without a Data Acquisition system (DAQ), the data would be lost at the instant that is detected. DAQ systems store the data for later computations. The saved value can be a current or a voltage, and with a proper interface, it is possible to measure non electrical values, as such as temperature, pressure, sounds and images. The measuring hardware, consisting, among the other parts, of amplifiers and analog to digital converters. This requires the conditioning of the analog source.

Metabolimeter VO2000 MedGraphics.

According to the previous discussion, a device that can measure the gas flow using a Pitot tube. The measure of oxygen is provided by a Galvanic Fuel Cell, whereas the CO₂ is measured by infra-red systems. The working principle is similar to Douglas bag, but in this case an electronic device records the measurement during the time.



Figure 24- Metabolimeter VO2000.

Metabolimeter VO 2000 by MedGraphics is a compact device that can be used for metabolic measurements. The sensors are connected to a respiratory mask. The sensors are connected to a respiratory mask. Several experiments had been made in subjects freely moving on the field where their aerobic energy expenditure was obtained by wearable metabolimeters from the MedGraphic company[63,72, 77,78,82].

STEVAL-MKI 121V1.

The STEVAL-MKI121V1 is a product evaluation board. The communication protocol is based on a USB virtual COM,

INEMO-M1.

Inemo-n1 is a 9 axis accelerometer.

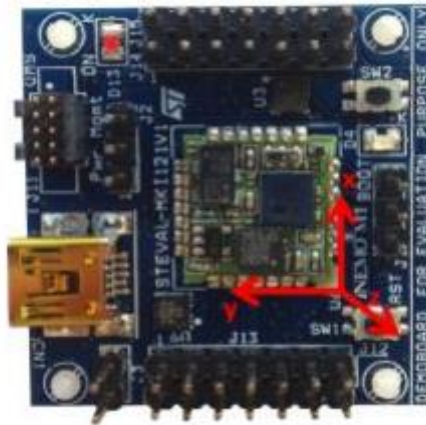


Figure 25 – INEMO M1 accelerometer.

The sensor is based on chip LSM303DLHC, that contains a 3-directional accelerometer and a 3- dimensional magnetometer.

Component	Property	Value
MEMS accelerometer LSM303DLHC	Sensitivity [LSB/g]	[1000, 500, 250, 83.3]
	Frequency range [Hz]	0÷[1, 10, 25, 50, 100, 200, 400, 1344]
	Available bandwidth [Hz]	Frequency range /9
	Measurement range pk [g]	[2, 4, 8, 16]
	Size: cubic edge [m]	$(36 \times 36 \times 20) \cdot 10^{-3}$
	Weight: device [kg]	$52 \cdot 10^{-3}$

Table 2-Characteristics of LM303DLHC in chip accelerometer.

Figure 2. Pin connections

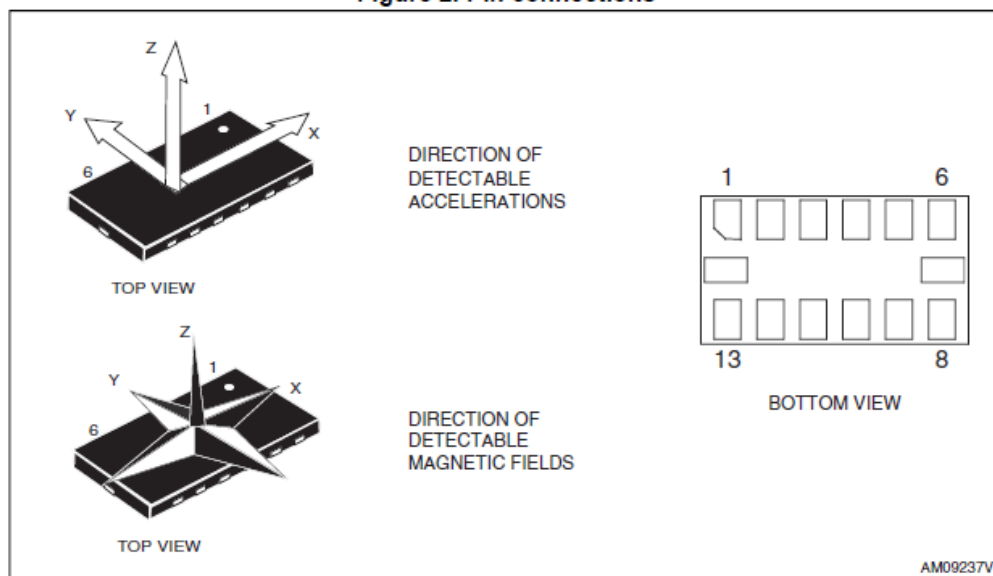


Figure 26- Constructive details of the chip.

WT901SDCL accelerometer from Wit Motion.



Figure 27- WT901SDCL 3-axis accelerometer

The WT0901sdcl datalogger is a multisensory device used in many fields. The device is able to detect the acceleration, the angular velocity, the angle and the orientation of the magnetic field. The device is available with a set of custom libraries that perform immediate conversion and transmission of detected data. Moreover, a special algorithm that automatically correct bias at cold start. The device can be directly connected to a personal computer via USB cable.

Armband SenseWear Pro3.



Figure 28- Armband SenseWear Pro3.

The SenseWear Pro3 armband is a multiple signal device capable of detecting the skin temperature, the Galvanic skin response, the heat flux and it is also equipped with a 2-axis accelerometer.

The device has an autonomy of two weeks. The software provided with the device can also identify the rest time and the periods of activity of the bearer, accordingly to the producer, but many researchers tested and validated the device.

The acceleration on two axes allows to reconstruct the activity of the bearer, while, the temperature and moisture can be related to caloric consumption through a complex set of relations, however, as written above, different validation techniques were developed in order to validate the computed parameters.



I dati contenuti nel referto non possono essere utilizzati a scopo diagnostico.

Figure 29- Results of armband SenseWear Pro3 measurements.

Thanks to these parameters, it is possible to roughly estimate the efficiency of locomotion or at least of total activity

The main output of interest provided by the armband are:

- estimated basal metabolism calories.

- estimated total caloric output.

- activity time.

- path followed by the bearer.

Other pieces of information of clinical interest concerns sleeping time and time sleeping proficiency of the subject. Many validation techniques were developed by researchers for this or similar device. Validation techniques were developed in order to determine the validity of this approach [79,89,91,93].

Use of Disposable electrodes.



Figure 30- On the right an ECG disposable electrode with the male component of the press stud near its contact side whit conductive gel. On the left the tag with the technical and safety data.

Electrodes must be set on the trunk in order to detect the variation of the impedance, accordingly to the position of blood in the organism. Blood is in fact an acid fluid that conduce electricity and the position of the blood in the tissues changes the resistance of the portion of the human body examined by the researcher. This variation is exactly what is investigated in the present work.

Detection of cardiac impedance.

In the present work, as it will explained in the following paragrapher, one of the main goals was to detect the thoracic impedance using four electrodes. In order to detect the signal, a commercially available mono-frequency evaluation board must be used and, in this work, the ADAS-1000 board (Analog Devices, USA) was chosen. The board contains an alternate current supply at a constant value of 1mA. The ADAS-1000 board, implemented into the wearable device NEW CORE” which, in turn, is part of the e-Physio ICT platform (2C Technologies Ltd & Nomadyca Ltd associated proprietary), consented to assess

cardiodynamic profile in subjects engaged in extreme in field physical activities [80,81].

The relatively high frequency (65 kHz) of the current injected into the thorax is such as to short-circuit all the electrical capacities of the cell membranes, thus nullifying the reactive component of the electrical impedance so that the latter only consists of its resistive component. The blocks diagram represents the e-Physio platform for the remote cardio-dynamic variables of which an example of acquires analogic instrumental traces. Roughly speaking, it consists of three separate blocks: a sampling front-end, a command and control system and a data transmission system.

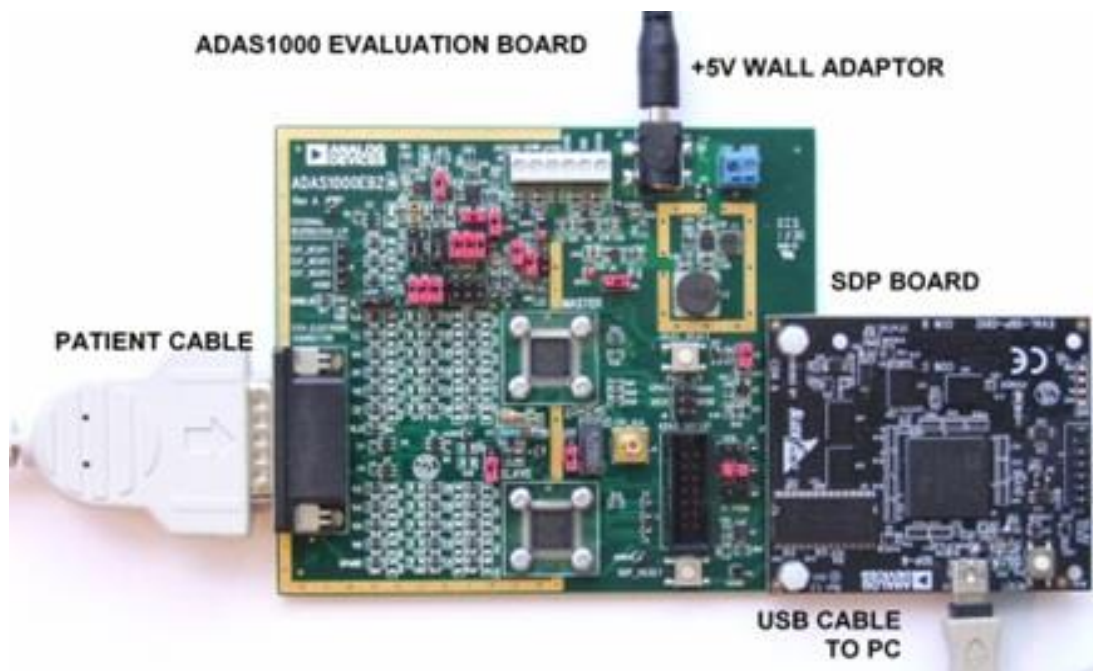


Figure 31 –the electronic evaluation board for bioimpedance electrical measurements (see text for specifications).

The sampling front-end contains the ADAS-1000 electronic board to inject the electrical current into the subject's thorax (current supply block in figure) which voltage difference is assessed by a module containing the electrical signals amplifier (amplifier block). It also contains a three stages filtering section to ensure the elimination of frequencies outside of the range of interest from the acquired signals (filtering block) and a 10bit analogical-digital converter appropriately calibrated (A/D converter block). The command-and-control block in figure supervises the sampling sessions by initializing and driving the ADAS-1000's operations and shares all the information to a controlling software operating on a personal computer by means of a data acquisition system. A Bluetooth microchip fully supporting the radio frequency communication protocol enables a totally wireless operation mode of the thoracic impedance device (see the same block in figure). The WEB block (in figure with dashed lines) consents the device to be remotely controlled by a Personal Computer running a proprietary software.

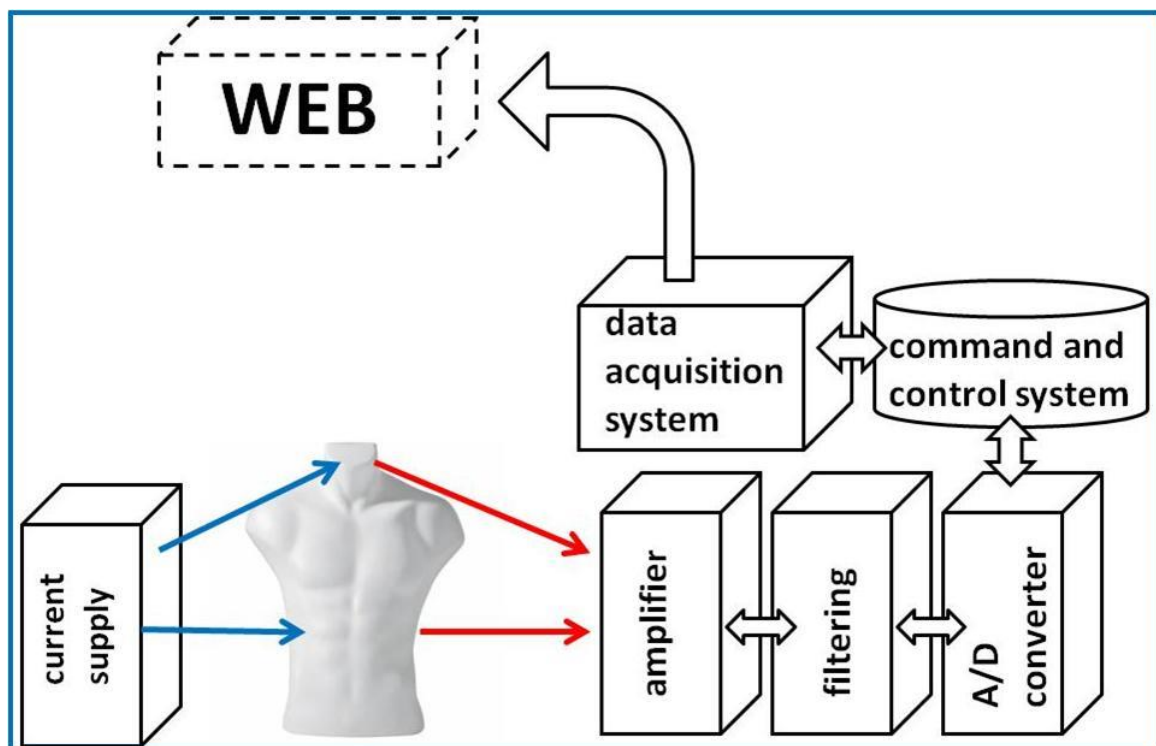


Figure 32 – Blok diagram of the e-Physio platform. Impedance signals were assessed from the subject thorax by means of two couples of disposable ECG electrodes attached at the roots of neck muscles and in the thorax at the level of the xiphoid process while an AC current was injected by other two couples of electrodes placed 5 cm externally respect to those for the impedance assessment (see text for further particulars).

Mechatronics in biomedical engineering.

The rapid development of information technology provided the researchers of new means of inquiry in the scientific discipline. And this is certainly true for the biomedical engineering, whose goal is to assist physiologists and medical academics in the exploitation of such resources of new conception, whose full potentiality would otherwise remain unexpressed. In this, mechatronics plays a relevant role. The development of new instruments, analysis techniques, methods etc. represents a great occasion for the mechatronic engineer who is interested to work into field full of challenges and opportunities, that can be almost considered at a pioneering stage. In sport medicine latest improvements and development allow a deeper comprehension of adaptation of the human body to different environmental conditions. Researchers are interested in the determination of connection between the environmental conditions and the adaptation of the human body to variations of these conditions. For general medicine it can be interesting to develop new clinical techniques that can reduce the invasiveness of medical treatment and prognosis as well. The importance of electroimpedance techniques is related with arrhythmia disorders, that can, in some cases, lead to the sudden death of the subject.

Bolton's Fabrice Muamba collapses during Spurs-Bolton match

🕒 17 March 2012 | ⚽ Football |

Bolton Wanderers midfielder Fabrice Muamba was left critically ill after collapsing during an FA Cup quarter-final tie against Tottenham.

The 23-year-old was rushed to the intensive care unit of the heart attack centre at the London Chest Hospital.

Medics spent six minutes trying to resuscitate him on the field after he fell to the ground with no other players around him.

Figure 33-Electrophysiology has important implications in prevention and diagnostics. Underestimating clinic examinations leads sometimes to bitter consequences (source: CNN announces the stroke of a soccer player occurred on the field, <https://www.bbc.com/sport/football/17417973>) .

Bioelectromagnetism.

Bioelectromagnetism is the discipline devoted to the determination of electric and magnetic properties of biological materials and tissues. Electricity was already known in the ancient time, like the Greek etymology of the name itself suggests, but it was only during the age of

Enlightenment that a linking between physiology and electromagnetism was described by the Italian physician Luigi Galvani, that published his results in his work *de Viribus Electricitatis in Motu Musculari Commentarius* (essay on the forces of electricity in muscular displacement) from 1791. Galvani based his assumptions on the famous experiment of the frog legs, when he demonstrated that the retraction of the legs was still possible even the upper half of the frog was disconnected from the brain, injecting current in it.

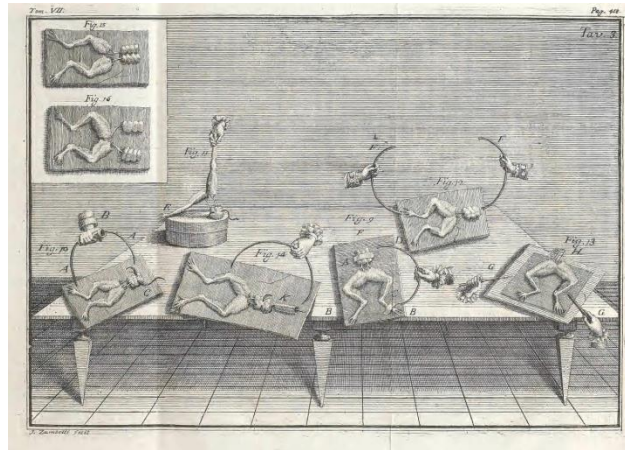


Figure 34-Galvani's experiments represent a milestone in electrophysiology.

Starting from Galvani's work, scientists of different disciplines in XIX century dedicated great effort and time in the investigation of further aspect of bioelectromagnetism, but the laws behind the phenomena, if not the phenomena itself, remained conceived to researchers for decades, and the whole discipline was often associated to paranormal and parapsychological wisdom, like the fortunate Mary Shelley's masterpiece *Frankenstein or the modern Prometheus* shows. Still in 1846 the German zoologist and philosopher Carl Vogt could write:

"the connection between the act of thinking and the brain is the same as between the bile and the liver, or the urine and the kidneys", underlying an analogy with fluid mechanics, similarly to other unfortunate assumptions in physics, as such the theory of the caloric fluid theorized by the pioneers of thermodynamics and luminiferous aether in electromagnetic wave propagation. It must not be forgotten that a scientific and rigorous mathematical approach to electromagnetism was yet to come. It was only in 1865 that James Clark Maxwell described the fundamentals of electromagnetic field theory, in his paper on Physical Lines of Force, published on the Philosophical Magazine and Journal of Science, even if Hans Christian Ørsted had already observed that a current can generate a magnetic field, to be considered as the down not only of electrophysiology and biomagnetism but also of electromagnetic theory. It was only in 1887 that the first electrocardiogram was recorded, by the British physiologist Augustus Desiré Waller. At the time, however, further developments of the discipline were limited not only because theoretical issues, but also due to the lack of a mature electronic industry, so that the cost of electronic materials and elements discouraged further experiences. For example, the first pacemaker was theoretically conceived by Mark C.

Lindwill in 1926, but it was only in 1950 that the first external pacemaker was designed by the Canadian Electrical engineer John Hopps.

It was only with the World Wars and the cold war, when the political and social rivalry shifted in the academic field, that research in biomedical diagnostics blossomed in URSS, Europe and United States of America and were boosted by local governments. For the first time in history, the realization of a Universal health care was conceived. Between 1950s and 1970s a wide range of electronic instruments were adapted for biomedical applications. At the time, the electronic devices were still bulky, expensive and required many ours of training to operators. A first step into the mass diffusion of electronic technology was done when the vacuum tube technology was outclassed by semiconductors. If the pacemaker designed in 1958 by the Colombian doctor Alberto Vejarano Laverde and the Colombian engineer Jorge Reynold Pombo weighted 45kg, the American engineer Earl Bakken developed the first wearable pacemaker. At that time, sensors were coupled to analogic scopes as such as oscilloscopes. A second revolution was experienced during the blossoming of digital technology and continues at the point the present work is written. Wireless technologies and miniaturization of the devices allow the realization of a great number of applications, the limit of which seems due to human imagination. Today IoT systems allow an ubiquitous monitoring of vital, physiological parameters, cardiac frequency, weight, and so on.

Electrophysiology of biological tissues.

At the present time, electrophysiology and biomagnetism are applied to almost every aspect and field of medicine. Among the others, one of the greatest advantages for diagnosis is to provide information without invasive techniques on the biological tissues.

Electrophysiological techniques find their natural application for a wide range of fields, including animal and human wellness. Some methods were also applied to plants and fruits. The essential activities in electrophysiology[96] can be identified in:

- measurement of electric and magnetic fields, for example, magnetic field generated by neuron synapsis.
- injection of stimuli, generating an electrical or magnetic field.
- measurement of magnetic properties, as such as inductance, resistivity or susceptibility of a biological tissue.

At the time of publication of this work, the most important branches of human electrophysiology are devoted to the study of the brain, the eye, and the heart. The study of brain waves represents an important field of research since it makes possible to treat disabilities such as blindness and deafness. In the last decades, researchers developed remote control techniques for artificial arms or legs, directly with the patient [51,53].

Electrophysiology of the brain uses the magnetic fields generated by brain waves related to psycho-motorial activities and attempt to reconstruct a map of the neural path connected to a specific action willingly conceived by the subject. Electroencephalogram (EEG) techniques are widely used not only in the study of languages and cognitive processes, but also in the identification of the mechanism of locomotion.

Trans-cranic Magnetic Stimulation (TMS).

The contemporary computational technology allows the detection of large datasets containing different mappings of the brain. The goal is to link the path with the behavior of the subject. Progress in this research field allowed some researchers to claim that mind read is at hand and it will be soon realized.

Electrophysiology of the heart.

Methods exploited in electrocardiography are totally different. The classical case in electrophysiology is the study of the electrocardiogram (ECG). Among the main properties of ECG analysis, arrhythmia can be detected, avoiding severe consequences to the patient [49,57,58]. The main advantage of these methods is the non-invasivity.

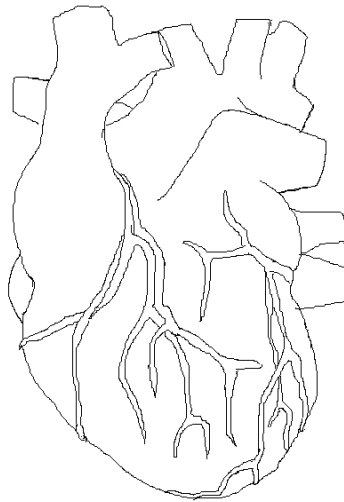


Figure 35-Electrophysiology of the heart is of paramount interest in contemporary medical research.

Electrophysiology of equilibrium and locomotion.

Locomotion[50,52] is controlled by the brain by means of two mechanisms:

- voluntary movements.
- involuntary movements.

Voluntary movements are usually related to the execution of a certain action, for example, in sport, the act of hitting a ball in soccer, whereas the central nervous system cope with a series of secondary muscles necessary to exploit the action. The control action of locomotion is the result of a fragile balance of the two system, the disturbance of which can have severe and pathological consequences, as such as experienced in Parkinson disease.

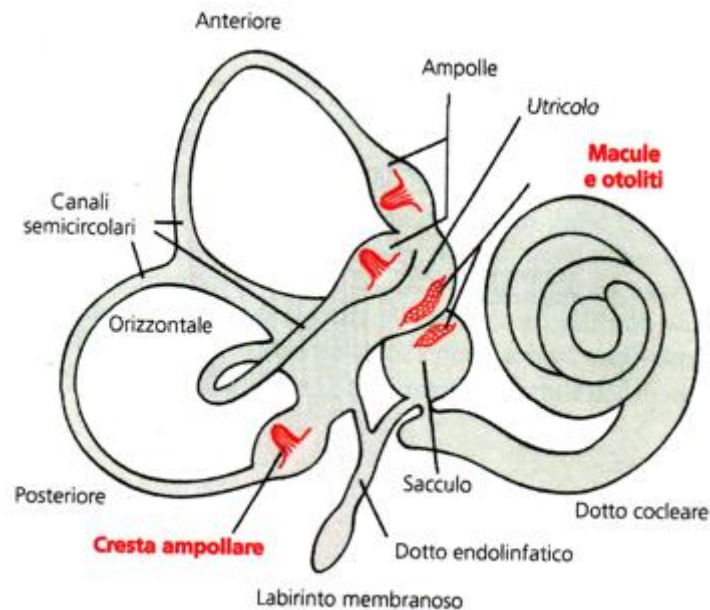


Figure 36 – membranous labyrinth in ear (from J. E. Hall, A.G. Guyton, ,Fisiologia Medica, Milano, Edra, 2012).

A paramount role in locomotion is played by the equilibrium organs, and, by the membranous labyrinth. In the internal ear, important organs called utriculi (lat. *Utriculus*, small bag) and ampullas can be considered as natural accelerometers, capable of measuring the acceleration of 3 axes. This means that the nervous system is able to detect not only the variation of inclination of the body (especially of the head), but also the inclination itself.

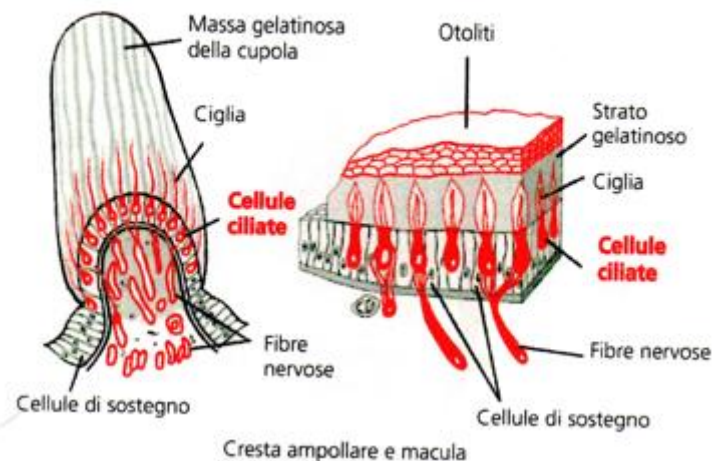


Figure 37- Ampullas, otoliths, and cranial nerves. (from J. E. Hall, A.G. Guyton, ,Fisiologia Medica, Milano, Edra, 2012).

In ampullas threads called cilia are used to detect the motion transmitted to cranial nerves. Random accelerations and gravity acceleration change the orientation of the cilia. Otoliths are particles inside the ampulla involved in the whole process. Considering an analogy in control signal theory and robotics, the internal ear represents a sensor to be used in feedback.

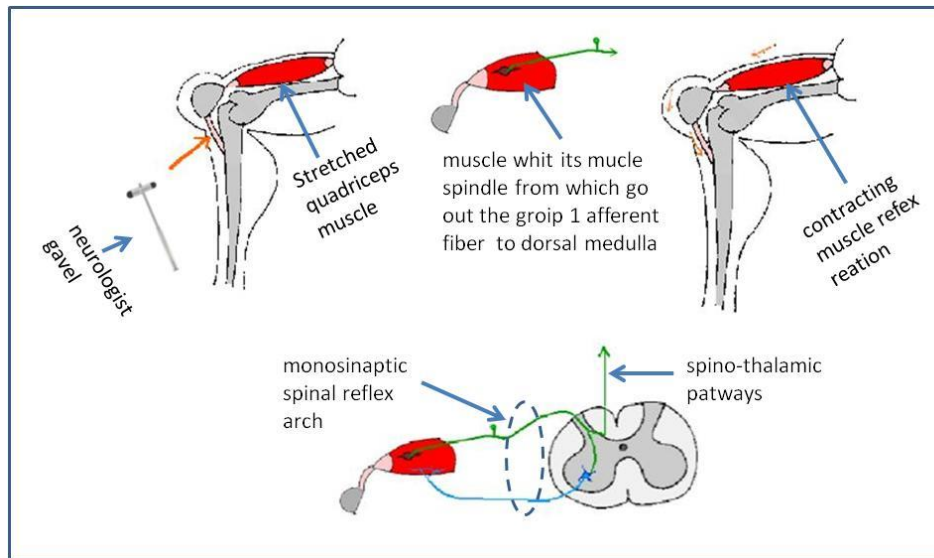


Figure 38- The central nervous system sends the motor impulses to the musculoskeletal apparatus and received muscle status information by spino-thalamic pathways. In figure is represented a monosynaptic spinal reflex acting in the legs quadriceps muscle. When the distal tendon is washy by an involuntary knee flexion (as for instance was what happens when the neurologist strikes it with his gavel) then the quadriceps was stretched as well as its muscle spindre proprioceptor which send this information, towards dorsal horn of the spinal cord, to the homologue muscle motoneurons in the ventral horn from which goes out nervous signals towards the same muscle which in turn contracts up to recover primary knee position. However the same information, coming from the muscle spindles, also travels through the nerve fibers of the spino-thalamic tract and from here it radiates the information of muscle contraction to various body structures including the cardiovascular system. The latter is then informed of the need to supply more blood to the contracting muscles and responds with an increase in its activity. Thanks to this anatomic-physiology basis the leg muscle contractions as a postural reaction to body displacements due to sea wavy way could also induce changes in cardiac output.

e.

Locomotion is performed by muscles, controlled by the central nervous system via the spinal cord. The impulses are sent to the muscles motor end plates from the activated muscle fibers during contraction. On the other hand, another “feedback” mechanism is provided by receptors in the muscle, that, using the analogy to robotics, can be seen as extensimeters, aimed to avoid excessive stretch of the muscles. One of the aim of the present work is to investigate the connection between the cardiac activity and the nervous system, due to inertial accelerations.

Energetic consideration. Metabolism.

Metabolism is of great interest for scientists and physicians. Metabolic activity is related to health state of the subject and a great effort was done in last decades for the comprehension

of the mechanisms aimed to improve performances of athletes in sport medicine, or for the detection of pathological conditions. The human body is an amazing machine, a bioreactor, able to convert chemical energy stored in food into mechanical energy. As much as the organic life is surprising, it is also incredibly fragile, and it must always strive with a complex balance of biochemical processes. It is of uttermost interest for physicians to develop a sufficient comprehension of complex phenomena related to the matter, so to treat disorders and pathologic conditions, such as hypertension. On the other hand, experts in sport medicine, aiming to increase the output of the athletes, decrease the occurrence of injuries or decrease fatigue and recovery time after severe performance, greatly benefit from the discoveries in the field.

Main sources of energy can be divided into:

- aerobic process, connected to the expenditure of oxygen.

- anaerobic process, related to fat and lipids consumption.

Biomechanical mechanisms such as homeostasis of Hydrogen ions and muscle oxygenation are of plain interest. But also, aerobic condition represents an important field of study. Experimental techniques were developed to monitor the oxygen level in respiration, in order to understand the influence of aerobic and anaerobic phase. For this reason, carbohydrate oxidation(glycogenolysis) is also of great interest, and it is in fact related to the fatigue threshold of the athlete. During sport activity, carbohydrates are depleted and muscles exploit the fat oxidation process. Such process is widely controlled by hormones. Theoretically, the energy expenditure can be derived from the detection of oxygen intake (VO_2) and the correspondent CO_2 values. This requires spirometry techniques. Many procedures were developed for the measurement of energy expenditure, on different activity conditions [70,73,82,92]. The relation with energy expenditure and acceleration greatly depends on the kind of activity performed. Triatic accelerometers are widely used in energy expenditure estimation.

Mechanical energy.

Mechanical energy is the output of the human being considered as a system. Mechanical considerations provide an important tool that can be exploited to increase the comprehension of the physiological and metabolic process both in healthy and pathological conditions[55,56,84,87]. Simple concepts such as Newton's laws, conservation of energy and momentum end so on, allow to study a wide range of locomotion and give some insights on metabolism as well. The human body can either be seen as a whole rigid body or as a multibody systems, where each part(arms, legs, chest, head) has an inertia and a mass and it is connected by pair joints (elbows, shoulders, knees, pelvic junctions etc.). The kinematic relations between the body parts are determined by the shape of the bones, straight muscle and tendons[50,52,85]. As well know from dynamics of rigid body, the mechanical work produce by a force is equal to the parallel component of the force multiplied by the displacement on the same direction, whereas the variation of the gravitational potential energy, that is, the variation of the position of the body regarding the gravitational field, is the work associated to the gravitational energy.

In some special cases, also elastic energy is involved in the computation of the total mechanical energy consumed by athletes.

One of the most important equation is the work due to gravitational potential energy:

$$\Delta E = W = mg(z_f - z_i)$$

Where z is the variation of the position according the isopotential gravitational surfaces.

Chemical energy and metabolism.

Energy during biological activity depends on biochemical conversion of nutrient from food into energy delivered to tissues and organs. Oxidation of nutrient is performed from the cells of the tissues, this is why oxygen is carried to the tissues[48,52,100].

Efficiency of locomotion.

The efficiency of the human body during activity [76,82,86,87] can be measured by the ratio of mechanical energy with respect to the metabolic energy.

$$\eta = \frac{E_m}{E_m}$$

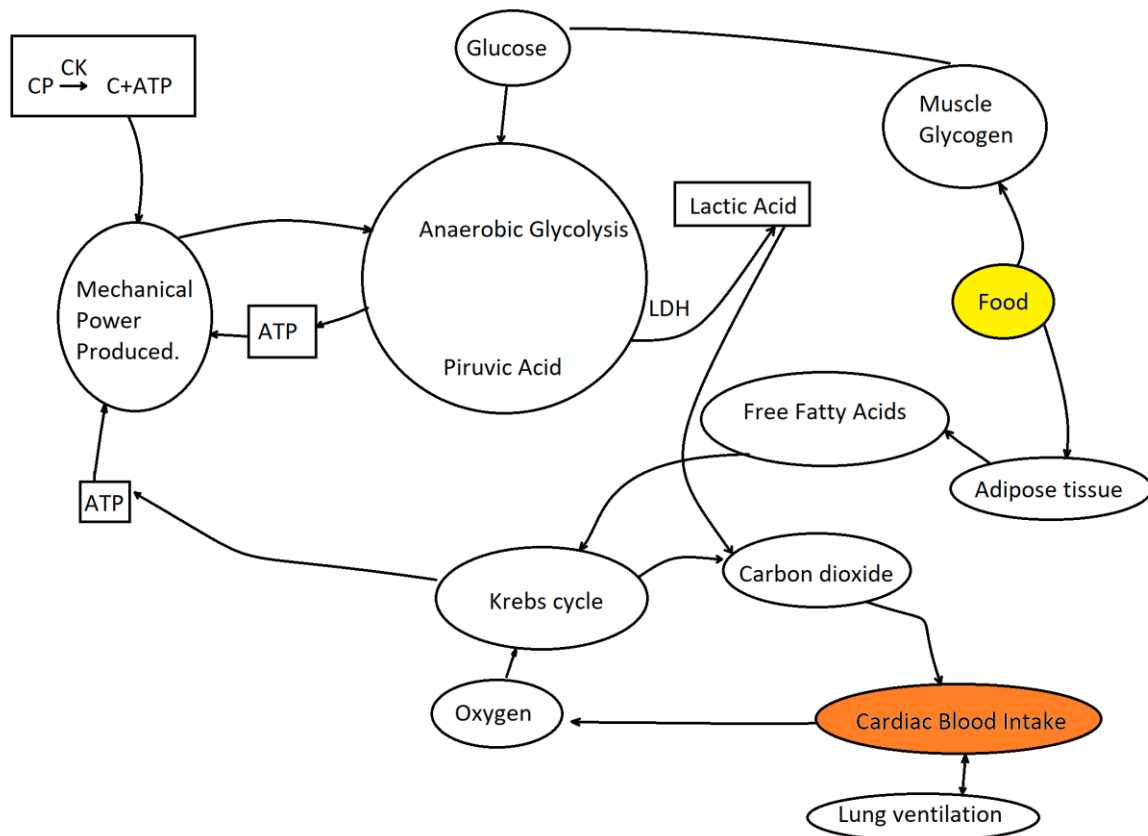


Figure 39-Main processes in metabolism[48,50],.

Many studies suggested a linear relation between the signal of the accelerometer and caloric consumption. Caloric consumption is also regulated by hormones.

Correlation between mechanical energy and metabolic energy.

From the previous discussion, it can be easily understood the relation between mechanical energy and oxygen consumption. Many researchers investigated methods and developed models for the comprehension of the relation of the two phenomena [70,86]. The mechanical work in human activity is generally related to the position of the centre of mass of the whole body, or, if no other work is involved, in the displacement of the centre of mass of moving parts of the body, usually arms and legs, for example, considering gait on a single plan.

This is true in locomotion or other physical activities, but it is worth notice that mechanical energy is also involved in basal metabolism(that is, at rest), considering cardiac circulation and endocrine system, or, generally speaking, in all those processes that requires the displacement of body fluids, especially against gravity. In general, however, mechanical energy is related to the muscle-tendon systems of the locomotion apparatus.

Indirect calorimetry.

Indirect calorimetry is aimed to detect the caloric consumption in human activity. Caloric consumption is related to basal metabolism and locomotion or physical work[90].

As already seen in the previous sections, the determination of mechanical energy and work can be determined using proper test set up, or can be easily computed considering masses and displacement that can be accurate measured.

For chemical energy an exact computation of expenditure is not possible. The determination of chemical energy spent during the activity cannot be obtained directly with the measuring of the data. Of course, there are parameters, as such as temperature, and skin galvanic conductivity, that can be measured, too many variables, however, influence the process.

At any rate, many researchers suggested models and estimation techniques for this purpose. Accordingly to Fick., the Oxygen concentration can be computed from the stroke volume using the relationship[83]:

$$VO_2 = SV \times HR \times \Delta O_{2a-v}$$

So, it is relevant to study the relationship between heart rate and respiratory cycle.

The human gait.

A simple phenomenon to study is the human gait. This is advised for the simplicity of the test definition and for the important results that can be derived. If, in fact, it is possible to derive the mechanical energy developed in locomotion thanks to the motion of the centre of mass of members of the body and the centre of mass of the whole body[54,60,94].

Researchers developed techniques for the measurement of the energy consumption in human gait also using auxiliary devices as such as elastic stilts[85,95].

Transthoracic electrical bioimpedance cardiography.

The first attempts to measure the impedance of biological tissues were performed, among the others, by Geddes[65,73,96], who injected a saline solutions in dogs and detected the current injected was performed with electrodes positioned on the limits of the thorax. The detection of the impedance and its variation was amplified using saline injection directly into the ventricle of the animals.

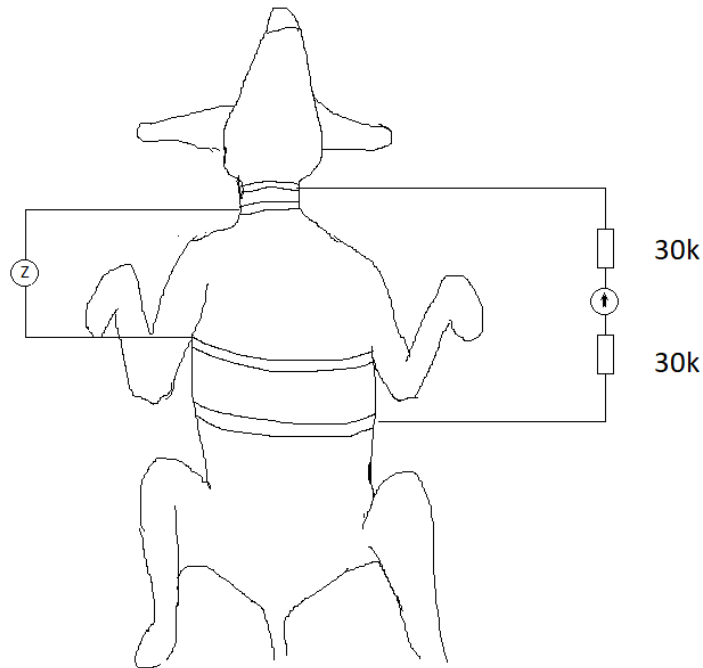


Figure 40- ICG experiments on dogs.

The variation of the impedance is detected by the electrodes, and it is assumed to be dependant from value of cardiac flow.

The goal is to derive a computed value called stroke volume, that is a measure of the equivalent blood pumped by heart on a specific period. It is usually given in milliliters. The cardiac flow is assumed to depend on the impedance measured at the terminals of the electrodes, placed on the thorax of the subject. The measurement is possible since blood is an acid fluid with conductivity properties. The variation of blood quantity in tissues varies according to systolic and diastolic phases. A low voltage AC current is generated and let flow in the tested person. The value of the voltage is detected and recorded during a test of at least three minutes. The test must be performed at rest since motion can influence the outcomes of the recording session. Respiration process can also influence the data collecting and must in fact removed filtering the recorded signal. A typical value of the stroke volume varies around 40mL/s for slightly overweighted person, to 95mL/s for male athletes.

ICG.

Cardiac impedance variation is plotted on time and the result is called Impedance CardioGram(ICG)[67,74]. This technique is especially appreciated since the information is

obtained via a non-invasive method. In ICG, an alternating currents is used to measure the impedance of a portion of the human body delimited by the position of the electrodes. Researchers developed different techniques to predict the stroke volume.

Kubicek's method.

The computational method developed by Kubicek[75] consists in the determination of a cylinder with a base equal to the thorax circumference. The cylinder has a Height L in cm, where the electrodes are connected at the hypoid process and the base of the neck. The thoracic variation in pulse of the aortic blood flow caused the variation of the measured impedance at the terminals of the electrodes. The maximum value of the first derivative of the variation of the impedance is proportional to peak ascending aortic blood flow. A value of fundamental impedance, computed as the average of the impedance on the total period, is exploited in the final formula. According to Kubicek, it is possible to compute the aortic blood flow as:

$$PF = \rho_b \frac{L^2}{Z_0^2} \left(\frac{dZ}{dt} \right)_{max}.$$

Where ρ_b is a specific resistance of the portion of the human body considered. Multiplying for the ventricular ejection time, the suggested stroke volume equation is:

$$SV = T_{lve} \rho_b \frac{L^2}{Z_0^2} \left(\frac{dZ}{dt} \right)_{max}.$$

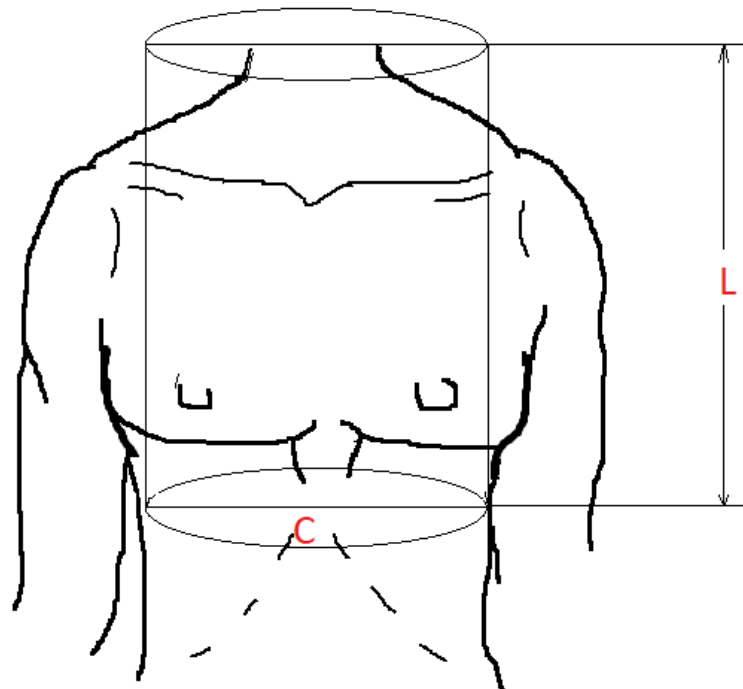


Figure 41- Relevant anthropometric dimensions for the computation of the electrically involved volume in ICG technique according to Kubicek.

As it is obvious, the first objection to the validity of this approach is that the resistivity value ρ_a is unknown and the Stroke Volume would be undetermined.

Quail approach.

Quail et al. developed the previous relations, deriving the value of the impedance considering

$$Z = \rho \frac{L}{A}$$

The equation, expressed in terms of average impedance is, is useful to derive the value of the resistivity:

$$\rho_0 = \frac{Z_0 A}{L}.$$

The thoracic cylinder hypothesis allows to carry out the following relations:

$$\rho_0 = \frac{Z_0 A(circle)}{L}$$

$$\rho_0 = \frac{Z_0 \pi r^2}{L}$$

Substituting in the Kubicek's equation, the final result is:

$$SV = \frac{(Z_0 \pi r^2)}{L} T_{lvi} \frac{L^2}{Z_0^2} \left(\frac{dZ}{dt} \right)_{max}$$

$$SV = volume(cylinder) \frac{T_{vli}}{Z_0} \left(\frac{dZ}{dt} \right)_{max}$$

Šramek et al. demonstrated that the magnitude of arterial resistivity is constant.

Stroke volume equation.

Different methods for measuring the stroke volume equations were proposed by researchers. One of them is the Šramek equation. The impedance can be related to the stroke volume using the equation of the volume.

Relevant parameters are:

The derivative of the detected impedance at its peak.

The time of ejection.

A nomogram, that is related to the body of the patient.

Most of the mentioned values are detected by experimental data. The last is derived from a parametrization suggested by Šramek and his equip. The parameter is fixed and can be considered as a coefficient dependent on the height of the person under observation, her or

his weight, accordingly to a corrective coefficient that takes into account the difference from the ideal weight.

Šramek equation.

Another more sophisticated techniques were conceived by Šramek[64,65,66] and developed by Bernstein. The Sramek equation, suggested by Bernstein in the paper Continuous Bioimpedance, consists of a multiplication of 4 terms that provides an estimation of the stroke volume.

The stroke volume is the volumetric hearth intake. The Sramek equation is obtained as:

$$SV = VEPT * VET * TFI * EVI$$

The four terms having the meaning:

- VET :Ventricular Ejection Time.
- TFI: Theoretical Fluid Index
- EVI: Ejection velocity index
- VEPT: Volume of Electrically Participating Tissues.

In this case, the new equation is obtained with the assumption that the thorax cylinder can be represented by a truncated cone, whose larger base has a circumference equal to:

$$C = 3L$$

Where L is the height of the truncated cone. This leads to the definition of the radius:

$$r = \frac{C}{2\pi}$$

$$r = \frac{3L}{2\pi}$$

The volume of the cylinder is expressed by:

$$\pi r^2 L = \pi \left(\frac{3L}{2\pi} \right)^2 L$$

And substituting, the new stroke volume equation is equal to:

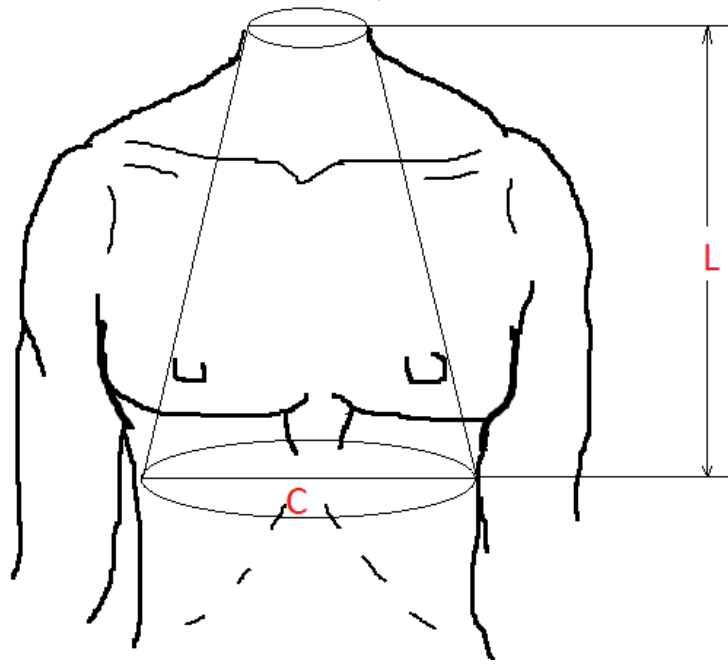


Figure 42- Anthropometric dimensions in the Šramek-Bernstein model.

$$V = \frac{L^3}{1.4Z_0} T_{lve} \left(\frac{dZ}{dt} \right)_{max}$$

According to the author, it is possible to derive the VEPT from anthropometric considerations, since it is related to the height of the patient. Considering evidences collected by researchers, the height of this truncated cone is equal to 0.17 the height of the subject and the smallest base square has a radius equal to 1/3 of its height.

The whole equation becomes:

$$SV = \left[\frac{(0.17H)^3}{4.2} \right] T_{lve} \left(\frac{dZ_0}{dt} \right)_{max} \frac{1}{Z_0}$$

This theoretical approach was corrected by other researchers (Feldshuh and Enson), who suggested a correlation with the blood volume Q of the patient and its weight. A new coefficient was developed, in order to correct the initial data:

$$\delta = \beta \left(\frac{W_{observed}}{W_{ideal}} \right)$$

Where W is a weight in kg. The new corrected equation that takes into account this correction factor is:

$$SV = \delta \left[\frac{(0.17H)^3}{4.2} \right] \frac{T_{lve}}{Z_0} \left(\frac{dZ}{dt} \right)_{max}$$

As previously stated, the first member of the equation is equal to:

$$TFI = \delta \left[\frac{(0.17H)^3}{4.2} \right]$$

For a man of 175cm height, a little overweight, the VEPT is equal to 6270. According to the previous equations, it is necessary to derive the value of the derivative of the impedance.

Typical shape wave of Impedance.

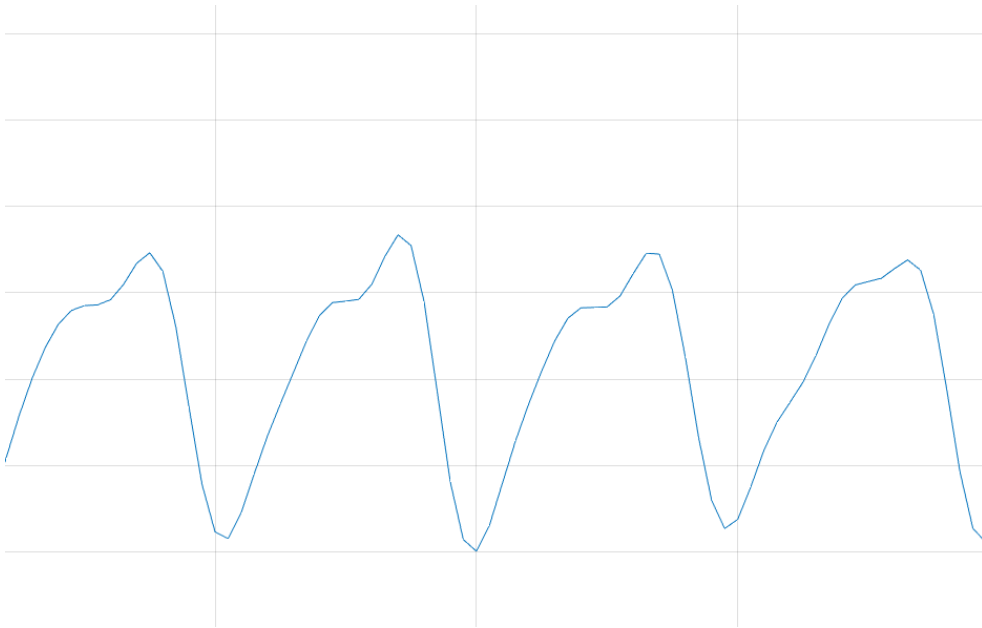


Figure 43- The impedance cardiogram characteristic shape.

The impedance has a typical wave shape resembling a triangular or saw tooth wave. In the present work, the measured impedance ranged between 27 and 35 Ohm. Only resistive behavior was taken into account, whereas capacitive and inductive behaviour were ignored. In the equation, the value of the impedance to be used in the computation is the average value of the impedance on the period under consideration.

The shape wave of the derivative of the impedance

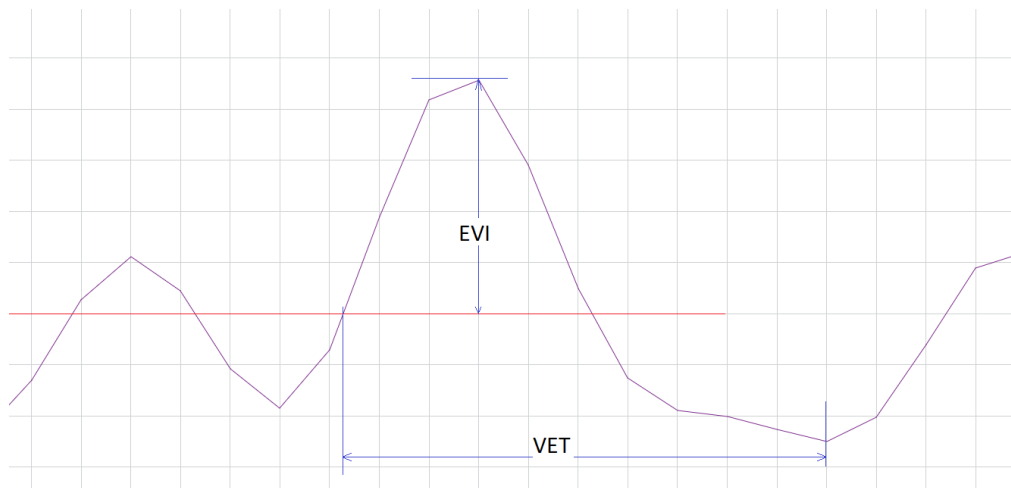


Figure 44- Typical shape of the derivative of the impedance and values necessary for the stroke volume computation according to Šramek's method.

Usually, the maximal value of the derivative of the impedance has a variation of 0.2 Ohm/s, and a mean value of 0.8 Ohm/s. The mean value of the impedance is computed in the same data set, delimited by the previous automatic procedure. According to Šramek, the value of the impedance and its derivative can be used for the computation of the stroke volume.

Feature extraction.

Once the data is filtered, it is necessary to implement an automatic routine for the determination of specific features and trends of the data series. In this case, the main goal is to derive the impedance characteristics.

A classical problem in feature extraction is related to recording of brain activity, since electroencephalogram(EEG), consisting in the reading of magnetic signals from the brain, is usually a mixture of quite different signals, as such as sensorial impulses, biorhythm signals, locomotion and muscular activity. The receiver can only observe the process as a whole, and the main goal is to isolate specific signals representing a certain brain activity.

Feature extraction is possible taking into account a probability distribution function that minimizes the error of the model in respect to the original data. The main goal can be performed using neural network properly arranged to derive the data obtained from filtering.

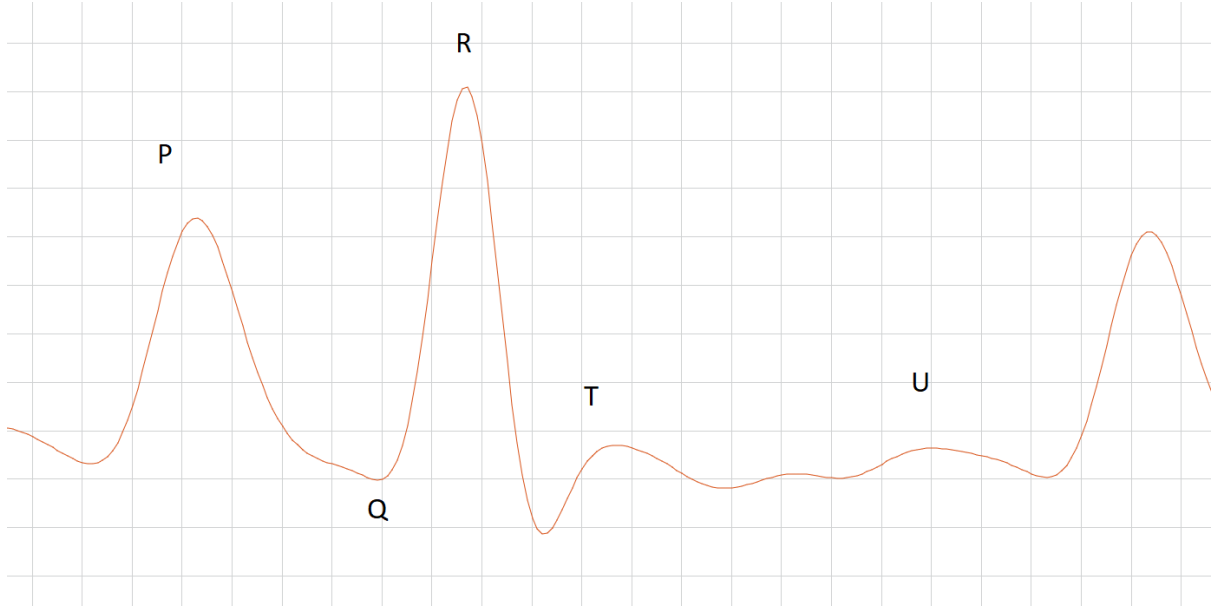


Figure 45- Main features of an ECG signal, with P,Q,R,S,T,U waves.

A wide literature was produced on Electrocardiographic techniques. In this case, a modelling of a signal can be performed using

ECG model suggested by McSharry.

McSharry[1,3,5] introduced the reconstruction of the ECG signal considering the equation of a Dynamic system and using the technique of the Independent Components Analysis(ICA). The system can be represented by a 3 dimension differential equation.

$$\dot{x} = \alpha x - \omega y$$

$$\dot{y} = \alpha y + \omega x$$

$$\dot{z} = - \sum_{i \in P, Q, R, S, T} a_i \Delta \theta_i \exp\left(-\frac{\Delta \theta_i^2}{2b_i^2}\right) - (z - z_0)$$

Where:

$$\alpha = 1 - \sqrt{x^2 + y^2}$$

And θ angles are obtained for every single portion of the ECG according to P,Q,R,S,T waves.

The estimation of the parameters must be undertaken using the equation:

$$S(f) = \frac{1}{\sqrt{2\pi c_1^2}} \exp\left(\frac{f - f_1}{2c_1^2}\right) + \frac{1}{\sqrt{2\pi c_2^2}} \exp\left(\frac{f - f_2}{2c_2^2}\right)$$

That are two Gaussian with average value and impedance.

The solution of these problem can be found using a Runge-Kutta numerical integration method of the 4th order. The result is an “artifact” ECG, that is, the best estimation of the original signal. The estimation of the parameters of the system can be obtained thorough deep learning techniques, that is, by averaging the input data on a certain span of time and deriving the model for statistical systems.

Peak detection.

In peak detection it is important to obtain the equation of the problem using the new equation. In order to detect a peak, it is possible to use the maximum routine, that returns the maximal value of a vector. However, considering a set of data, it is necessary to have a “window” of a single heart beat. To do that, it is necessary to consider only a limited amount of cells of the memorized vector(in this case, a single hearth beat). To do that, it is possible to write a “flip flop” method, where a memory logic element is used to set an initial time and a second element that set the final element. The “flags” are reset when the peak is detected and another cycle is analysed, until the end of the vector. The peak detection allows to create a map of the collected data at the points of interest, that can be used in a routine that finds the maximal amount of the derivative of the impedance. Fortunately, Matlab provide the findpeaks routine, that saves the local maxima of a vector, including the number of the cell where they are detected on a different array. The output can be re-sized using a for cycle and the result can be plotted according to the original time flow.

Adaptation of human body during navigation.

Human body is an excellent machine that is capable of adaptation according to the environmental conditions and their variations, when these do not occur too sharply or abruptly. During a prolonged period of navigation, metabolic and physiologic parameters are influenced and modified. The main goal of the present model is to underline any correlation in the variation of these parameters. Energy in metabolic power and energy costs can usually be related to the adaptation, during navigation, of cardio-respiratory and metabolic activity variation.

Among the others, the main interest is to detect the variation of the homeostasis of the subject, especially in relation to the average temperature, pH, glycaemic levels, osmolarity. Changes in aerobic efficiency were observed. Sailors also experimented changes in sleep rhythm. A typical activity that provides an example of variations of environmental activity are sailing, space navigation, aeronautical travelling. In a previous attempt from Concu et al., the data was observed on a transoceanic sail, when the variation of many physiological values was observed, as such as blood saline concentration, and chemical element concentration as such as Calcium, Phosphorus, Potassium and Sodium. An increase of glycemic level was also observed, coherently with the fructosamine protein concentration. Moreover, It was observed that after 3 months of oceanic navigation MAO enzymes decrease, a substance related to the cerebral transmission in synapsis. In these conditions, the production and level of Creatin Kinase enzymes, as well as LDH enzymes (related to explosive force) suffer an appreciable decrease. The variation of these parameters influences physiological processes, that was, in fact, observed.

Role played by random acceleration on stroke volume and cardiac activity.

Random accelerations on human body generate inertial forces and influence cardiac activity, since they trigger the equilibrium mechanism starting from the inner ear organs. The reactions to equilibrium are transmitted to muscles and consequently, an increase of cardiac output is measured.

Sperimental data.

METHODS

1. SUBJECTS

To carry out this experimental study it has been engaged (see figure 46) a crew of three very skilled senior sailors (75 ± 5 years, 73 ± 11 kg, 169 ± 4). The crew captain was also owner of the boatt with many years of navigation and command experience on ships (subject A), one the other two crew members was an expert marine meteorologist (subject B) and the other had experience in sailing maneuvers (subject C).



Figure 46– the photo shows the three sailing crew members while they were posing in the stern of the boat before leaving for the cruise.

Before starting the sailing cruise the crew members underwent to check by a sports medicine medical team to aim at ascertaining the absence of psycho-physical conditions such as not to make the subject suitable with the planned experimentation.



Figure 47 – The photo shows the sports medicine physician engaged in the medical examination of the sailors, inside the living room of the boat, before their departure for the cruise.

The study was conformed to the standard set by the latest revision of the Declaration of Helsinki. Prior to testing, experimental procedures were explained to participants and subjects provided written informed consent.

2. EXPERIMENTAL PROTOCOL

The data used in the present work are related to the travel of the engaged 3 sailors around south Sardinia during June 26th and July 16th 2021. Data collection was performed on the crew of the cruise boat, a Bavaria yacht 41. The members of the crew repeated the sampling process every day, at 10:00 am and at 18:00 pm



Figure 48– Course of navigation related to the collected data. Cruise route is subdivided in two phases: A and B, around the coast of south Sardinia. The numbered starts indicate the places in which the boat was moored.

Day	Log events
June 26th	Leaving from Cagliari
June 27th	Landing at Sant'Antioco Island
June 30th	Arriving at Carloforte dock
July 3rd	Course to Cagliari, night stop at Teulada Cape
July 4th	Landing in Cagliari
July 12th	Landing at Porto Corallo, Villasimius, from Cagliari
July 13th	Course from Porto Corallo to Arbatax dock
July 14th	Course from Arbatax to Santa Maria Naverrese
July 15th	Return to Cagliari with a stop at Porto Corallo

Table 3-The chronological order of the navigation.

The sailors were equipped with the armband Pro3, in order to track the already mentioned physical parameters. Since Cardiac impedance can also be influenced by the position of the electrodes, but also by the state of the subject and motion of the subject, for the test procedure requested to subjects to perform the measurements after at least 10 minutes of total rest and without moving, since every movement causes the variation of the blood density in the tissues and the variation of the current lines.



Figure 49-The members of the crew during a coastal cruise phase.

Moreover, the boat was equipped with a multi-sensor datalogger, WT901SDCL.

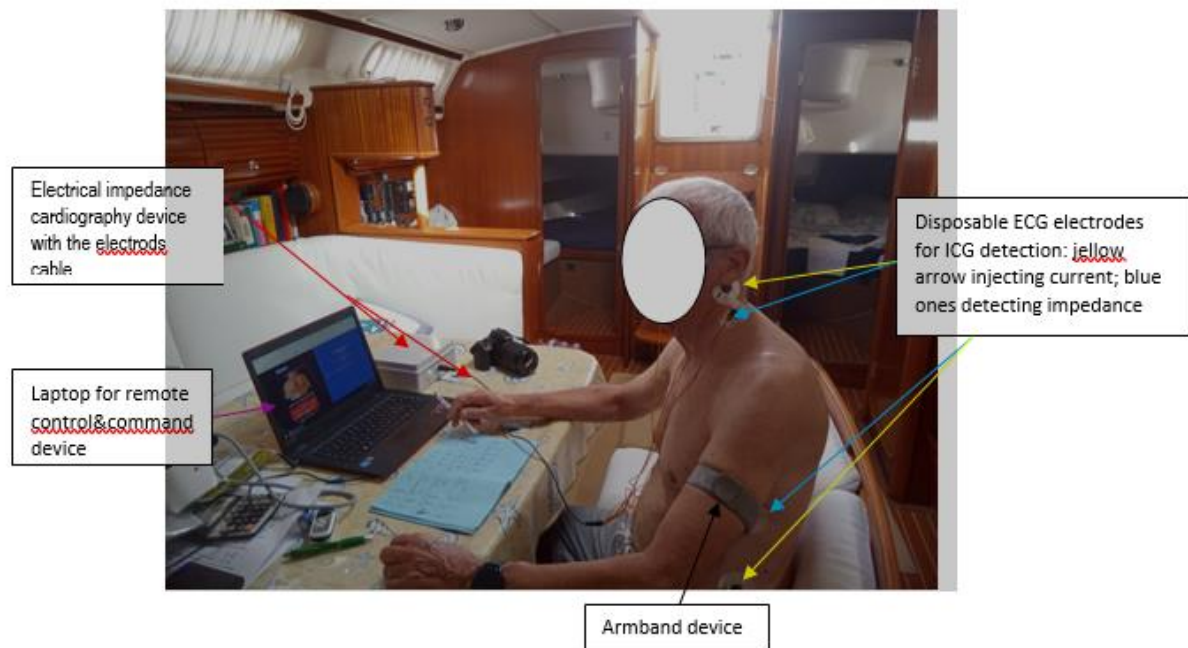


Figure 50- The captain during ICG data collecting.

With the ICG, an ECG of the subject was recorded.

Armband Pro3 results.

The results of the captain armband show an adaptation of human body to navigation

Day	km	kCal	efficiency	%	Day	km	kCal	efficiency	%
Jun-28	4.40	260.00	0.02	1.69	Jul-07	5.50	129.00	0.04	4.26
Jun-29	-	-	-	-	Jul-08	2.10	97.00	0.02	2.16
Jun-30	7.20	845.00	0.01	0.85	Jul-09	5.30	174.00	0.03	3.05
Jul-01	6.80	1,060.00	0.01	0.64	Jul-10	8.10	239.00	0.03	3.39
Jul-02	11.60	557.00	0.02	2.08	Jul-11	6.30	164.00	0.04	3.84
Jul-03	8.10	508.00	0.02	1.59	Jul-12	5.10	202.00	0.03	2.52
Jul-04	2.00	126.00	0.02	1.59	Jul-13	4.50	373.00	0.01	1.21
Jul-05	4.70	248.00	0.02	1.90	Jul-14	9.50	452.00	0.02	2.10
Jul-06	2.80	195.00	0.01	1.44	Jul-15	8.10	338.00	0.02	2.40

Table 4-Comparison among bioenergetic parameters assessed from the Armband device, dressed from the boat captain at the beginning and at the end of the cruise.

Table 4 shows the variation of the ratio between the path followed by the subject in km and the estimated metabolic energy spent. It is possible to observe the decrease of this ratio and it can be assumed that the overall efficiency increased during time. And this can be explained considering that prolonged physical activity in sailing caused the optimization of metabolic processes of energy conversion.

PARAMETR	2021/06/26	2021/07/16
Kcal (total/h(<u>be address</u>))	101,3	113,5 (+12%)
Kcal (<u>activity</u>)/min	4,48	4,8 (+7%)
<u>Space travelled</u> (Km)	2,7	4,4 (+63%)
Kcal <u>activity</u> /km	97	84,5 (-13%)

Table 4.1.

Table 5 shows that at the end of the cruise, in the boat captain both the overall energy cost per hour and that relating only to motor activities per min, performed on the boat, were higher than the corresponding values recorded at the beginning: +12% and +7% respectively. Furthermore, the energy cost of motor activities on the boat (Kcal activity/km) at the end of

the regatta was 13% lower than at the beginning of the sailing test. This last data clearly shows that in our sailor the 20 days spent in pleasure sailing activities have considerably improved his bioenergetic/metabolic efficiency.

Data collected by the ICG device.

Sample	Time	Subject			
	June 26 th Morning			July 8 th Morning	
			62 06:48:08		C
1	06:15:37	C	63 08:20:53		B
2	06:30:15	A	64 09:00:13		A
	Evening			Evening	
3	18:23:35	B	65 11:48:40		A
4	18:45:31	C		July 9 th Morning	
5	18:57:06	A	66 06:46:34		C
	June 27 th Evening		67 08:26:16		A
6	15:18:16	C	68 08:40:58		B
7	15:32:36	B		Evening	
8	15:43:08	A	69 15:16:47		A
	June 26 th Morning		70 15:30:24		B
9	06:06:10	C		July 10 th Morning	
10	06:30:15	B	71 08:00:51		C
11	06:41:18	A		July 12 th Morning	
	Evening				
12	18:56:56	C	72 04:40:55		B
13	19:08:24	B	73 05:26:37		A
14	19:33:36	A	74 05:43:53		C
	June 29 th Morning			Evening	
15	06:11:57	B	75 18:06:24		A
16	06:29:44	C	76 18:18:40		B
17	06:33:42	C	77 18:36:17		C
18	06:56:50	A		July 13 th Morning	
	June 30 th Morning		78 04:55:21		C
19	04:05:50	C	79 05:46:53		A
20	05:05:58	B	80 06:10:50		B
21	05:46:55	A		Evening	
	Evening		81 16:38:41		C
22	18:09:25	C	82 16:48:53		A
23	18:20:15	B	83 17:08:25		B
24	18:41:43	A		July 14 th Morning	
	July 7 th Morning		84 04:58:40		C
25	05:32:29	C	85 05:26:29		A
26	05:49:53	A	86 05:39:53		B
27	06:12:56	B		Evening	
28	07:35:57	C	87 17:50:00		C
29	07:45:17	B	88 19:07:47		A
	Evening		89 19:21:27		B
30	17:17:33	B		July 15 th Morning	
31	17:29:13	C	90 05:33:15		A

91	05:59:2	C
92	06:16:38	B
		Evening
93	17:42:09	C
94	17:54:25	A
95	18:06:28	B
		July 16 th
		Morning
96	04:32:19	C
97	05:19:20	A
98	05:28:43	B
		Evening
99	15:50:42	A
100	17:39:05	C
101	18:03:49	B

Table 5-Chronological order of the files.

Data treatment.

The main goal of the data analysis was to detect the computation of the Stroke Volume among the period of the survey. From the previous discussion, we can identify two main problems in the analysis of impedance data to be processed. First of all, the original signal is affected by random noise, due to environmental conditions. It was necessary to filter the noise. On the other hand, it was desired to study the influence of inertial accelerations on human body. For these reasons, filtering procedure had to be performed paying attention not to cancel frequencies associated to boat displacement and motion.

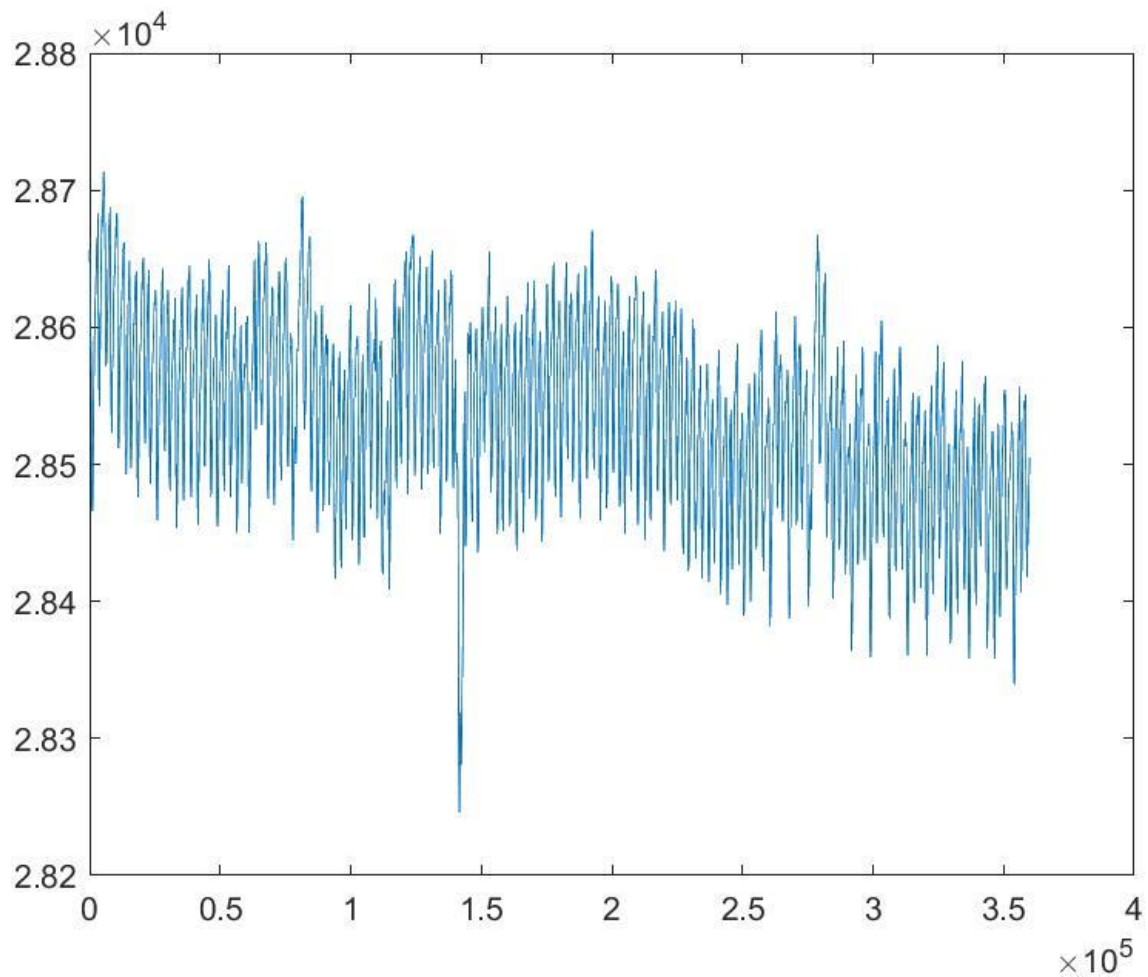


Figure 51- A typical graph of the Impedance detected in the test.

Original names of the data.

In order to treat the data on Matlab, the name of the original files had to be changed, since matlab must work with .TXT file as input.





 dati_00099-2021-07-16_052843	05/10/2021 15:19	Text Document	5,274 KB
 dati_00100-2021-07-16_155042	05/10/2021 15:19	Text Document	5,274 KB
 dati_00101-2021-07-16_173905	05/10/2021 15:19	Text Document	5,274 KB
 dati_00102-2021-07-16_180349	05/10/2021 15:19	Text Document	5,274 KB

Figure 52-Original file names in the folder.

It would have been necessary to open every single file one by one. Instead, the names of original files were changed using a python code that read the file name, copy the data and rename the file with a cardinal order, so that the chronological sequence is preserved.

```

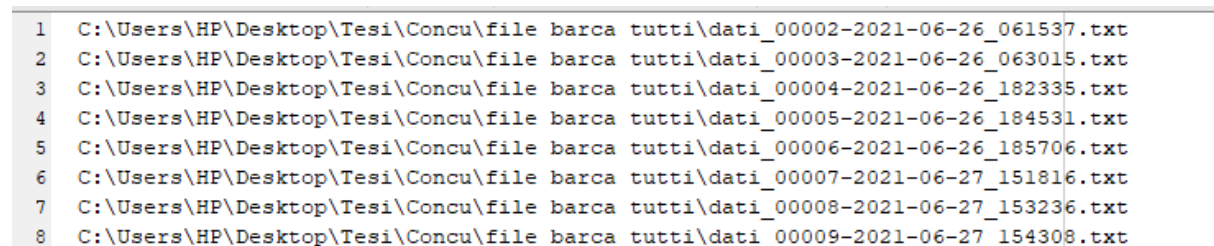
f=open('FileNames.txt')
f1=open('FileNames2.txt','a')
for x in f.readlines():
    p = len(x)
    p = p-2

    x = x[1:p]
    # x = ""+x +""
    f1.write(x)
    q = '\n'
    f1.write(q)
f.close()
f1.close()

```

Code used to change the names of the file.

The python code allowed to write the name of the files plus the address, so that the files could be opened by the load() MATLAB function. The list of the file names was saved in “FileNames2.txt” file.



```

1 C:\Users\HP\Desktop\Tesi\Concu\file barca tutti\dati_00002-2021-06-26_061537.txt
2 C:\Users\HP\Desktop\Tesi\Concu\file barca tutti\dati_00003-2021-06-26_063015.txt
3 C:\Users\HP\Desktop\Tesi\Concu\file barca tutti\dati_00004-2021-06-26_182335.txt
4 C:\Users\HP\Desktop\Tesi\Concu\file barca tutti\dati_00005-2021-06-26_184531.txt
5 C:\Users\HP\Desktop\Tesi\Concu\file barca tutti\dati_00006-2021-06-26_185706.txt
6 C:\Users\HP\Desktop\Tesi\Concu\file barca tutti\dati_00007-2021-06-27_151816.txt
7 C:\Users\HP\Desktop\Tesi\Concu\file barca tutti\dati_00008-2021-06-27_153236.txt
8 C:\Users\HP\Desktop\Tesi\Concu\file barca tutti\dati_00009-2021-06-27_154308.txt

```

Figure 53-Address of the names used to load the data in matlab.

In this way, MATLAB can open the files starting from the file names and using importdata() command.

```

data = importdata('FileNames2.txt')
fileNamesNum = []
[p q] = size(data);

```

In order to save the output, a MATLAB code with a new set of file names developed, with a for cycle:

```
f = ".mat";
```

```
w = "DImpThree.mat"
```

```
w1 = "Max.mat"
```

```
w2 = "Max.jpg"
```

```
for i=1:p
```

```
    fileNamesNum(i,1)= i;
```

```
    S = string(fileNamesNum(i,1));
```

```
    fileNamesStr(i,1)= strcat(S,w);
```

```
    Q = strcat(S,w)
```

```
    fileNamesOut(i,1)=Q
```

```
    fileNameMax(i,1) = strcat(S,w1);
```

```
    fileNameMaxP(i,1) = strcat(S,w2);
```

```
end
```

The output of this code is of the kind: cardinal number of the file+type of the file + either .mat extension or .jpg extension.

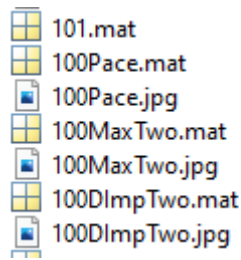


Figure 54-The file output obtained by matlab.

Identification of main frequencies of the spectrum in ICG.

The output data refers to the Bode diagram of the amplitude of the signal allows to identify the main frequencies of the ICG signal.

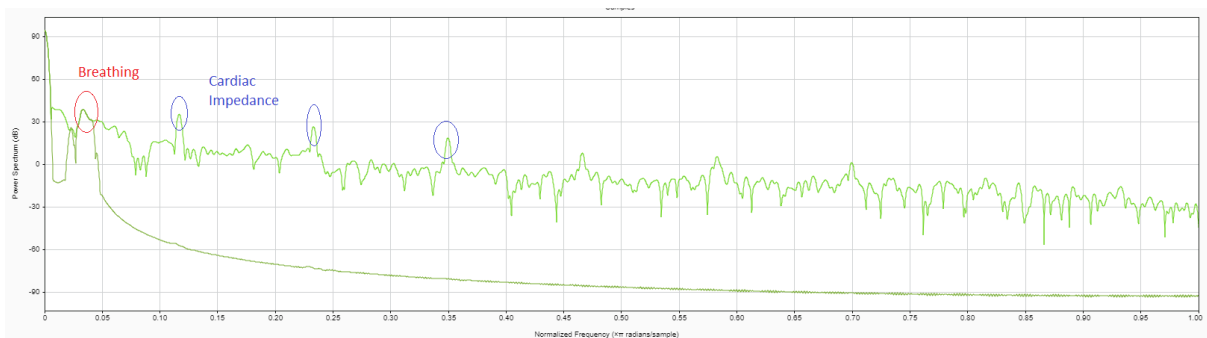


Figure 55-The detection of the main peaks in the spectrum of the impedance.

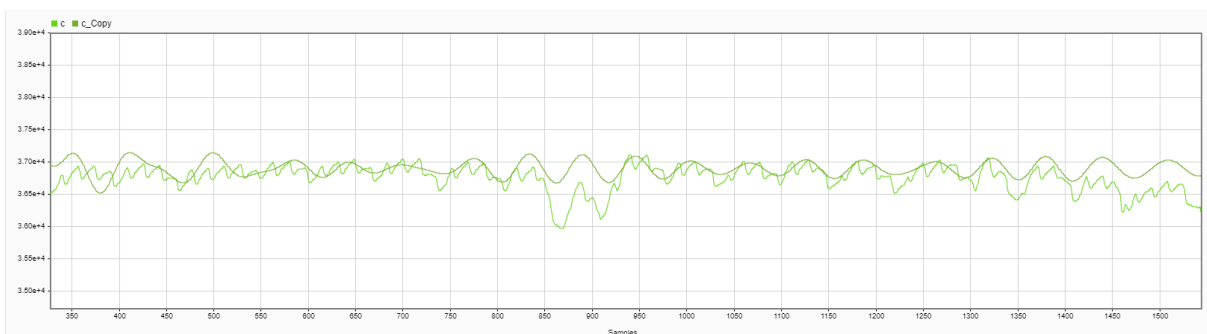


Figure 56-The original time series and the breathing reconstruction time series.

Frequency analysis allowed to identify the breathing frequency on around 0.8-1Hz, whereas the cardiac impedance was found as a composition of three fundamental waves, with oscillation frequency of around 2Hz, 4-5Hz and 6-7Hz.

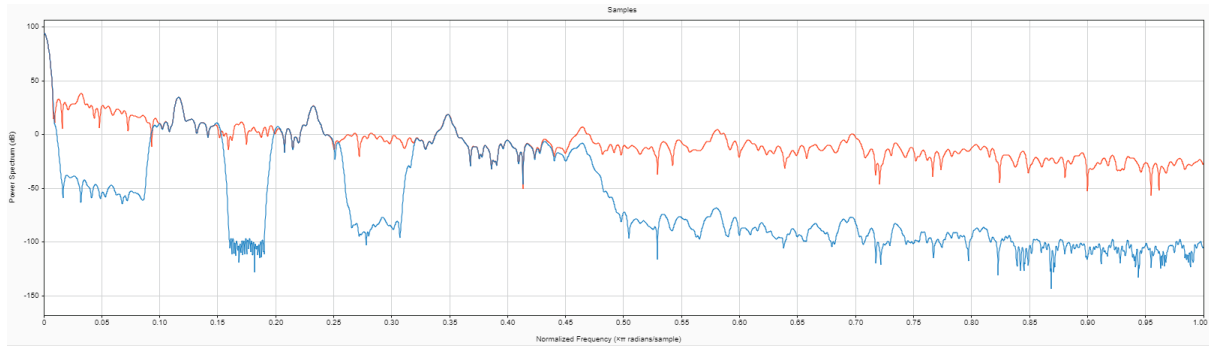


Figure-Filtering of the signal considering the three dominant frequencies necessary for the representation of significant data.

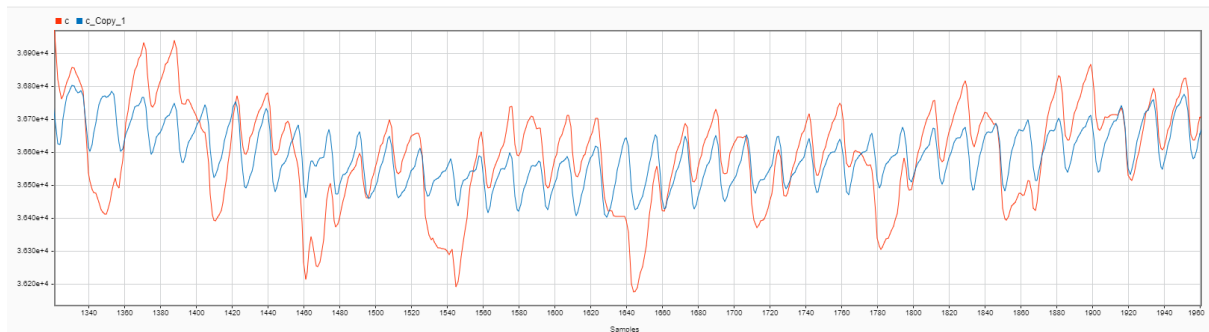


Figure 57-Original signal and signal without the breathing influence.

Identification of impedance features.

As previously stated, the SV equation depends on two characteristics that must be extracted from the diagram of the variation of impedance. As usual in machine learning it is possible to detect a set of representative points that help to identify the shape of the wave to be analyzed. In the derivative of the impedance the interesting points are:

- points where the derivative is zero.
- points where the derivatives assume maximum and minimum value.

A code that performs the computation of VET and TFI can take into account three points where the variation of the impedance is zero. The points are the limits of two intervals, where the interest of the

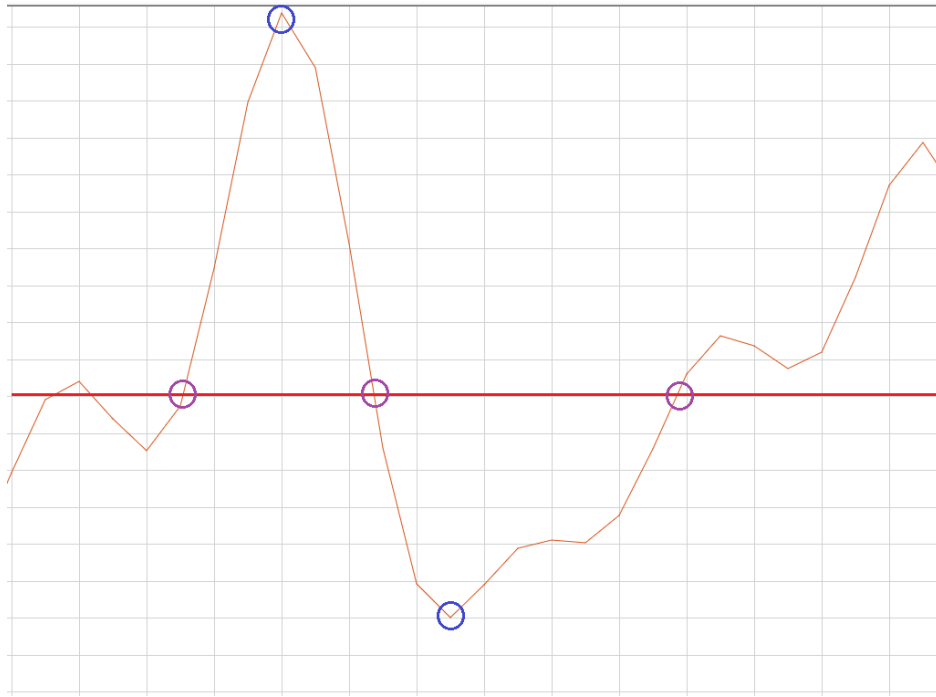


Figure 58-Main features necessary to be identified in the computation of the stroke volume.

For example, the code for the investigation of the first interval was written as follows:

```
for aa = 1:N
```

```
    if c(aa)>0 && ab==0
```

```
        aMinus = aa;
```

```
        ab =1;
```

```
    elseif c(aa)<0 && ab==1
```

```
        aPlus = aa;
```

```
        bb = 1;
```

```
    end
```

```
    if ab ==1 && bb==1
```

```

    mm = max(c(aMinus:aPlus))
    ab =0;
    bb =0;
    for ex=aMinus:aPlus
        if c(ex)==mm
            Max(ex) = mm;
            Pos(ex) = ex;
        end
    end
end

end

for vv=1:N
    if Max(vv)>0
        ll = ll+1;
        gg = Max(vv)+gg;
    end
    Ave = gg/ll;
end
for as=1:N
    if Max(as)<Ave
        Max(as)=0;
    end
end

```

The algorithm can be so explained:

-aa contains the value of the impedance.

-if the value of the impedance is greater than zero, aMinus is the index to take into account and represent the poin where the maximum value of impedance is to be searched. The

parameter a_b is set equal to one. -when the value is smaller than zero and a_b is equal to one, the second zero is found and a_{Minus} is found. A new parameter is set to one.

-once a_{Minus} and a_{Plus} are found, the maximum is found using matlab max routine.

-on the interval $a_{\text{Minus}}-a_{\text{Plus}}$ a search routine is repeated, comparing the elements with the maximum found at the previous step. The aim is to find the position of the maximum.

Accelerometer on the boat.

The mutlisensor datalogger WT901SDCL was set on the boat and was used to detect the acceleration of the boat during the navigation. The measuring regarded only one week of navigation: from June 29th to July 6th 2021.

	Start	End
29-Jun	1	220973
30-Jun	220974	652973
01-Jul	652974	1084972
02-Jul	1084973	1516971
03-Jul	1516972	1948971
04-Jul	1948972	2380970
05-Jul	2380971	2812969
06-Jul	2812970	3116442

Table 6-Detection of acceleration from WT901SDCL.

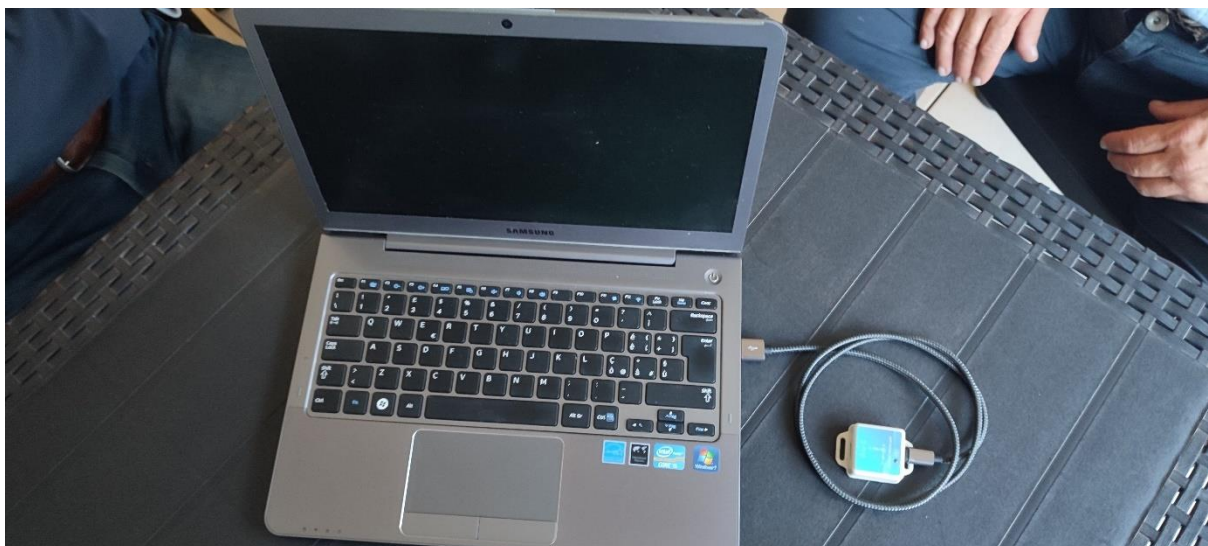


Figure 59-layout of 3 axis accelerometer WT901SDCL connected to a personal computer.

The 6 axis accelerometer had to provide information on the state of the sea. Sampling is repeated 5 times a second.

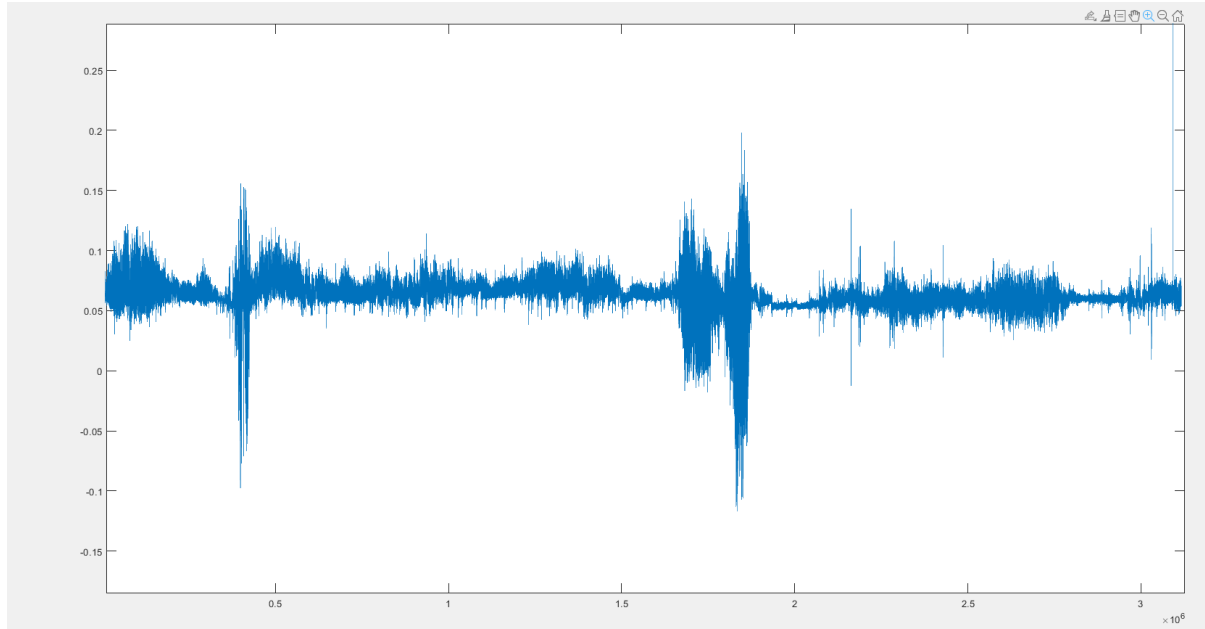


Figure 60-Acceleration on x axis during navigation as multiple of g.

Results for the acceleration for x axis.

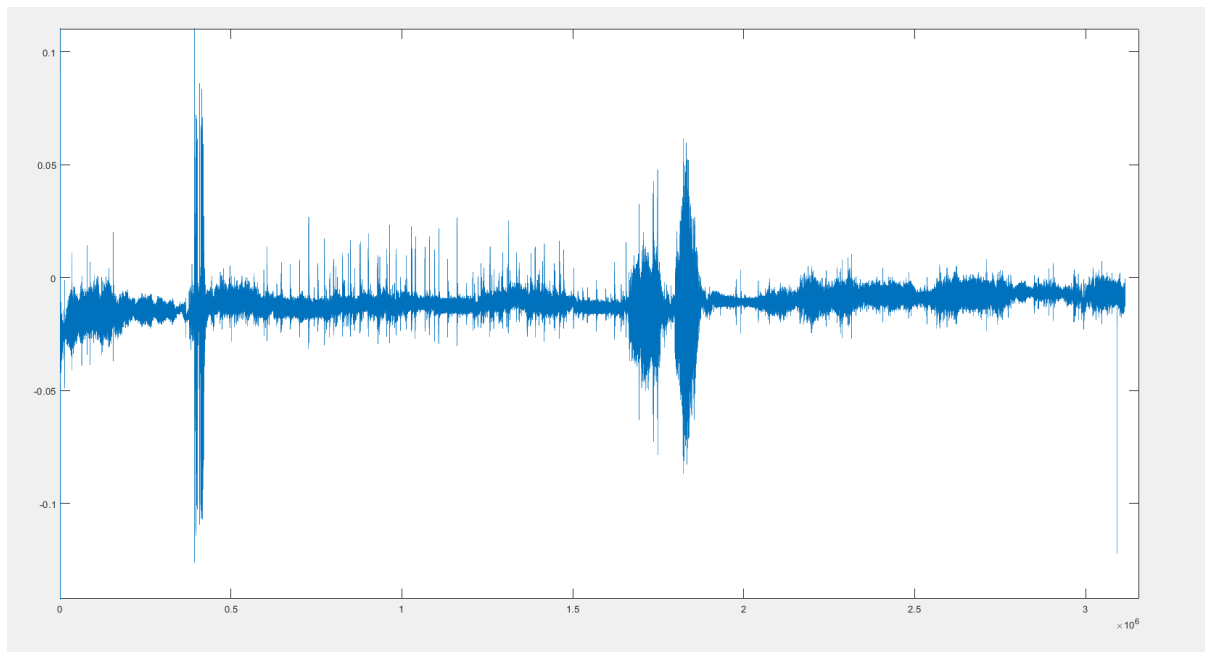


Figure 61-Acceleration on y axis as multiple of g.

results for acceleration on y axis.

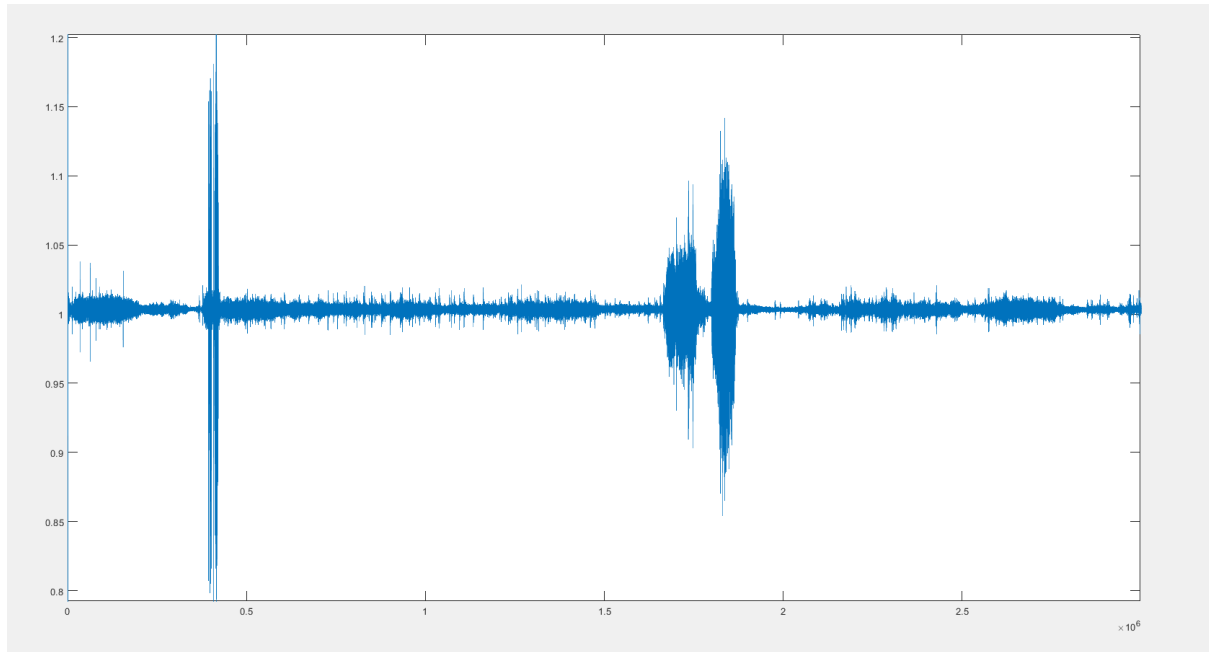


Figure 62-Acceleration of z axis as multiple of g.

The period of interest must be extracted and a correspondence between the acceleration on the boat and the test of the ICG device, in order to underline a linking between the two data. Linear accelerations are provided by the instrument as multiple of gravity acceleration g . It is possible to see that on z axis, the acceleration oscillates around the value 1, since it is influenced by the gravity acceleration. Since the sampling time is equal to $1/5$ seconds, it is necessary to match the data of the bioimpedance with acceleration and temperature with decimation and timing.

The graphs of impedance used in the comparison are reported in Appendix D.

Temperature during the navigation.



Figure 63-HOBO device for the measurment of the moisture and temperature.

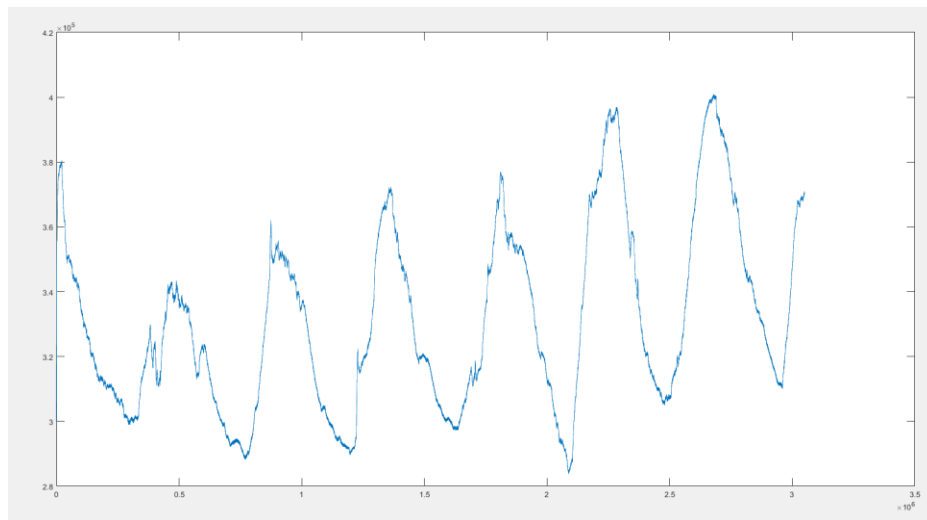


Figure 64-Temperature oscillation during the time of 6 days of navigation.

A further data, the temperature during navigation was also detected and stored in memory, using a HOBOTemp datalogger.

Filtered time series.

After identifying the main frequencies of frequencies and the samples of interest (from sample 19 to sample 58), the filtered time series of the impedance was plotted and saved for the other steps in the computation of the stroke volume. The graph is reported in Appendix B, where ARMA models for 38 samples are reported. ARMA model of sample 29 was rejected.

Stroke volume graphs.

As previously stated, the main goal in this stage is to compute the stroke volume. A MATLAB code was developed to perform the automatic computation of the Stroke volume, reported in appendix A. The algorithm identifies the main maximal value of the derivative of the impedance, the ejection time and the average value of the impedance during one beat and multiplies for the value of EPI, dividing by the mean value of the impedance. It was found that the ejection time is averagely equal to 0.3s. The results are plotted in this section, as tens of millilitres. The test performed are used as validation and confirmation of the data acquired.

Relation between accelerations and Stroke Volume.

The main goal of the present work is to underline the linking between inertial accelerations and cardiac output. In the previous sections the main inputs necessary to the determination of this connection were developed.

- the stroke volume was computed and plotted.

- the acceleration on x axis was identified on the same periods of the samples.

In this section, the relation between acceleration and Stroke Volume will be examined.

Subject A

Regression equation.

Dependent Y	Sv
Independent X	X

Least squares regression

Sample size	12
Coefficient of determination R^2	0,3674
Residual standard deviation	4,8574

Regression Equation

$y = 16,9942 + 67,0396 x$					
Parameter	Coefficient	Std. Error	95% CI	t	P
Intercept	16,9942	17,6038	-22,2296 to 56,2180	0,9654	0,3571
Slope	67,0396	27,8170	5,0594 to 129,0198	2,4100	0,0367

Analysis of Variance

Source	DF	Sum of Squares	Mean Square
Regression	1	137,0391	137,0391
Residual	10	235,9404	23,5940

F-ratio	5,8082
Significance level	P=0,0367

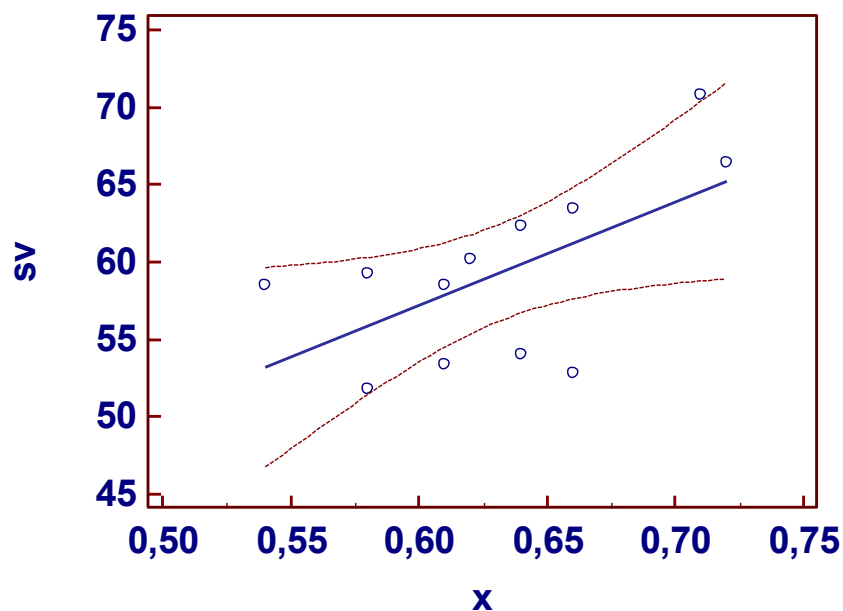


Figure 64-relation between acceleration and stroke volume, in m/s^2 and ml, for subject A.

Subject B.

Regression

Dependent Y	Sv
Independent X	X

Least squares regression

Sample size	10
Coefficient of determination R^2	0,4094
Residual standard deviation	6,1778

Regression Equation

$y = 93,3210 + -64,0659 x$					
Parameter	Coefficient	Std. Error	95% CI	t	P
Intercept	93,3210	17,0349	54,0384 to 132,6036	5,4782	0,0006
Slope	-64,0659	27,2066	-126,8045 to -1,3273	-2,3548	0,0463

Analysis of Variance

Source	DF	Sum of Squares	Mean Square
Regression	1	211,6252	211,6252
Residual	8	305,3180	38,1647

F-ratio	5,5450
Significance level	P=0,0463

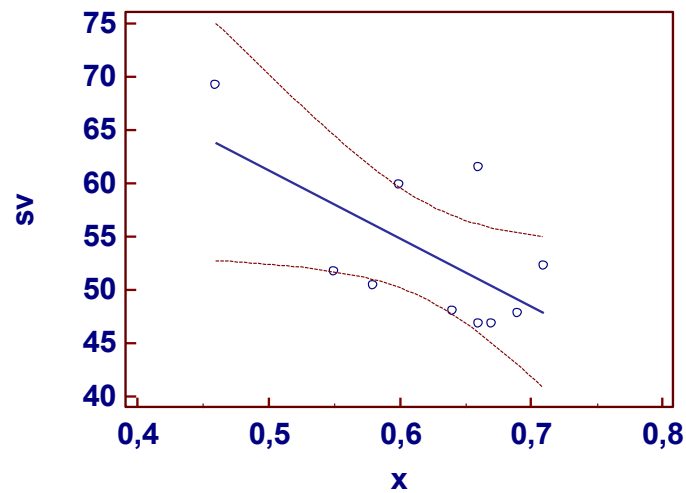


Figure 65-relation between acceleration and stroke volume, in m/s^2 and ml, for subject B.

Data from the linear regression equation of SV versus X axis linear acceleration show a statistical significance since the P value was lower than 0.05.

Subject C.

Regression

Dependent Y	sv
Independent X	x

Least squares regression

Sample size	11
Coefficient of determination R^2	0,5633
Residual standard deviation	3,6855

Regression Equation

$y = 85,9721 + -41,6054 x$					
Parameter	Coefficient	Std. Error	95% CI	t	P
Intercept	85,9721	7,2789	69,5062 to 102,4380	11,8112	<0,0001
Slope	-41,6054	12,2113	-69,2292 to -13,9816	-3,4071	0,0078

Analysis of Variance

Source	DF	Sum of Squares	Mean Square
Regression	1	157,6791	157,6791

Residual	9	122,2469	13,5830
----------	---	----------	---------

F-ratio	11,6086		
Significance level	P=0,0078		

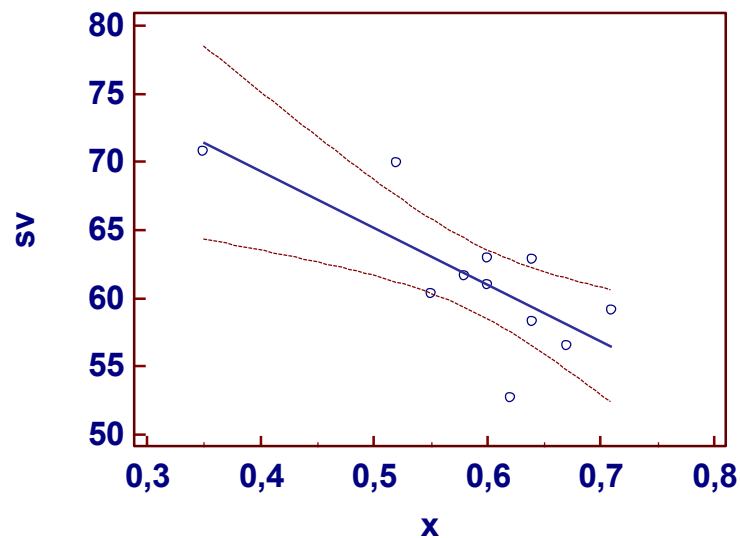


Figure 66-relation between acceleration and stroke volume, in m/s^2 and ml, for subject C.

Data from the linear regression equation of SV versus X axis linear acceleration show a statistical significance since the P value was lower than 0.05.

Data from the linear regression equation of SV versus X axis linear acceleration show a statistical significance since the P value was lower than 0.05.

The results allow to compute a linear regression model of the relationship between acceleration on x axis and the Stroke Volume.

Hemodynamic considerations.

As a further validation, the stroke volume was computed manually and compared to the automatic procedure.

a	m	giorno	ora
58,49	58,76	2021/06/30	4:40
66,46	67,72	2021/06/30	18:09
70,79	71,87	2021/07/01	5:32
52,08	66,44	2021/07/01	17:29
63,41	63,89	2021/07/02	5:38
62,42	69,83	2021/07/02	16:51

Table 7-Stroke Volume manually computed and stroke volume obtained from the automatic procedure.

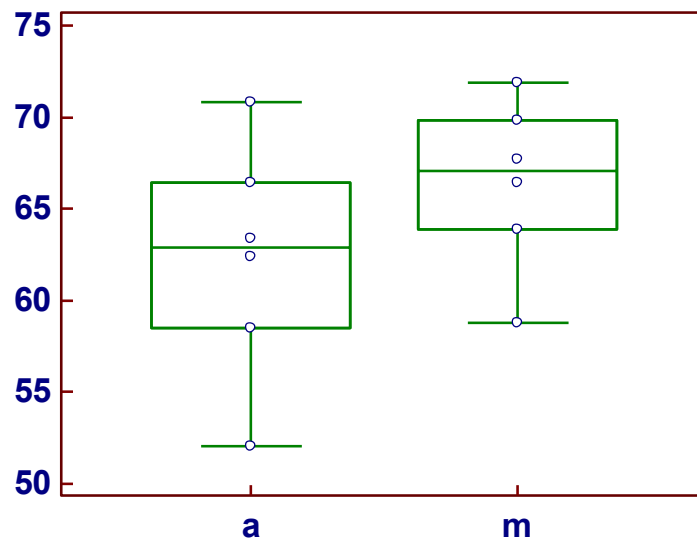
Mann-Whitney test.

Sample 1	
Variable	SV automatico (a)
Sample 2	
Variable	SV manuale (m)

	Sample 1	Sample 2
Sample size	6	6
Lowest value	<u>52,0800</u>	<u>58,7600</u>
Highest value	<u>70,7900</u>	<u>71,8700</u>
Median	62,9150	67,0800
95% CI for the median	53,3243 to 69,9494	59,7559 to 71,4740
Interquartile range	58,4900 to 66,4600	63,8900 to 69,8300

Mann-Whitney test (independent samples)

Average rank of first group	5,1667
Average rank of second group	7,8333
Mann-Whitney U	10,00
Large sample test statistic Z	1,281
Two-tailed probability	P = 0,2002



Box and whiskers representation, that shows how the second quartile of the set of Stoke Volume obtained from tests, can be compared to the third quartile. Mann-Whitney test performed on the averages did not provide statistically relevant differences (P=0,2002).

Tests on human gait.

Accelerometric measures in human gait.

In order to provide a validation data of the acceleration detected by the 3-axial accelerometers, a test on human gait was undertaken. A standard procedure was adopted for the tests. According to this procedure, the test is to be repeated at least two times, with the following requirements:

- The accelerometer must be positioned on the leg of the subject.
- The test consists of 10 m straight walking; whereas the stance period (time from BAC1 to BAC5 (gait), i.e. time to place a foot longitudinally in front of the other one) stance $t = 1$ s.
- It is requested to maintain a whole step period of about 2 s. In order to maximize the reliability of the measurement, the pavement material must be tile or marble, as flat as possible, as –anelastic as possible, since elastic properties of the ground can decrease the measured acceleration, due to absorption of the kinetic energy related to the gait.
- Finally, it is requested the walker to walk with bare feet., again, to reduce to total amount of lost energy due to the elasticity of the shoes.

Concerning the walkers who performed the test, the following biometric parameters were detected:

- 90÷100 kg of mass;
- 1.85 m of height.

The experimental setup has to be arranged as follows:

1 Inertial Measurement Unit (IMU) must be placed on the ankle of the walkers, according to a right-hand reference system with X direction as longitudinal direction of walking and Z direction the vertical direction floor-to-ceiling;

In order to cancel aliasing effects, a minimum IMU sampling frequency $s f = 100$ Hz.

Test performed in Turin at Politecnico.



Figure 67-Position of the accelerometer for the test.

The test was performed using the STEVAL-MKI121V1 board equipped with INEMO-M1 accelerometer.

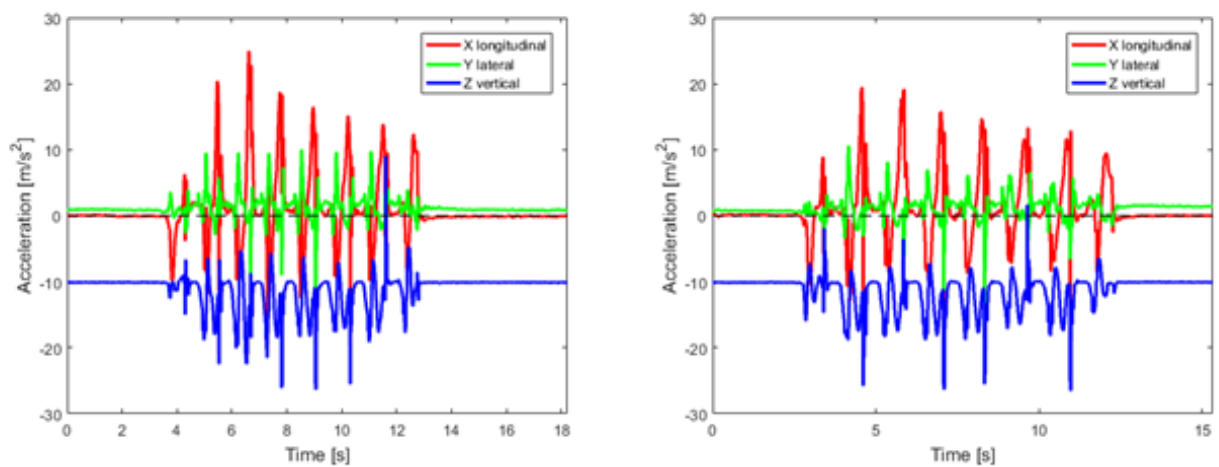


Figure 68- 3 axis-accelerations of test 1 and test 4.

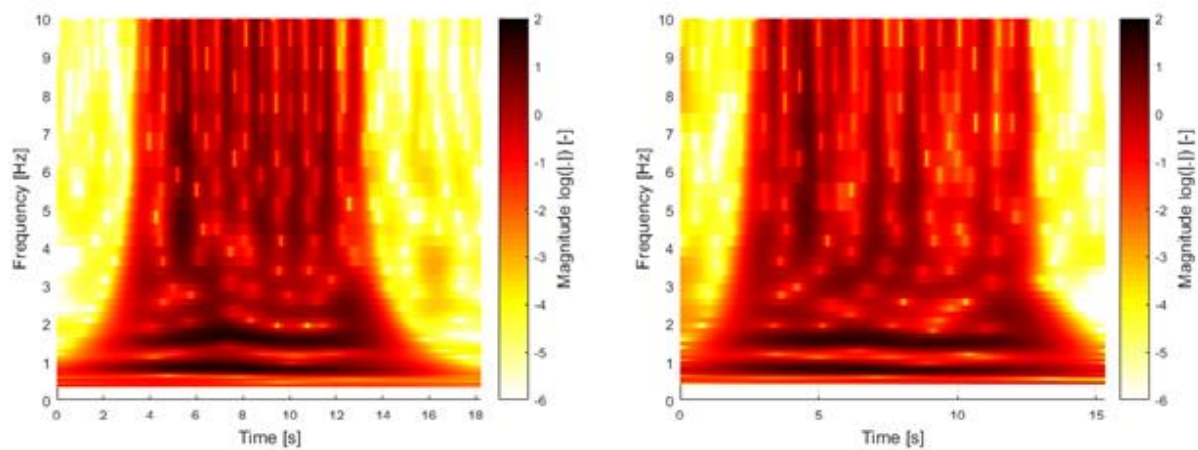


Figure 69-Spectrograms of X vertical direction, test 1 and test 4.

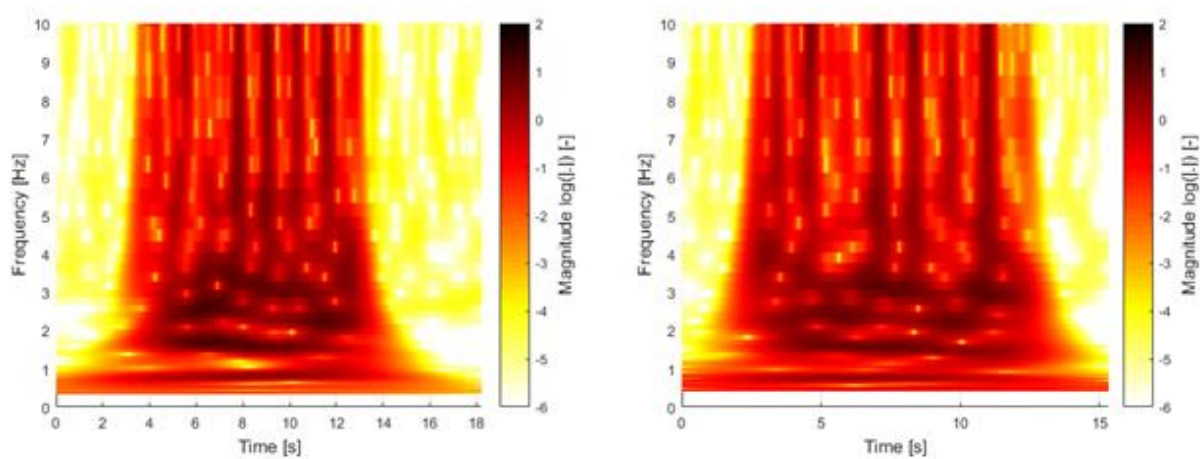


Figure 70- spectrograms of Z in vertical direction, test 1 and test 4.

Test performed at Cagliari.

The same test was performed in Cagliari using the WTI accelerometer.

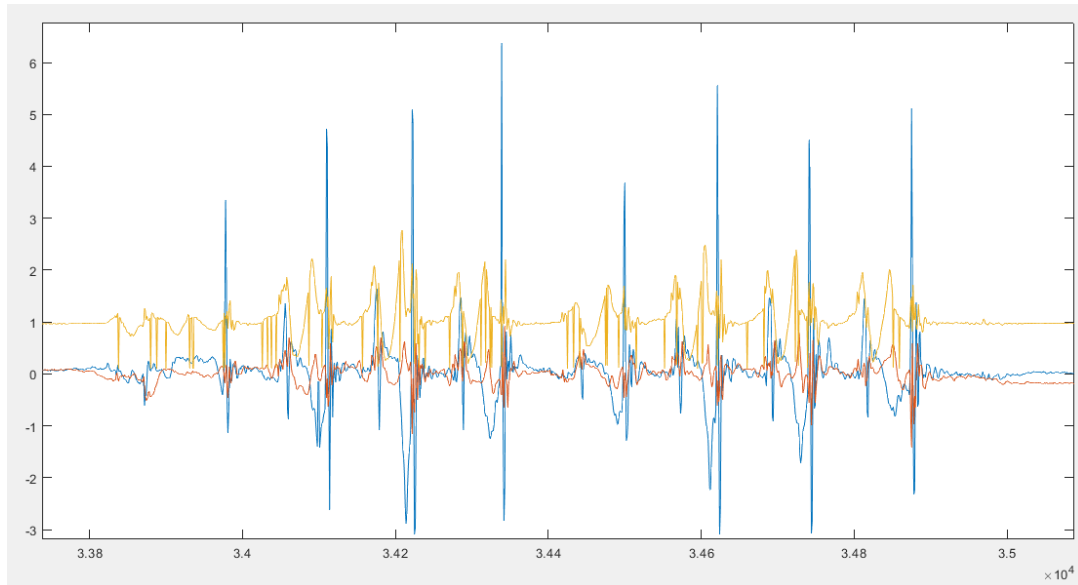


Figure 71- first test on WTI accelerometer. Yellow line represents the z axis, the blue line is the x axis as multiple of g.

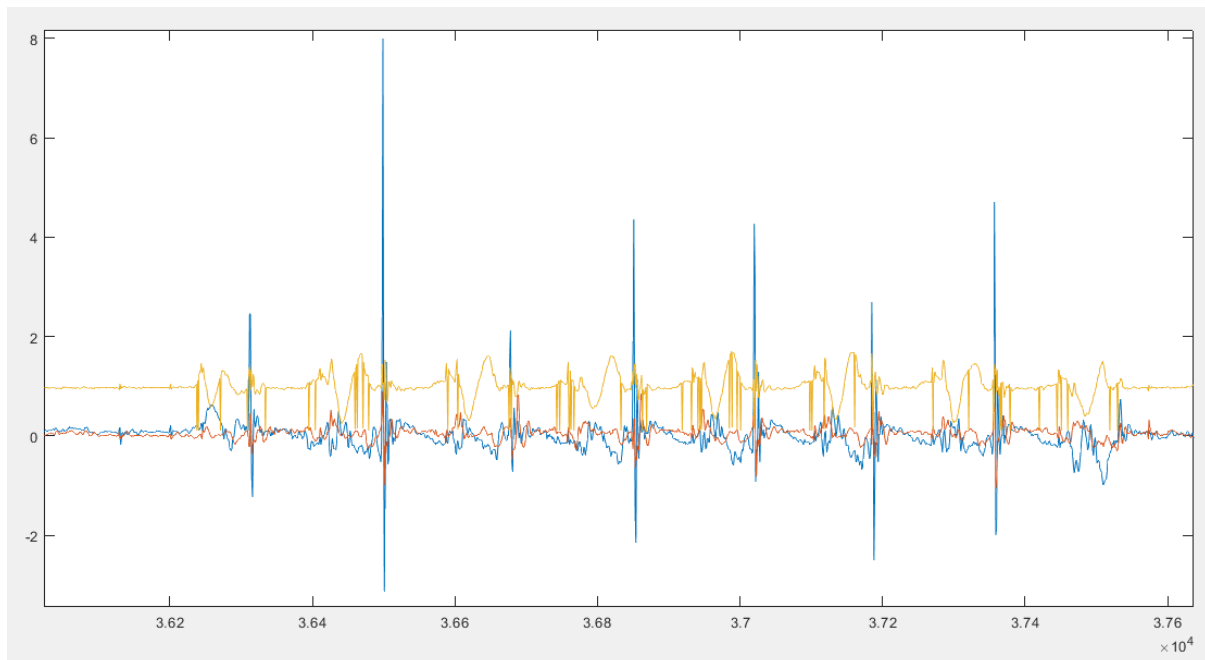


Figure 72-second test on WTI accelerometer. Yellow line represents the z axis, the blue line is the x axis as multiple of g.

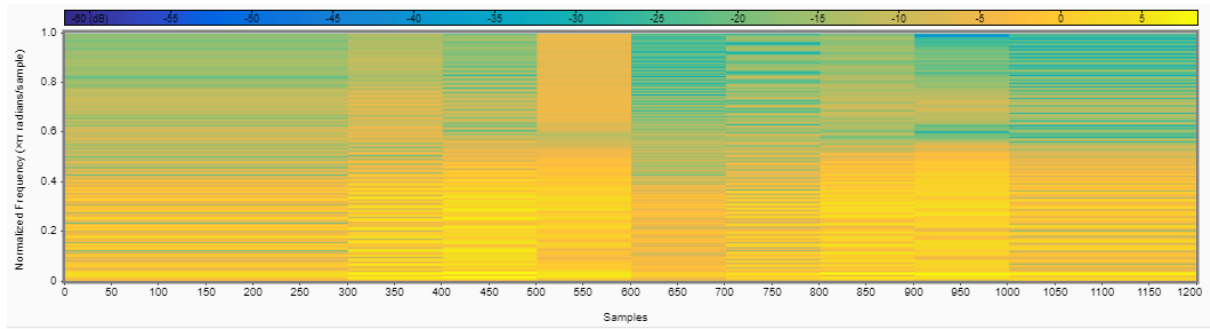


Figure 73-scalogram of the x axis for first sample.

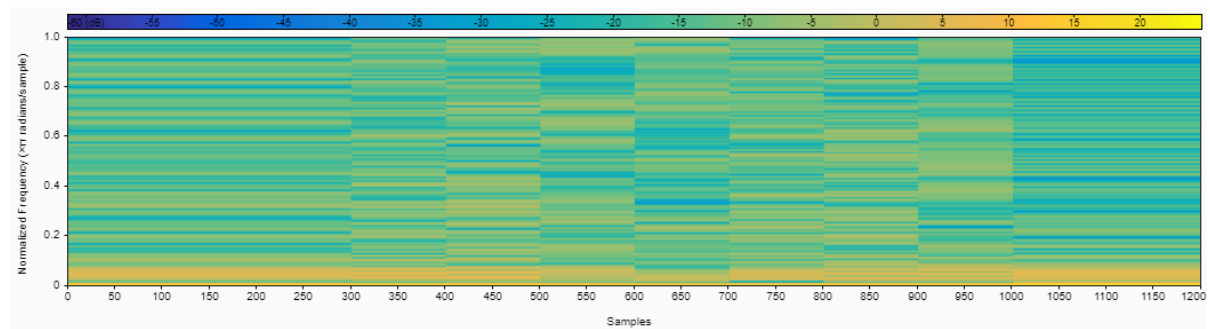


Figure 74-scalogram of the z axis for the first sample.

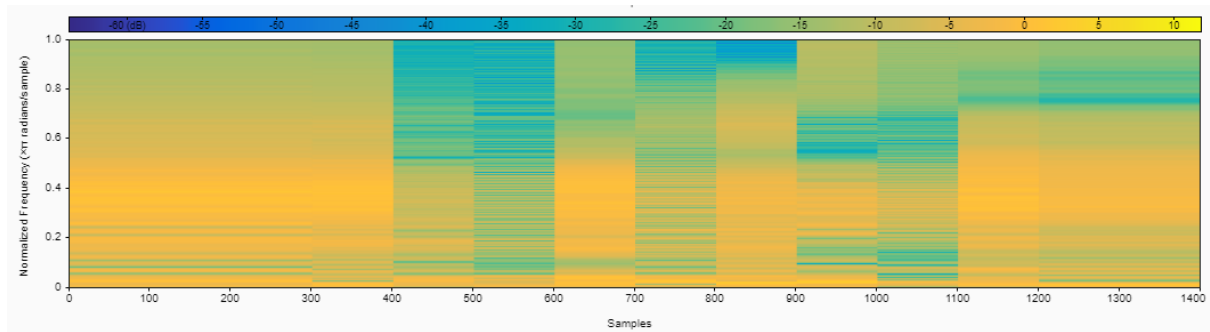


Figure 75-scalogram of the x axis of the second sample.

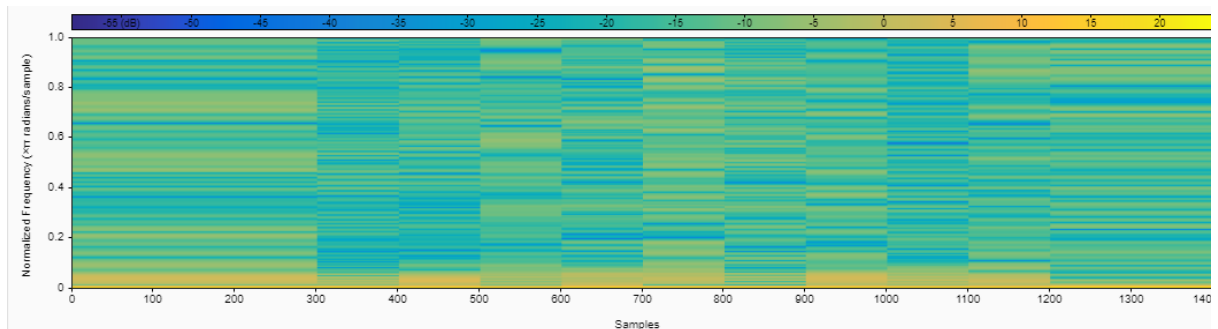


Figure76-Scalogram for z axis for the second sample

Analysis of the results of tests on accelerometers.

As it can be seen from the graphs, only x and z axes were chosen for comparison, since y axis is assumed to have negligible effect in gait.

The comparison of the two accelerometers shows a similar shape of the acceleration trend. On the other hand, a sensible difference in the peak intensity can be observed.

This was due to the different gate of the two subjects. In fact, the peak value of the acceleration is roughly three times bigger than the peak acceleration of the tests performed in Turin. On the other hand, in the first case, the peak occurs for 0,3 seconds, while in the other case it was observed an average length of 0,1 seconds.

Since the length of the step is the same, accordingly to the protocol of the test, it is necessary to have a greater peak of acceleration in the latter case. The problem is similar to “pick and place” procedure in robotics, where two similar robots performing the same task of moving an object, in the same time, the accelerations measured on the joints are different, due to different tolerances, time constants of the drives and actuators, if not a different kinematic path followed by the robots.

Discussion of Results.

In all the 3 engaged subjects, results from these experiments clearly show a linear dependence of the SV beat-by-beat changes from the boat acceleration changes along the chosen spatial X axis, even though in one of them this linear relationship was direct while in the other two ones it was of reverse kind. To explain why these occurrences, a mechanics-neurophysiological model is proposed as follows.

A) Vestibulo-spinal bases of body posture adjustments when external forces, generates by sea waves motion, induce changes in the body's gravity acceleration

As is known, vestibular apparatus in each of the two internal ear are deputies to receipt information concerning the changes in the head position, referred to that of body trunk, in such a way of induce neuromuscular activations producing specific muscles reactions to re-align both head and body trunk.

For this purpose the labyrinth of the ear is equipped with particular receptor structures, i.e. the semicircular canals, three in number on each side, and the utricle with the saculus. In fact, the semicircular canals are particularly sensitive to the variations of the components of the angular velocity of the head on each of the three anatomical planes in which it is virtually inserted: horizontal, frontal and sagittal, while both the ampullae of the saculus and utricle contribute to acquire the linear variations of speed of the head in all directions of space.

In figure 76, the photo towards the right down corner in the section A shows the boat crew captain sitting at the long side of the table in the living room of the boat while the latter was moored. Aided by the composition of photos in which a repertoire sailboat is positioned in mooring with the stern viewed distally and this is placed in correspondence, through a blue arrow, with the inside of the experiment boat to highlight the position of the stern of this latter, it can be deduced that the subject in the experiment was seated so as to have the stern on his right and the prow on his left.

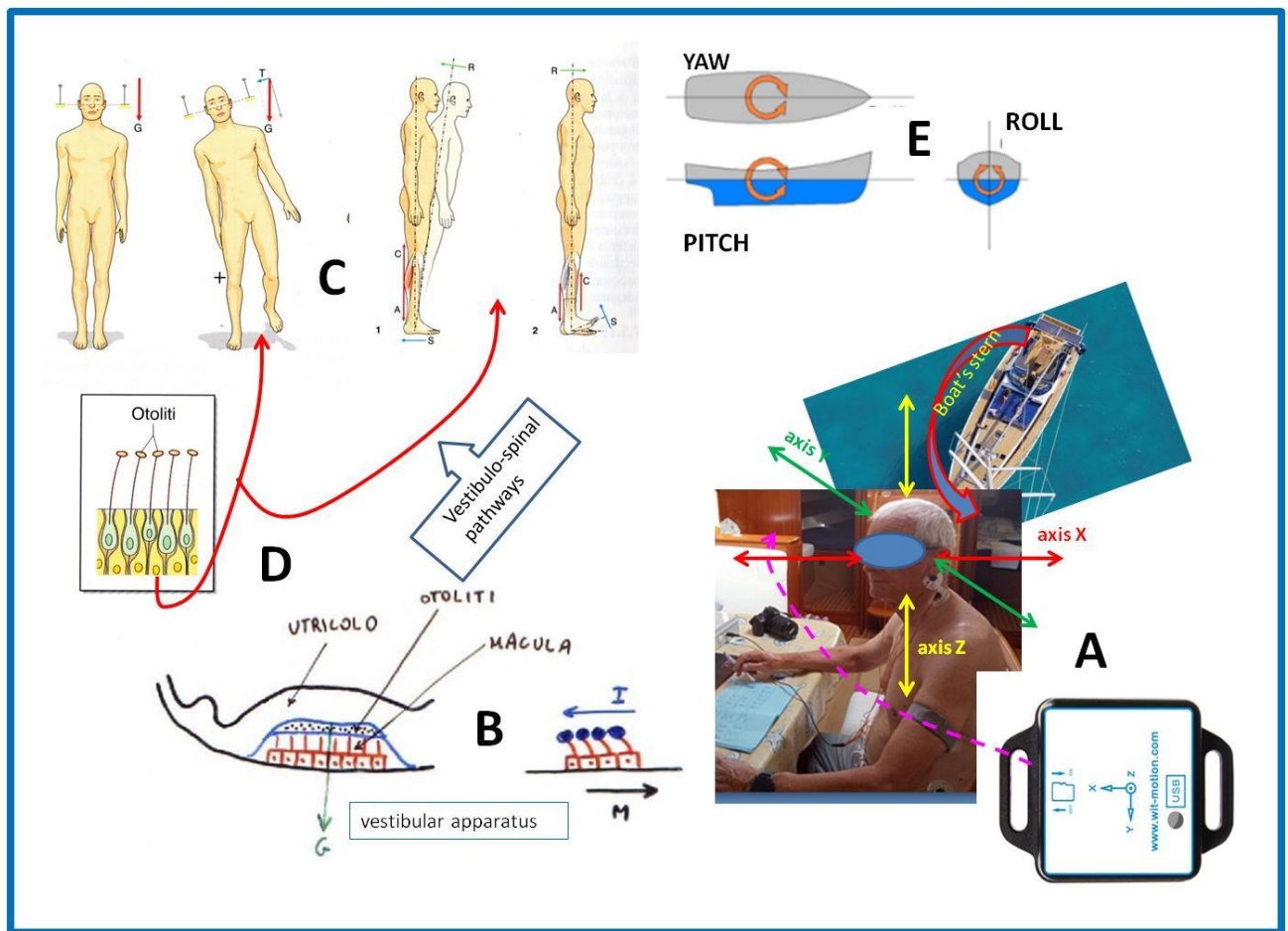


Figure 78 - Section A shows the subject (A) while sitting at living room table of the moored boat while assessing bioimpedance signals. around his head are drawn the 3 accelerometer device longitudinal axis (device showed at the right corner). Section B shows a schematic composition of utricle chamber in the vestibular apparatus. Section C shows dummies simulating different vestibular excitations while staying in the moored boat. Section D concerns a representation of the vestibule-spinal pathways from which the antigravity muscle reactions depend. Section E show typical boat oscillations around each accelerometer axis.

In this way, this studied sailor was subjected to the boat roll or having body movements around the X axis of the accelerations device (positioned magnified in the extreme right-down corner of section A in the exact position as was in the chart desk of the boat indicated by the purple dashed arrow) which corresponded to the transverse axis of the boat and generate lateral left-right movements of the head-trunk of the sailor. At the same time, the wave motion could also produce linear movements of the head-trunk along the X axis or antero-posterior linear oscillations of the body. Otherwise pitching of the boat occurred around its longitudinal axis which lay along the Y-axis of the accelerometer and induced antero-posterior head-trunk movements. Also in this case, the wave motion could produce linear movements of the head-trunk along the Y axis or linear lateral oscillations of the body.

In this way, this studied sailor was subjected to the boat roll or having body movements around the X axis of the accelerations device (positioned magnified in the extreme right-down corner of section A in the exact position as was in the chart desk of the boat indicated

by the purple dashed arrow) which corresponded to the transverse axis of the boat and generate lateral left-right movements of the head-trunk of the sailor. At the same time, the wave motion could also produce linear movements of the head-trunk along the X axis or antero-posterior linear oscillations of the body. Otherwise pitching of the boat occurred around its longitudinal axis which lay along the Y-axis of the accelerometer and induced antero-posterior head-trunk movements. Also in this case, the wave motion could produce linear movements of the head-trunk along the Y axis or linear lateral oscillations of the body.

In the section B of the figure 78 is manually drawn down the scheme of the vestibular utricle chamber where is shown the sensible layer cells with the otoliths located at the distal ends of the villi. When the head moves longitudinally increasing its speed, due to the inertia of their mass the otoliths tend to maintain their initial position in space thus generating a deformation of the villi in the opposite direction to that of the movement (see lateral scheme where, due to inertia (I), the villi bend in the opposite direction to that of the movement (M)). This gives rise to a depolarization of the cell membrane with the generation of discharges of action potentials along the nerve fibers efferent from them (the frequency of which is proportional to the imposed linear acceleration) which, via the vestibulo-spinal nerve pathways (see section D), affers to the motor neurons of the anti-gravity muscles of interest, generating a motor reaction that puts the head back in line with the trunk.

Section C on the left of figure 78 shows two human dummies which, subjected to the roll action that the wave motion generates on the moored boat (see the specific boat roll scheme in section E of figure), starting from the postural condition of standing still in which the action of the acceleration of gravity is constant (see the red arrow pointing downwards in the still subject) and therefore the vestibular sensors are not excited, when his was subjected to the action of roll that the wave motion generates on the moored boat, the subject's head undergoes a lateral displacement causing the excitation of the vestibular sensors which, via the vestibulo-spinal nerve pathways, induced an increase in the muscular tone of the postural musculature in the homologous lower limb which in turn generates reaction forces against those produced by the roll, thus adjusting the body posture in order to avoid falling. As a consequence, there is a mechanical deformation of the muscles/tendons of the affected limb from whose proprioceptors of strength and length, trains of electrical action potentials inputs afferent to the lumbo-sacral spinal cord, from where they will be distributed to the various organs and systems involved in maintaining of the postural homeostasis of the subject.

On the right of section C the human dummies are shown in profile to better highlight the action of the boat pitch. It can be shown that when the boat pitch displaces the head-trunk forward vestibulo-spinal nervous pathways send informations from the utricles sensitized cells towards the motoneurons of the triceps surae muscles, i.e. the calf highlighted in red, which contraction straighten the body by generating a backwards reaction (R). Otherwise, when the boat pitch pushes head and trunk backwards (see the dummy on the right) a vestibular volley of impulses travel towards the tibialis muscles motoneurons which, producing a dorsal contraction of the foot, causes the body to straighten forward.

In the light of what above considered, and also considering what was the subjective feeling about each of our three sailors, due to the particular stabilisation of the moored boat, non relevant entity of the angular accelerations changes, caused by the wave motion of the sea, had been recorded by the accelerometer device as well as they were not consciously

perceived by our sailors while each of them was sitting at the table in the living room of the boat to acquire the data relating to the cardiodynamic measurements carried out using the e-Physio device.

On the contrary, as show the experimental data, linear acceleration changes had been registered by the device especially along the X axis of the accelerometer (which was coherent with the transverse axis of the boat) both concerning the boat captain, i.e. named subject A, while he was sitting at the long side of the table, and the other two crew sailors, named in turn subject B and C, while each of them was sitting at the short side of the table just at right to the captain's position. Interestingly, while he was seated to carry out the cardiodynamic measurements, subject A perceived antero-posterior movements of the head-trunk, along the reference X axis, similar to what is shown on the right of section C in figure Z. Differently, both subjects B and C perceived movements alternating of the head-trunk in a transverse direction, similar to what is shown on the left of section C in figure 78.

Practically, all the 3 subjects tested while seated, due to the rolling movements of the boat, were slightly displaced along the X axis, subject A alternately forwards and backwards and both B and C in the left and right directions. Obviously, these differences in the behaviour of the head-trunk movements had given rise to the action of acceleration along the X axis in different parts of the body, thus exciting different areas of the utricle and saccule otoliths from which the recruitment of different muscle groups for the purposes of some specific postural adjustments aimed at recovering postural homeostasis in the upright position. Returning now to the dummies of figure 76, the subject A underwent an anti-gravity muscle reaction as in the case of the examples on the right of section C while both subjects B and C produced an anti-gravity muscle reaction as exemplified from the dummies on the left of section C.

B) Cardiovascular adjustments from extravascular mechanocetive stimuli of the limb muscles recruited by the vestibular antigravity reaction to the body displacement induced to the moored boat by wave motion of the sea

Figure 77, on the right, schematically shows cardiovascular control mechanisms. There is highlighted that nervous motor commands that arise in the brain to perform exercise tasks may interfere with cardiocirculatory homeostasis by cortical and subcortical/hypothalamic radiation of stimuli that act as a feedforward mechanism involving parallel activation of motor, respiratory and cardiovascular centres. To these latter brain stem nuclei also converge mechanocetive and chemoceptive stimuli of intravascular origin, the former ones mainly from receptors placed into the aortic arch and the second ones from receptors mainly placed in the bifurcation of the two carotid arteries. Both these receptors modulate the activity of the brainstem centers determining central and peripheral adjustments of the hemodynamic profile as a function of metabolic demand. In fact, changes in mean arterial blood pressure and in oxygen and carbon dioxide partial pressure in the arterial blood give rise to sympathetic or parasympathetic impulse volleys towards the primary heart pacemaker, i.e. the sinus node, and the myocardium muscle. In this way, arterial mean blood pressure increases above a set value induces a reflex parasympathetic/colinergic hypertone from vessel rerceptors towards the sinus node which reduces the heart rate, from which the blood pressure was reset.

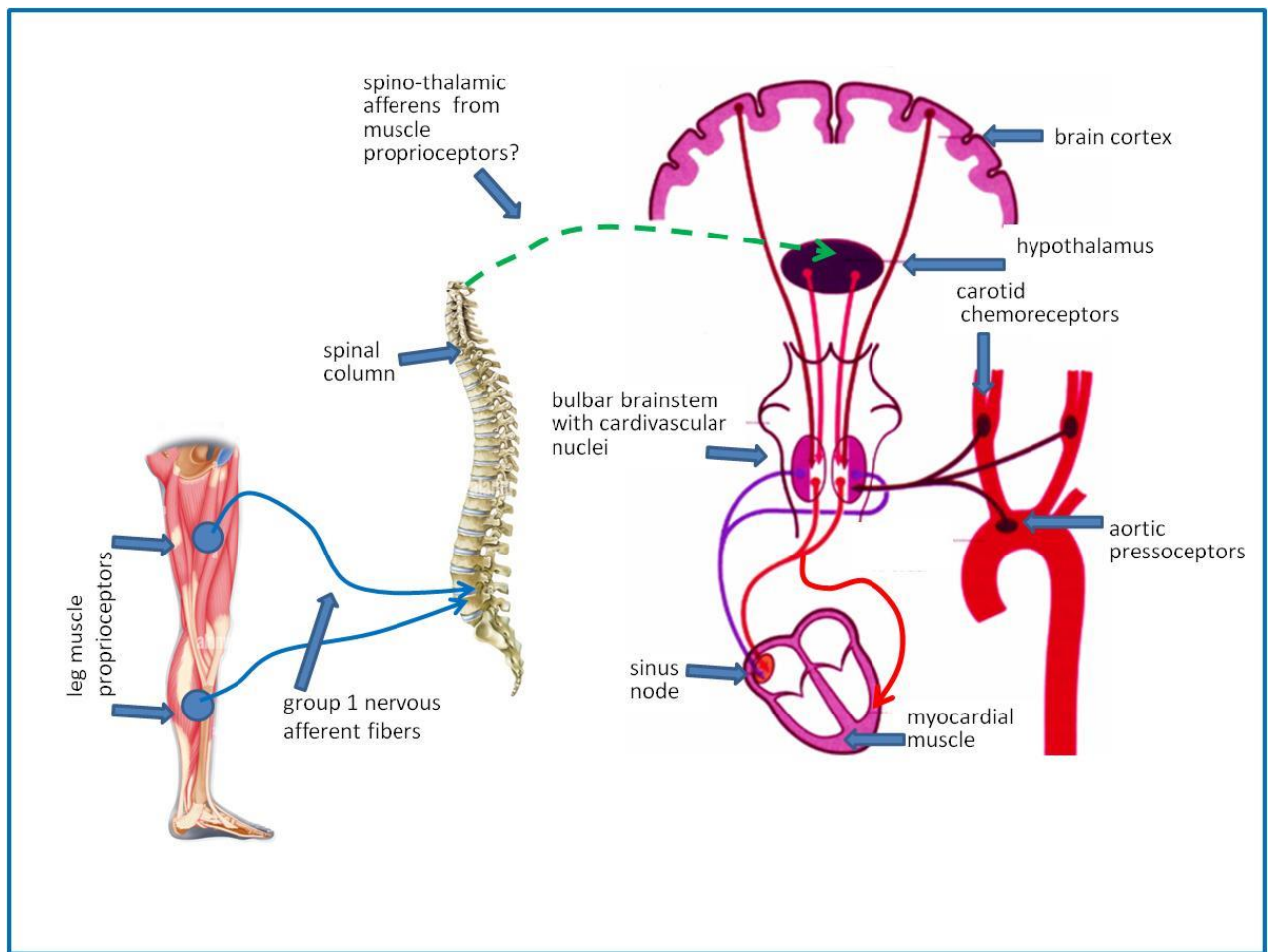


Figure 79 – On the figure's right side a schematic anatomy of the cardiovascular nervous control is represented. In the middle of figure is shown an image of the human spinal column where after the group 1 nervous fibers from leg muscles proprioceptors and exit towards the brainstem possible nervous pathways reaching the limb muscles proprioception informations.

On the contrary, arterial blood hypoxia and hypercapnia together with a falling arterial blood pressures in turn induces induce a reflex sympathetic/adrenergic hypertone towards both the sinus node and the myocardium muscle resulting, by induced tachycardia and myocardial ipercontractility, in increased cronotropic and hinotropic activities of the heart from which normopressure, normoxia and capnia of arterial blood are reset.

It is therefore evident that the activity of both the brainstem and intra-arterial structures per se are able to keep the cardiocirculatory homeostasis constant at values which are compatible with a condition of physical and mental rest.

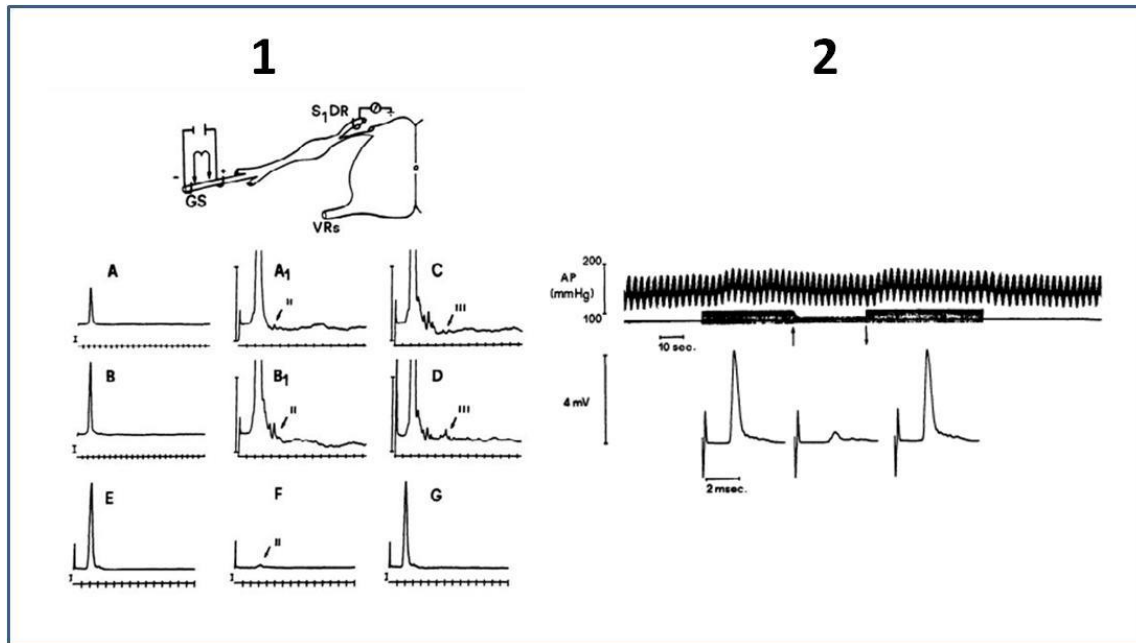


Figure 80 - Section 1 - Experimental arrangement used to record afferent volleys from S1 dorsal rootlet (SIDR) disconnected from the spinal cord to stimulate gastrocnemius-soleus and medial gastrocnemius (GS) nerve and to block fast afferent volleys by applying anodal current at sides of stimulating electrodes. (VRs, ventral roots.) Traces show computer plots of afferent volleys after analog-to-digital conversion at 20 kHz. Each trace represents mean of 500 sweeps triggered by stimuli applied to GS nerve at 3 Hz. Distance between stimulating and recording electrodes was 16 cm. First afferent volley of each trace, except F, belongs to group I fibers because conduction velocity was >72 m/s.

Section 2 – Effects of stimulation test on carotid pressure performed with Intermittent stimulation after curarization. Enlarged traces represent averaged values of afferent volleys recorded in sequence in intermediate trace. During test, group I afferent fibers were reversibly blocked by anodal current. During testing period before application of anodal current, afferent volleys consist of a fast component attributable to group I fibers (100 m/s, distance between stimulating and recording electrodes being 16 cm) followed by small volleys attributable to group II fibers. During this period, arterial pressure (AP) increases without adaptation. At arrow, anodal current is applied and increased slowly. Its blocking value (50 μ A) is reached in 4 s. Consequently, amplitude of fast component of afferent volleys decreases progressively until complete disappearance. AP returns to control values despite presence of volleys of group II fibers. As soon as anodal current is interrupted (2nd arrow), fast volleys recover their original amplitude and AP begins to increase toward values recorded at beginning of test. During this period, arterial pressure (AP) increases without adaptation. At arrow, anodal current is applied and increased slowly. Its blocking value (50 μ A) is reached in 5s. Consequently, amplitude of fast component of afferent volleys decreases progressively until complete disappearance. AP returns to control values despite presence of volleys of group II fibers. As soon as anodal current is interrupted (2nd arrow), fast volleys recover their original amplitude and AP begins to increase toward values recorded at beginning of test.

However, as the diagram in figure 79 shows, both cortical and subcortical nervous structures could interfere with the base activity of the bulbar vasomodulatory nerve nuclei. In fact, it has been found that central commands from brain motor cortex as well as from subcortical/thalamic nervous structures could operate in reaching bulbar neurons deputed to modulate heart and vessel activity. This could occur in response to increased fuel demand by parallel activated skeletal muscles as well as to mental stressors occurrence which per se may influence cardiovascular homeostasis in preparation for possible fight or flight reactions.

Nevertheless, the left section of figure 79 shows a possible flow of information from the extra-vascular muscle proprioceptors of the limbs towards the bulbar cardiovascular control centers.

Previous experiments on anesthetized cats, made in the 70-80s of the past century at the cardiorespiratory experimental electrophysiology laboratory of the University of Cagliari, in Italy (in which prof. Alberto Concu was research fellow), examined cardiorespiratory activity during excitation of large afferent fibers from muscle proprioceptors [56].

As shown in figure 79, in the above cited mile stones experiments, the selective stimulation of group I fibers from muscular muscle spindle receptors with electric impulses at 200-300 Hz (side 1) induced an increase in mean systemic arterial pressure from control value of 151 \pm 2 to a maximum of 160 \pm 2 mmHg (side 2). Neither of these increases was produced by the same stimulation when applied during anodal block of volleys of group I fibers.

in subsequent experiments conducted by the electrophysiology team of Cagliari (, in the same kind of animal samples was investigated if on anesthetized and curarized cats the increase in blood pressure caused by electrical stimulation of group I afferent fibers is related to a direct reflex effect on the heart. The reflex effect of electrical stimulation of group I afferent fibers from the gastrocnemius-soleus muscles on the arterial pressure, the left ventricular pressure, the inotropic state of the left ventricle (dp_{50}/dt) and the heart rate were compared before and after beta-blockade with propranolol (0.1 mg/kg intravenously) to reduce a possible direct effect on the heart. The same comparison was made before and after alpha-blockade with phentolamine (2.5 mg/kg intravenously) to keep the peripheral resistance constant. Electrical stimulation of group I afferent fibers caused an increase in the blood pressure, the left ventricular pressure and, to some extent, the inotropic state of the left ventricle and the heart rate. The beta-blockade had no significant effect on these increases, while the alpha-blockade abolished the increase in blood pressure. It is concluded that the effect of stimulation of group I afferent fibers on the blood pressure is not dependent on a direct reflex effect on the heart, but can be better explained by a reflex increase in the peripheral resistance .

Starting from the above miles stone experimental results, subsequent research confirmed also in humans a robust connexion of the muscle mechanoreceptors in contributing to fine conditioning the cardiovascular behaviour in the aim of optimize the skeletal muscles activities [55,57].

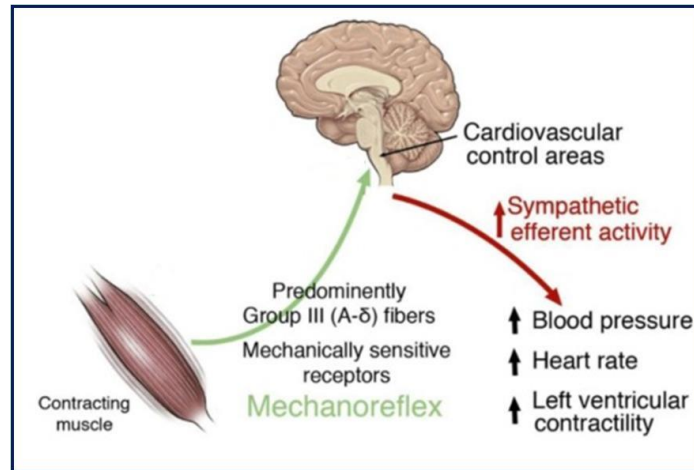


Figure 81 – Schematic picture of the effects of the contracting muscles in controlling the left ventricle stroke volume through the sympathetic brainstem efferens controlling the ventricle contractility.

In conclusion, figure 81 clearly highlights the possibility of induce changes in left ventricle stroke volume by skeletal muscles contractions by acting on the homeometric/contractility mechanism via the brain bulbar nuclei efferens towards the myocardium muscle.

The above sentence reasonably consents to functionally connect the beat-to-beat changes in SV showed by our sailors when they were submitted to wave motion induced body displacement and they engaged postural reflexes to recover the body position in reaction to the externally applied body accelerations. In fact, since reflex reactions implied not voluntary legs muscle contractions, stretched muscle spindle proprioceptors generated an action potential volley towards spinal medulla and then triggering in this way a cardiovascular reflex. In our sailors this reflex induced SV changes which were linearly coherent whit the acceleration changes applied to their bodies along the X axis. In the case of the subject A, this reflex gave rise to a direct regression of SV on acceleration temporally correlated together; in the case of both subjects B and C gave rise to an inverse regression among the same variables. Obviously, the different pendency of the regression straight line depended by the fact that the subject A and both the subject B and C were orthogonally positioned in the table of the boat dining all, so in the former one subject, as shown by section C on the right in figure X, acceleration induced displacement of body was of the anterior-posterior type while in the other two subject was of the lateral right-left type, and complex interactions among stimuli generated in different muscle groups, concerning the two cases, could justify different pendency in the regression equations here observed.

Conclusions.

The navigation is an example of the variation of the activity that influences physiological activities. In the present work it was noted an increment in the mechanical efficiency, based on the arm band pro3 and the metabolic data. On the other hand, Stroke volume data suggest a correlation between the inertial acceleration on cardiac activity, such as to increase cardiac activity. All the previous results suggest a beneficial effect on the overall health of human subjects, especially those in the elderly age range.

Also considering the more purely mechatronic aspects of this experimentation, the validation of the e-Physiol ICT platform is of no negligible importance for the purpose of a prolonged non-invasive monitoring in subjects/patients engaged in activities with a high cardio-metabolic demand, thanks also to the absolute innovation concerning the possibility of in real time automatic calculation of the beat-by-beat values of the systolic ejection volume, i.e. the most important hemodynamic variable for cardiovascular homeostasis.

References.

Artifacts of ECG.

- [1] G. D. Clifford, F. Azuaje, P. McSharry, *Advanced methods and tools for ECG data analysis*, Artech House, Norwood, 2006.
- [2] A. Hyvärinen, J. Karhunen, E. Oja, *Independent Component Analysis*, Wiley publications, 2001.

Papers.

- [3] P.E. McSharry, G.D.Clifford, L. Tarassenko, L. A. Smith, *A Dynamical model for Generating Synthetic Electrocardiogram Signals*, IEEE transaction on biomedical engineering, vol 50, n.3, March 2003.
- [4] *A Signal Decomposition Model-Base Bayesian Framework for ECG Components Separation*, IEEE transactions on signal processing, vol. 64, no.3, February 1, 2006.
- [5] N.V. Thankor, Y.S. Zhu, *Applications of Adaptative Filtering to ECG Analysis: Noise Cancellation and Arrhythmia Detection*. IEEE transactions on biomedical engineering, vol. 38, no.8, August 1991.
- [6] P.Laguna, G.B. Moody, R.G.Mark, *Power Spectral Density of Unevelly Sampled Data by Least-Square Analysis: Performances and Application to Heart Rate Signals.*, IEEE transaction on biomedical engineering, vol. 45, no.6, June 1998.

Dynamical systems, digital signal processing and filtering.

- [7] S. M. Alessio, *Digital signal processing and spectral analysis for scientists. Concepts and applications*. Springer, 2016.
- [8] V.I. Arnold, *Mathematical Methods of Classical Mechanics*, Springer Verlag, 1978.
- [9] S.L. Brunton, J.N.Kutz, *Data Driven Science and Engineering*, Cambridge University Press, 2019.
- [10] H. Gassmann, *Einführung in die Regelungstechnik*, , Harri Deutsch Verlag, 1993.
- [11] L. Ljung, *System Identification, Theory for the user*, second edition, Prentice Hall, 1999.
- [12] A.V. Oppenheim, R.W. Schaffer, J.R. Buck *Discrete Time Signal Processing*, second edition, Prentice-Hall, 1999 .
- [13] S.M. Kay, *Modern Spectral Estimation, Theory and Applications*, Prentice Hall.
- [14] A. Svoboda, *Computing Mechanisms and linkages*, New York, Dover Publications, 1965.

- [15] A. Tarantola, *Inverse Problem Theor and Methods for Model Parameter Estimation*, SIAM.
- [16] S. Winder, *Analog and Digital Filter Design* , Newnes, Elsevier Science (USA), 2002.

Papers.

- [17] H. Akaike, *Statistical Predictor Identification*, Annals of the Institute of Statistical Mathematics, vol.22, pp. 203-217, 1970.
- [18] L. Cohen, *Time-Frequency Distributions, a review*, Proceedings of the IEEE, vol. 77, No7. July 1989.
- [19] F. J. Harris, *On the Use of Windows for Harmonic Analysis with discrete Fourier Transform*, proceedings of th IEEE, vol.66, Issue 1, 1978.
- [20] E. Kheirati Roonizi and R. Sassi *A signal Decomposition Model-Based Bayesian Framework for ECG Components Separation*, IEEE Transactions on Signal Processing, vol. 64, no.3, pp. 665-674. February 2016.
- [21] R.W. Pickford, *Smoothing Periodograms from Time-Series with Continuous Spectra*, Nature, vol. 161, May 1st,1948.
- [22] A. Savitzky, J.E. Golay, *Smoothing and Differentiation of Data by Simplified Least Squares Procedures*, Analytic Chemistry, vol 36, no.8, July 1964.
- [23] R.M. Todd, J.R. Cruz, *Frequency Estimation and the QD Method*, Control and Dynamic Systems, vol 75, Academic Press.
- [24] U. Yule, *On a Method of Investigating Periodicities in Disturbed Series, with Special Reference to Wolfer's Sunspot Numbers*, Philosophical transactions of the Royal Society, January 1927.
- [25] C.R. Vogel, M.E. Oman, *Iterative Methods for Total Variation Denoising*, SIAM J. Sci. Comput., vol 17, no. 1, pp. 227-238, January 1996.

Wavelet transforms.

- [26] P.G. Lemarié (ed.), *Les Ondelettes en 1989*, Séminaire d'Analyse Harmonique, Université de Paris-Sud, Orsay, Springer, 1990.
- [27] S.Mallat, *A wavelet tour of signal processing. The sparse way*, , Academic Press, Elsevier, 2009.
- [28] A. Mertins, *Signal analysis, wavelets, filter baks, Time-frequency transforms and applications*, Wiley publications, 1999.
- [29] M. Misiti, Y. Misiti, G. Oppenheim J-M. Poggi, *Wavelets and their applications*, ISTE USA, 2007.

[30] D.B. Percival, *Wavelet Methods for Time Series Analysis*, Cambridge University Press, 2000.

[31] C.D. Sidney Barrus, R.A. Gopinath, H. Guo, *Introduction to Wavelets and Wavelet Transforms. A Primer*, Prentice Hall, 1998.

Papers.

[32] D.L. Donoho, *Interpolating Wavelet Transforms* Technical report no. 408, Stanford University, Novembre 1992.

Mathematical background

[33] M.H. Hayes, *Schaum's Outline of Theory and Problems of Digital Signal Processing*, Mc Graw-Hill, 1999.

[34] G.A. Korn, T.M. Korn, *Mathematical handbook for scientists and engineers*, Dover Publications, 1968, reprinted 2000.

[35] U. Krengel, *Ergodic Theorems*. Walter De Gruyter, New York, 1985.

[36] A. Papoulis, *The Fourier Integral and its Applications*, McGraw Hill, 1962.

[37] W.H. Press, S.A. Teukolsky, W.T. Vetterling, B.P Flannery, *Numerical Recipes, the Art of Scientific Computing*, Cambridge University Press, 2007.

[38] V. Serov, *Fourier Series, Fourier Transform and their Applications to Mathematical Physics*, Springer, 2017.

[39] E.M. Stein, R Shajarch, *Fourier analysis: an introduction*. Princeton University Press.

Papers.

[40] F. J. Harris, *On the Use of Windows for Harmonic Analysis with the Discrete Fourier Transform*, Proceedings of the IEEE, vol. 66, no. 1, pp.51-83, January 1978.

Machine Learning and deep learning.

[41] Y. Bengio ,I. Goodfellow, A. Courville, *Deep Learning*,. The MIT press, 2016.

[42] C.M. Bishop, *Neural networks for Pattern Recognition*, Oxford, Clarendon Press, 1995.

[43] C.M Bishop, *Pattern Recognition and Machine Learning*, Springer, 2006.

Papers

[44] T. Plötz, *Deep Learning for Human Activity Recognition in Mobile Computing*. Computer, vol.51, no.5, pp.50-59, May 2018.

[45] J. Salamon, J.P. Bello, *Deep Convolutional Neural Networks and Data Augmentation for Environmental Sound Classification*, IEEE Signal Processing letters, vol. 24, no.3, pp. 279-283, March 2017.

Biomedical engineering and science.

- [46] J. Malmivuo, R. Plonsey, *Bioelectromagnetism, Principles and Applications of Bioelectric and Biomagnetic Fields*, Oxford University Press, 1987.
- [47] A. Turner, I. Karube, G. S. Wilson, *Biosensors. Fundamentals and Applications*, .
- [48] W. Marshall, M. Lapsley, A.P. Day, R.M. Ayling, *Clinical biochemistry. Metabolic and Clinical Aspects*, Churchill Livingstone, Elsevier, 2014.
- [49] A.Natale, *Handbook of cardiac electrophysiology*. United Kingdom, Informa Healthcare, 2007.
- [50] W.L. Kennedy, L.H. Wilmore, D.L. Costill, *Physiology of Sport and Exercise*, sixth edition, Human kinetics, 2004.
- [51] C. Fortsythe H. Liao, M.C.S. Trumbo, R. E. Cardona-Rivera, *Cognitive Neuroscience of Human systems*, CRC Press, 2014.
- [52] *Fisiologia dell'Uomo*, Concu et al., Edi Ermes, 2002, Milano.

Papers

- [53] V. Gallese and A. Goldman, *Mirror neurons and the simulation theory of mind-reading*. Trends in Cognitive Science, pp. 493-501, December 1998.
- [54] S.H. Collis, M.B. Wiggin, G.S. Sawicki, *Reducing the energy cost of human walking using an unpowered exoskeleton*, Nature, 522(7555), April 2015.
- [55] A. Concu, A. Crisafulli, *Exercise-induced cardiovascular adjustments by muscle receptors stimulation*. Focus on Exercise and Health Research, ,chapter VII, pp. 181-201, 2006;
- [56] Concu et al., *Respiratory Response to Stimulation of large fibers afferent from muscle receptors in cats*. Pfluger Archive, Vol. 399, No. 4, pp. 309-314, 1983.
- [57] A. Concu et al. *New Insight into Cardiovascular Apparatus during Exercise*. Physiological and Physio-pathological Aspects., pp. 61-83, 2007; Grotle et al. *Auton Neurosci*, Vol. 228, pp. 102698, 2020
- [58] D.B.Geselowitz, and W.T. Miller III, *Active Electric Properties of Cardiac Muscle*, Bioelectromagnetics, 3:pp.127-132(1982).
- [59] R. A. Shipley, Richard, E. Clark, D. Liebowitz, J.S. Krohmer. *Analysis of the Radiocardiogram in Heart Failure*, Ciruclation Research, vol.1, No.5, September 1953.
- [60] T. Stökel, R. Jacksteit, M. Behrens, R. Skripitz, A. Mau-Moeller *The mental representation of the human gait in young and older adults*, , Frontiers in Psychology, 6:943, July, 14, 2015.

Dissertations

[61] *Valutazione dei limiti di tolleranza cardiodinamica in piloti impegnati in simulazioni di attività critiche con l'utilizzo di strumentazione dedicata*. Politecnico di Torino, Tesi di Laurea dell'Ing. Carmen Serra.

[62] *Dispositivi Meccatronici di Diagnosi e Ausilio Funzionale*, Università degli Studi di Cagliari, Tesi di dottorato del Dott. Ing. Mario Garau.

Impedance Electrical Cardiography Validation.

[63] Angius L, Cominu M, Filippi M, Piredda C, Migliaccio GM, Pinna M, Milia F, Tocco F, Concu A, Crisafulli A, *Measurement of pulmonary gas exchange variables and lactic anaerobic capacity during field testing in elite indoor football players*. Journal of Sports Medicine Phys.Fitn. 53: 461-469, 2013

[64] D.P. Bernstein, *A new Stroke Volume equation for the thoracic electrical bioimpedance: theory and rationale*. Critical care medicine, vol 14, no. 10 1986.

[65] D.P. Bernstein, *Continuous noninvasive real-time, monitoring of stroke volume and cardiac output by thoracic electrical bioimpedance*, Critical care medicine, vol. 14, no. 10, 1986.

[66] D.P. Bernstein, H.J.M. Lemmens. *Stroke Volume Equation for Impedance Cardiography*, Medical and Biological Engineering and Computation, vol. 43, 2005.

[67] F. H. Bonjer, Jw. Van den Berg, M.N.J. Dirken, *The Origin of the Variation of Body Impedance Occurring during the Cardiac Cycle*, Circulation, 1952; June. Ppg..415-420

[68] Concu A, Marcello C, Rocchitta A, Ciuti C, Esposito *Telemetric measurement of heart-rate-matched oxygen consumption during a volleyball game*. A Med. Sci. Res., 20:149-151, 1992.

[69] A. Concu, C. Marcello, *Stroke Volume Response to Progressive Exercise in Athletes Engaged in Different Types of Training*, European Journal of Applied Physiology, vol.66, pp. 11-17, 1993.

[70] Crisafulli, A, Melis F, Laconi P, Tocco F, Lai C, Concu A. *External mechanical work versus oxidative energy consumption ratio during a basketball field test*. J. Sports Med. Physical Fitness, 42: 409-417, 2002.

[71] Crisafulli A, Pittau GL, Lorrai L, Carcassi AM, Cominu M, Tocco F, Melis F, Concu A. *Poor reliability of heart rate monitoring to assess oxygen consumption during field training*, Int. J. Sport Med., 27: 55-59, 2006.

[72] Crisafulli A, Vitelli S, Cappai I, Milia R, Tocco F, Melis F, Concu A. *Physiological responses and energy cost during a simulation of a Muay Thai boxing match.*, Appl Physiol Nutr Metab. 34:143-50, 2009.

- [73] L.E. Geddes, L.E. Baker, *Thoracic impedance changes following saline injection into right and left ventricles*, Journal of Applied Physiology, Vol.33, No.3, August 1972.
- [74] K.C. Huang, M. Stoddard, K. Tsueda, M. F. HEINE, M.H. Thomas *Stroke Volume Measurements by Electrical Bioimpedance and Echocardiography in Healthy Volunteers*, Critical Care Medicine, vol. 18, no. 11, pp. 1274-1278, November 1990.
- [75] W.G. Kubicek, *On the source of Peak First Time Derivative(dZ/dt) During Impedance Cardiography*, Annals of Biomedical Engineerign, vol. 17, pp459-462, 1989.
- [76] Laconi P, Melis F, Crisafulli A, Sollai R, Lai C, Concu A *Field tests for mechanical efficiency evaluation in matching volleyball players*. Int. J. Sports Med., 19:53-56, 1998.
- [77] Marongiu E, Crisafulli A, Pinna M, Ghiani G, Degortes N, Concu A, Tocco F *Evaluation of reliability of field test to predict performance during ironman triathlon*. Sport Sci Health. 9:65-71, 2013.
- [78] Pinna M, Milia R, Roberto S, Marongiu E, Olla S, Loi A, Ortu M, Migliaccio GM, Tocco F, Concu A, Crisafulli A. *Assessment of the specificity of cardiopulmonary response during tethered swimming using a new snorkel device*. J Physiol Sci. 63:7-16, 2012.
- [79] Pisanu S, Deledda A, Loviselli A, Huybrechts I, Velluzzi F . *Validity of Accelerometers for the Evaluation of Energy Expenditure in Obese and Overweight Individuals: A Systematic Review*. J Nutr Metab. Aug 4;2020:2327017, 2020.
- [80] Marongiu E, Crisafulli A, Ghiani G, Olla S, Roberto S, Pinna M, Pusceddu M, Palazzolo M, Sanna I, Concu A, Tocco F. *Cardiovascular Responses during free-diving in the sea*. Int J Sports Med. 36:297-301, 2015.
- [81] Tocco F, Marongiu E, Pinna M, Roberto S, Pusceddu M, Angius L, Migliaccio G, Milia R, Concu A, Crisafulli A. *Assessment of circulatory adjustments during underwater apnoea in elite divers by means of a portable device*. Acta Physiol (Oxf). 207:290-298, 2013.
- [82] Tocco F, Sanna I, Mulliri G, Magnani S, Todde F, Mura R, Ghiani G, Concu A, Melis F, Crisafulli A. *Heart Rate Unreliability during Interval Training Recovery in Middle Distance Runners*. J Sports Sci Med. 14:466-72, 2015.
- [83] L. Werkö, H. Lagerhöf, H. Bucht, B. Wehle, A. Holmgren, *Comparison of the Fick and Hamilton Methods for the Determination of Cardiac Output in Man*, Scandinavian Journal of Clinical and Laboratory Investigation, vol. 1, pp. 109-113, 1949.

Energy expenditure

- [84] *External, Internal and total work in human locomotion*, Cavagna, Willems, Heglund, Journal of Experimental Biology, 198, pp. 379-383, 1995.
- [85] S.H. Collins, M. Bruce Wiggin, G.S. Sawicki *Reducing the energy cost of human walking using an unpowered exoskeleton*, Nature, 522(7555). pp. 212-215, June 2015.

[86] Concu A. Manuello A., Solinas R. Wu W.C. Meloni L. Fois A. Loviselli A., Deledda A. Velluzzi F. Metabolic power and energy cost of mechanical work carried out by a sailor engaged in a solo ocean race: a case of study., *International Journal of Mechanics and Control*, vol. 19, pp-19-32.

Dissertation.

[87] *Analisi degli Aspetti Cinematici, Energetici, Dinamici e fisiologici dei Trampoli a Recupero Energetico*, Università degli Studi di Cagliari, tesi di laurea dell'ing. Matteo Lecca, 2020.

Indirect calorimetry.

[88] A. Krogh, *The respiratory exchange of Animals and Man*, Longmans, Paternoster Row, Greens and Co, 1916.

Papers

[89] K.Y. Chen, D.R. Bassett, *The Technology of Accelerometry-Based Activity Monitors: Current and Future*. *Medicine & Science in Sport and Exercise*, vol. 37, Issue 11, pp 490-50, November 2005.

[90] J. H. Choi, Heongwhan Lee, H. T. Hwang, J. P. Jim, Jae Chan Park, Kunsoo Shin. *Estimation of Activity Energy Expenditure: Accelerometer Approach*. *IEEE Engineering in Medicine and Biology*, 27th annual conference, pp.3830-3833, 2005.

[91] G. Geršak and J. Drnovšek, *Sensewear body monitor in psychophysiological measurements*, , IFMBE Proceedings, vol. 57, September 2016.

[92] D.L. Johannsen, M.A. Calabro, J. Stewart, W. Franke, H.C. Rood, *Accuracy of Armband Monitors for Measuring Daily Energy Expenditure in Healthy Adults*, *Medicine and Science in Sport and Exercise*, 42(11): pp.2134-40, April 2010.

[93] H. Kare, M. Patricia, *Validation of the SenseWear Pro3 Armband Using an incremental exercise test*. *Journal of strength and conditioning research*, vol.28, Issue 10, pp. 2806-2814, October 2014.

Human gait.

[94] N. Özkaya, D. Leger, D. Goldsheyder, M. Nordin, *Fundamentals of Biomechanics, equilibrium, motion, deformation* , Springer, 2017.

[95] A. Concu, M. Garau, A. Manuello, M. Ruggiu. *Correlation between Mechanical and Metabolic Energy During the Gait Cycle with and Without Jumping Stilts*, *International Journal of Mechanics and Control*, Vol. 19, pp. 33-38, 2018.

Sensor technology.

- [96] L.A. Geddes, L.E. Baker, *Principles of applied biomedical instrumentation*. Wiley Publications, 1991.
- [97] J.W. Gardner, V.K. Varadan, O.O. Awadelkarim, *Microsensors MEMS and Smart Devices*, Wiley publications.
- [98] J. Hoffmann, *Taschenbuch der Messtechnik*, Fachbuch Verlag Leipzig.
- [99] D. Prutchi, M. Norris, *Design and Development of Medical Electronic Instrumentation, a Practical Perspective of the Design, Construction and Test of Medical Devices*. John Wiley publications.
- [100] D.B. Geselowitz, *An application of Electrocardiographic Lead Theory to Impedance Plethysmography*, IEEE transactions on Biomedical Engineering, vol. BME-18, no.1, January 1971.

Dissertation.

- [101] *Untersuchungen zum Einsatz elektromagnetischer Mikroaktoren*. Dissertation von Dipl.-Ing. T. Frank, Technische Universität Hannover, 2002.

Datasheets and technical documentation.

- [102] User manual of WT901SDCL, inclinometer sensor, accelerometer, data logger, WIT Motion
- [103] UM1744 steval MKI121V1 Communication Protocol, user manual.
- [104] LSM303DLHC-Ultra compact high performance eCompass module: 3D accelerometer and 3D magnetometer.

Appendix A: MATLAB code for the computation of Stroke volume.

```
clear
close all
clc

f1 = "DImpFour.mat";
f2 = "FilteredImp.mat"

w = "StrokeVolume.mat"
w1 = "StrokeVolume.jpg"
w2 = "index.mat"

for i=17:60
    S = string(i);

    fileNamesDImp(i,1)= strcat(S,f1);
    fileNamesFilImp(i,1) = strcat(S,f2);

    Q = strcat(S,w)
    fileNamesSV(i,1)=Q

    fileNamePictureSV(i,1) = strcat(S,w1);
    fileNamesIndex(i,1) = strcat(S,w2);

end

for aa = 17:60

    File=fileNamesDImp(aa,1)
    load(string(File))

    File=fileNamesFilImp(aa,1)
    load(string(File))

    %% find the peaks on the graph

    figure(1)
    bb = size(DImp,1)
```

```

DImpP = DImp;

for ac = 1:bb
    if DImp(ac)<0
        DImpP(ac)=0;
    end
end
[pkk,loc]=findpeaks(DImp) ;

u = size(loc,1);

gg = zeros(3200,1);
for i = 1:u-1
    df= [1;loc;3200];
    for ab = df(i):df(i+1)
        if ab ==df(i+1) && pkk(i)>20
            gg(ab) = pkk(i);
        end
    end
    % plot(gg);
end
% hold
[pkk2, loc2] = findpeaks(-DImp);

u2 = size(loc2,1);

gg2 = zeros(3200,1);

for i = 1:u2-1
    df= [1;loc2;3200];
    for ab = df(i):df(i+1)
        if ab ==df(i+1)% && pkk(i)>0
            gg2(ab) = pkk2(i);
        end
    end
end
% plot(-gg2);
end

hh = gg-gg2;
[pkk4, loc4] = findpeaks(gg);

%% compute the stroke volume

%% find only positive peaks
z0 =0;

DzMax =0;

cc = size(pkk4,1);
loc5 = [1;loc4;3200]
SVol= zeros(cc,1);
for oo =1:cc-1
    ga = loc5(oo,1);
    gb = loc5(oo+1,1);
    z0 = mean(Imp(ga:gb,1));

```

```

DzMax=DImp (gb) ;
DzM(oo) = DzMax;
zZero(oo) = z0;

% find the stroke volume with the data provided

Ttime = 0.3;

SVola=7000*Ttime*DzMax/0.1/z0;
SVol(oo,1) = SVola;

end

%% create the stroke volume data set according to the time
fff= size(DImp,1);
ress= zeros(fff,1);
ca=1;
loc6 = [loc4; 3200];
for vhs = 1:fff
    fa = loc6(ca+1,1)
    if vhs ==fa
        ress(vhs,1)= SVol(ca,1);
        ca = ca+1;
    end
end

[pkk7,loc7]= findpeaks(ress);

pic = fileNamePictureSV(aa,1);

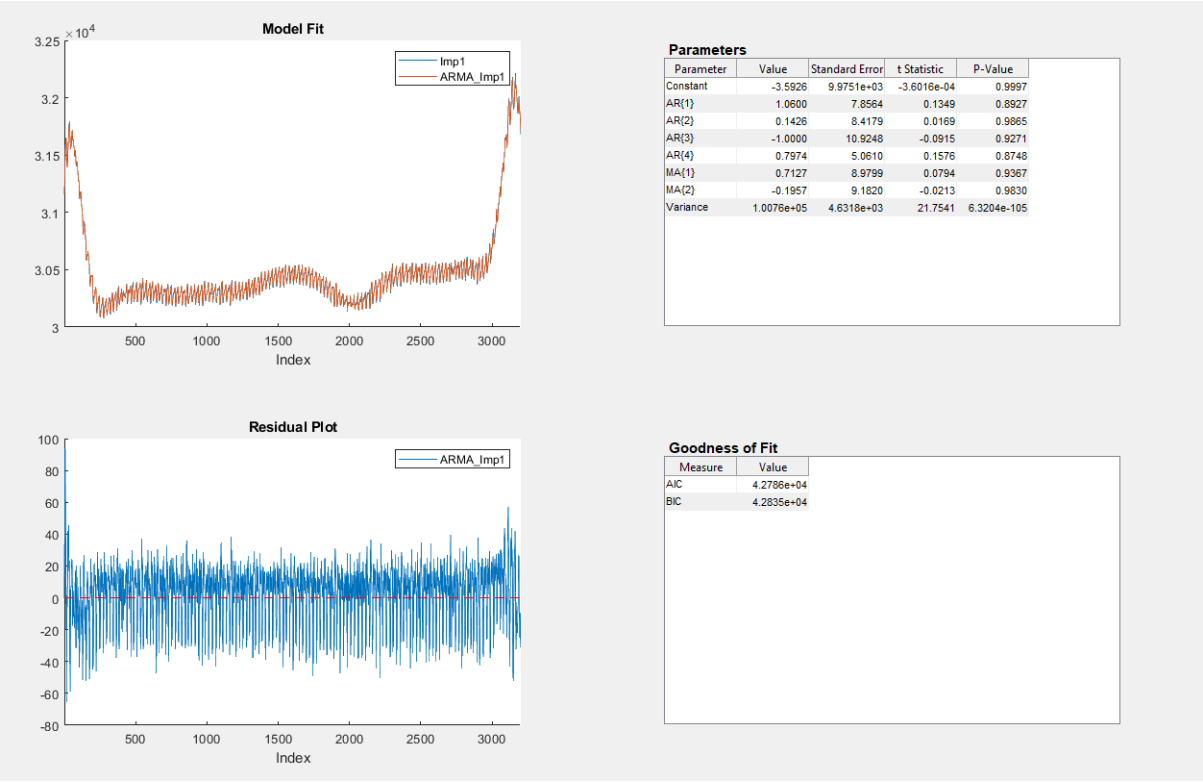
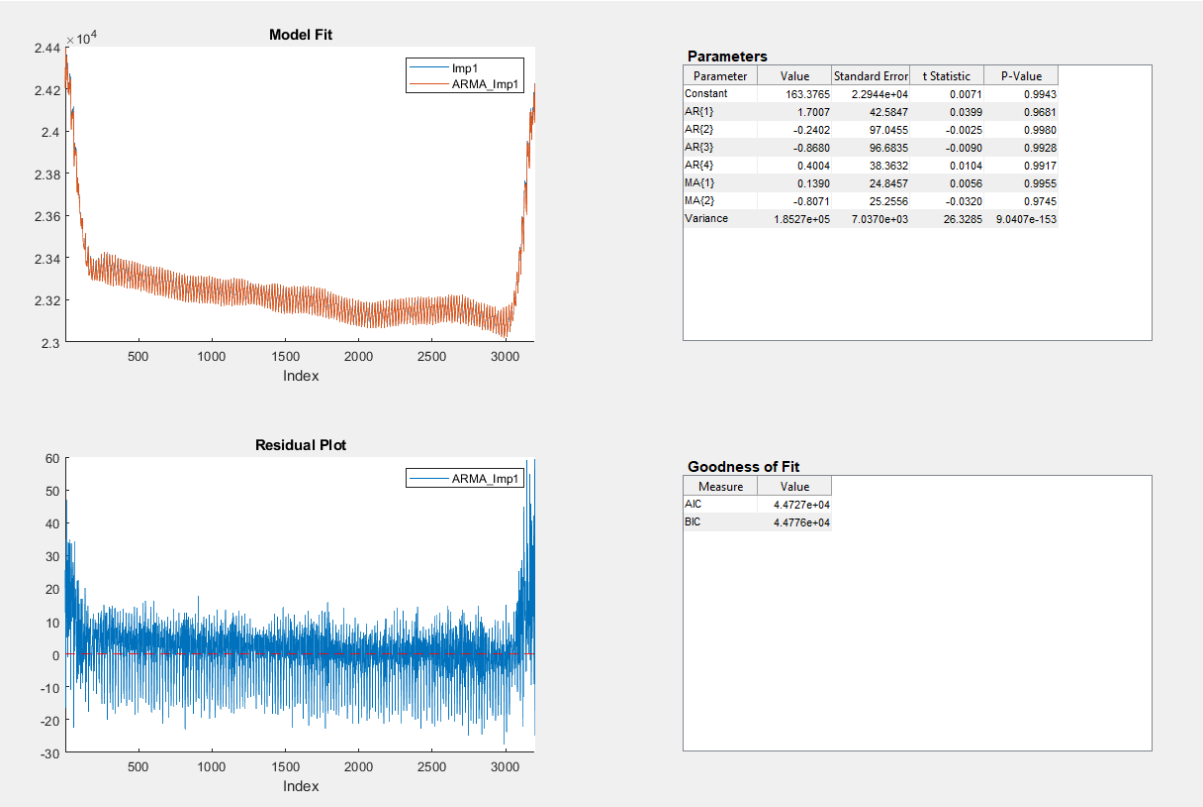
figure(1)
plot(SVol)
grid on
g=gcf;
exportgraphics(g,pic)
%% saving the mat file
ccv = fileNamesSV(aa,1);
ccvy = fileNamesIndex(aa,1);

save(string(ccv), 'ress')
Ind = loc7;
save(string(ccvy), 'Ind')

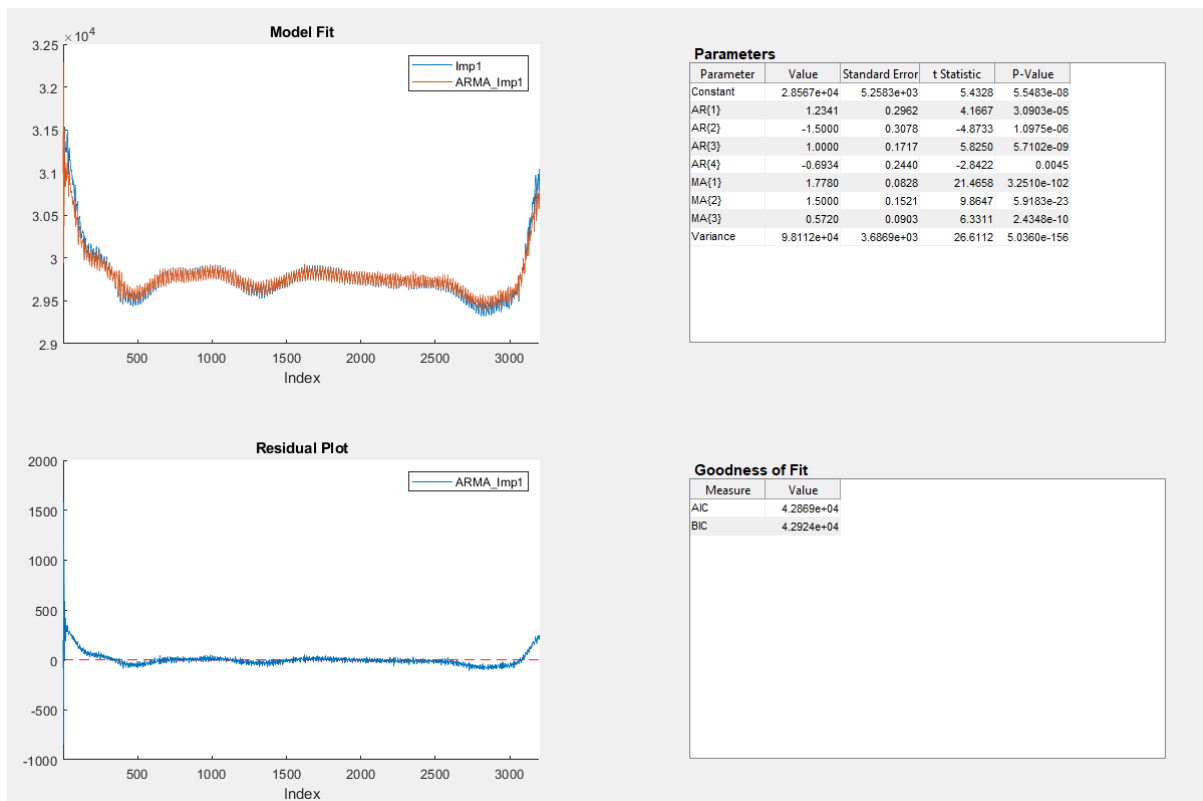
end

```

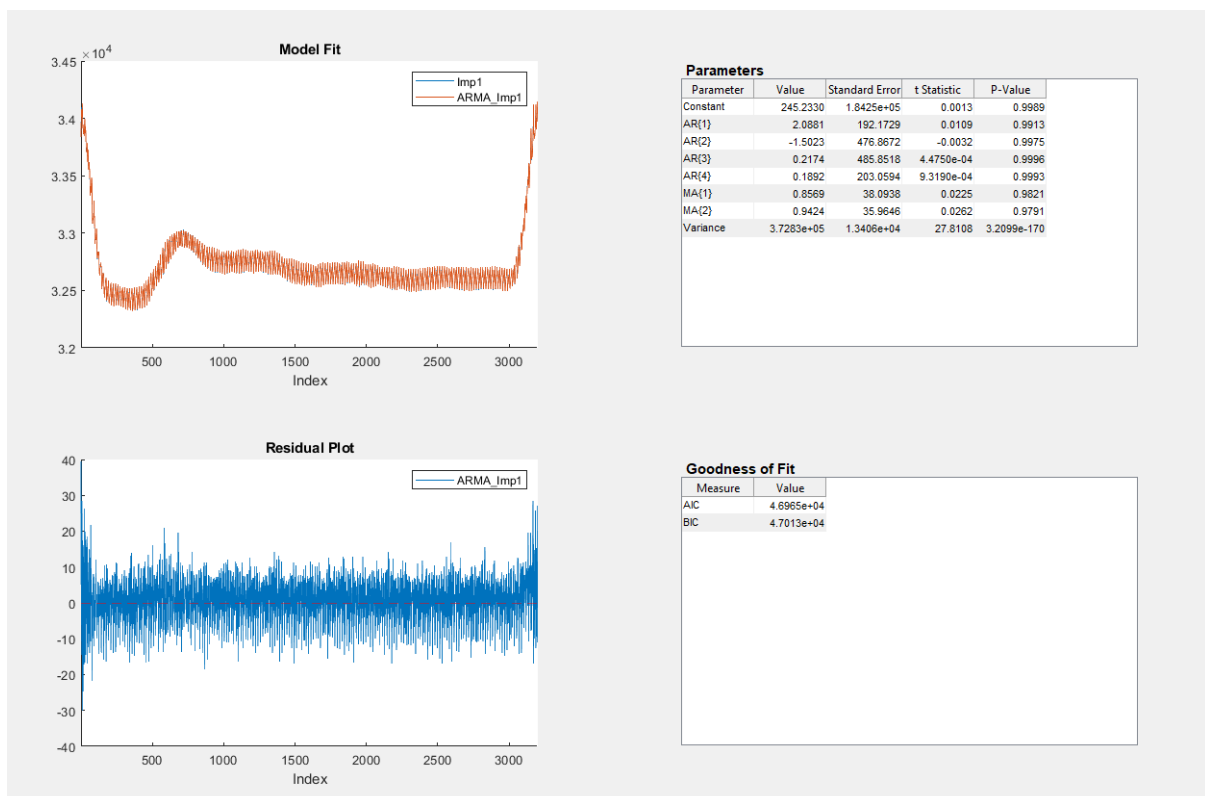
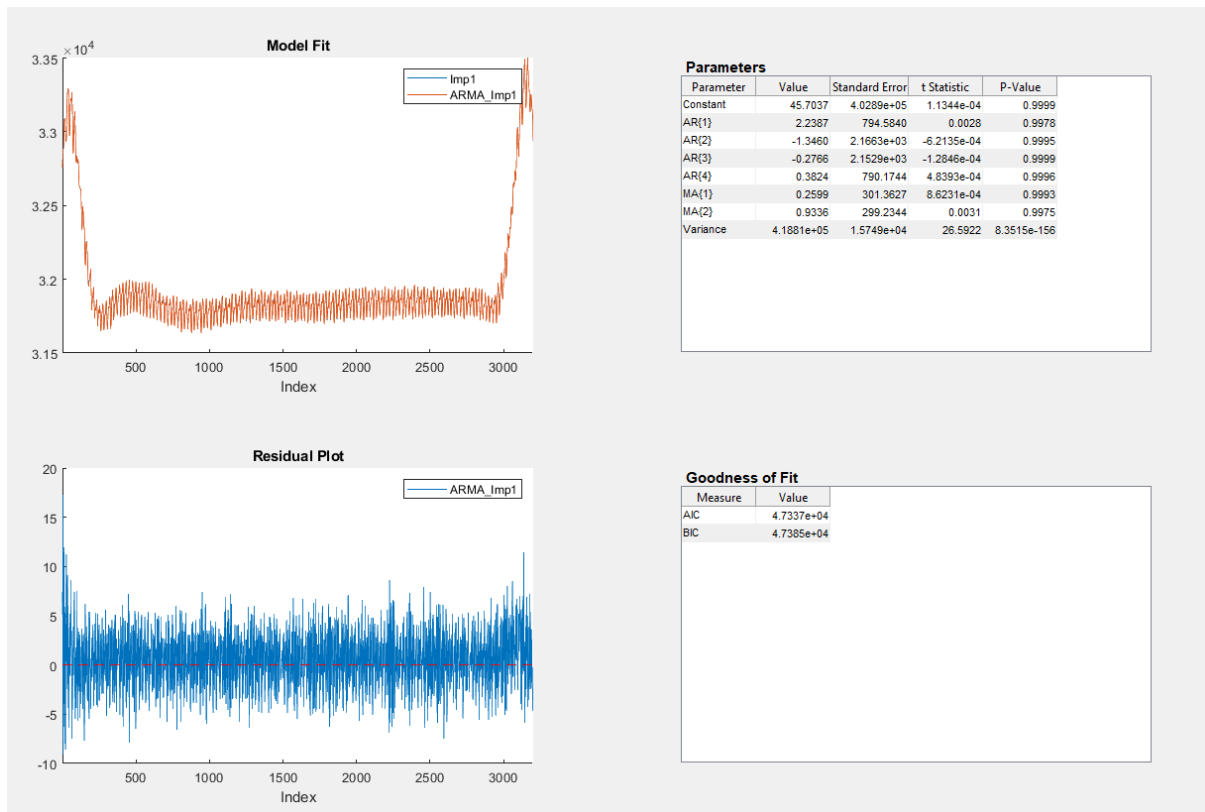
Appendix B: ARMA models of the filtered data.



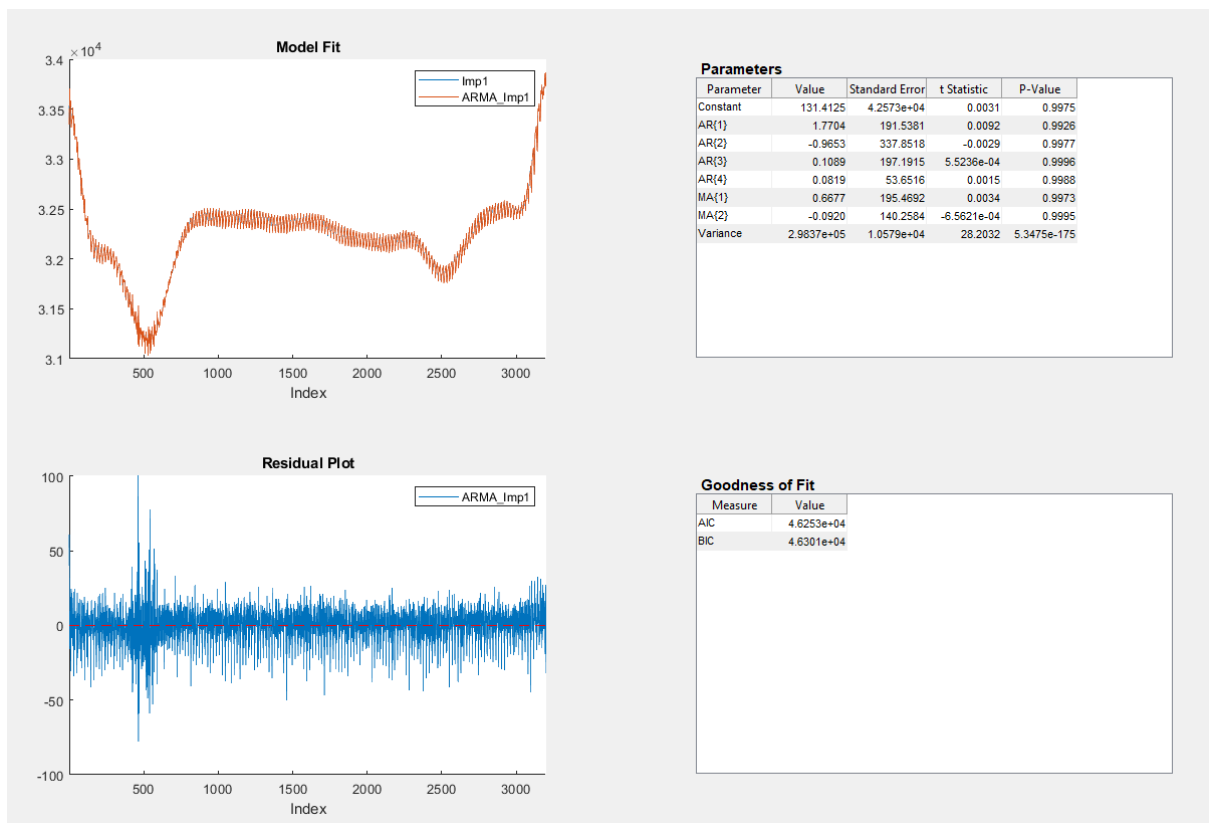
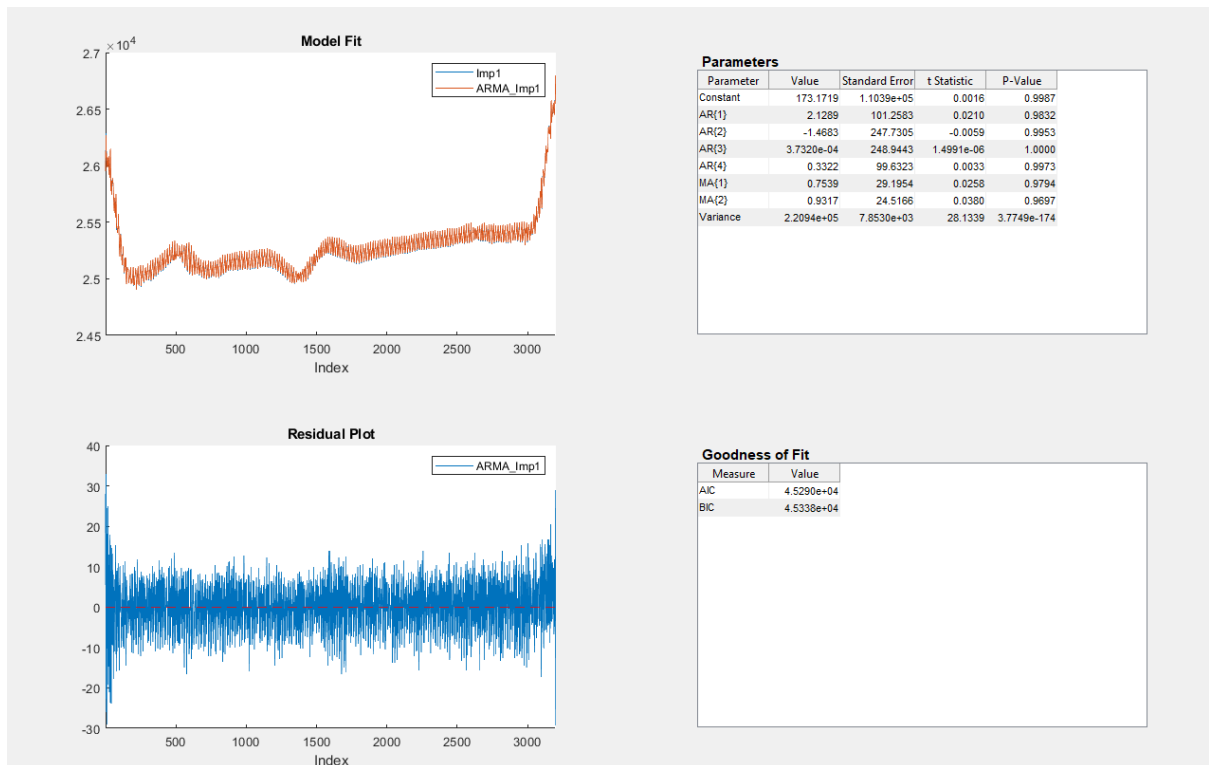
ARMA model for samples 1 and 2.



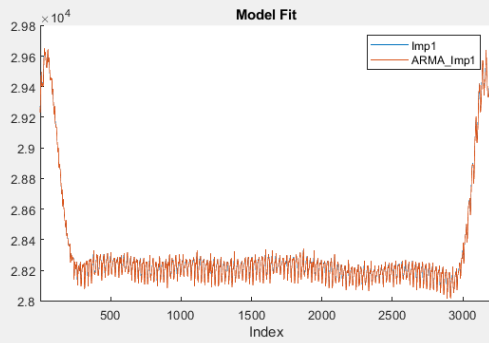
ARMA model for samples 3 and 4.



ARMA model for samples 5 and 6.

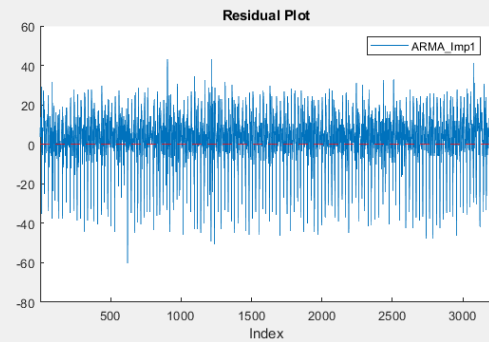


ARMA model for samples 7 and 8.



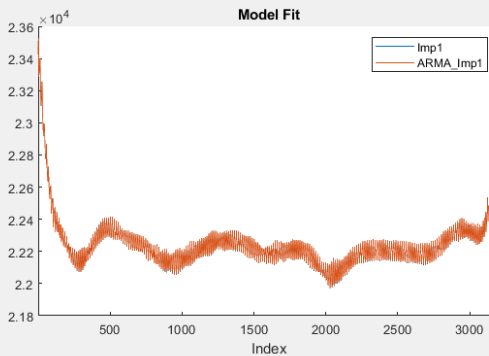
Parameters

Parameter	Value	Standard Error	t Statistic	P-Value
Constant	5.1732	9.2212e+03	5.6101e-04	0.9996
AR(1)	2.6633	123.4389	0.0216	0.9828
AR(2)	-2.4047	255.7516	-0.0094	0.9925
AR(3)	0.7554	207.0144	0.0036	0.9971
AR(4)	-0.0142	78.3526	-1.8155e-04	0.9999
MA(1)	-1.3363	117.3347	-0.0114	0.9909
MA(2)	0.5401	73.1133	0.0074	0.9941
Variance	3.7744e+05	1.5628e+04	24.1508	7.3214e-129



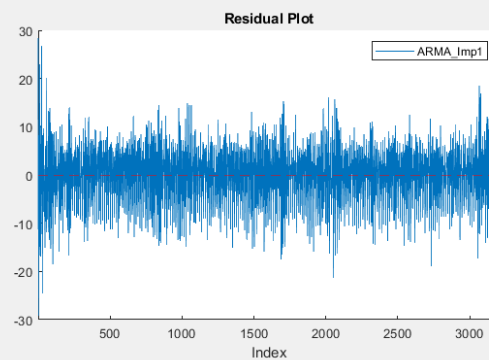
Goodness of Fit

Measure	Value
AIC	4.7005e+04
BIC	4.7054e+04



Parameters

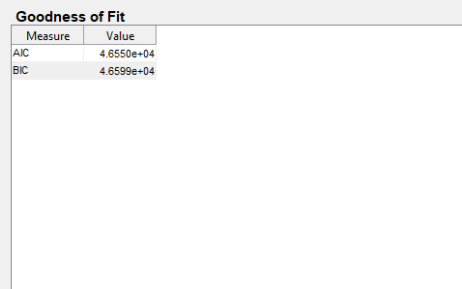
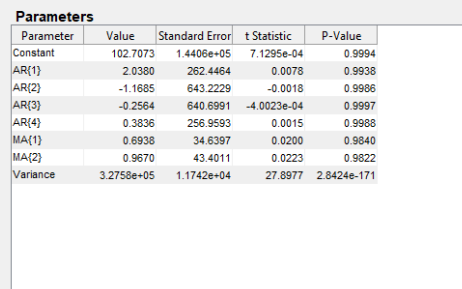
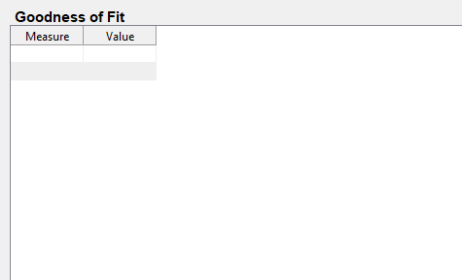
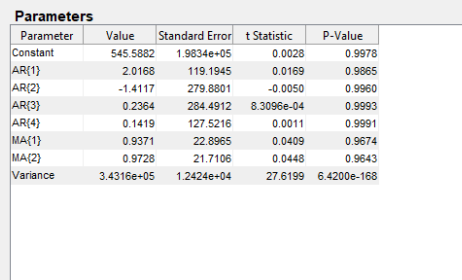
Parameter	Value	Standard Error	t Statistic	P-Value
Constant	85.9549	1.8983e+05	4.5280e-04	0.9996
AR(1)	1.8872	220.8025	0.0085	0.9932
AR(2)	-1.2063	479.7024	-0.0025	0.9980
AR(3)	0.1520	474.3125	3.2036e-04	0.9997
AR(4)	0.1633	204.2354	7.9961e-04	0.9994
MA(1)	0.9434	54.1736	0.0174	0.9861
MA(2)	0.9758	46.0863	0.0212	0.9831
Variance	4.5862e+05	1.6321e+04	28.0999	9.8281e-174



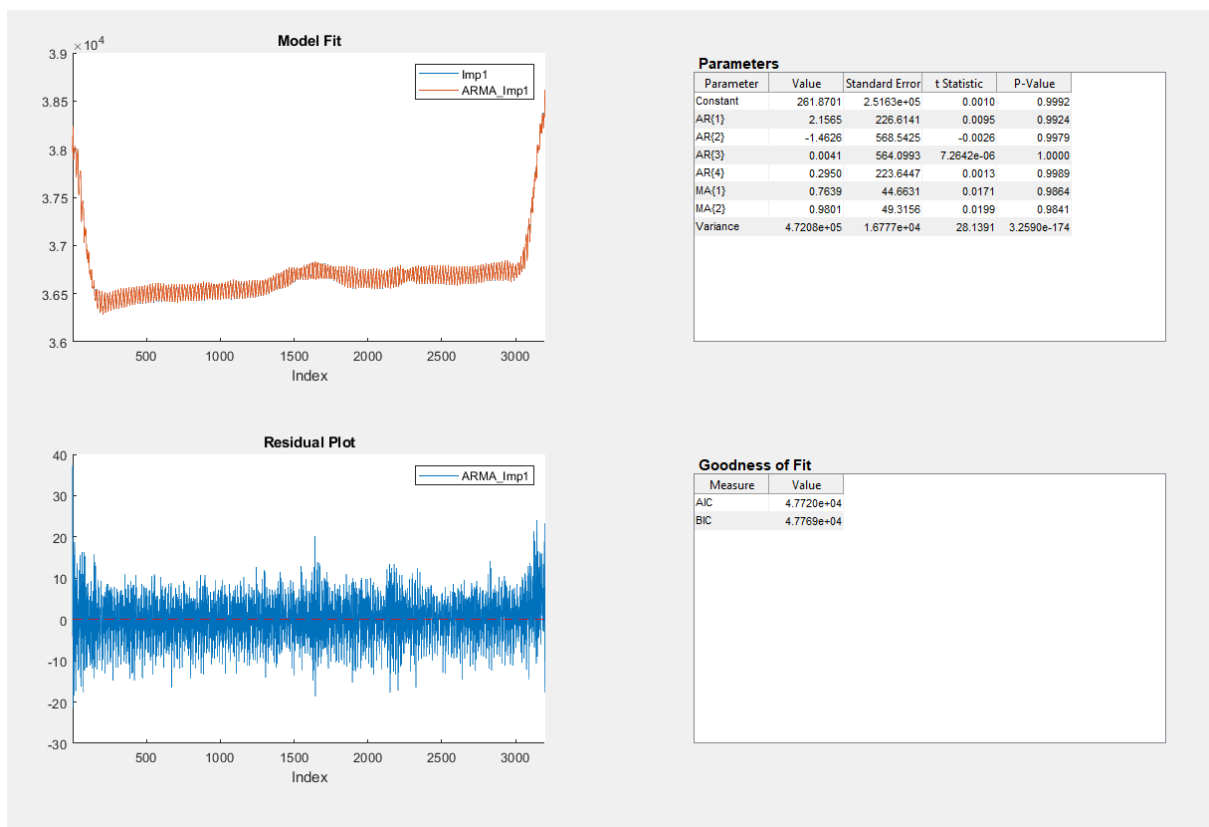
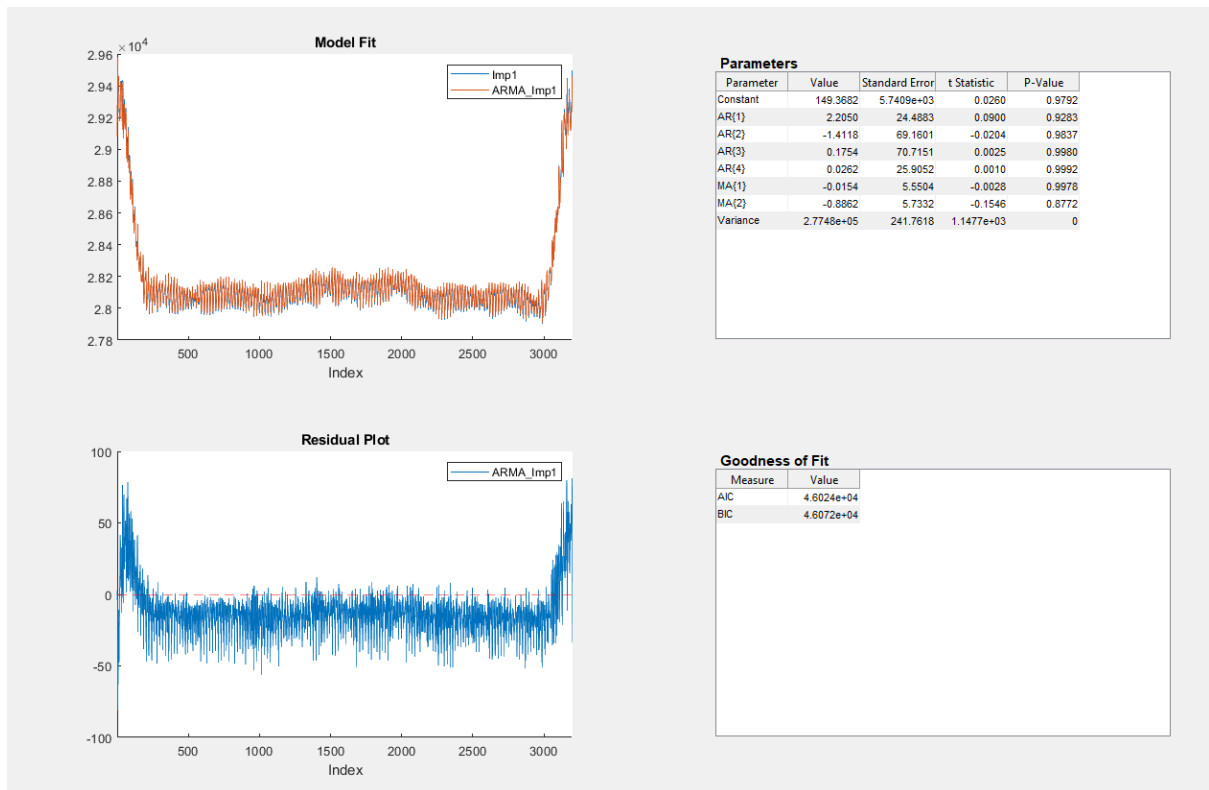
Goodness of Fit

Measure	Value
AIC	4.7627e+04
BIC	4.7676e+04

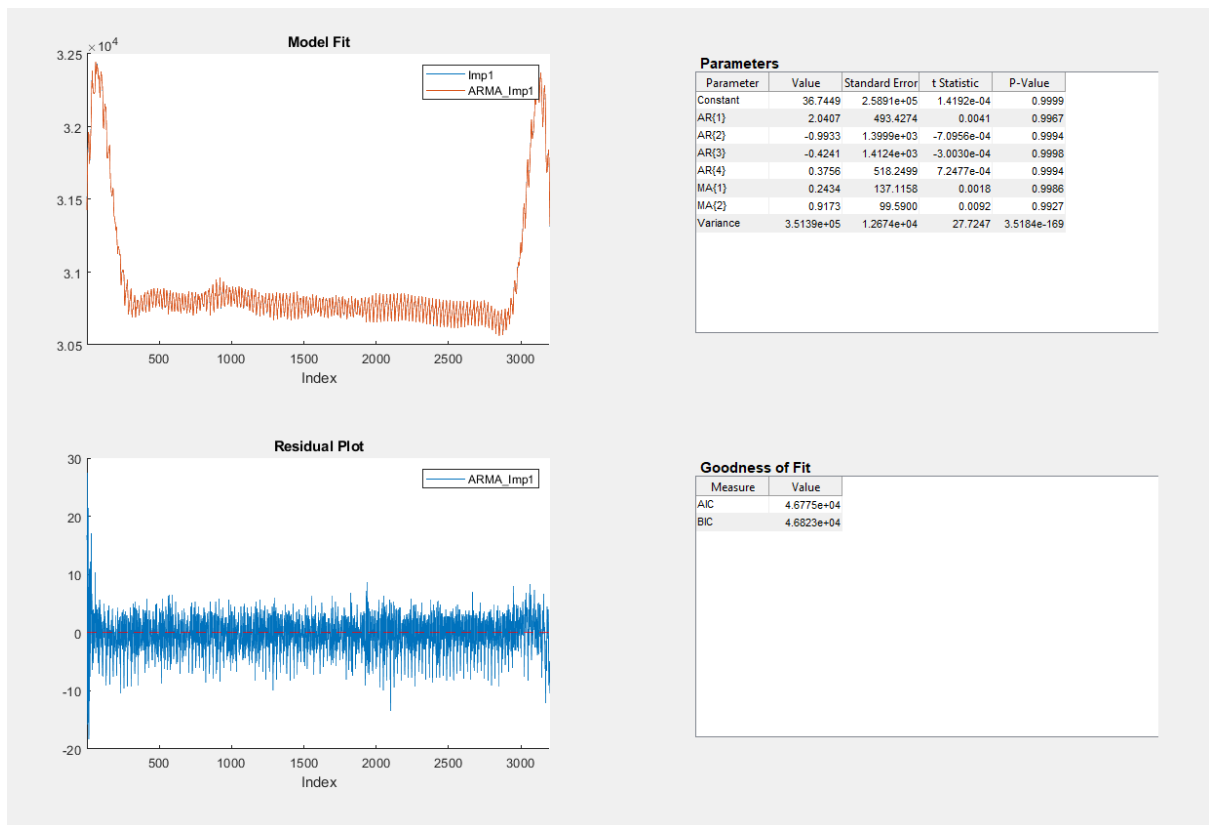
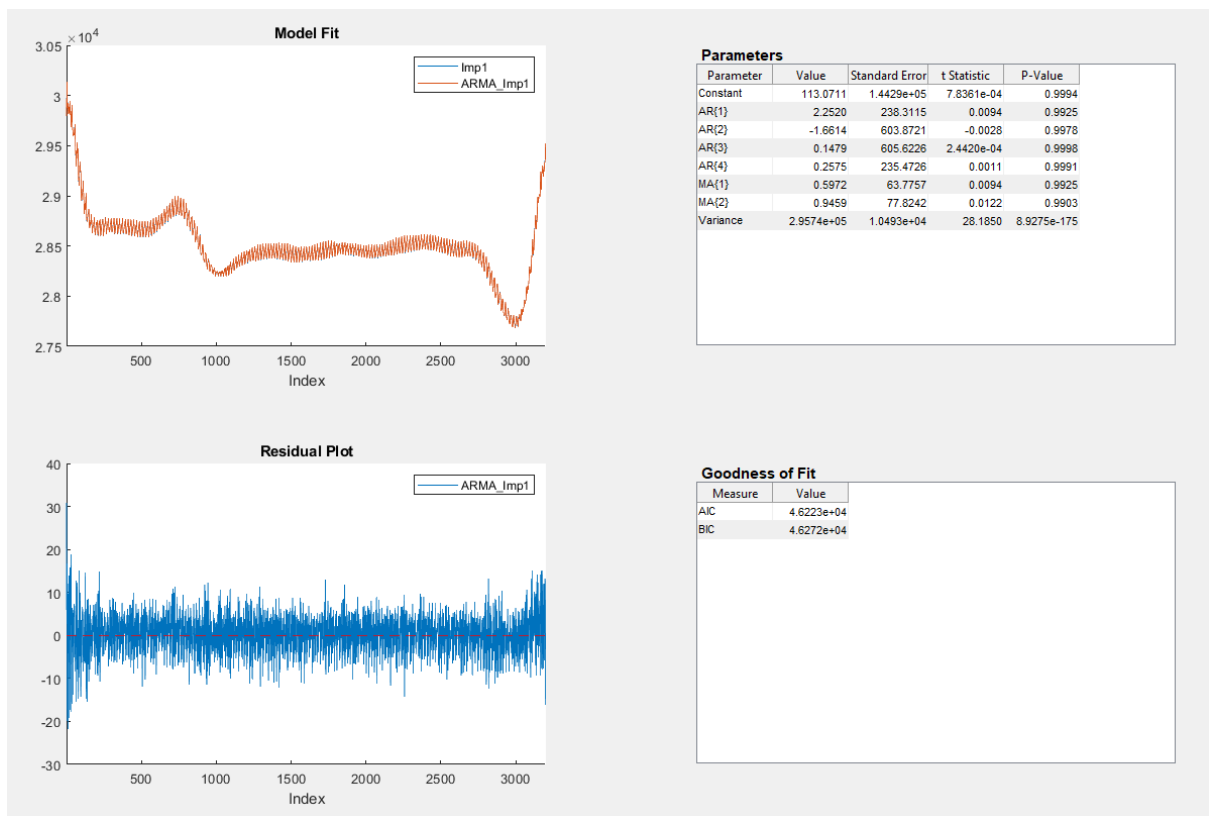
ARMA model for samples 9 and 10.



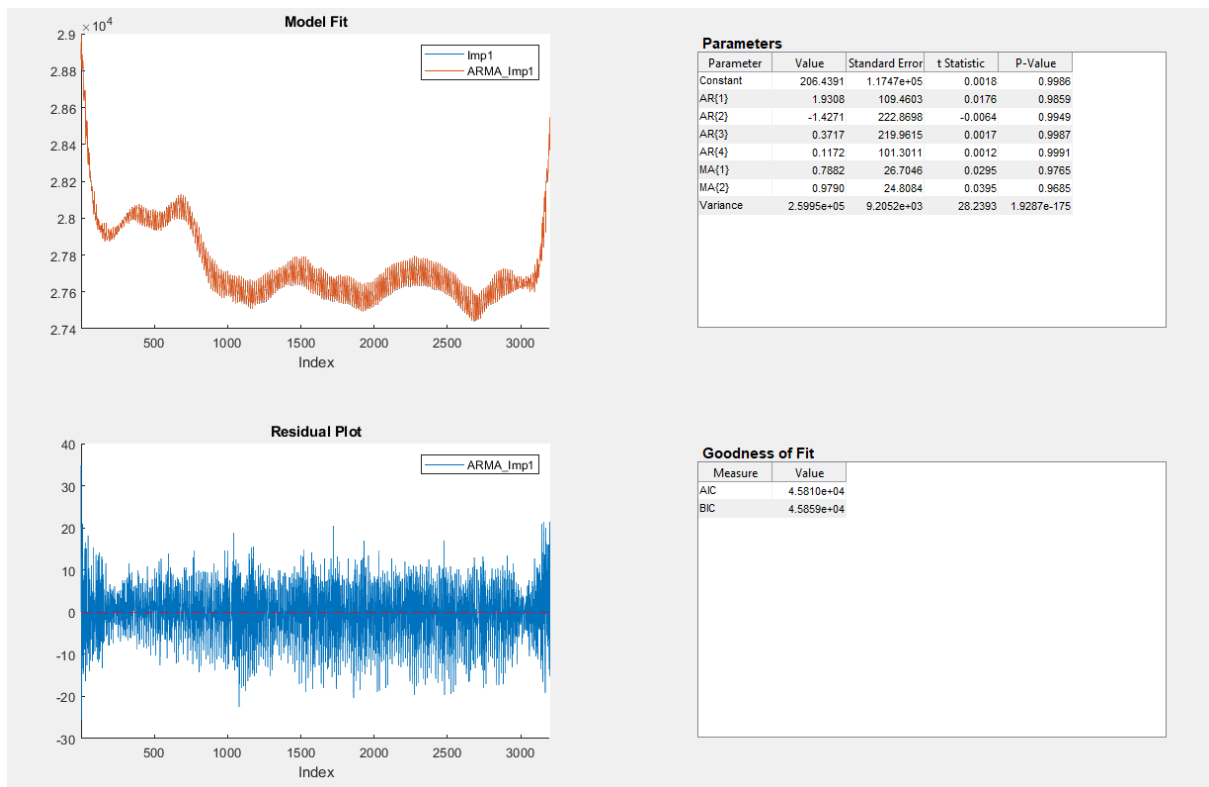
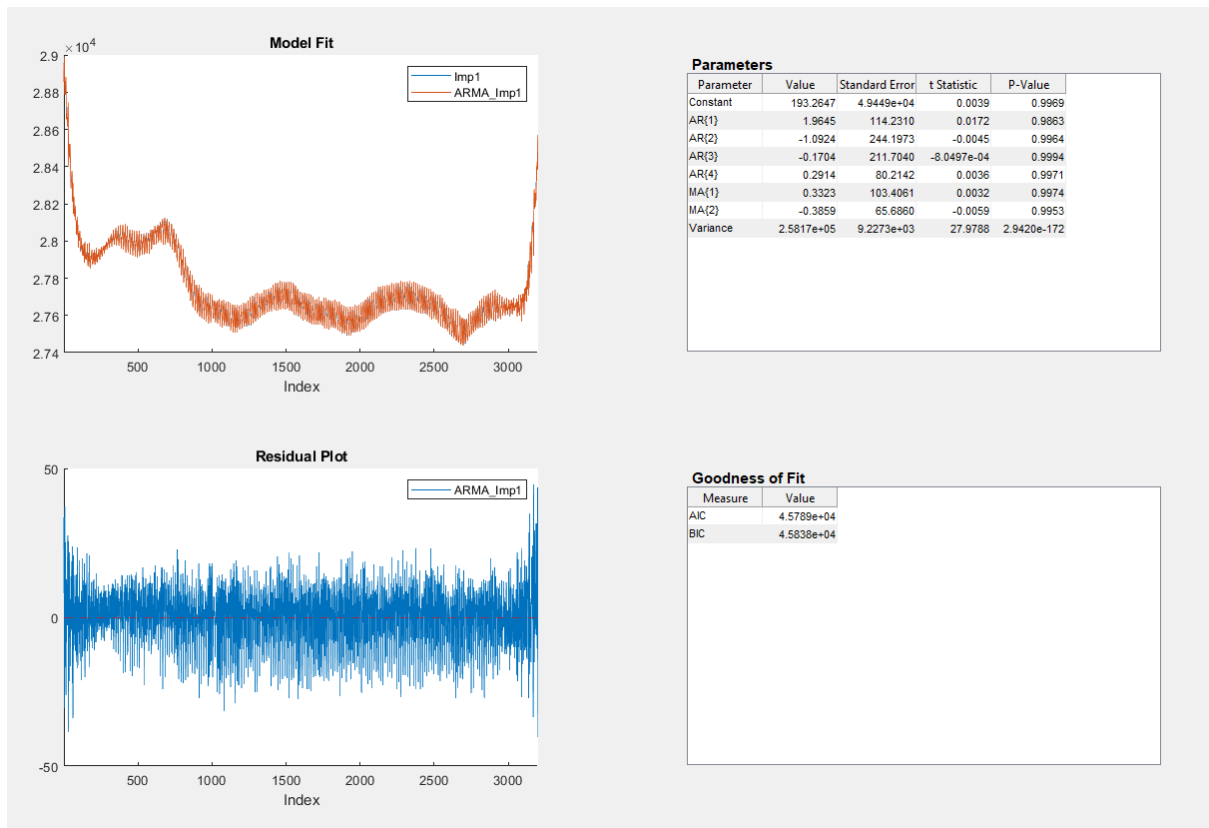
119



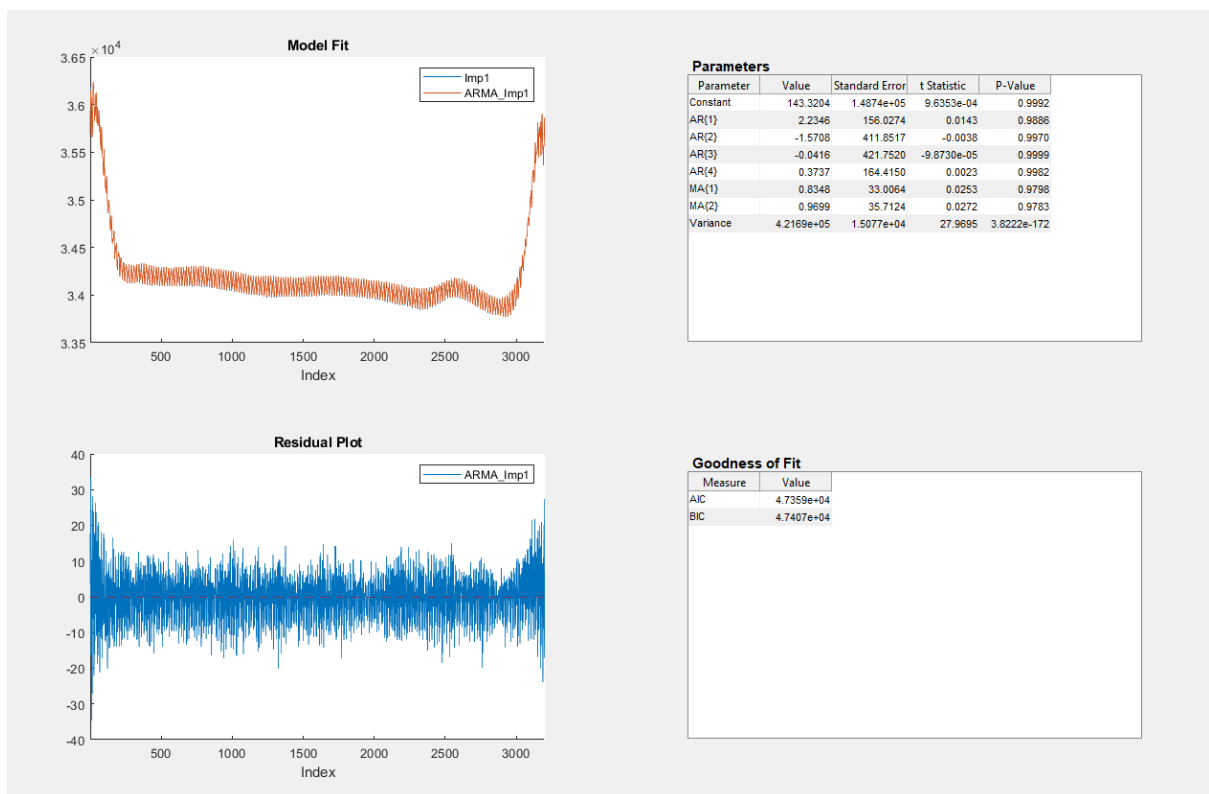
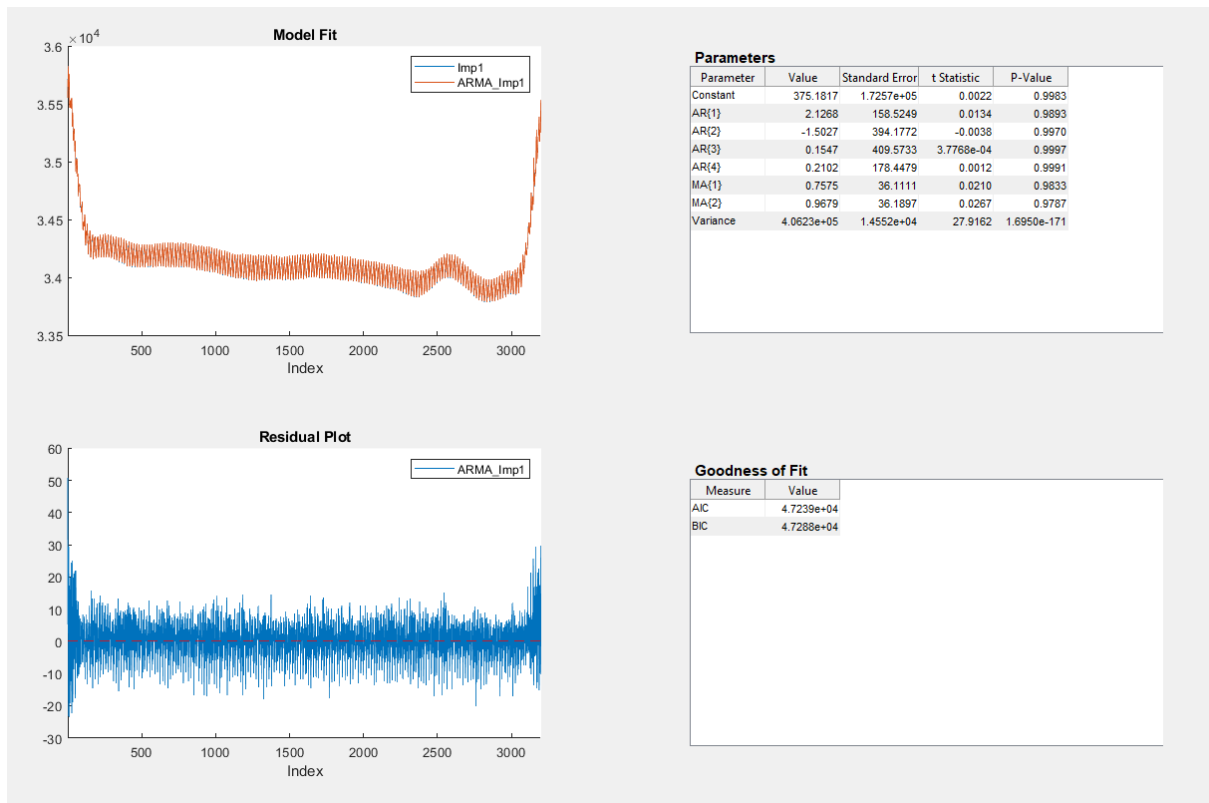
ARMA model for samples 13 and 14.



ARMA model for samples 15 and 16.



ARMA model for samples 17 and 18.



ARMA model for samples 19 and 20.

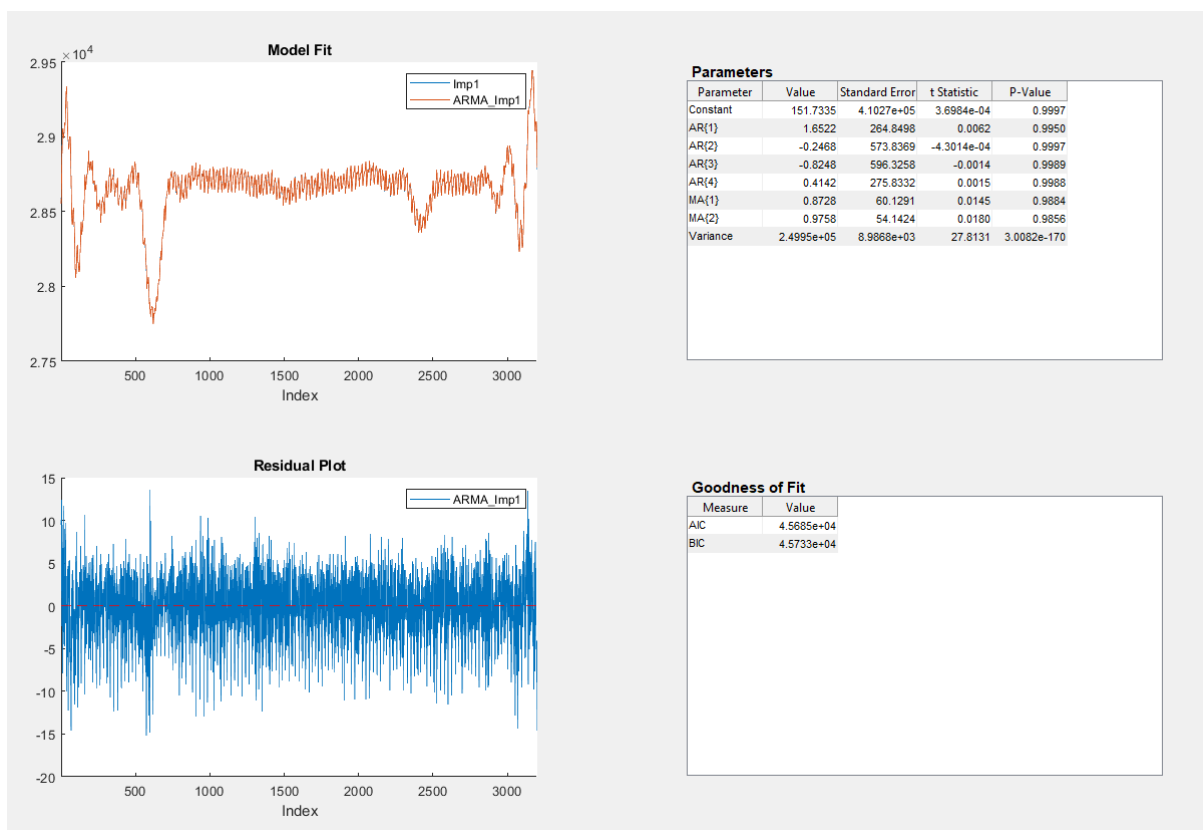
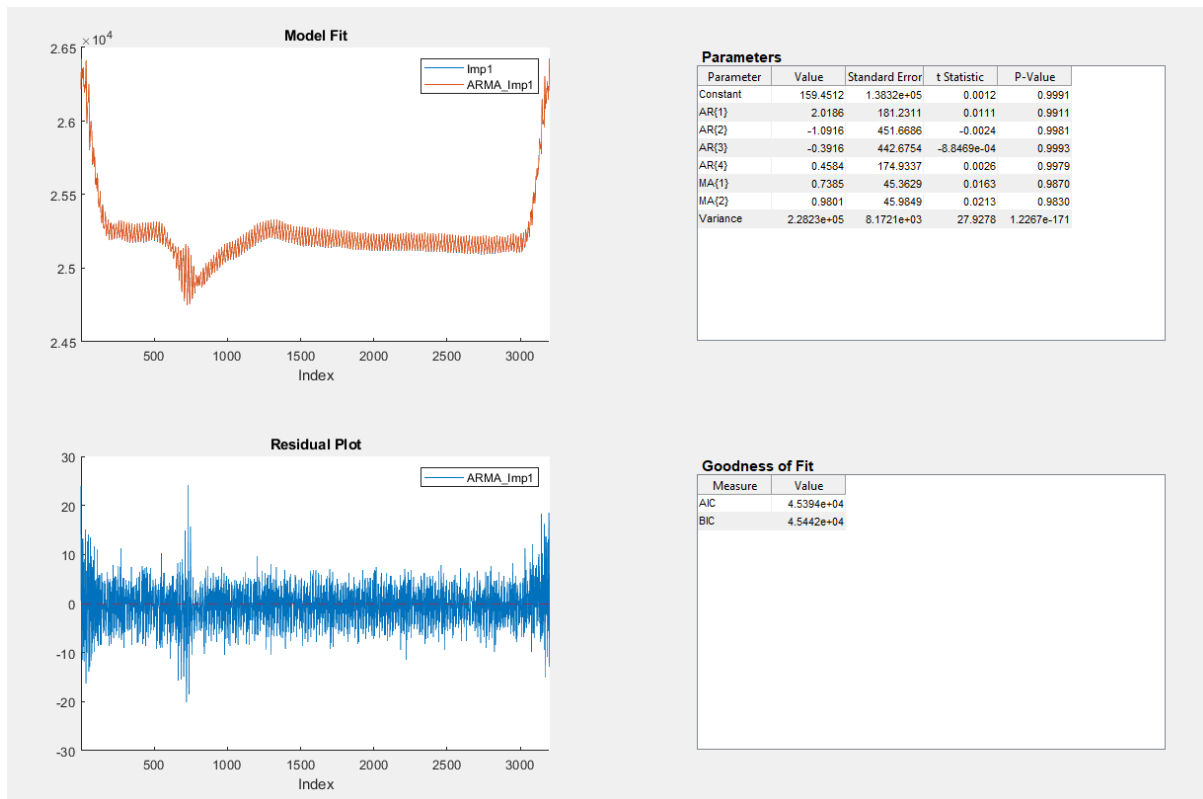


Figure-ARMA model for samples 21 and 22.



Model Fit

Imp1
ARMA_Imp1

Parameters

Parameter	Value	Standard Error	t Statistic	P-Value
Constant	24.8023	32.1362	0.7718	0.4402
AR(1)	2.0000	0.0374	53.5182	0
AR(2)	-1.2945	0.0836	-15.4880	4.1784e-54
AR(3)	0.0443	0.0791	0.5597	0.5757
AR(4)	0.2491	0.0336	7.4211	1.1614e-13
MA(1)	1.2875	0.0054	236.6229	0
MA(2)	0.9785	0.0054	181.7599	0
Variance	40.8135	1.6384	24.9099	5.8108e-137

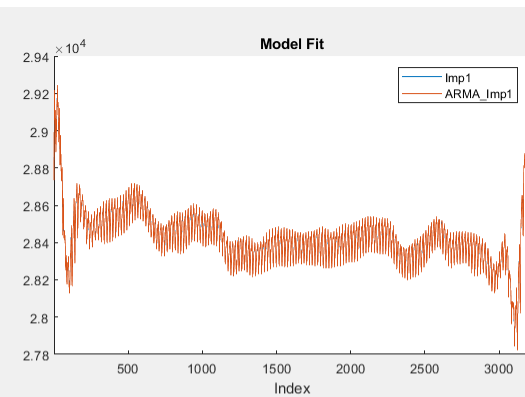
Residual Plot

ARMA_Imp1

Goodness of Fit

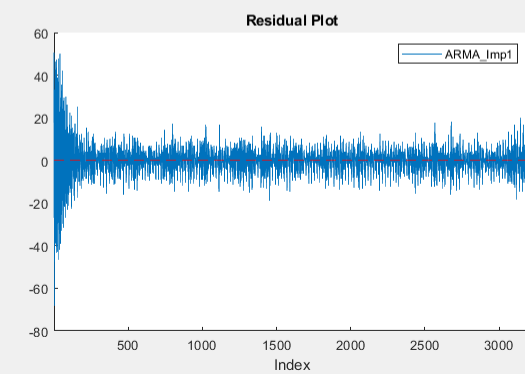
Measure	Value
AIC	1.9156e+04
BIC	1.9205e+04

Figure-ARMA model for samples 23 and 24.



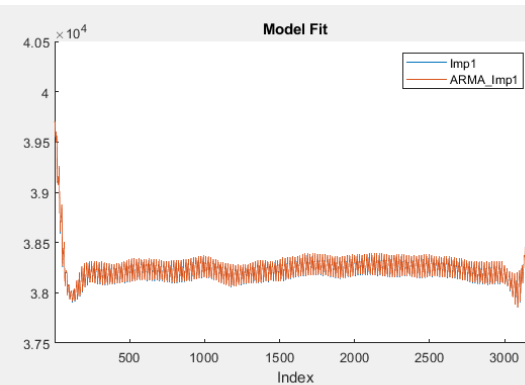
Parameters

Parameter	Value	Standard Error	t Statistic	P-Value
Constant	70.8934	28.9920	2.4453	0.0145
AR(1)	2.1709	0.0089	242.9429	0
AR(2)	-1.7759	0.0204	-87.0995	0
AR(3)	0.9149	0.0217	42.0989	0
AR(4)	-0.3124	0.0100	-31.3048	4.0120e-215
MA(1)	1.3955	4.2833e-04	3.2580e+03	0
MA(2)	0.9784	3.4434e-04	2.8357e+03	0
Variance	37.1323	0.8523	43.5665	0



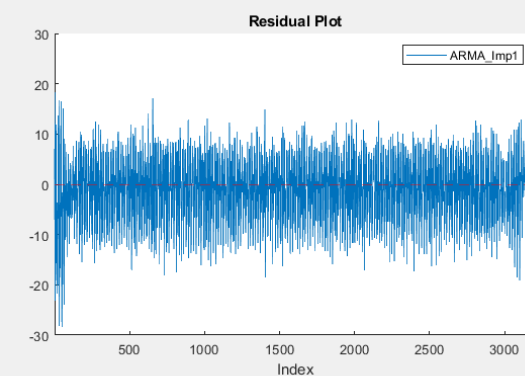
Goodness of Fit

Measure	Value
AIC	2.2046e+04
BIC	2.2094e+04



Parameters

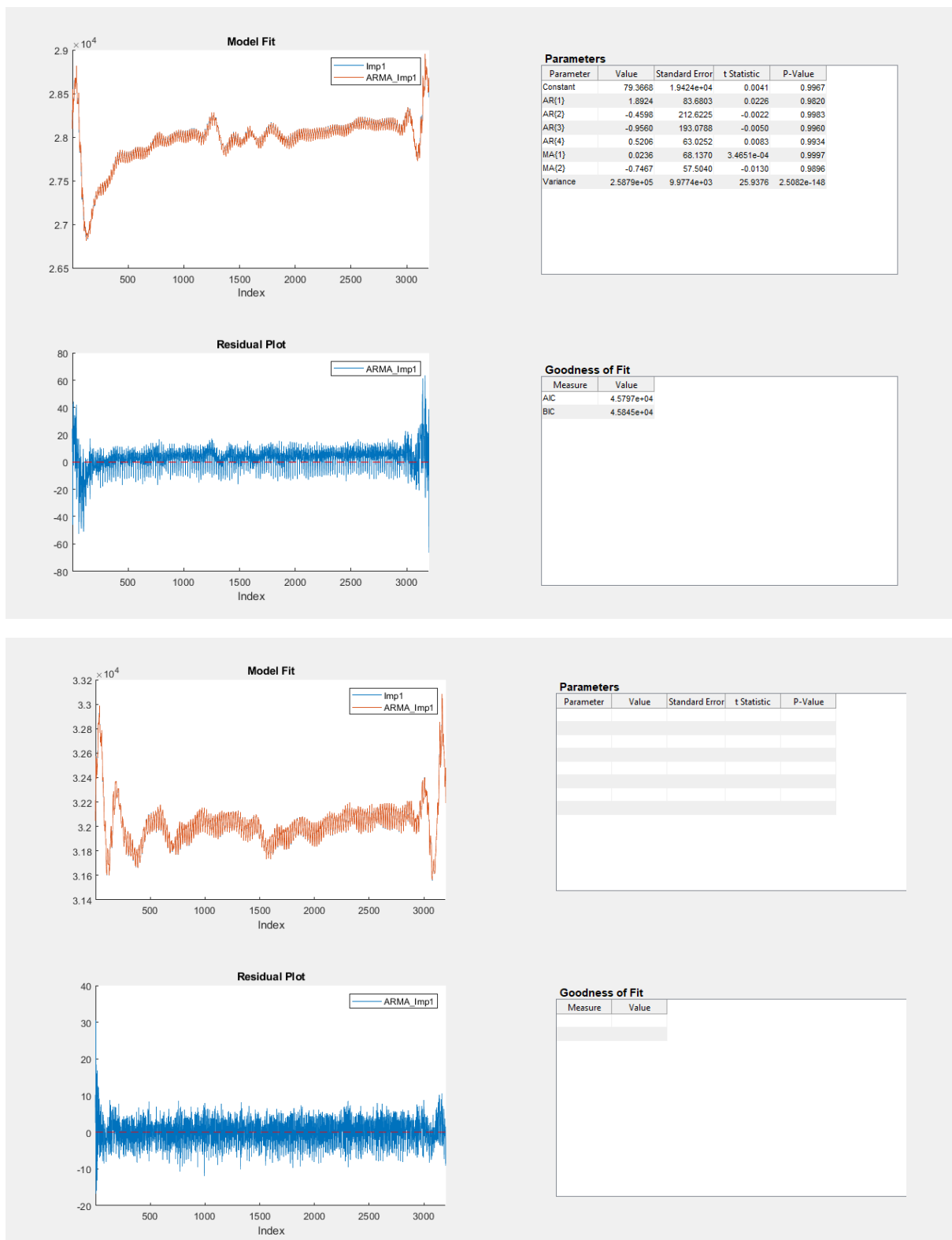
Parameter	Value	Standard Error	t Statistic	P-Value
Constant	173.7152	26.4914	6.5574	5.4751e-11
AR(1)	2.0003	0.0264	75.6829	0
AR(2)	-1.3210	0.0670	-19.7191	1.4786e-36
AR(3)	-0.0072	0.0674	-0.1076	0.9144
AR(4)	0.3236	0.0267	12.1280	7.5064e-34
MA(1)	1.1927	0.0287	41.5891	0
MA(2)	0.7156	0.0194	36.9493	7.4743e-299
Variance	35.8090	1.1086	32.3019	6.5818e-229



Goodness of Fit

Measure	Value
AIC	2.1107e+04
BIC	2.1155e+04

Figure-ARMA model for samples 25 and 26.



Model Fit

Imp1
ARMA_Imp1

Parameters

Parameter	Value	Standard Error	t Statistic	P-Value

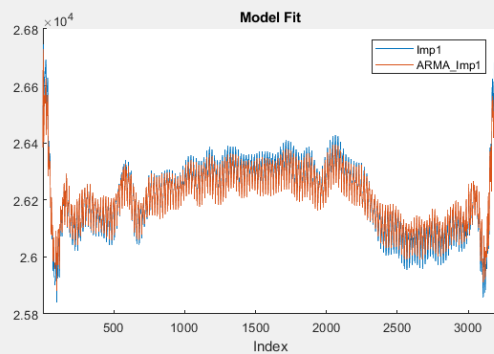
Residual Plot

ARMA_Imp1

Goodness of Fit

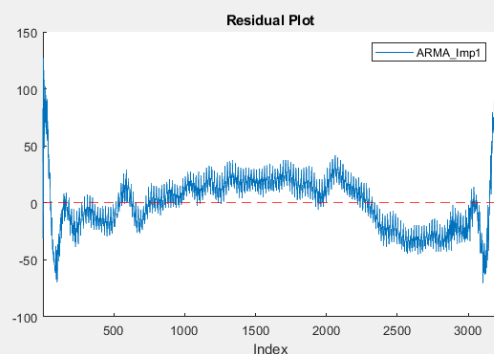
Measure	Value

Figure-ARMA model for samples 27 and 28.



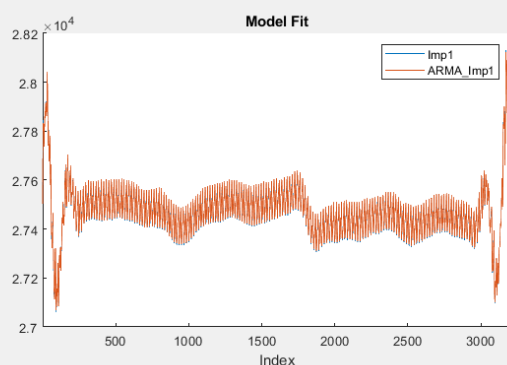
Parameters

Parameter	Value	Standard Error	t Statistic	P-Value
Constant	2.5398e+04	379.3308	66.9548	0
AR(1)	0.0279	0.0375	0.7430	0.4575
AR(2)	1.0124	0.0501	20.2133	7.4837e-91
AR(3)	-0.3908	0.0071	-55.0329	0
AR(4)	-0.6185	0.0202	-30.6155	7.6183e-206
MA(1)	2.0000	0.0236	84.8810	0
MA(2)	1.5000	0.0341	43.9267	0
MA(3)	0.4860	0.0199	24.4280	8.6135e-132
Variance	577.2574	21.2111	27.2149	4.3329e-163



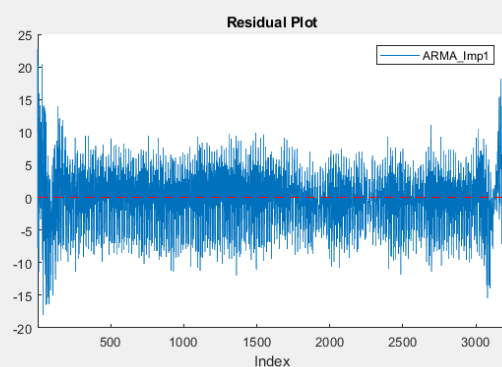
Goodness of Fit

Measure	Value
AIC	2.9459e+04
BIC	2.9514e+04



Parameters

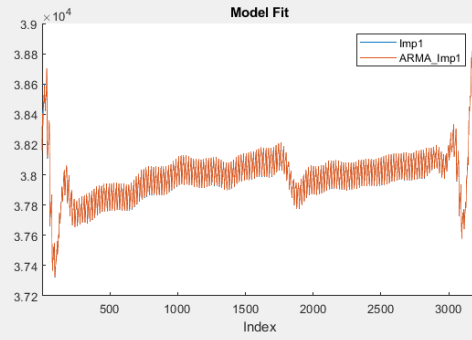
Parameter	Value	Standard Error	t Statistic	P-Value
Constant	955.0471	4.6246e+05	0.0021	0.9984
AR(1)	1.7244	112.9613	0.0153	0.9878
AR(2)	-0.4296	237.9460	-0.0018	0.9986
AR(3)	-1.0000	211.0669	-0.0047	0.9962
AR(4)	0.6704	84.4989	0.0079	0.9937
MA(1)	1.4708	19.3664	0.0759	0.9395
MA(2)	0.9873	16.9321	0.0521	0.9504
Variance	1.9475e+05	6.9708e+03	27.9363	9.1386e-172



Goodness of Fit

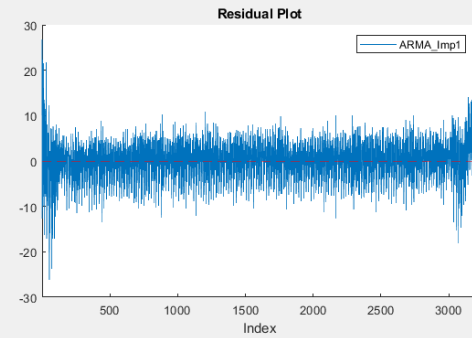
Measure	Value
AIC	4.4886e+04
BIC	4.4934e+04

Figure-ARMA model for samples 29 and 30.



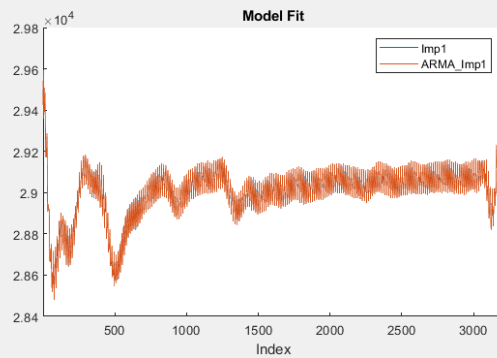
Parameters

Parameter	Value	Standard Error	t Statistic	P-Value
Constant	598.4362	9.0605e+05	6.6049e-04	0.9995
AR(1)	2.0056	373.8623	0.0054	0.9957
AR(2)	-1.0981	939.2122	-0.0012	0.9991
AR(3)	-0.3275	938.6995	-3.4888e-04	0.9997
AR(4)	0.4043	375.0667	0.0011	0.9991
MA(1)	1.3192	99.8175	0.0132	0.9895
MA(2)	0.9403	81.6600	0.0115	0.9908
Variance	4.6081e+05	1.6387e+04	28.1206	5.4813e-174



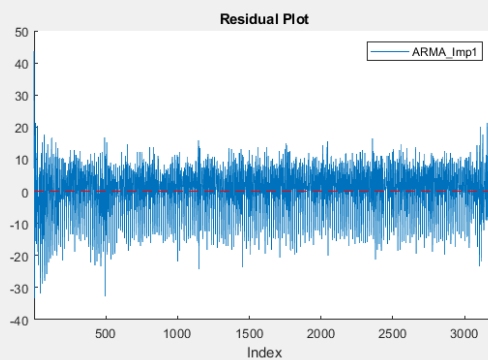
Goodness of Fit

Measure	Value
AIC	4.7643e+04
BIC	4.7691e+04



Parameters

Parameter	Value	Standard Error	t Statistic	P-Value
Constant	491.7850	45.7862	10.7409	6.5412e-27
AR(1)	1.9534	0.0679	28.7560	7.6232e-182
AR(2)	-1.5000	0.1448	-10.3626	3.6703e-25
AR(3)	0.5813	0.1213	4.7909	1.6602e-06
AR(4)	-0.0517	0.0447	-1.1560	0.2477
MA(1)	0.7623	0.0707	10.7807	4.2471e-27
MA(2)	0.2009	0.0412	4.8778	1.0728e-06
Variance	59.8023	1.8523	32.2849	1.1409e-228



Goodness of Fit

Measure	Value
AIC	2.2304e+04
BIC	2.2353e+04

Figure-ARMA model for samples 32 and 33.



Model Fit

Imp1
ARMA_Imp1

Index

Parameters

Parameter	Value	Standard Error	t Statistic	P-Value
Constant	498.6712	35.3369	14.1119	3.2082e-45
AR(1)	1.3976	0.0121	115.4570	0
AR(2)	-0.0590	0.0139	-4.2424	2.2114e-05
AR(3)	-1.0000	0.0156	-63.9910	0
AR(4)	0.6458	0.0110	58.9725	0
MA(1)	1.3638	0.0150	91.0161	0
MA(2)	0.3992	0.0149	26.7458	1.3819e-157
Variance	79.4851	2.1971	36.1774	1.3820e-286

Residual Plot

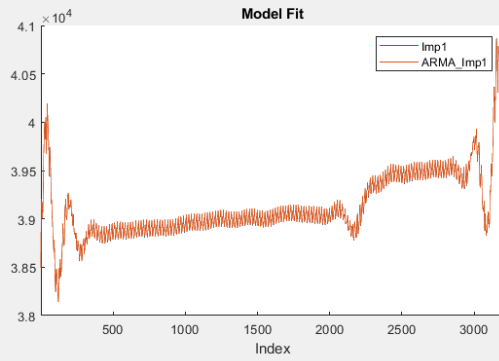
ARMA_Imp1

Index

Goodness of Fit

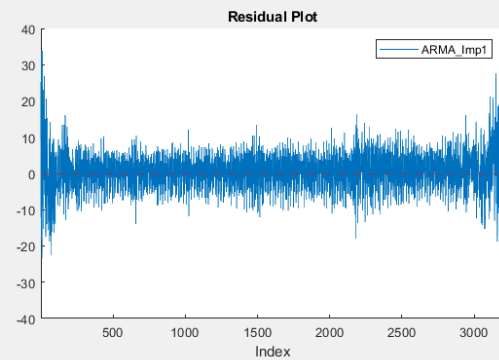
Measure	Value
AIC	2.2756e+04
BIC	2.2805e+04

Figure-ARMA model for samples 34 and 35.



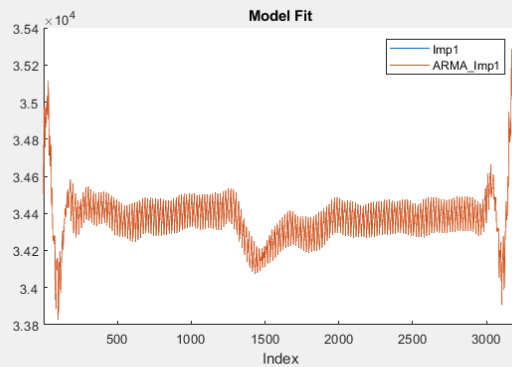
Parameters

Parameter	Value	Standard Error	t Statistic	P-Value
Constant	184.6708	3.9089e+05	4.7243e-04	0.9996
AR(1)	2.0617	197.9122	0.0104	0.9917
AR(2)	-1.0364	507.3846	-0.0020	0.9984
AR(3)	-0.5620	489.4467	-0.0011	0.9991
AR(4)	0.5319	185.1549	0.0029	0.9977
MA(1)	1.4105	61.2734	0.0230	0.9816
MA(2)	0.9502	61.8485	0.0154	0.9877
Variance	4.7903e+05	1.6990e+04	28.1944	6.8476e-175



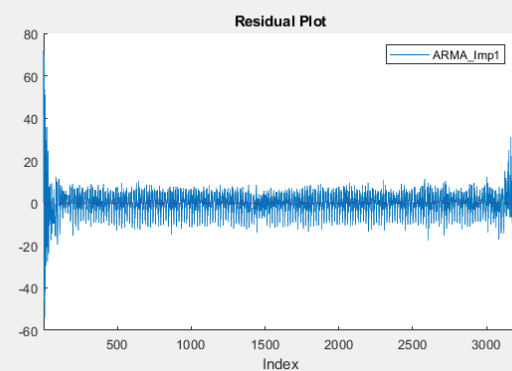
Goodness of Fit

Measure	Value
AIC	4.7767e+04
BIC	4.7815e+04



Parameters

Parameter	Value	Standard Error	t Statistic	P-Value
Constant	467.4057	30.6277	15.2609	1.3934e-52
AR(1)	1.8076	0.0060	300.3208	0
AR(2)	-1.0690	0.0127	-84.0779	0
AR(3)	0.0231	0.0144	1.6084	0.1077
AR(4)	0.2248	0.0071	31.6582	5.8471e-220
MA(1)	1.2819	0.0017	776.0949	0
MA(2)	0.9062	0.0012	770.6478	0
Variance	23.8206	0.3689	64.5760	0



Goodness of Fit

Measure	Value
AIC	2.0833e+04
BIC	2.0881e+04

Figure-ARMA model for samples 36 and 37.

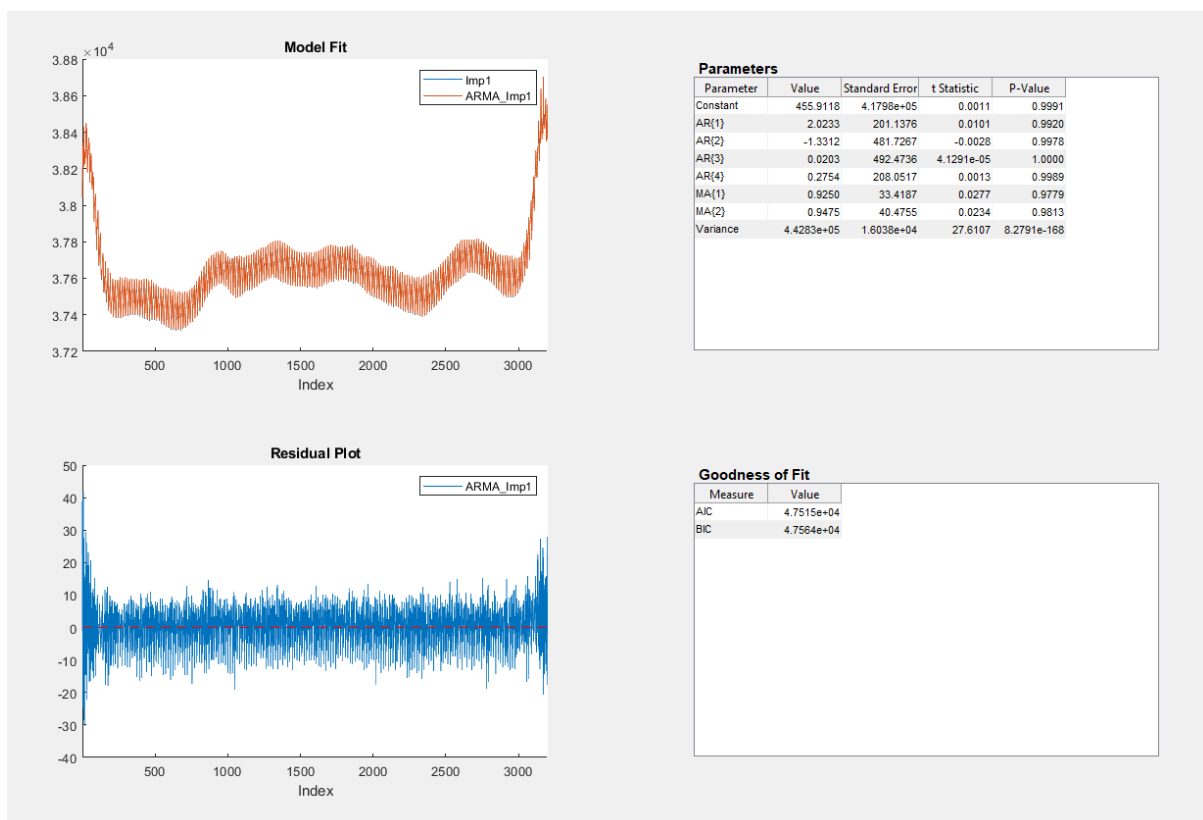
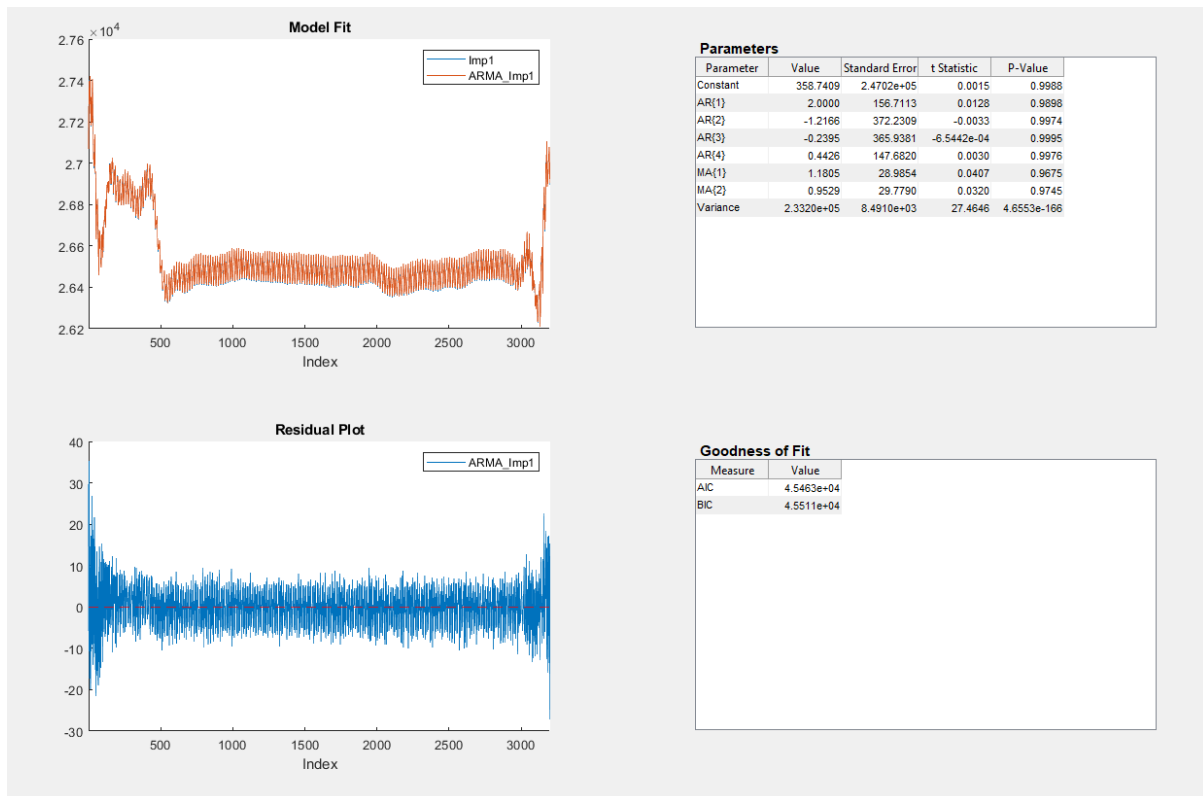


Figure-ARMA model for samples 38 and 39.

Appendix C: Stroke Volume graphs.

The following graphs represent the computed SV as 10ml per sample

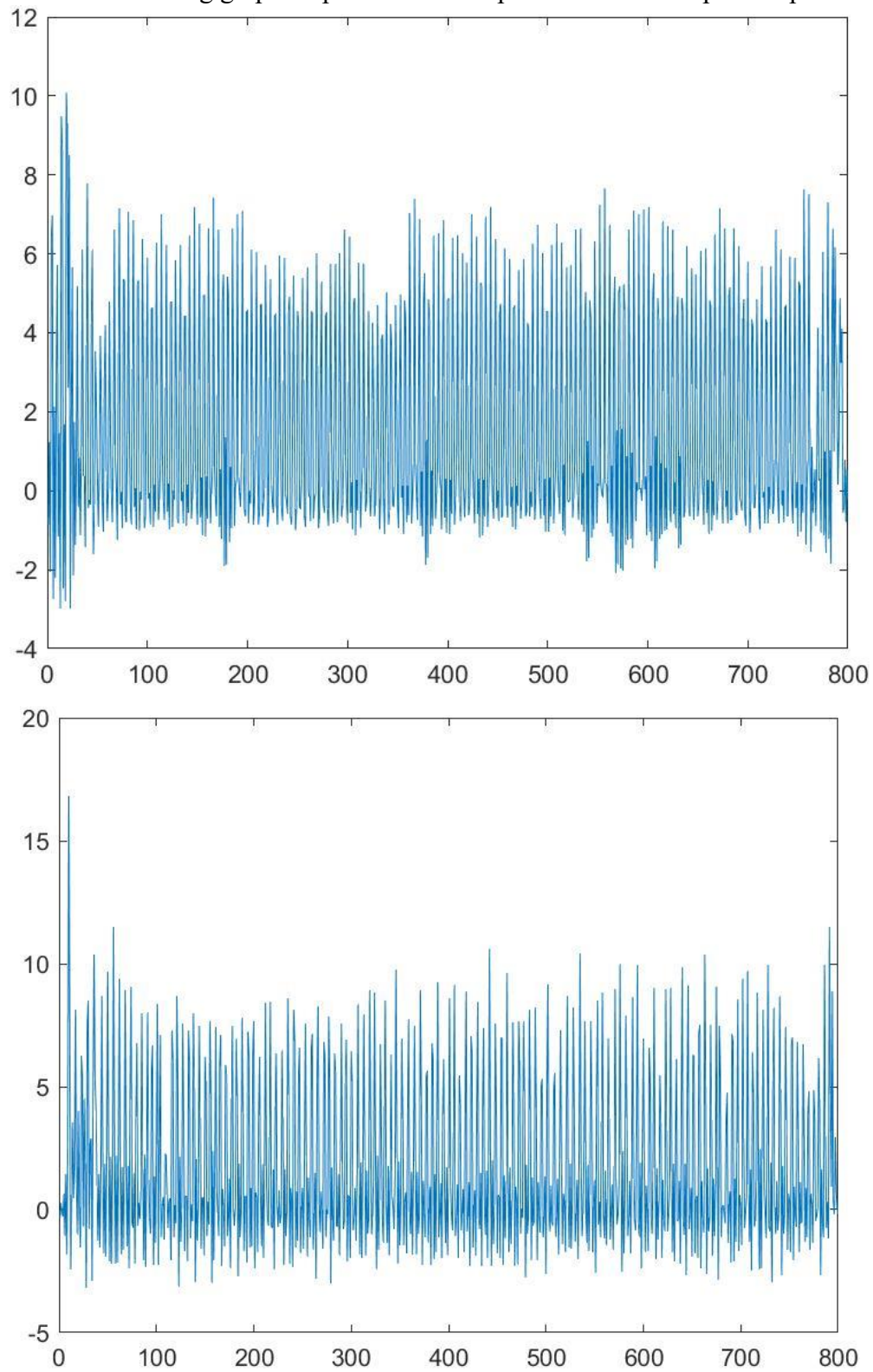


Figure-Stroke volume for 160 seconds for samples 1 and 2.

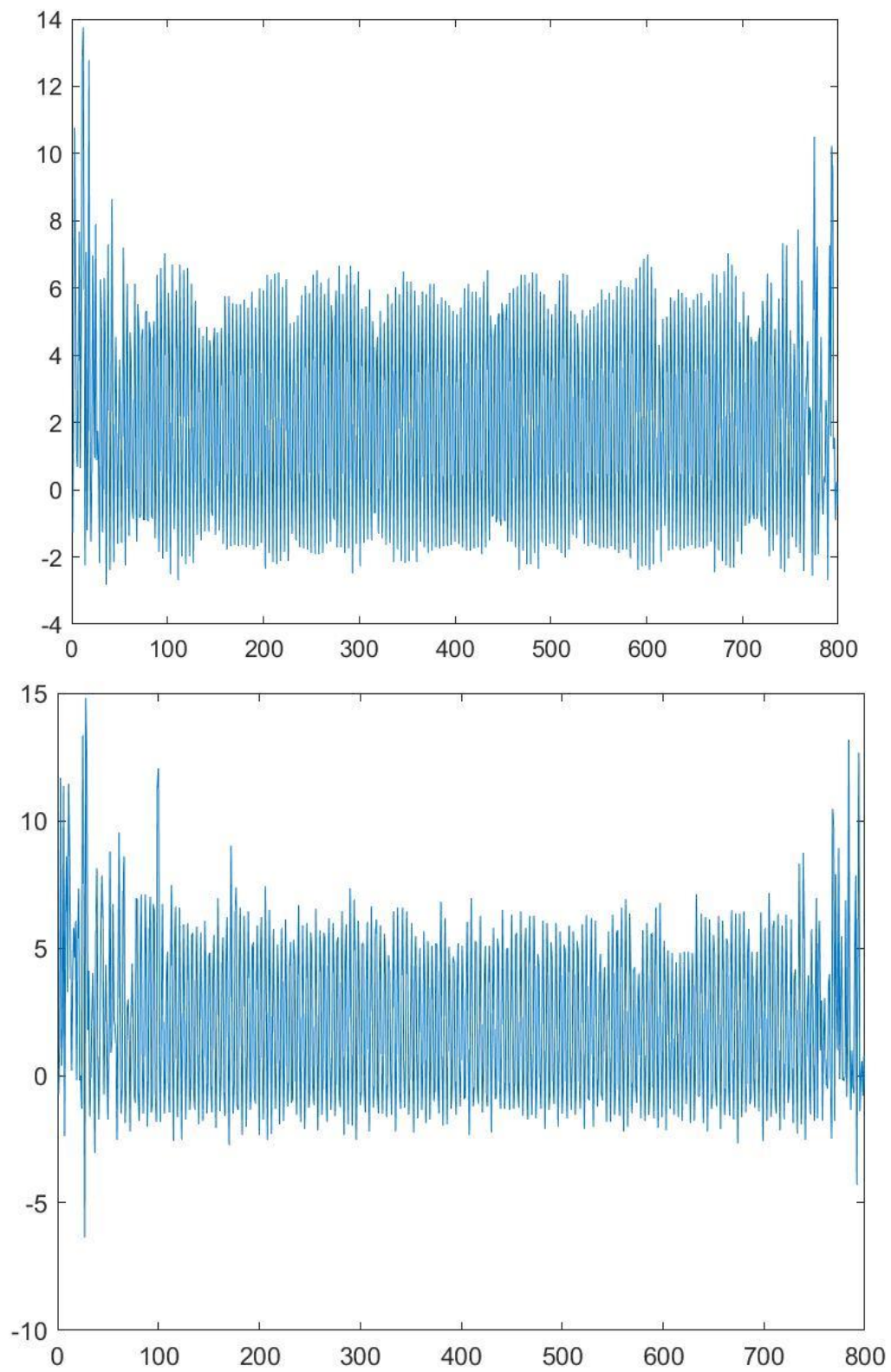


Figure-Stroke volume for 160 seconds for samples 3 and 4.

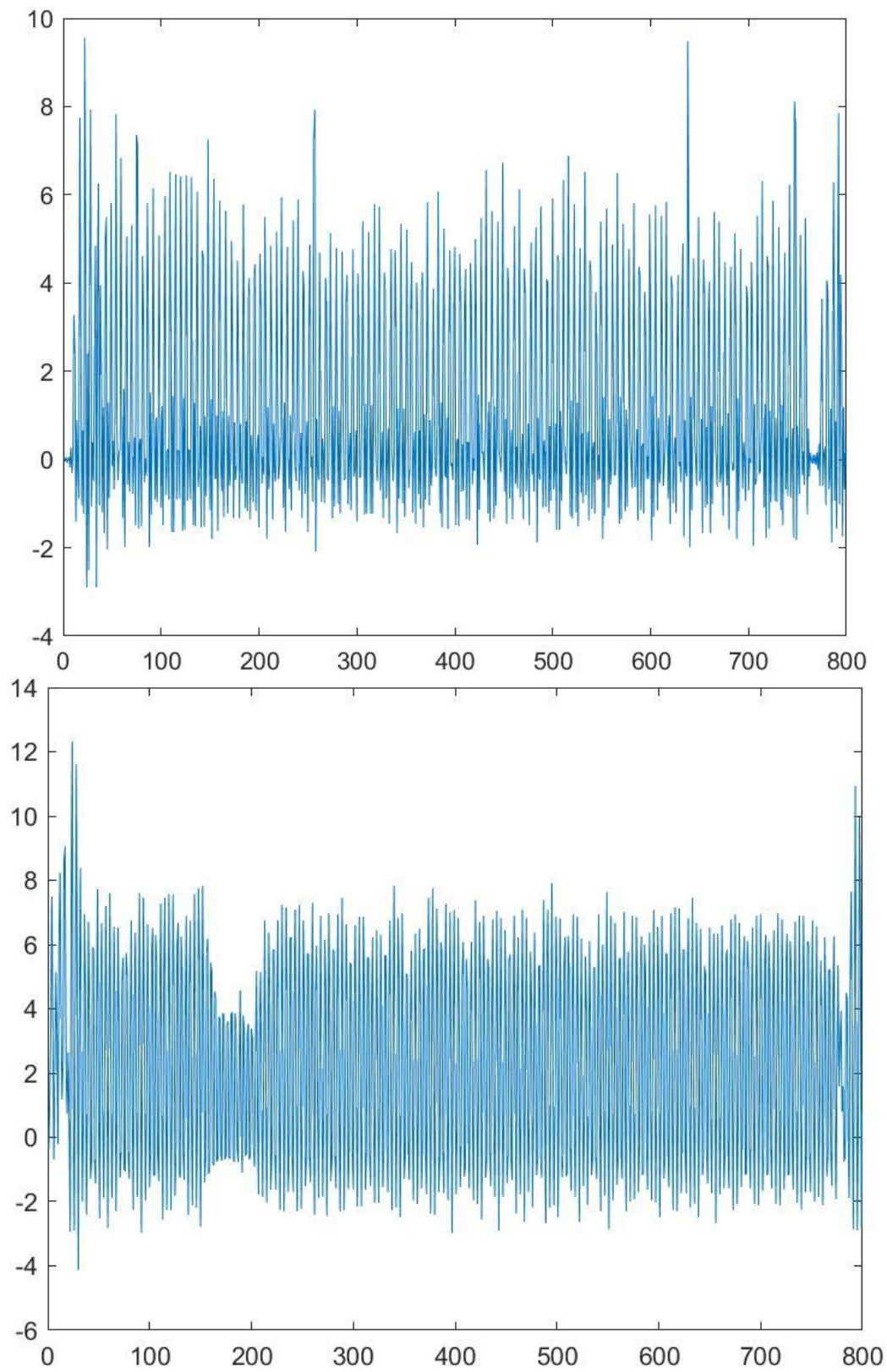


Figure -Stroke volume for 160 seconds for samples 5 and 6.

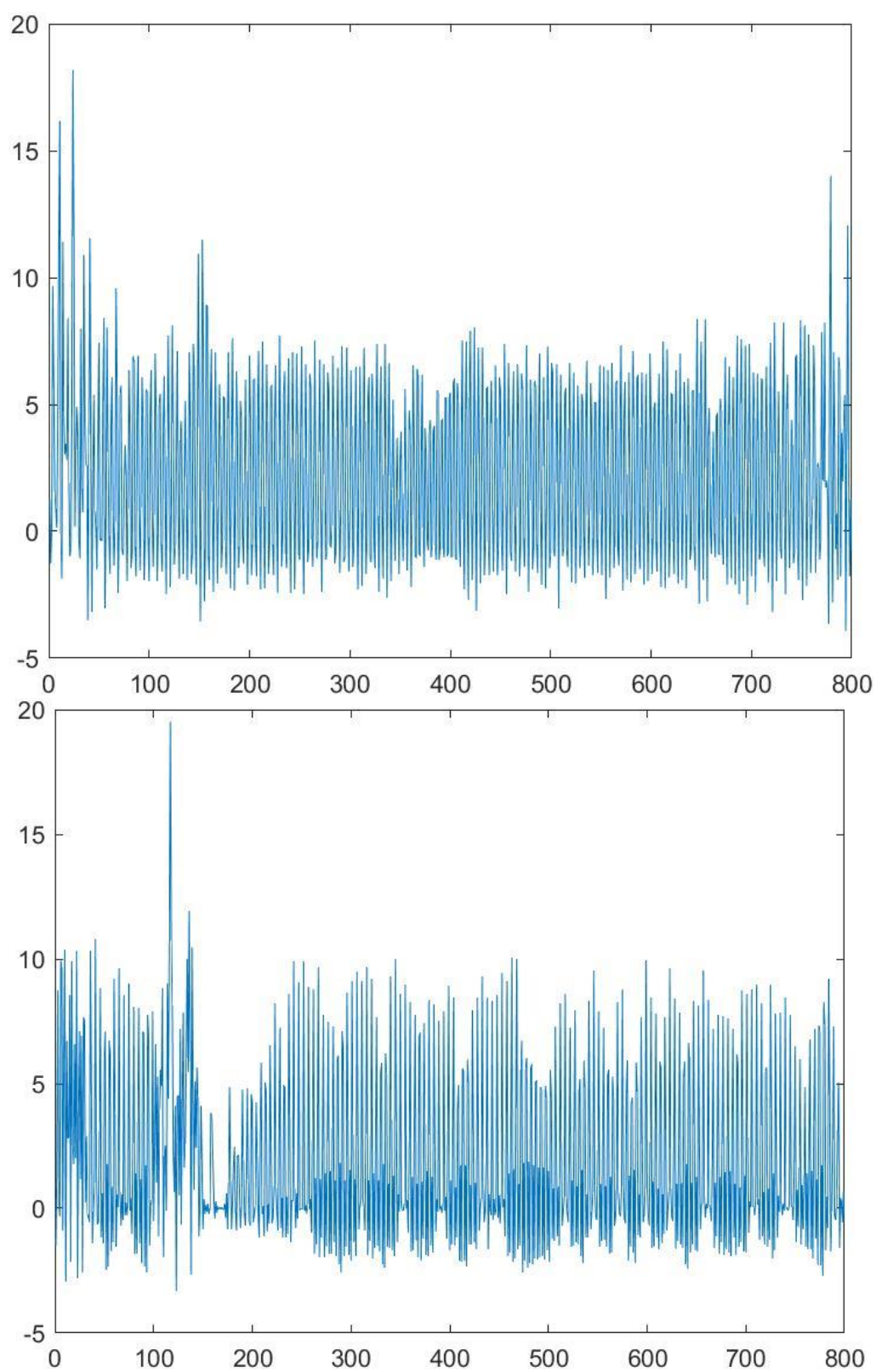
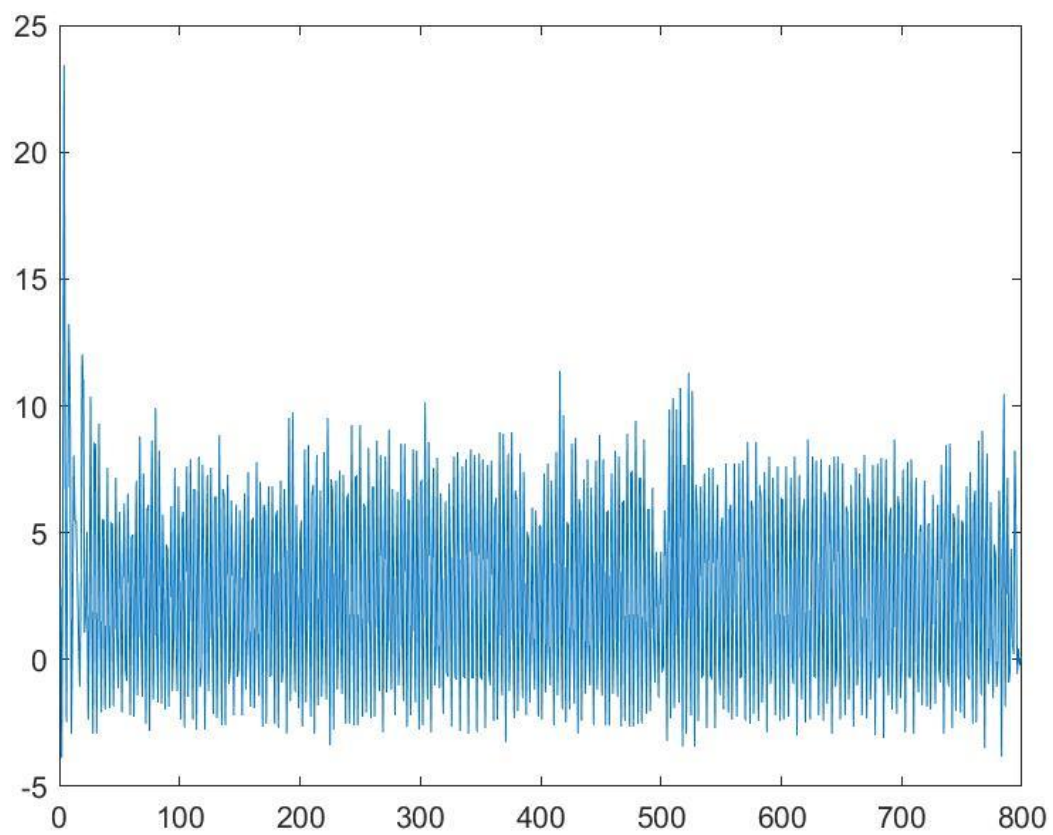
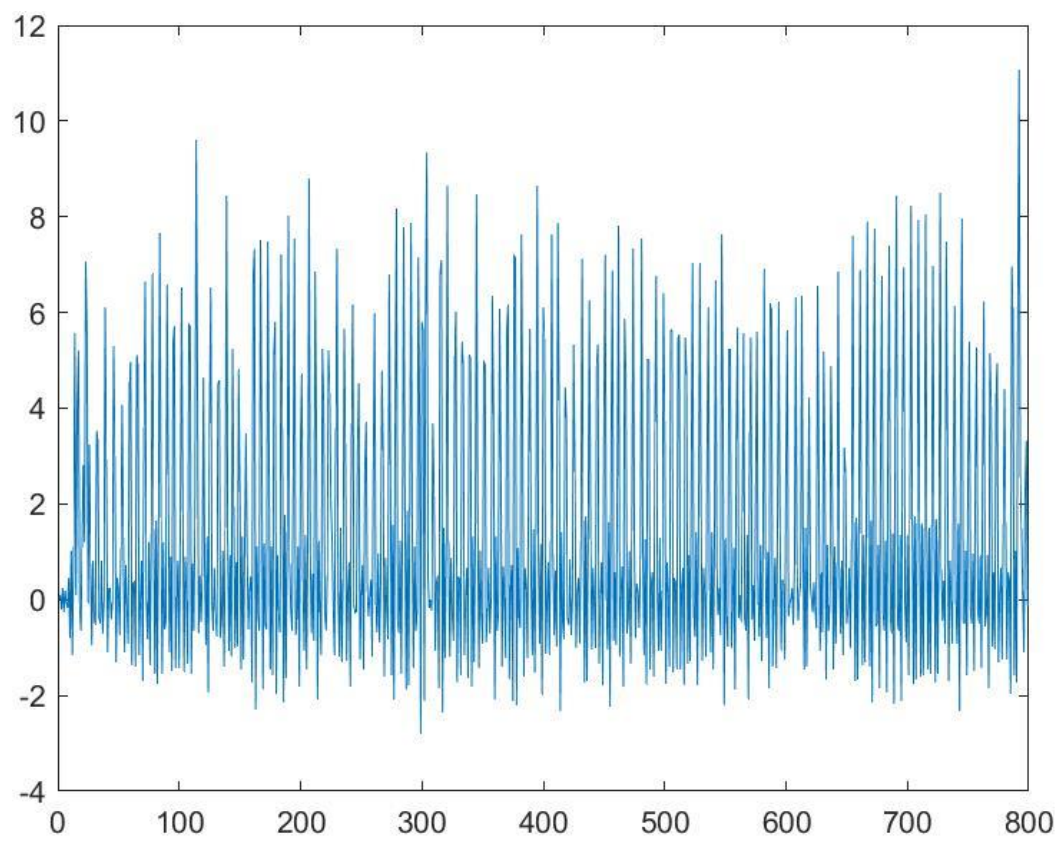
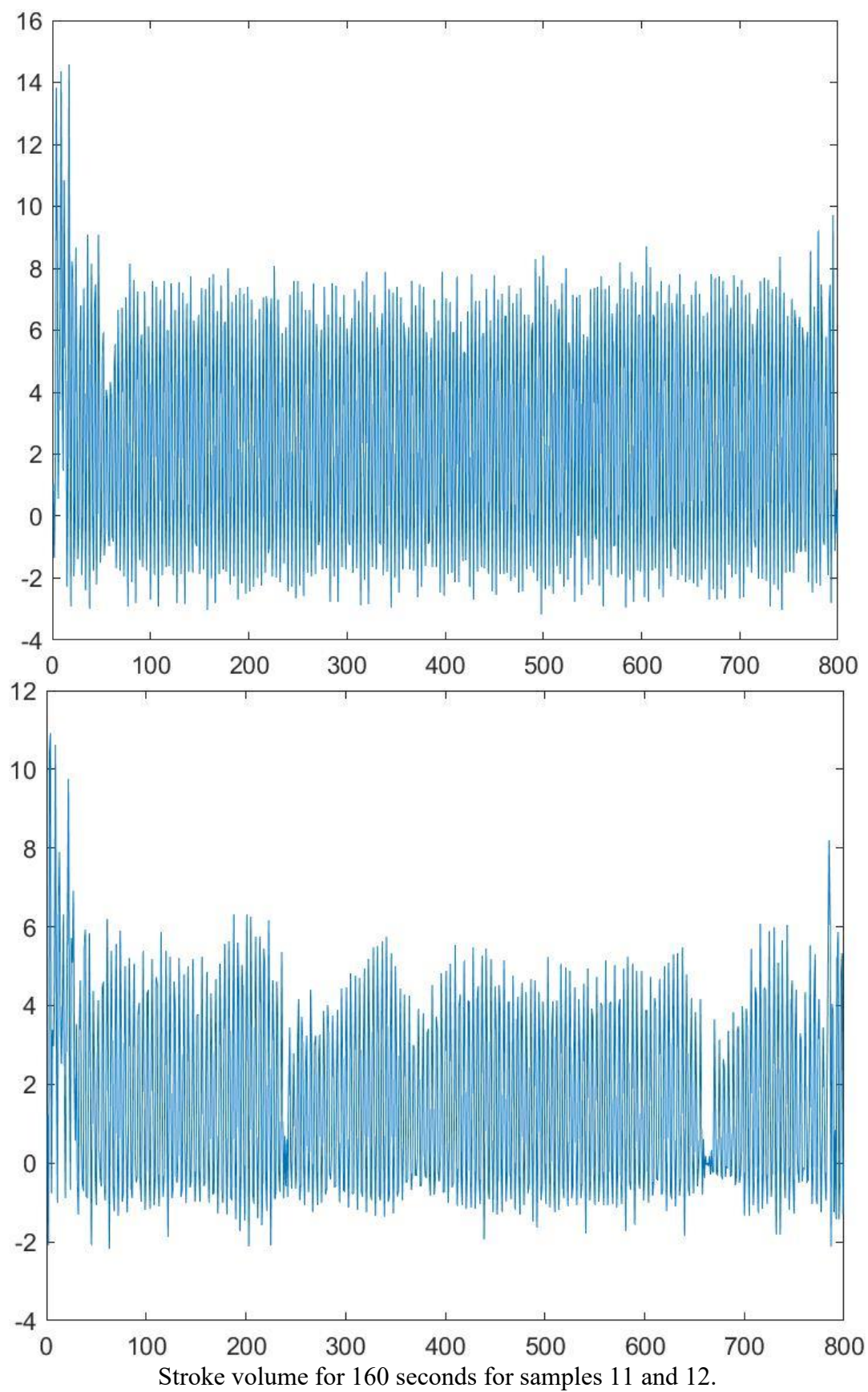
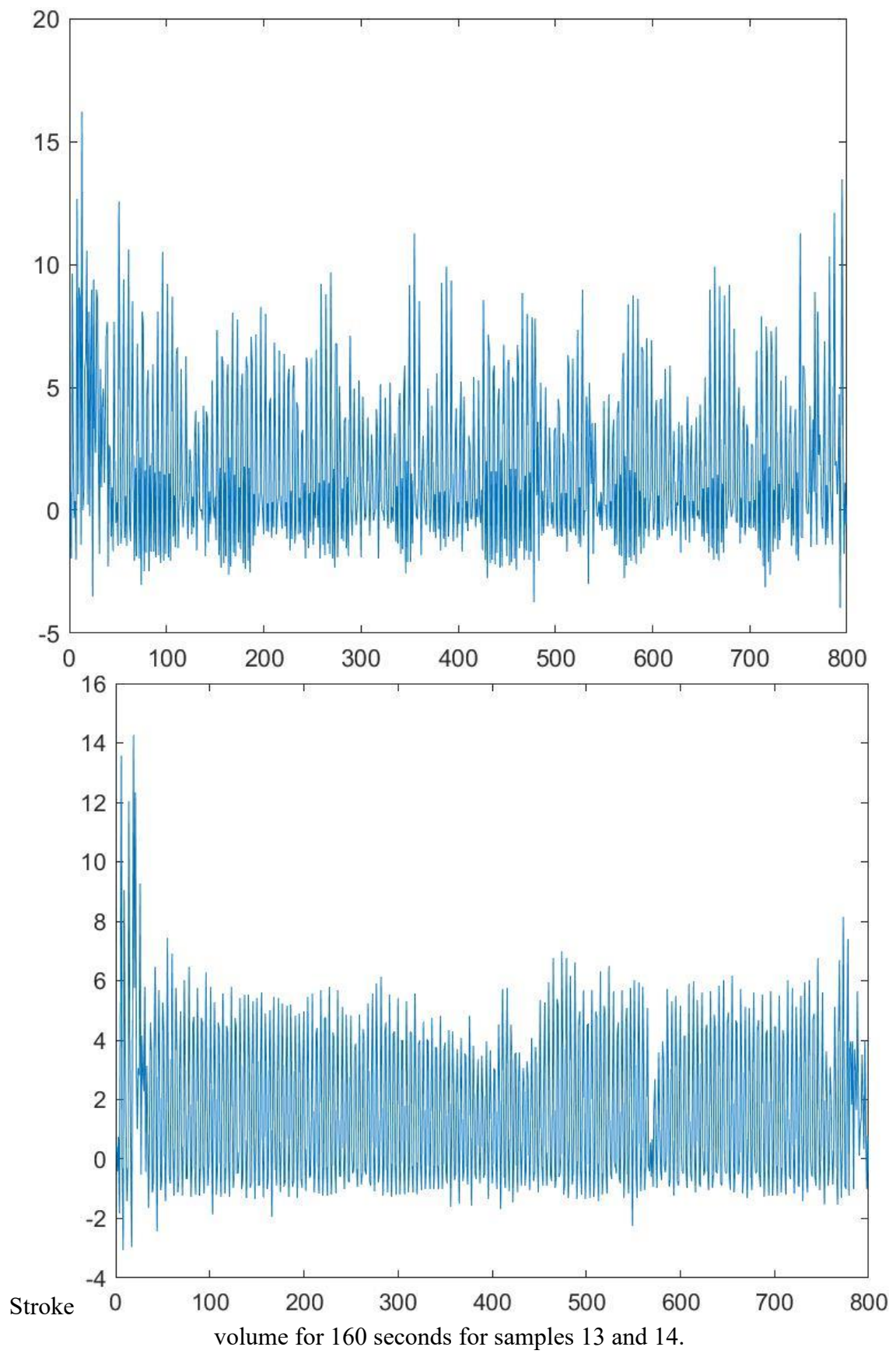


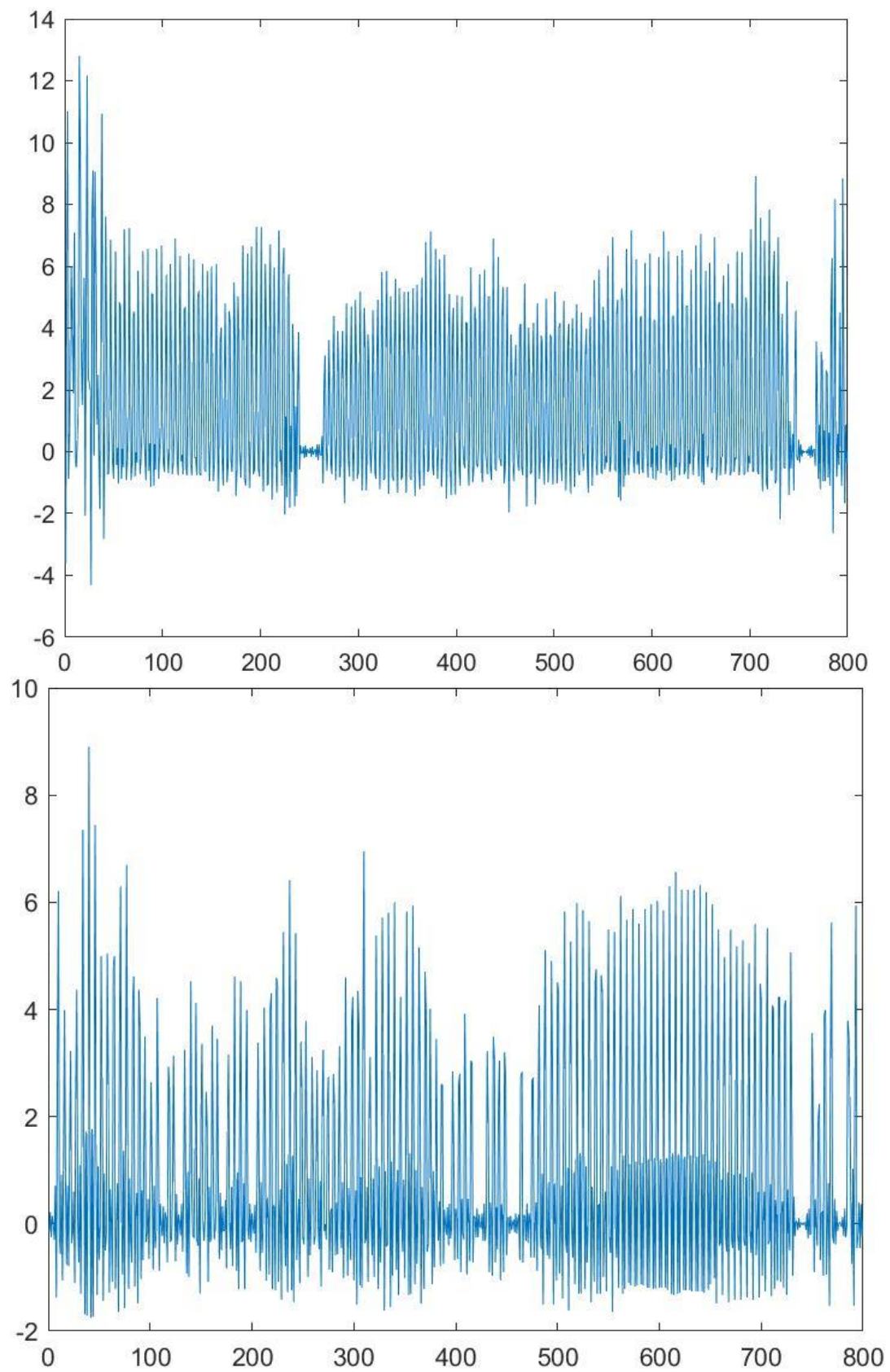
Figure-Stroke volume for 160 seconds for samples 7 and 8.



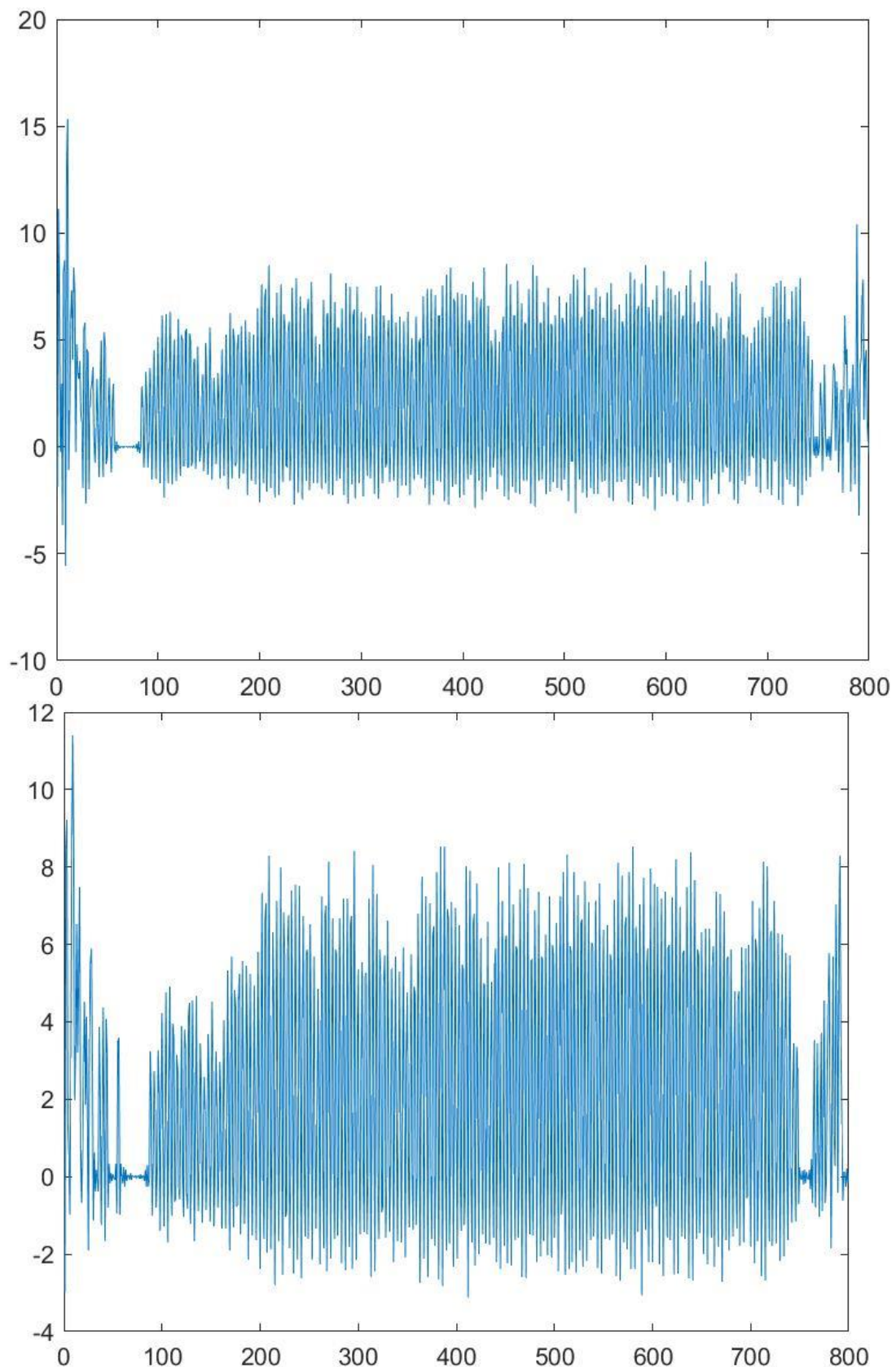
Stroke volume for 160 seconds for samples 9 and 10.



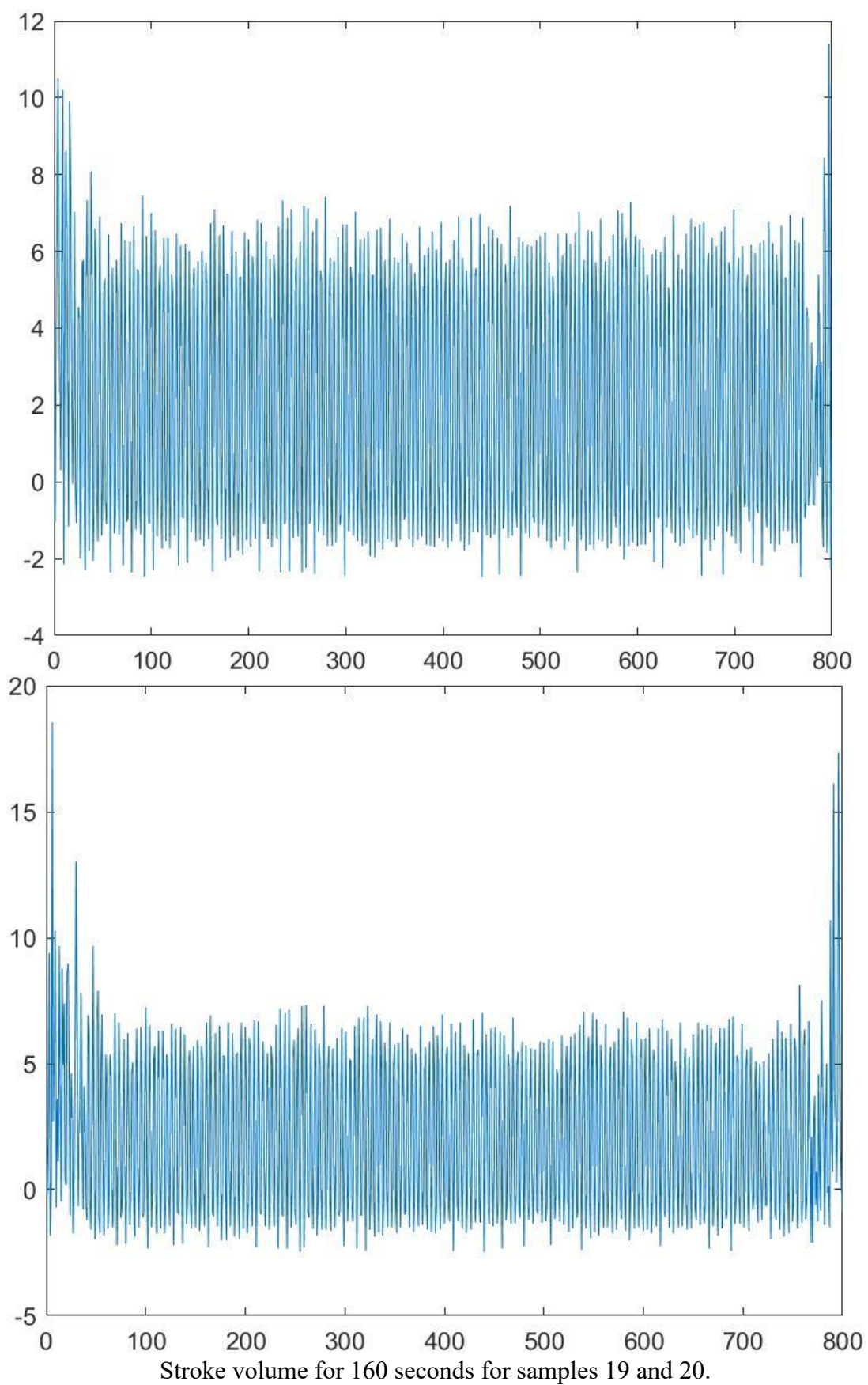




Stroke volume for 160 seconds for samples 15 and 16.



Stroke volume for 160 seconds for samples 17 and 18.



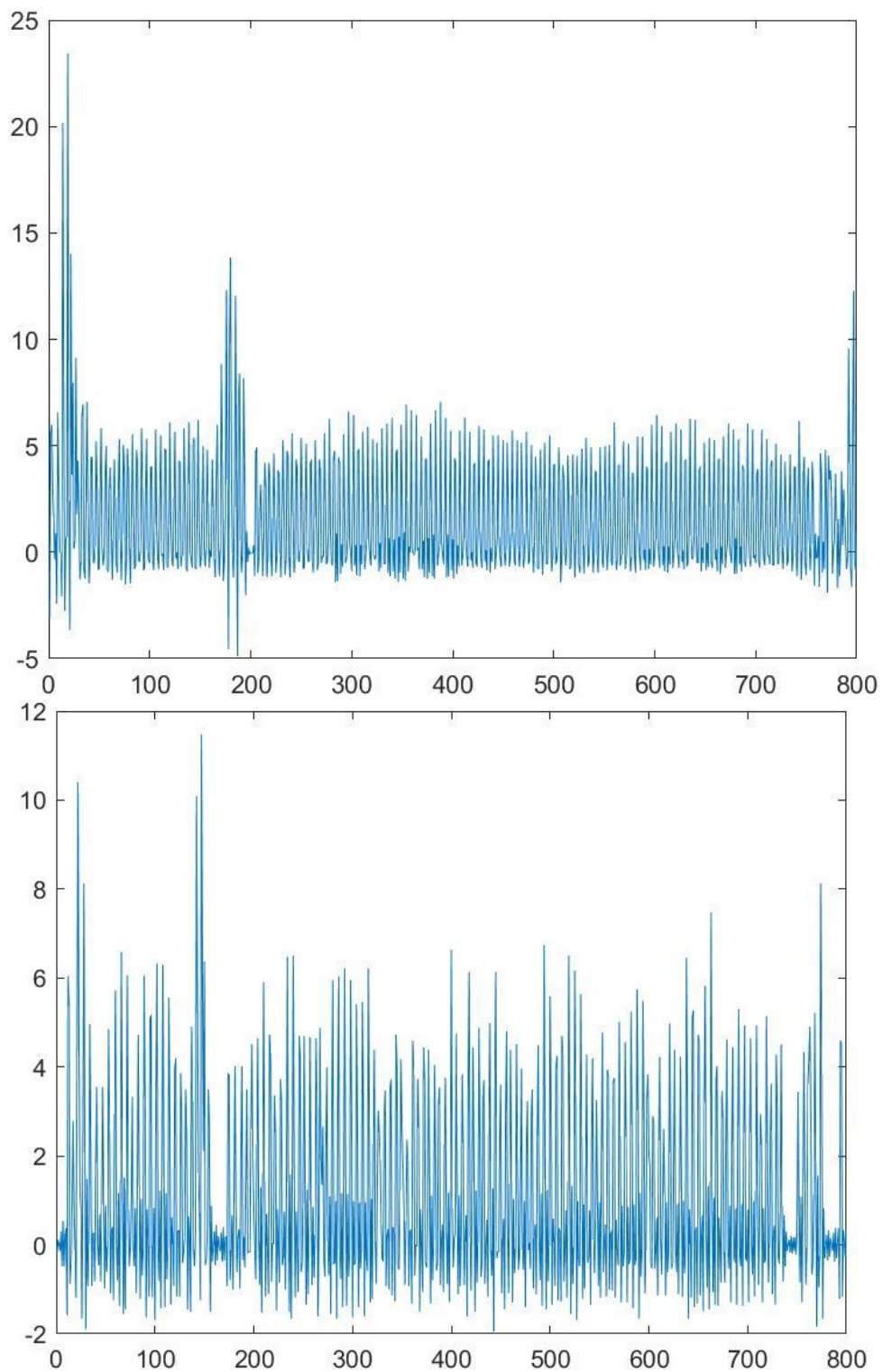


Figure-Stroke volume for 160 seconds for samples 21 and 22.

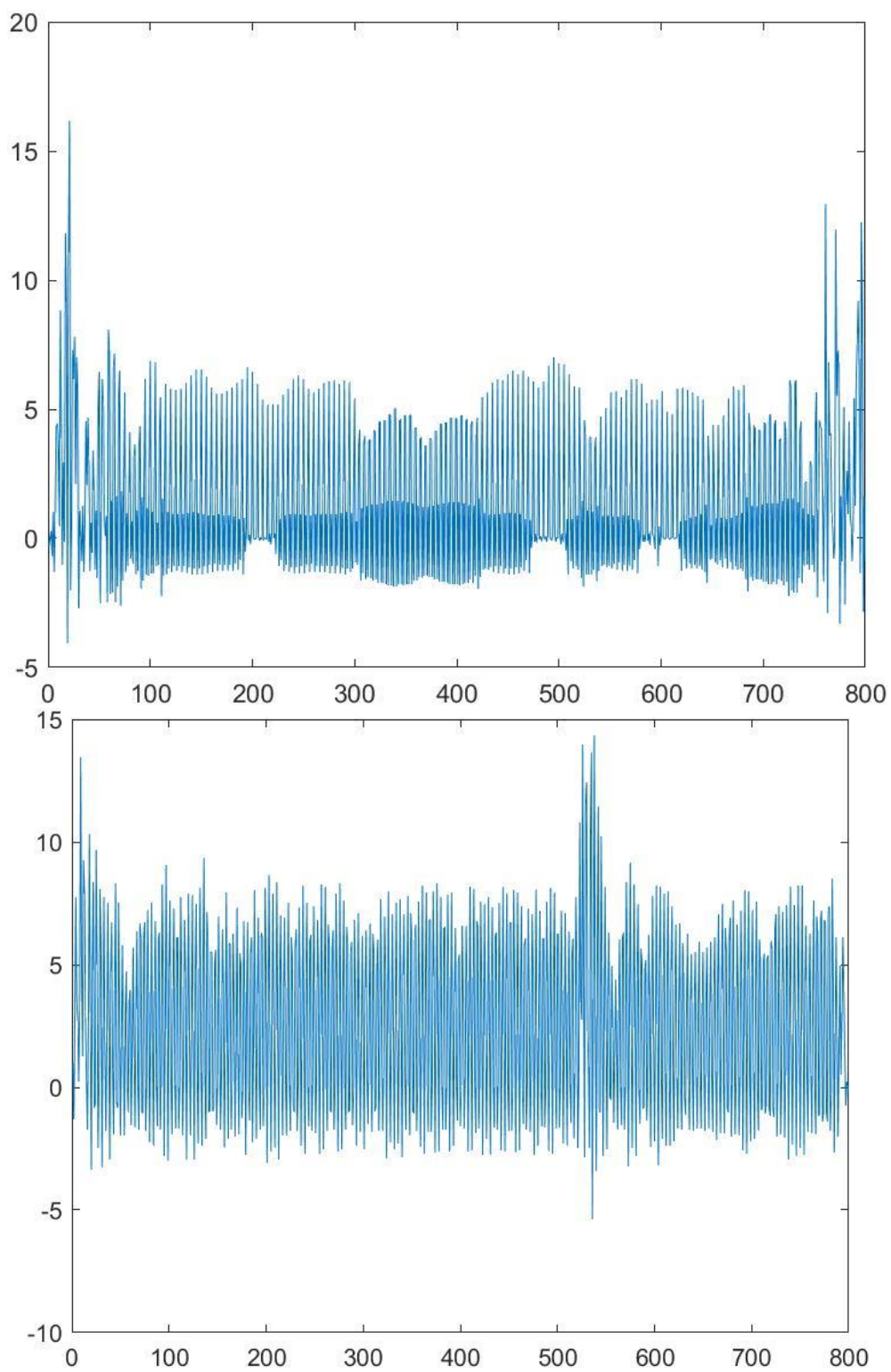


Figure-Stroke volume for 160 seconds for samples 23 and 24.

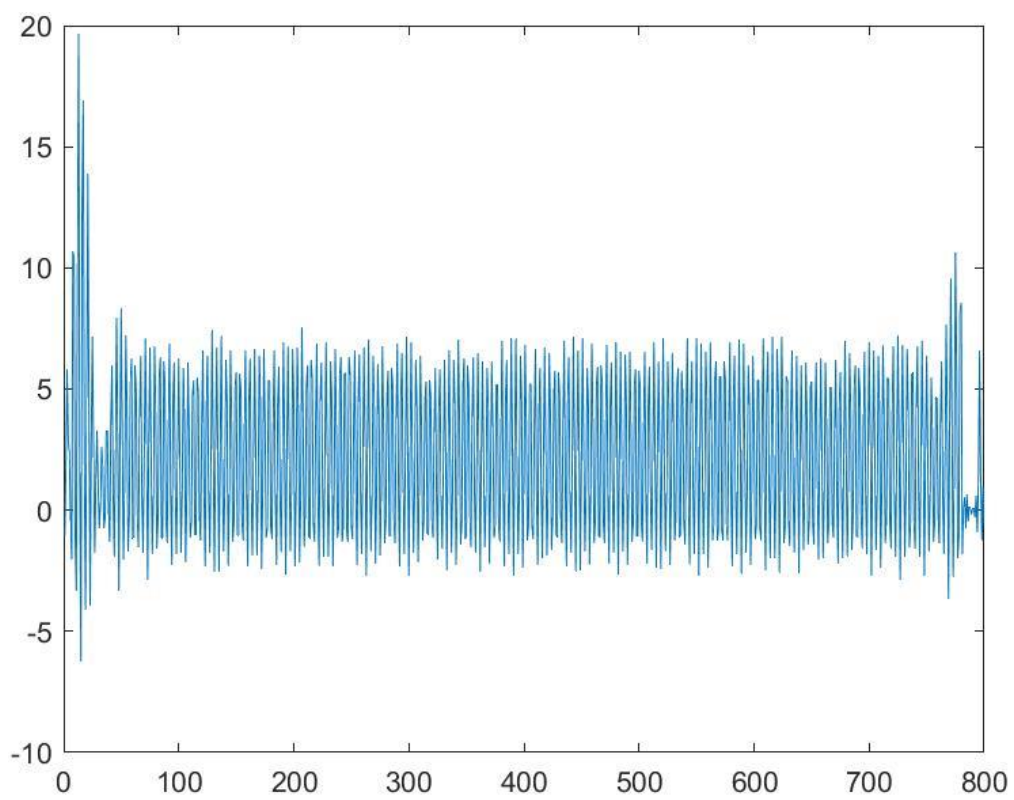
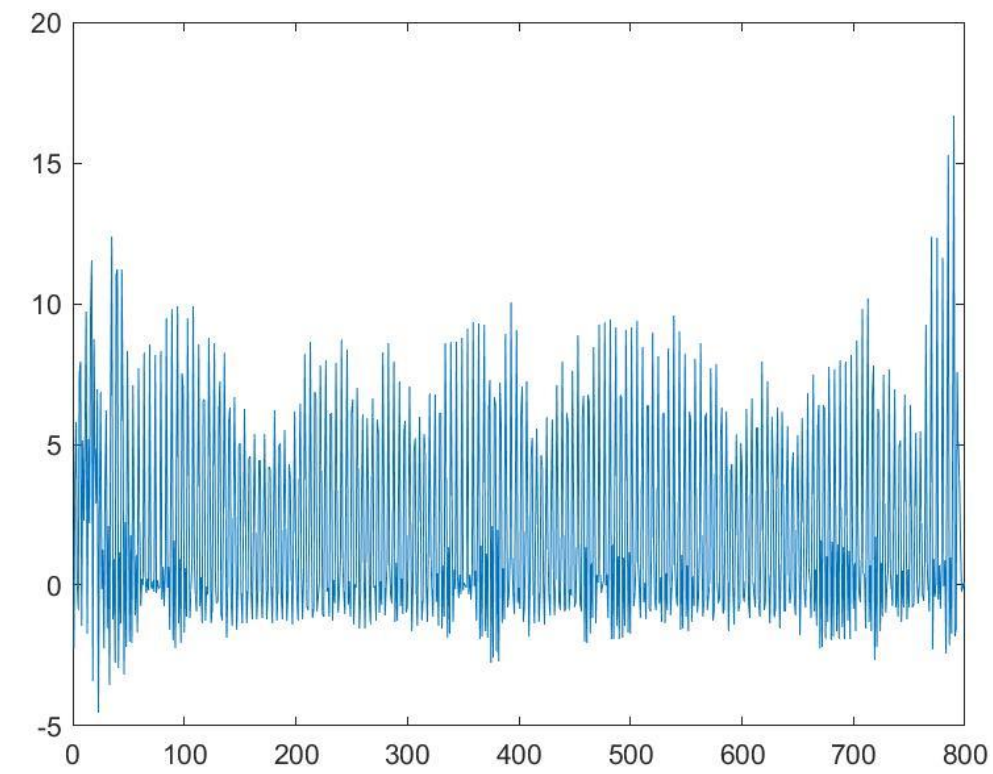
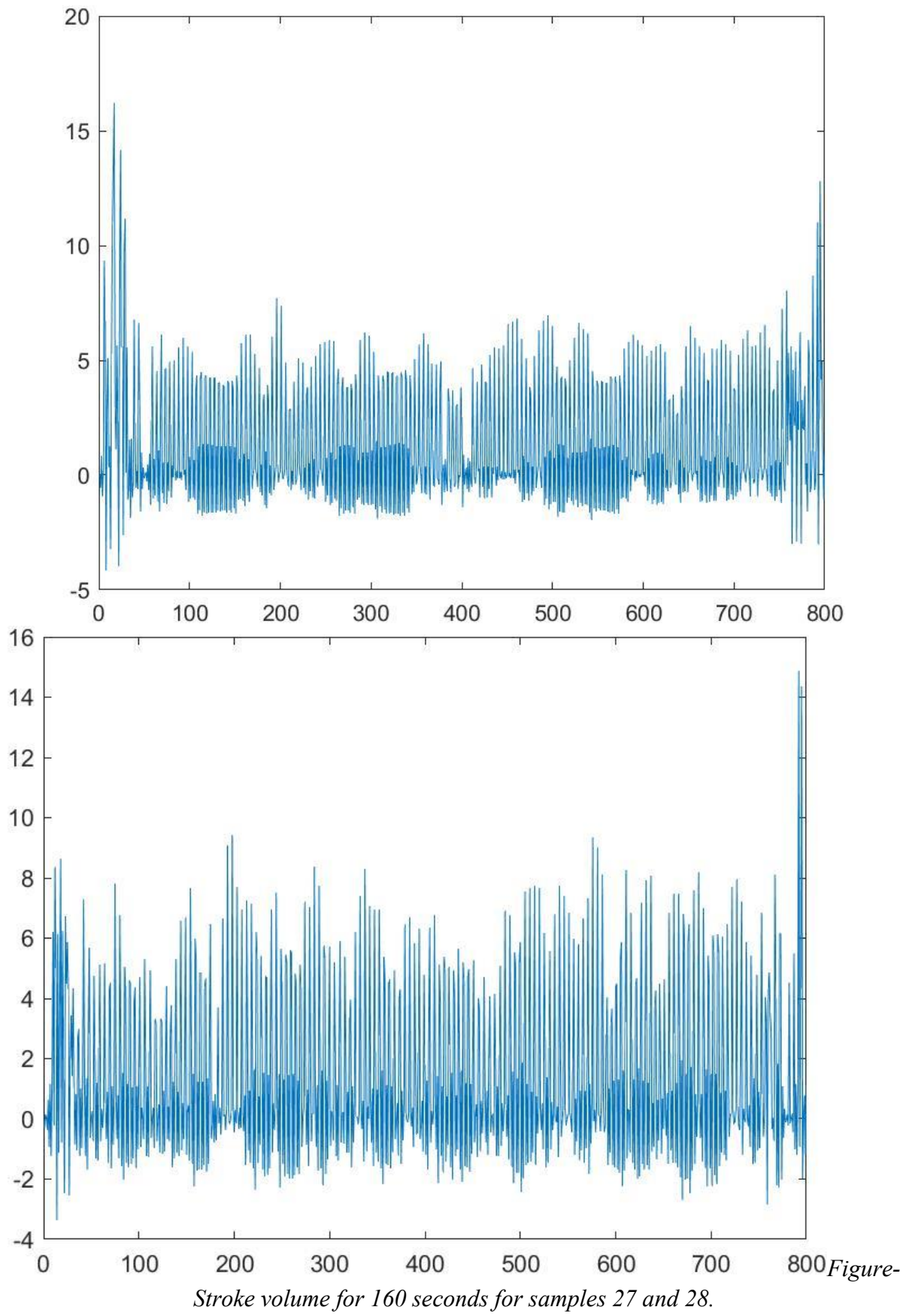


Figure-Stroke volume for 160 seconds for samples 25 and 26.



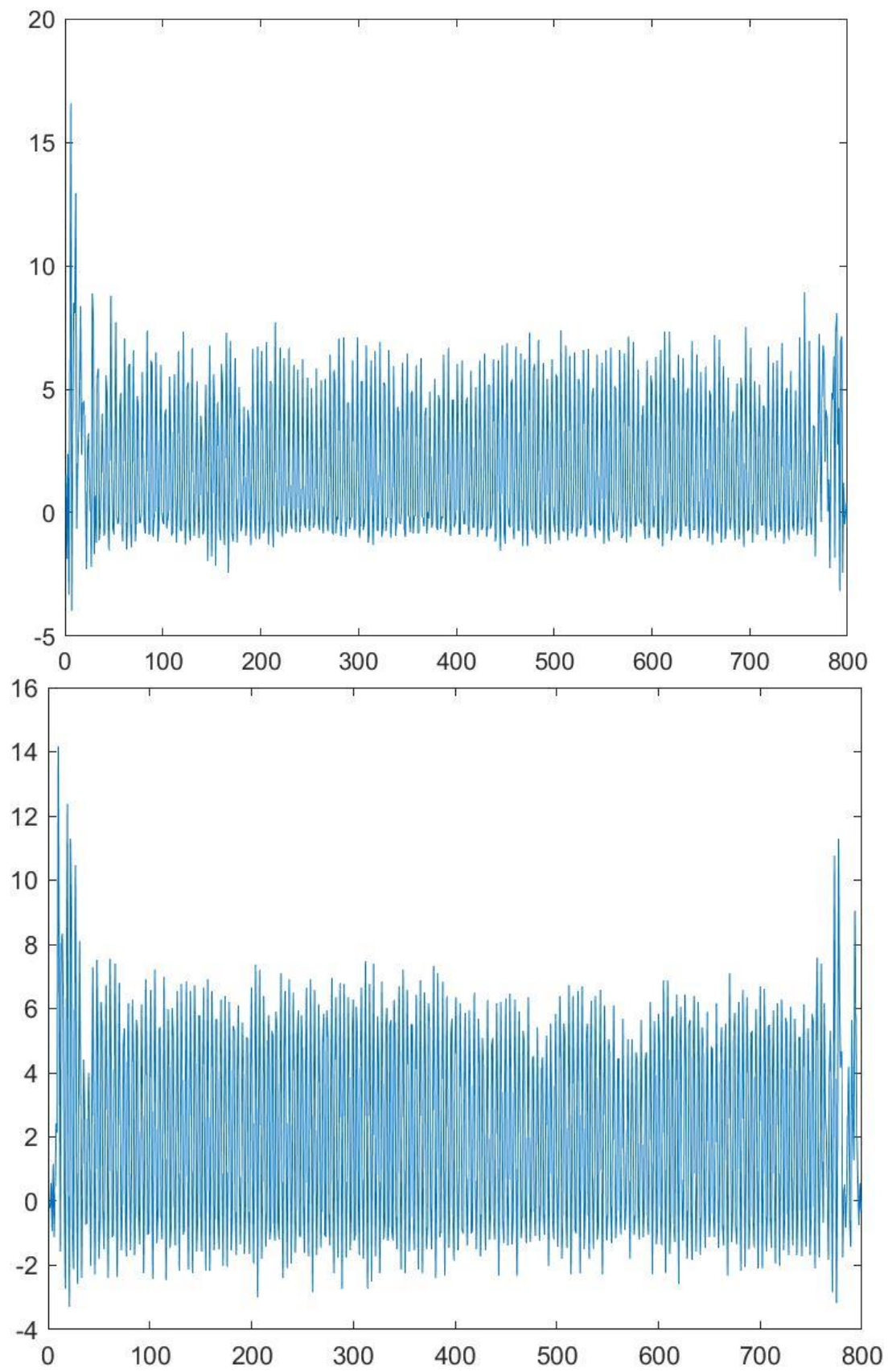
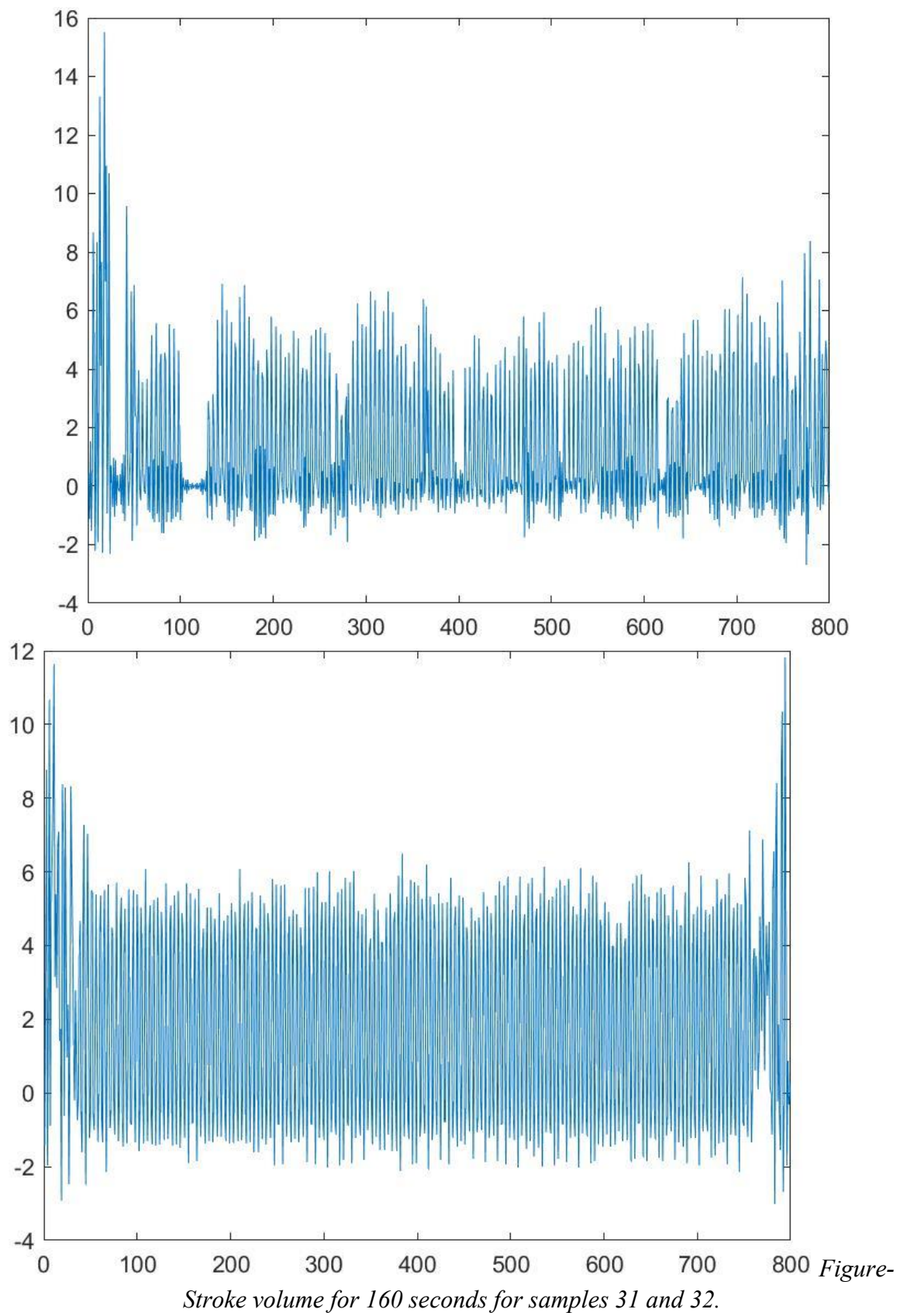


Figure-Stroke volume for 160 seconds for samples 29 and 30.



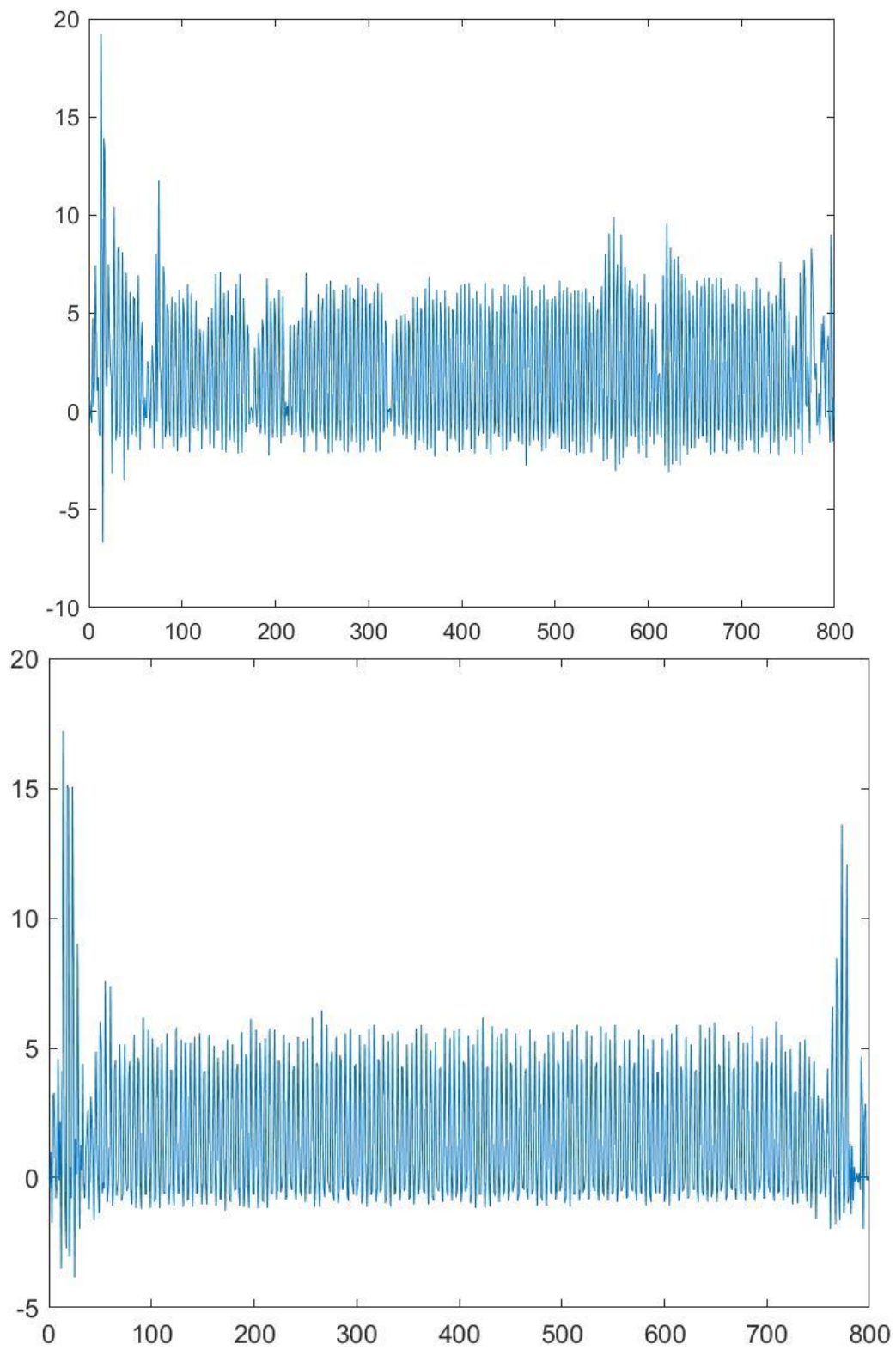
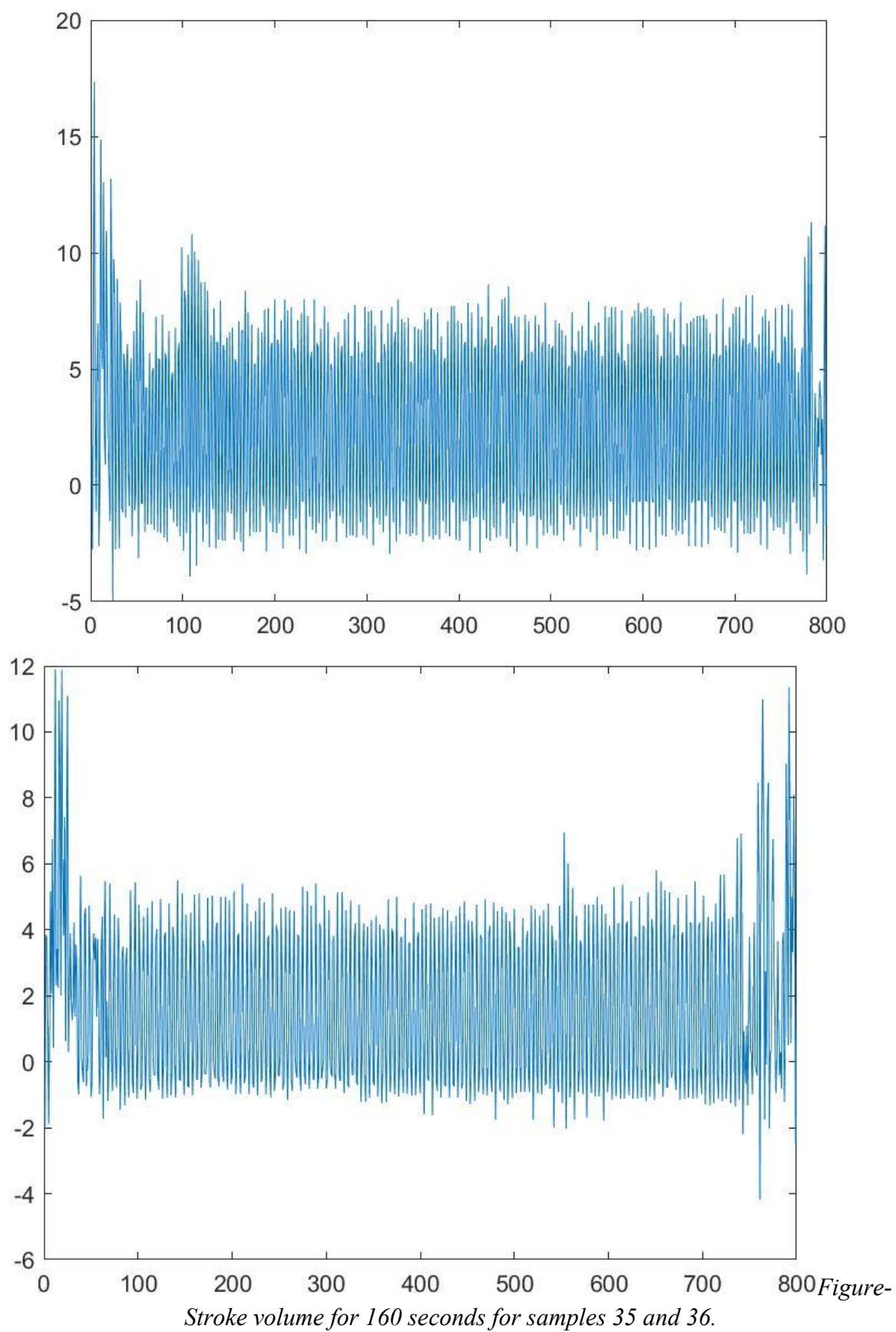


Figure-Stroke volume for 160 seconds for samples 33 and 34



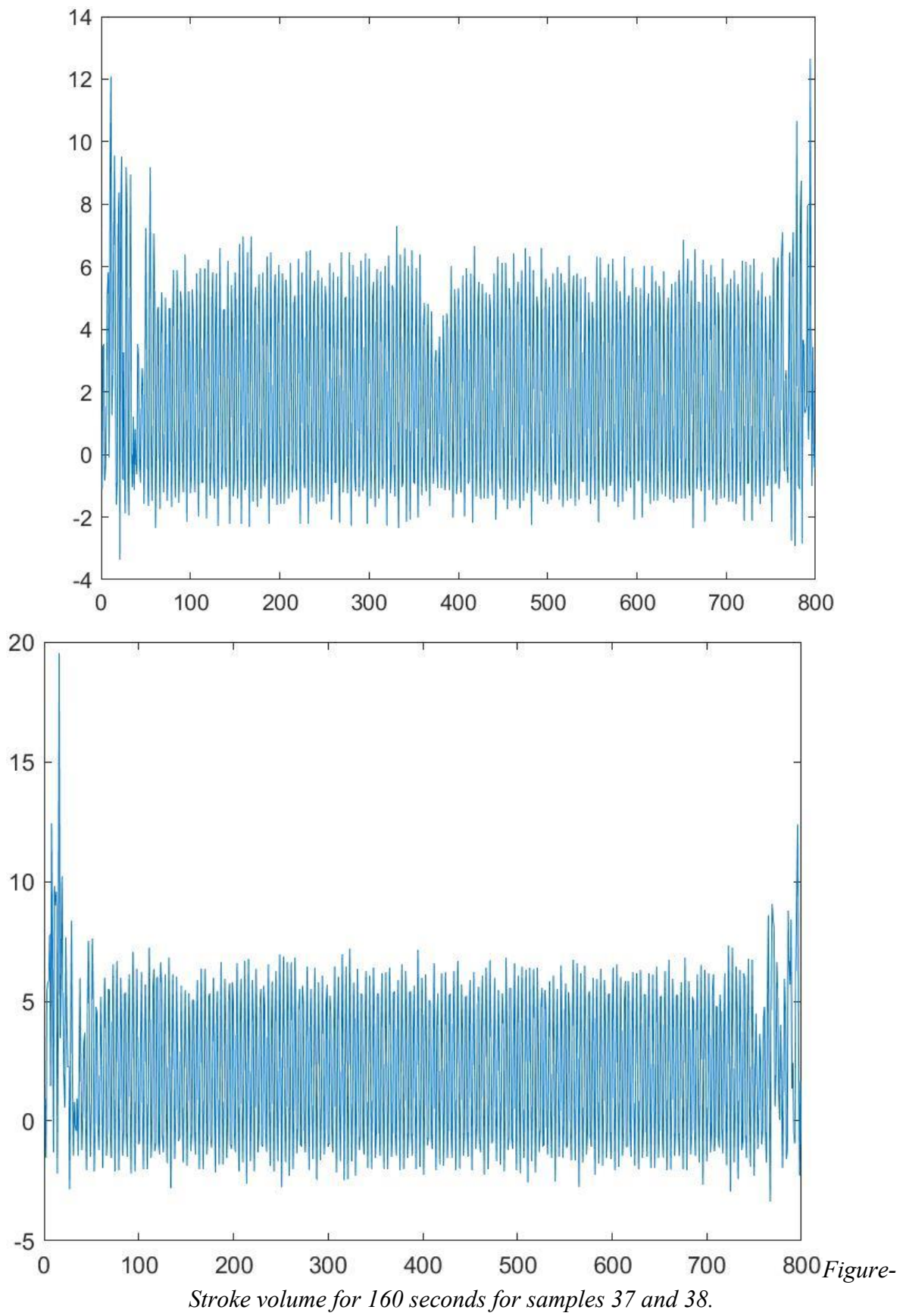


Figure-
Stroke volume for 160 seconds for samples 37 and 38.

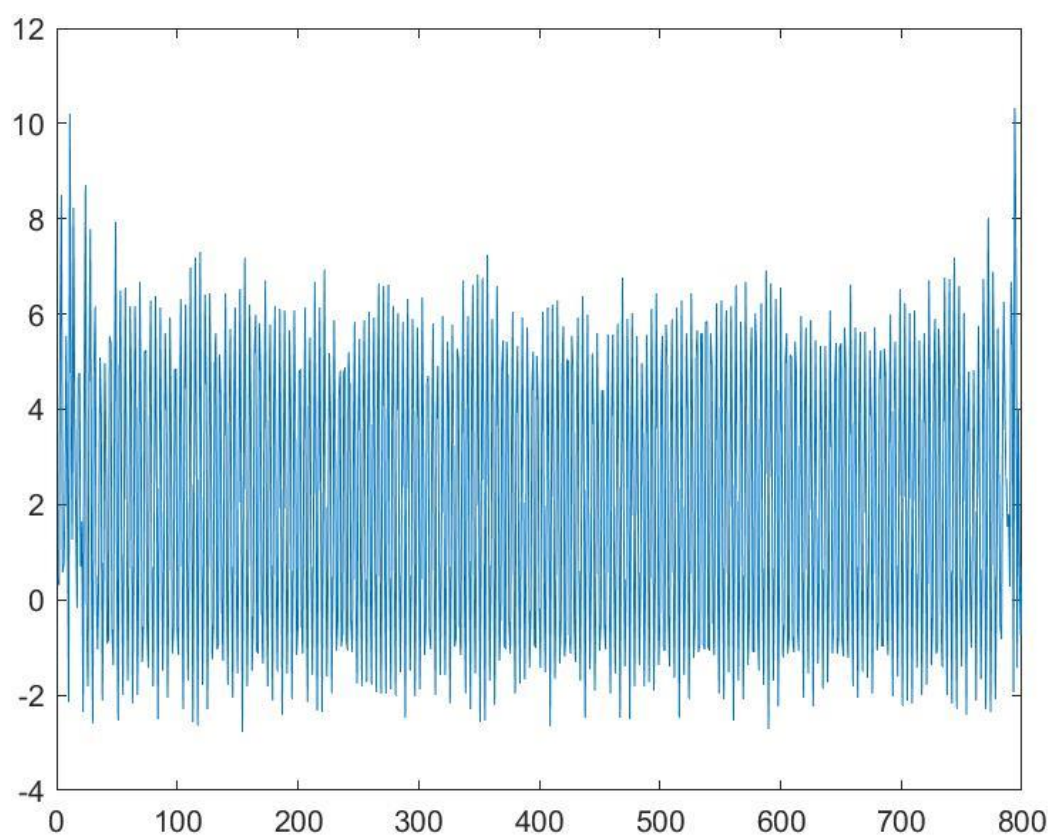
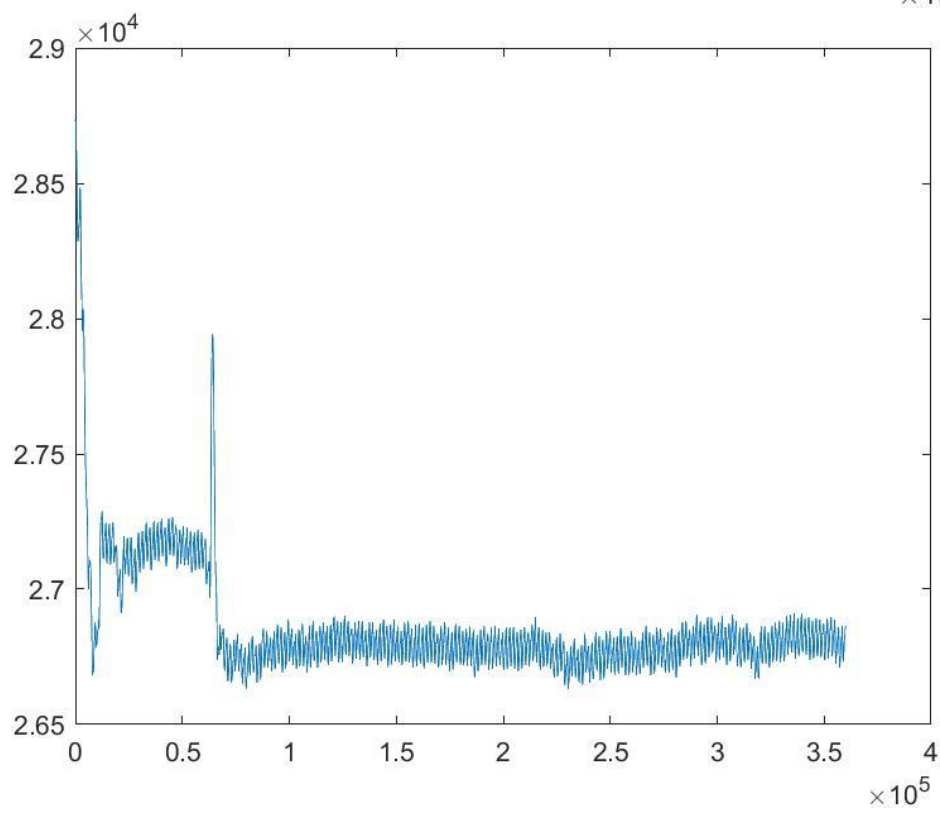
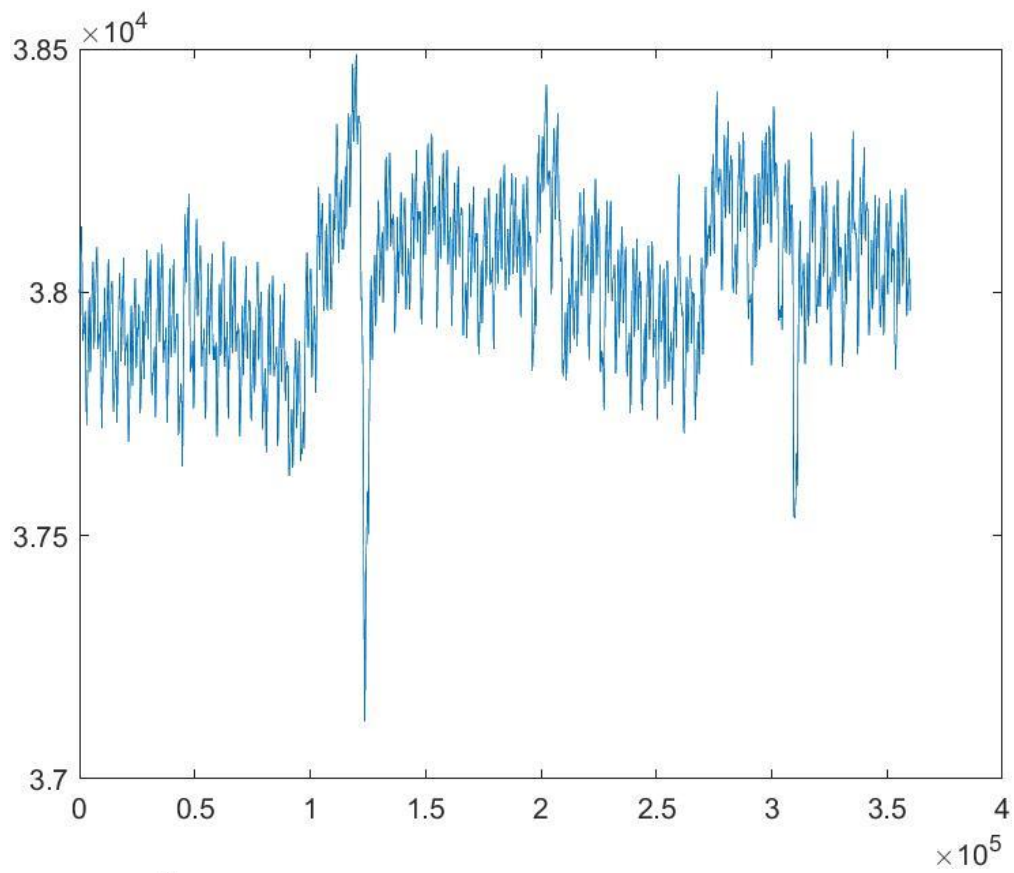
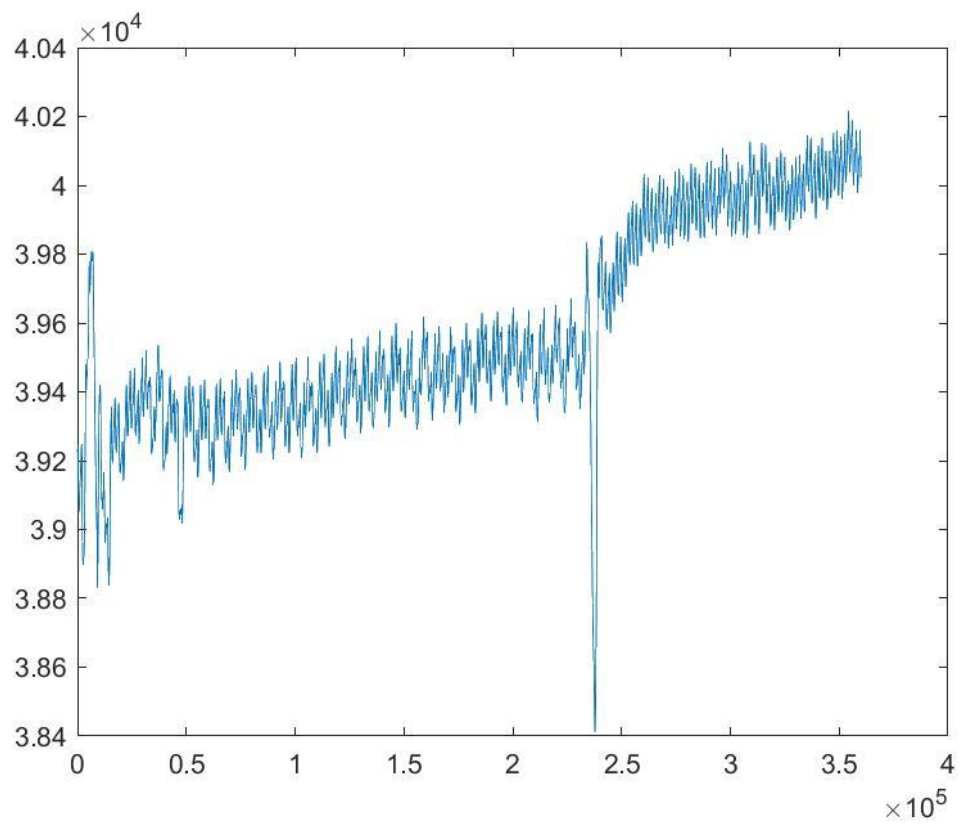
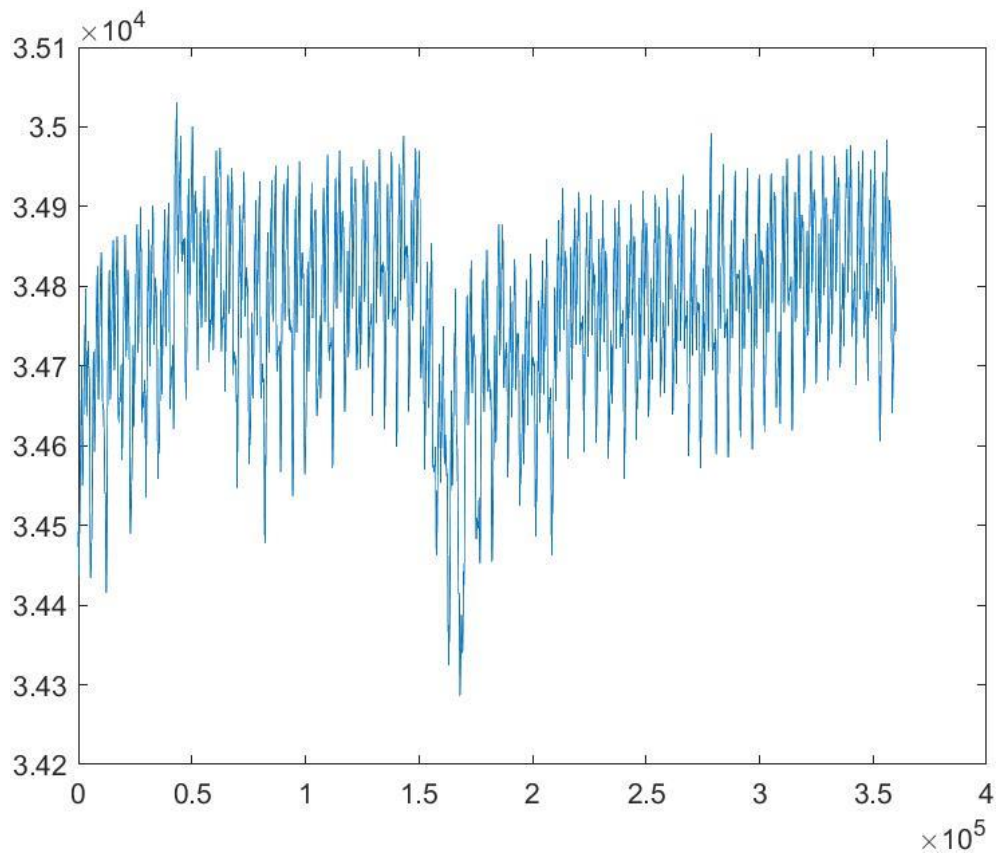


Figure-Stroke volume for 160 seconds for sample 39.

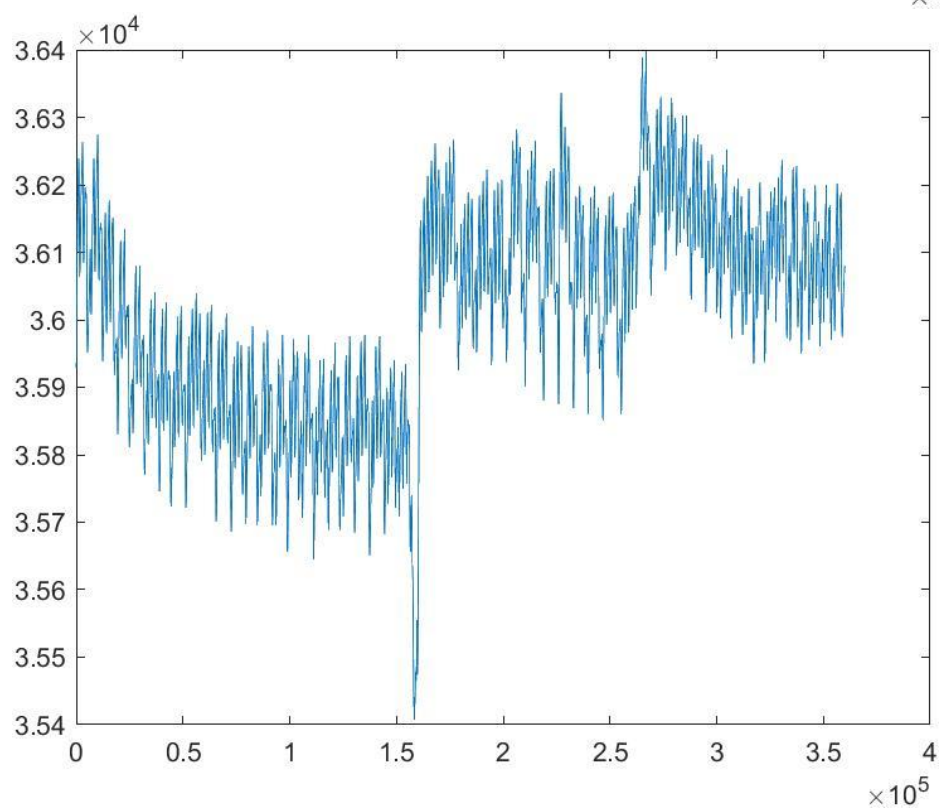
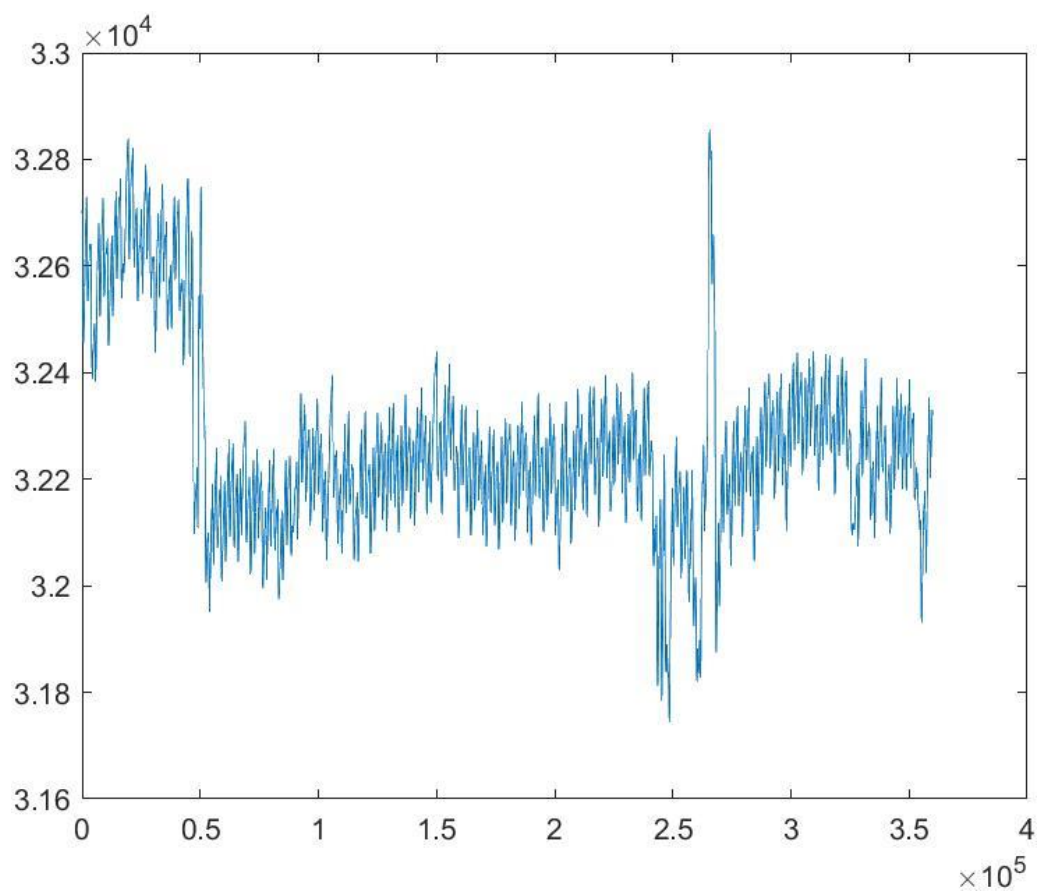
Appendix D: detected Impedance.



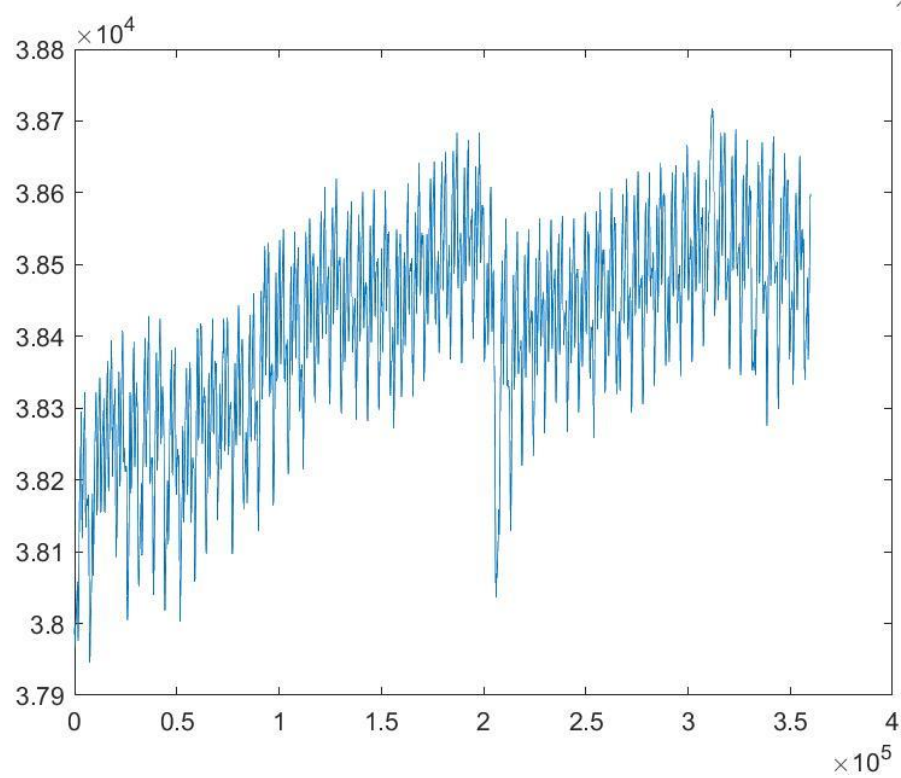
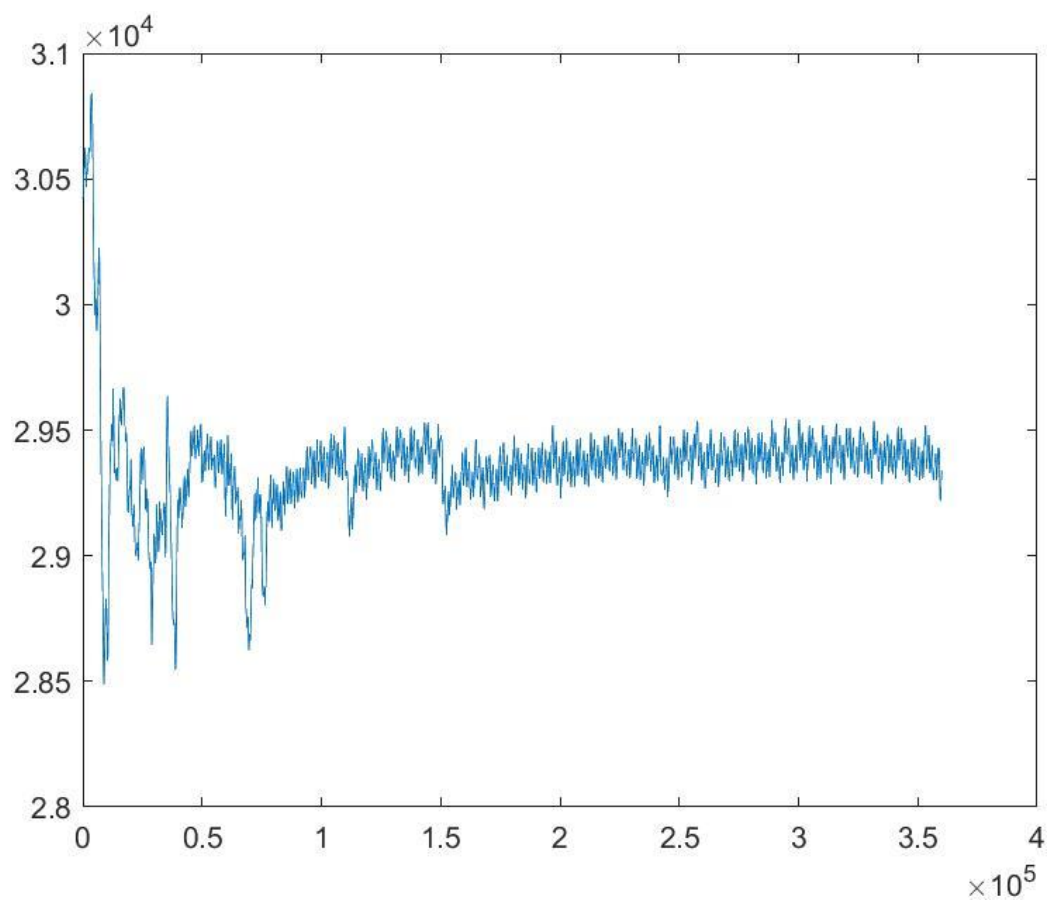
Impedance detected for sample 1 and 2.



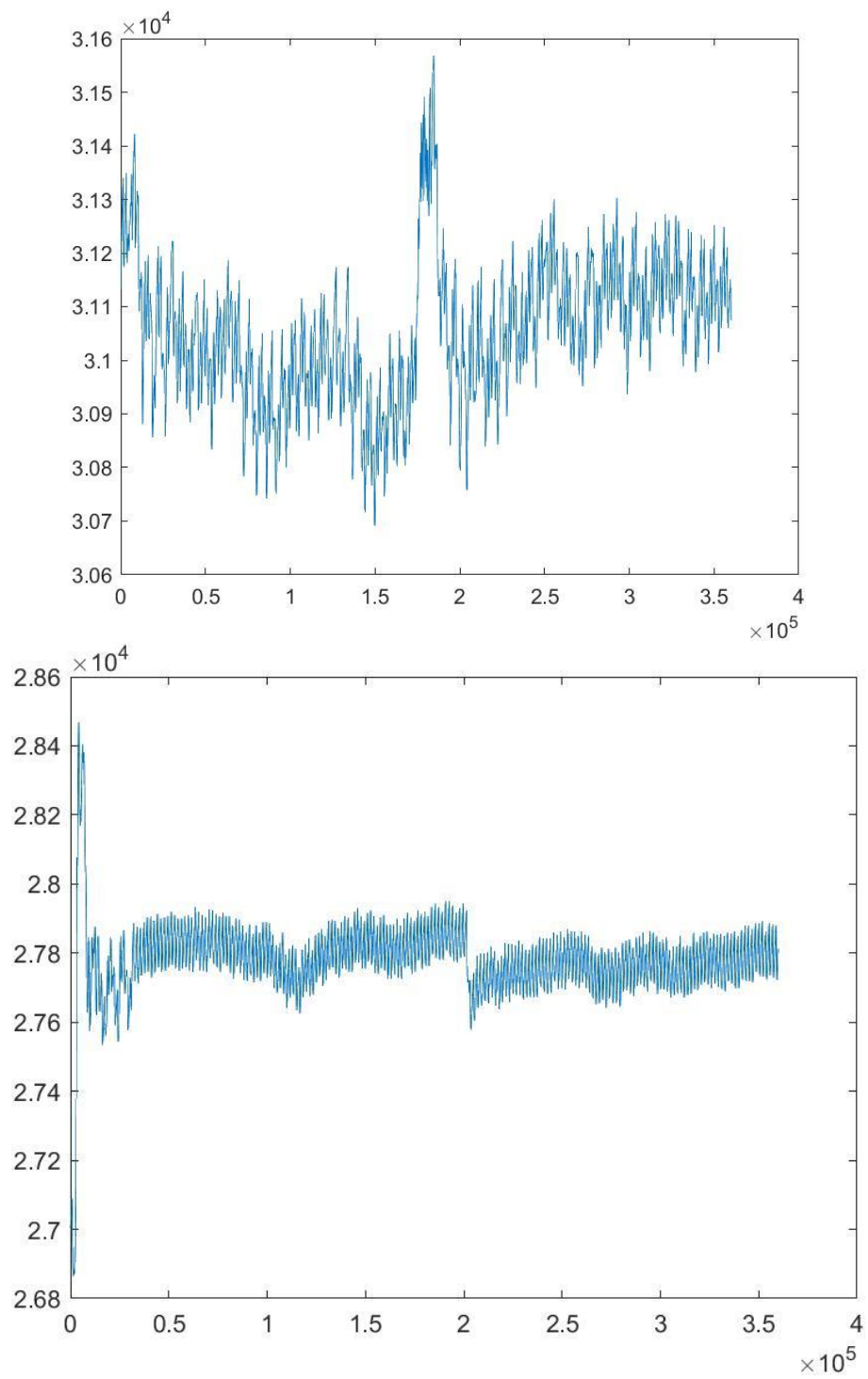
Impedance detected for sample 3 and 4.



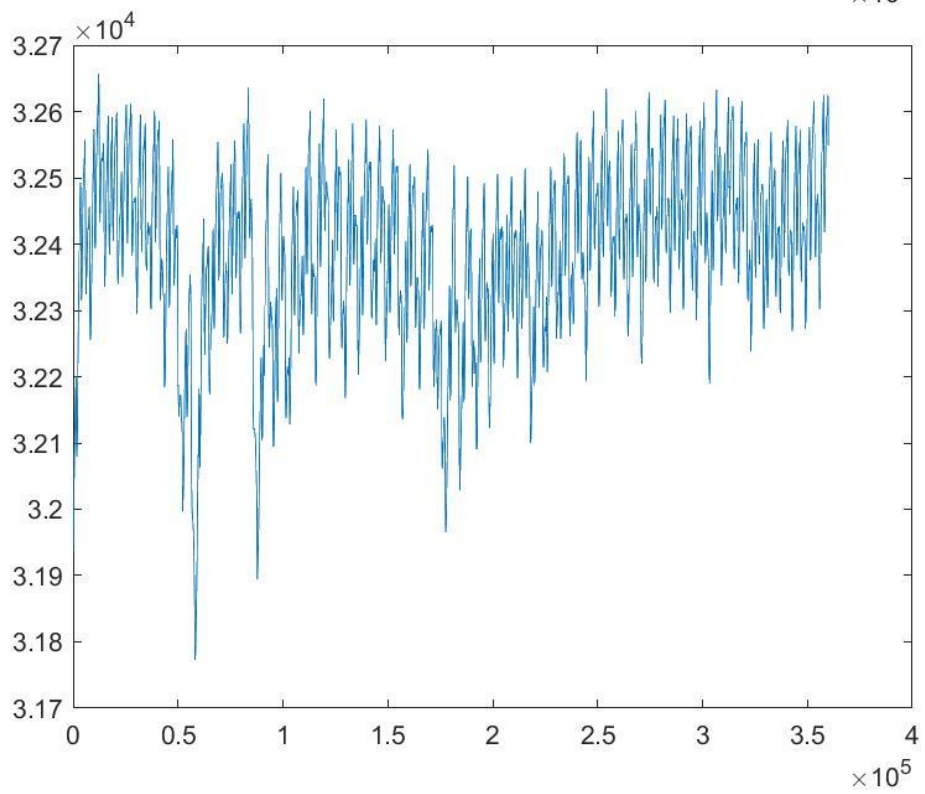
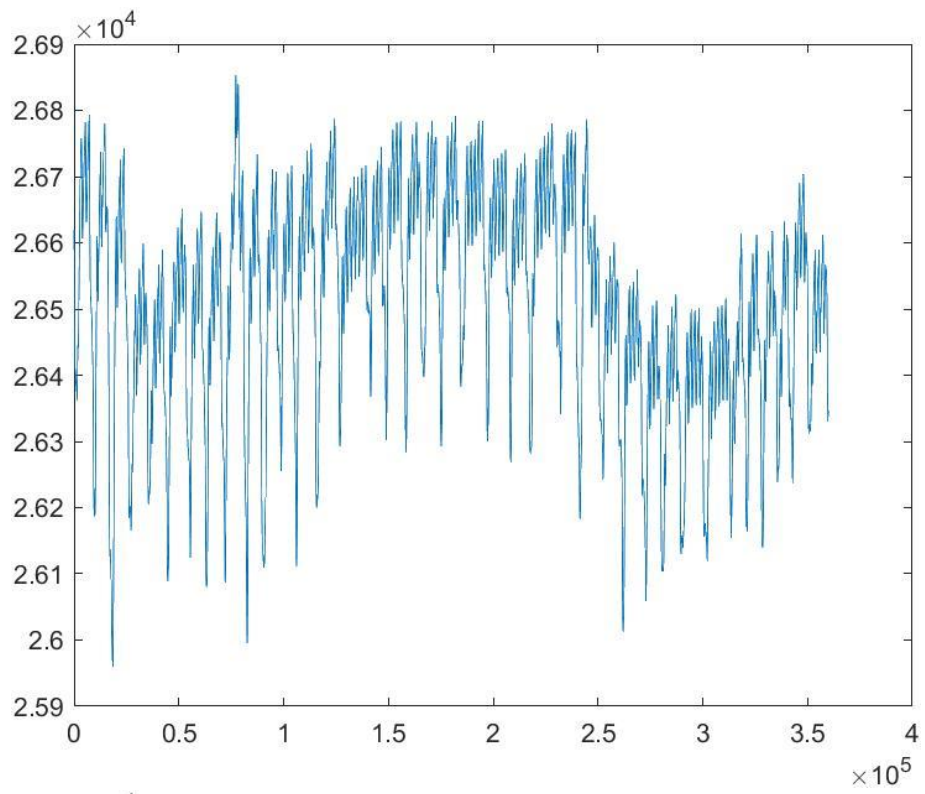
Impedance detected for sample 5 and 6.



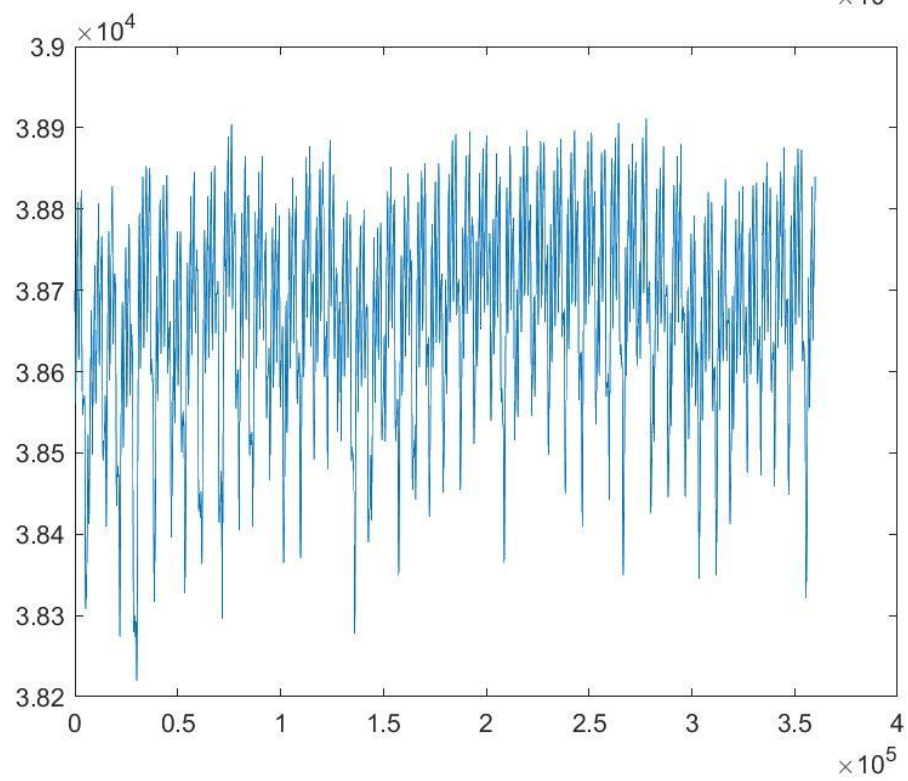
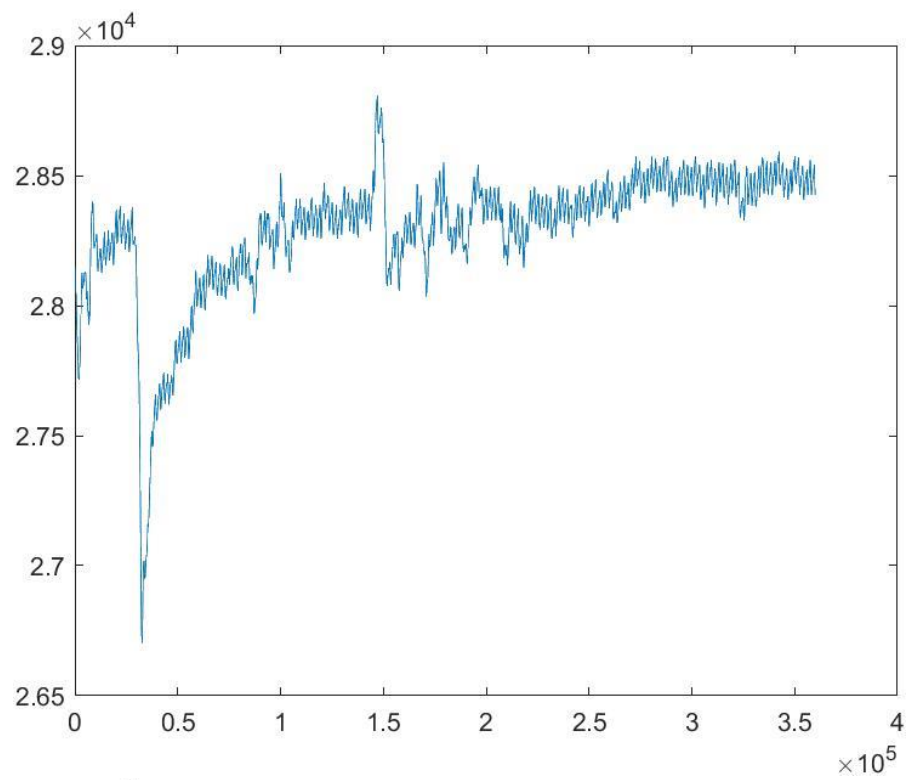
Impedance detected for sample 7 and 8.



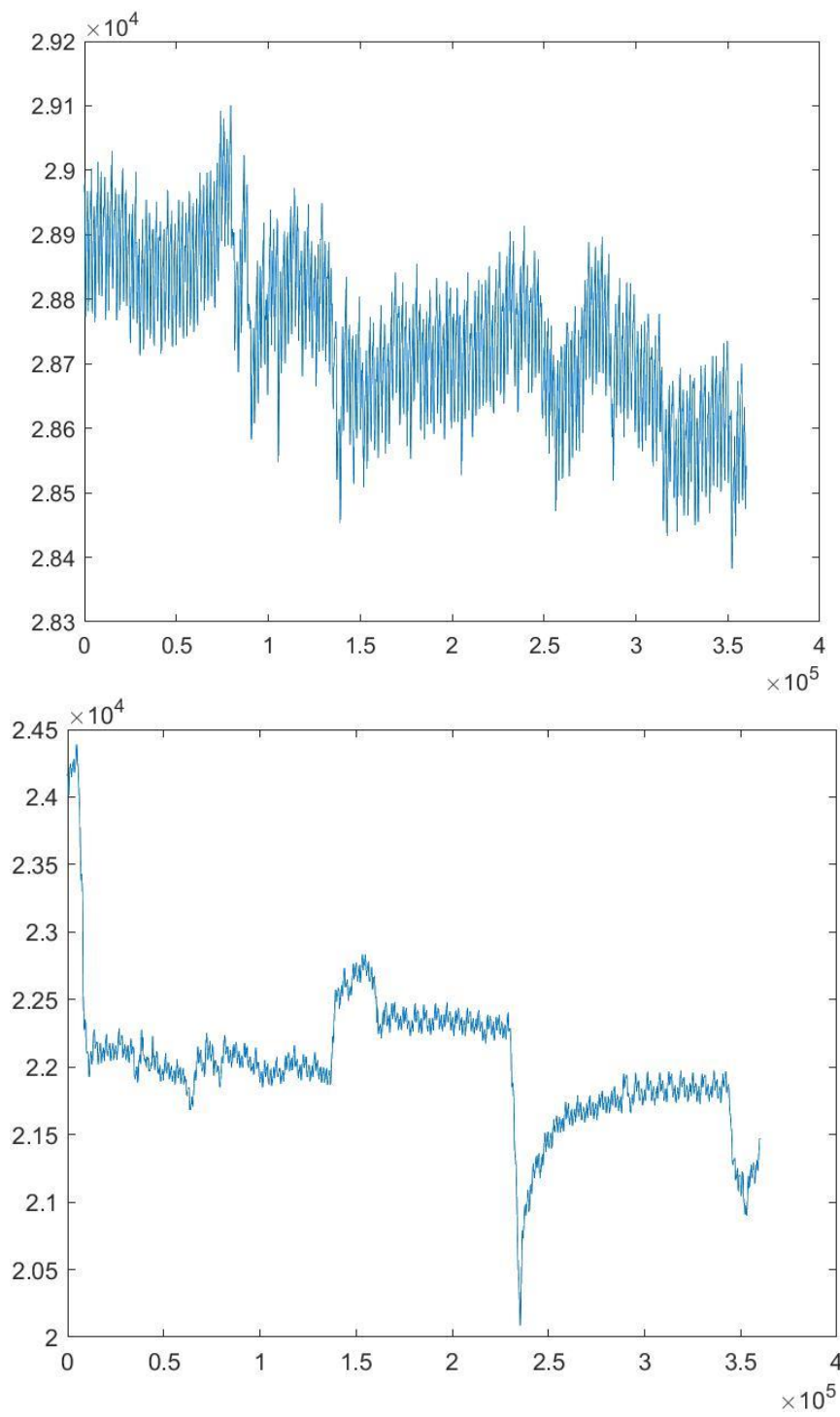
Impedance detected for sample 9 and 10.



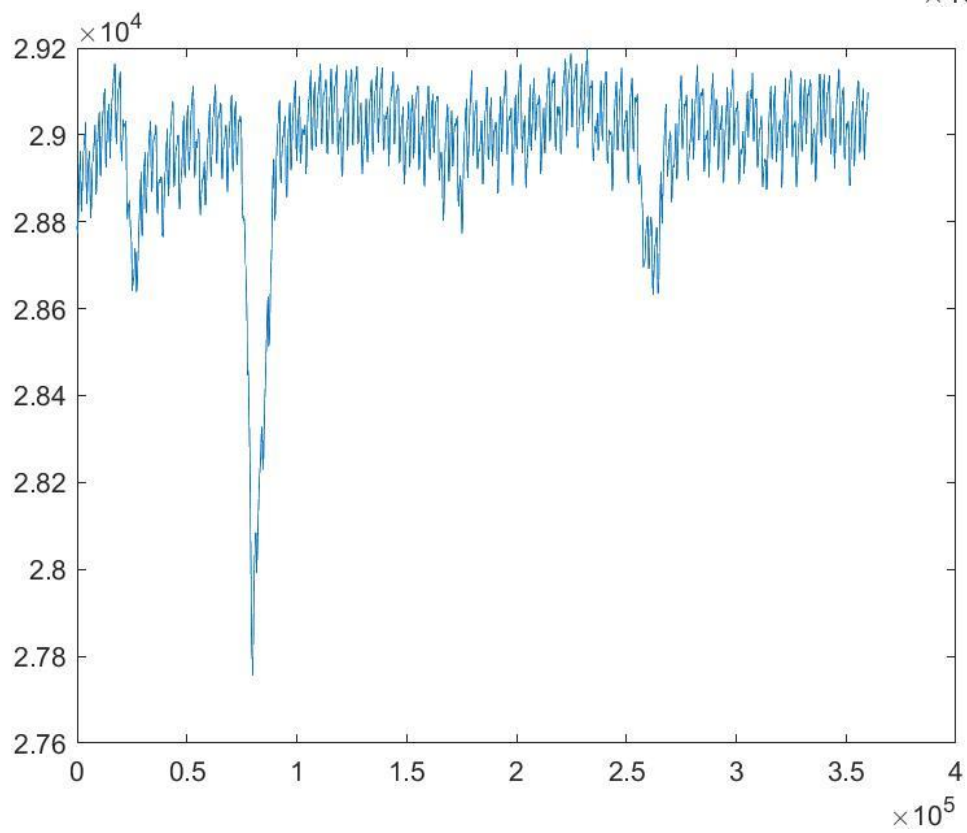
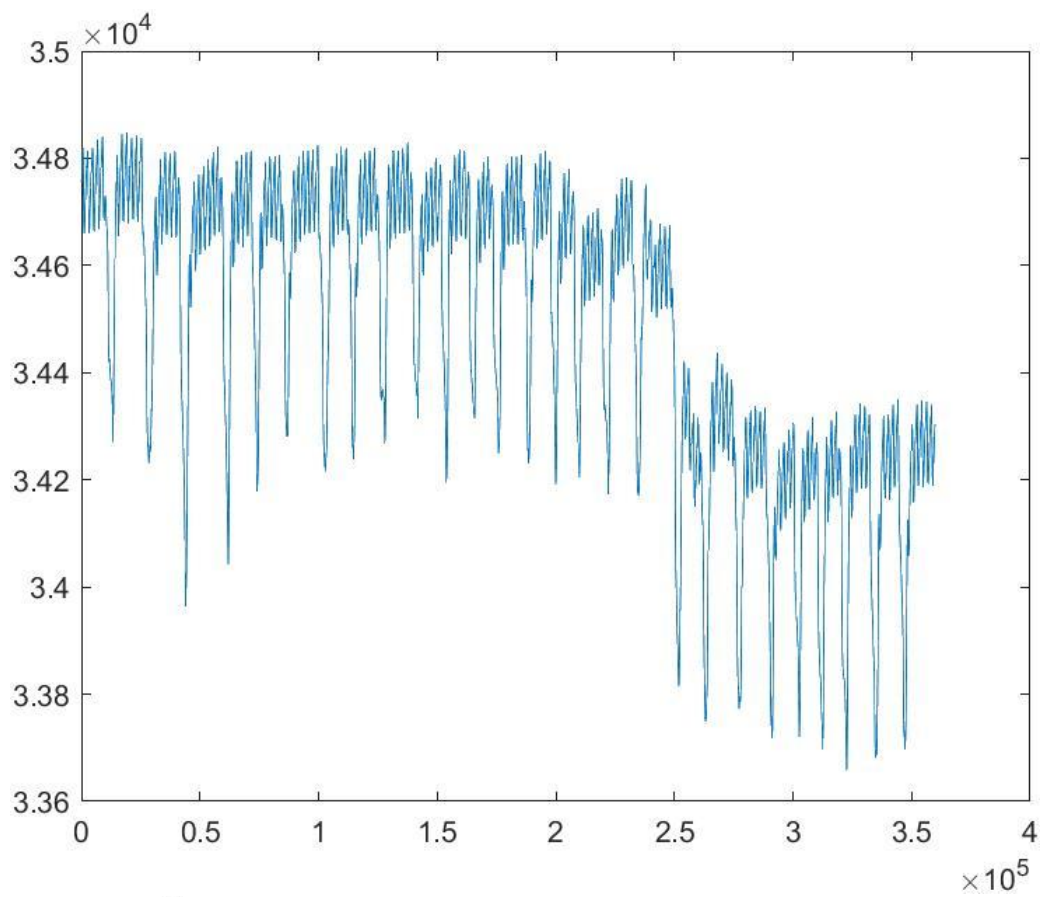
Impedance detected for sample 11 and 12.



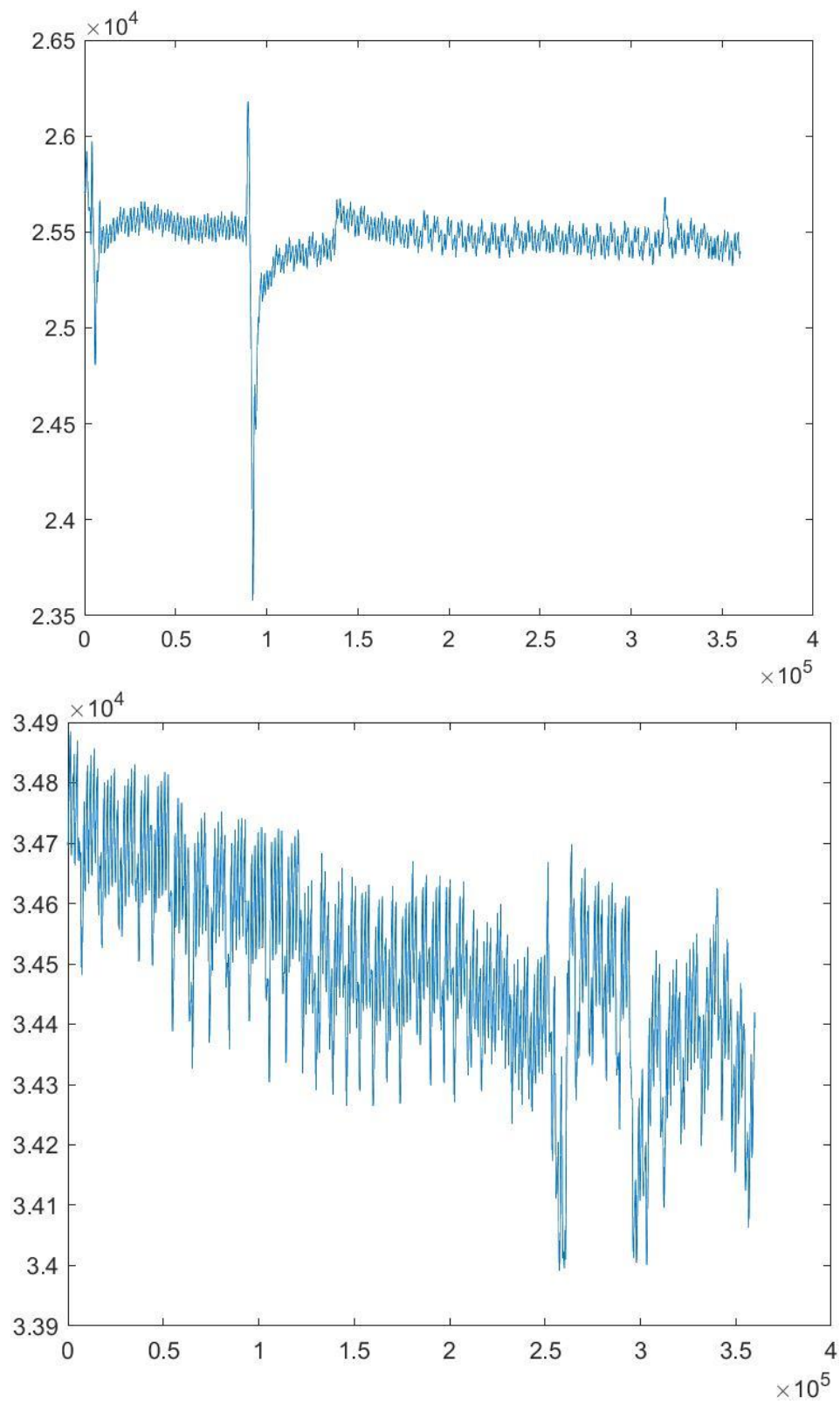
Impedance detected for sample 13 and 14.



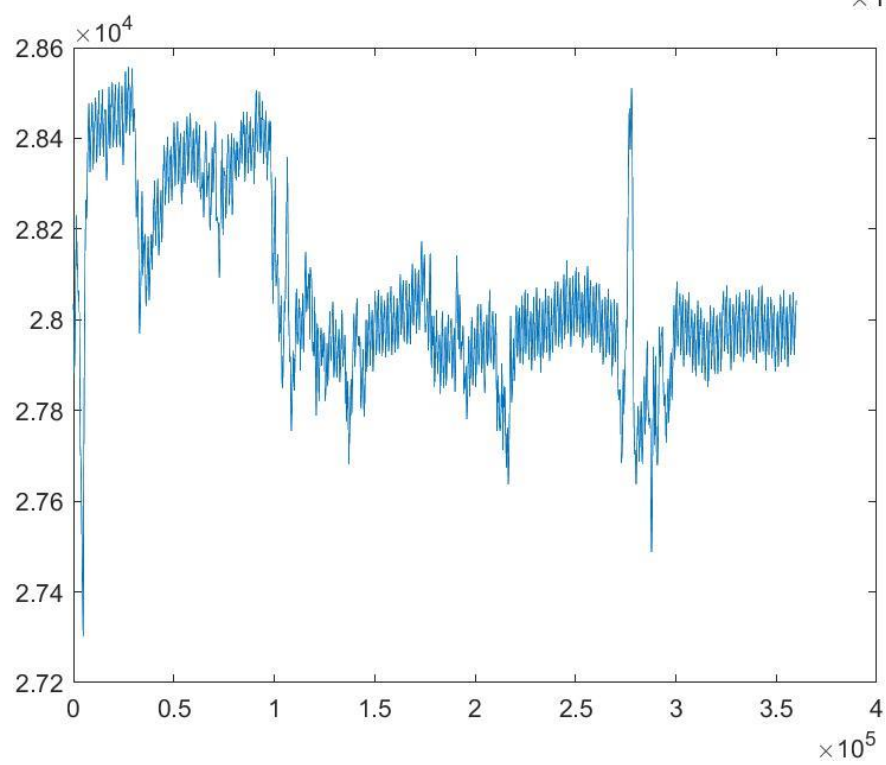
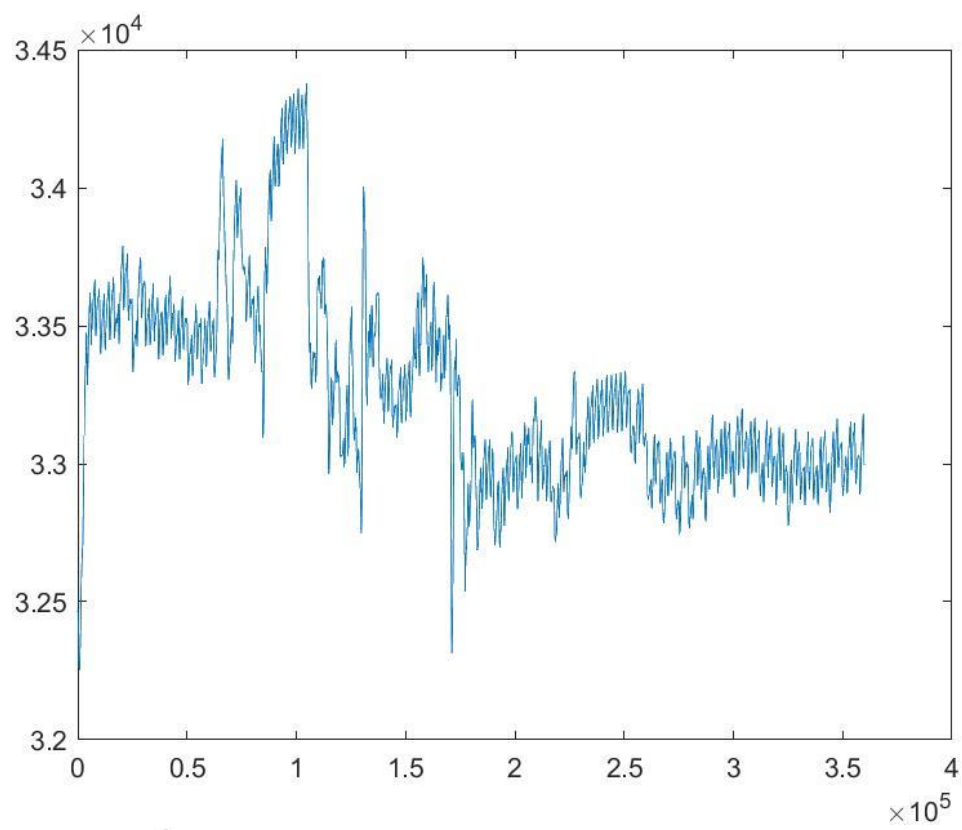
Impedance detected for sample 15 and 16.



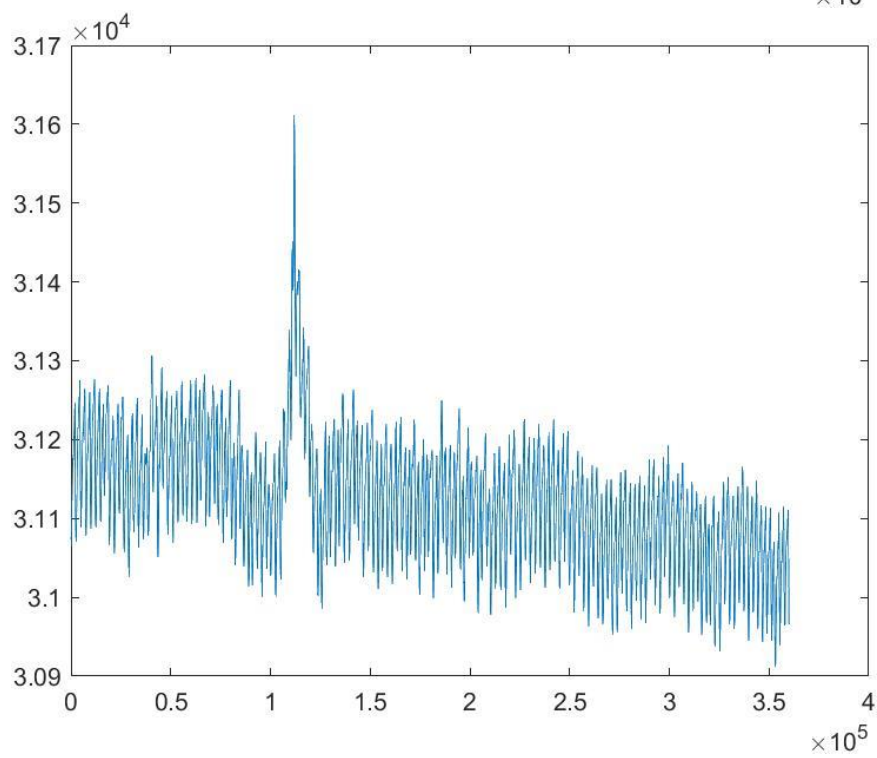
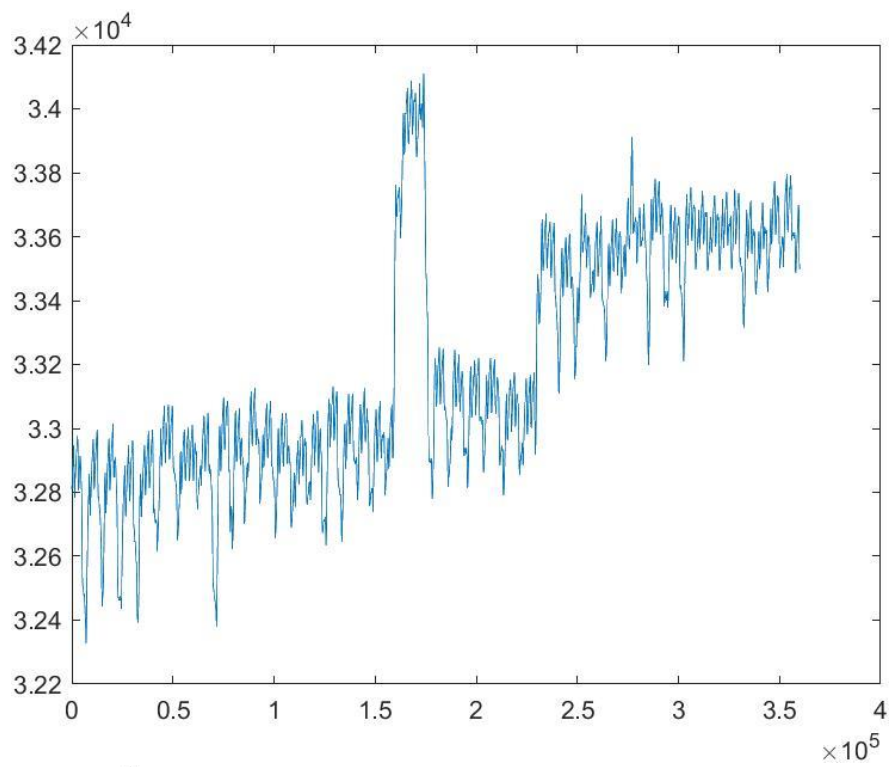
Impedance detected for sample 17 and 18.



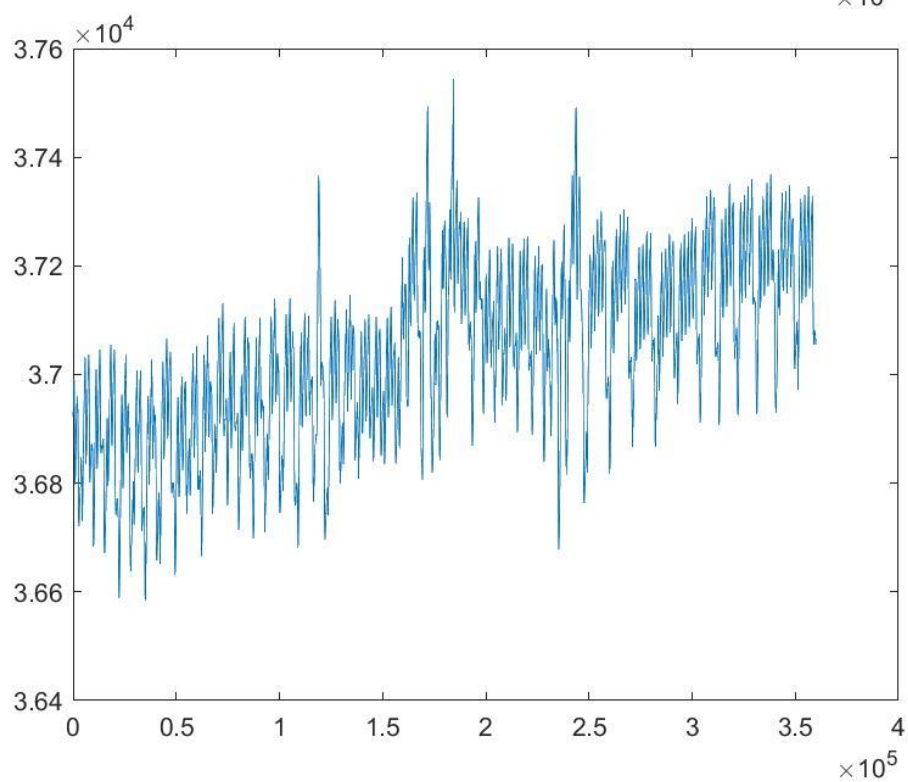
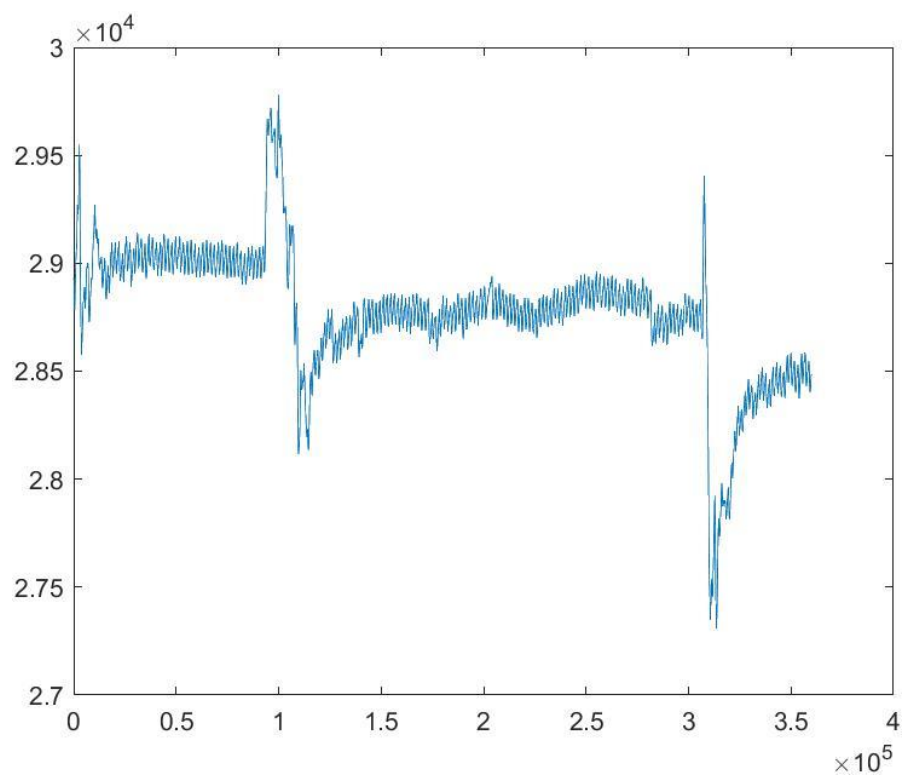
Impedance detected for sample 19 and 20.



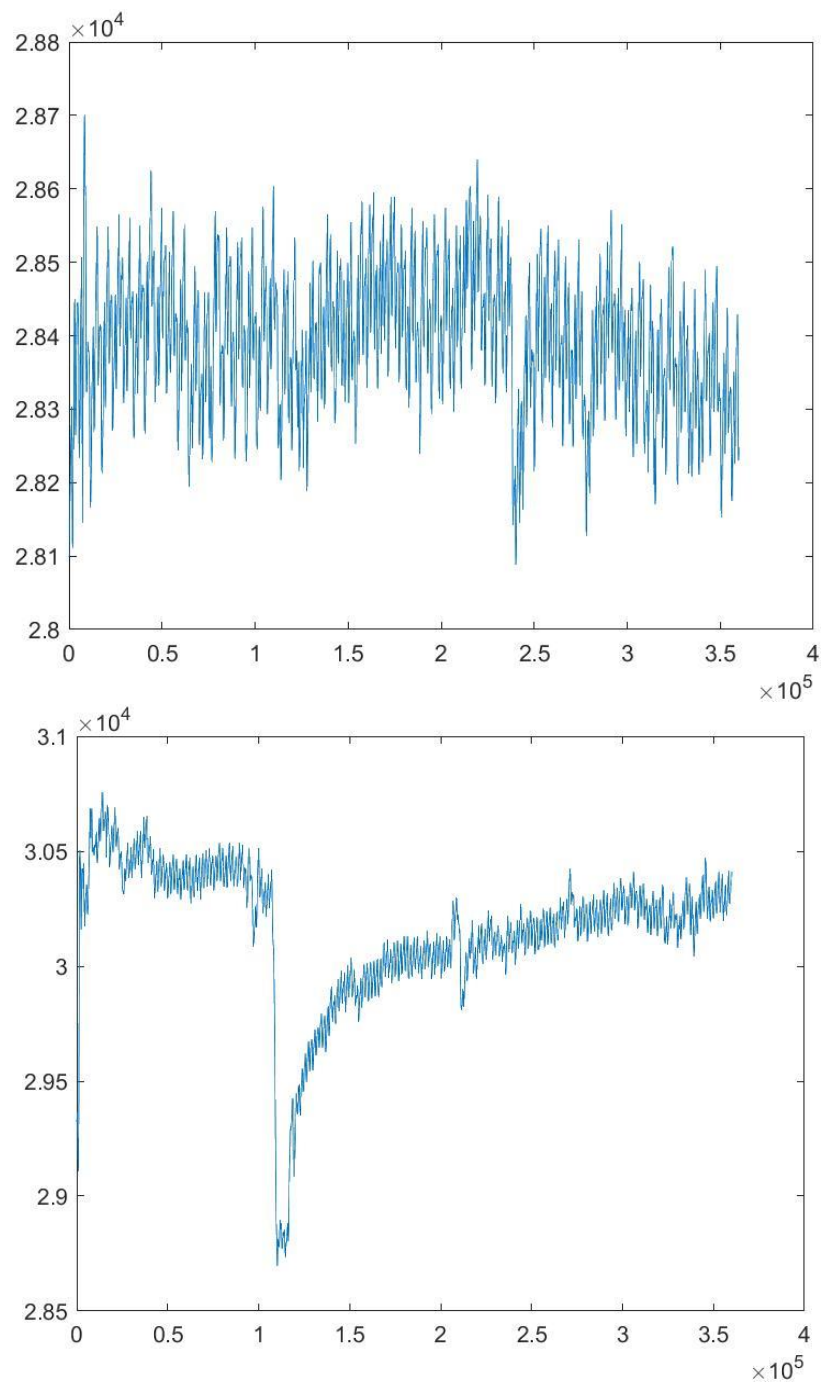
Impedance detected for sample 21 and 22.



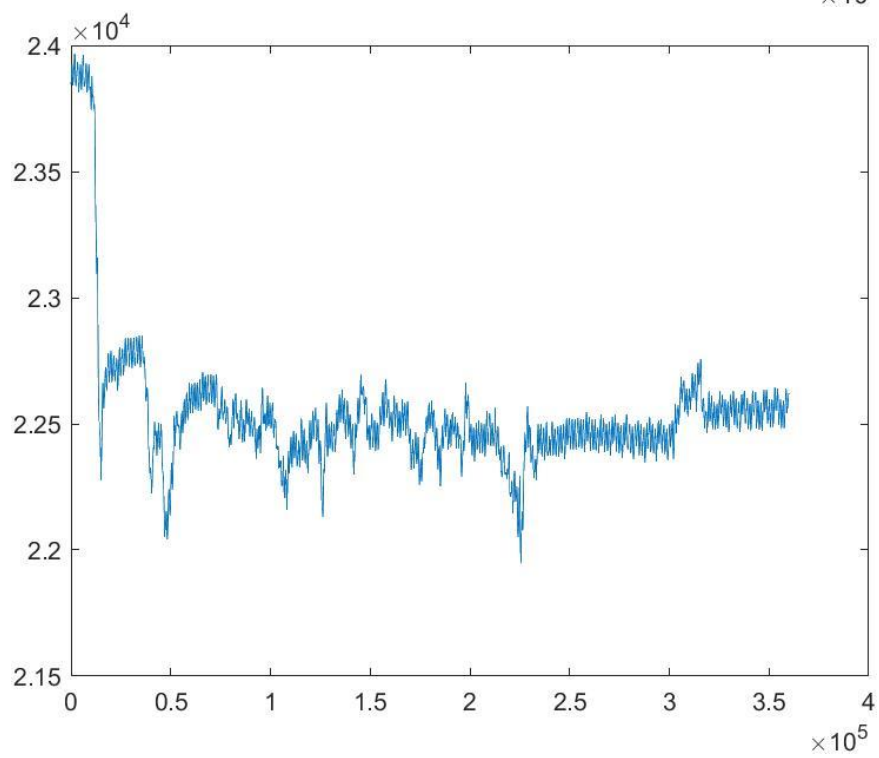
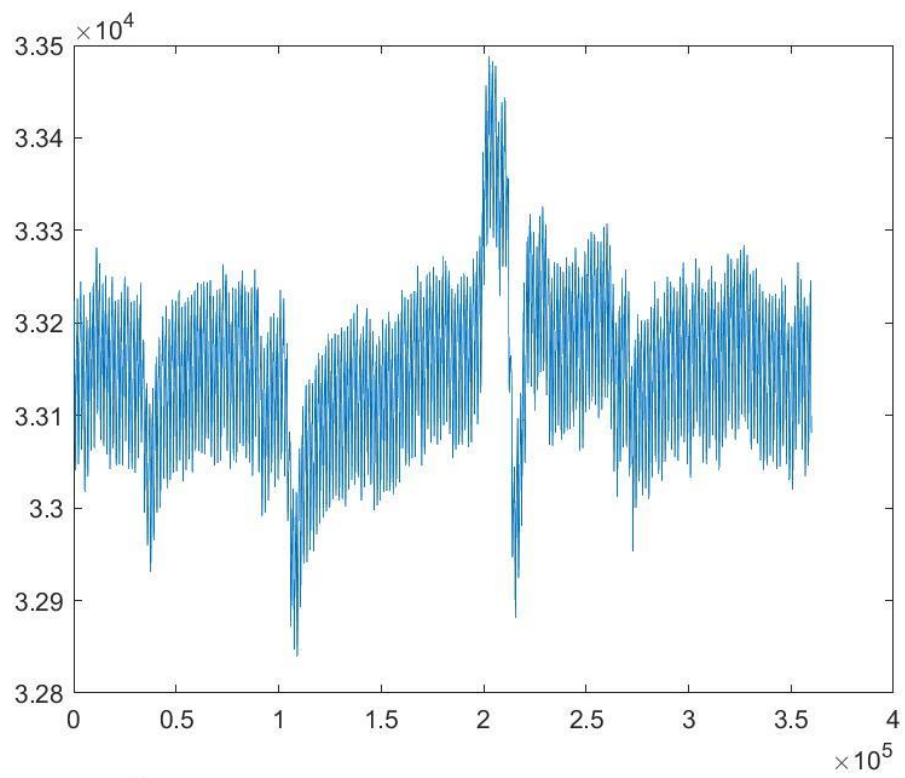
Impedance detected for sample 23 and 24.



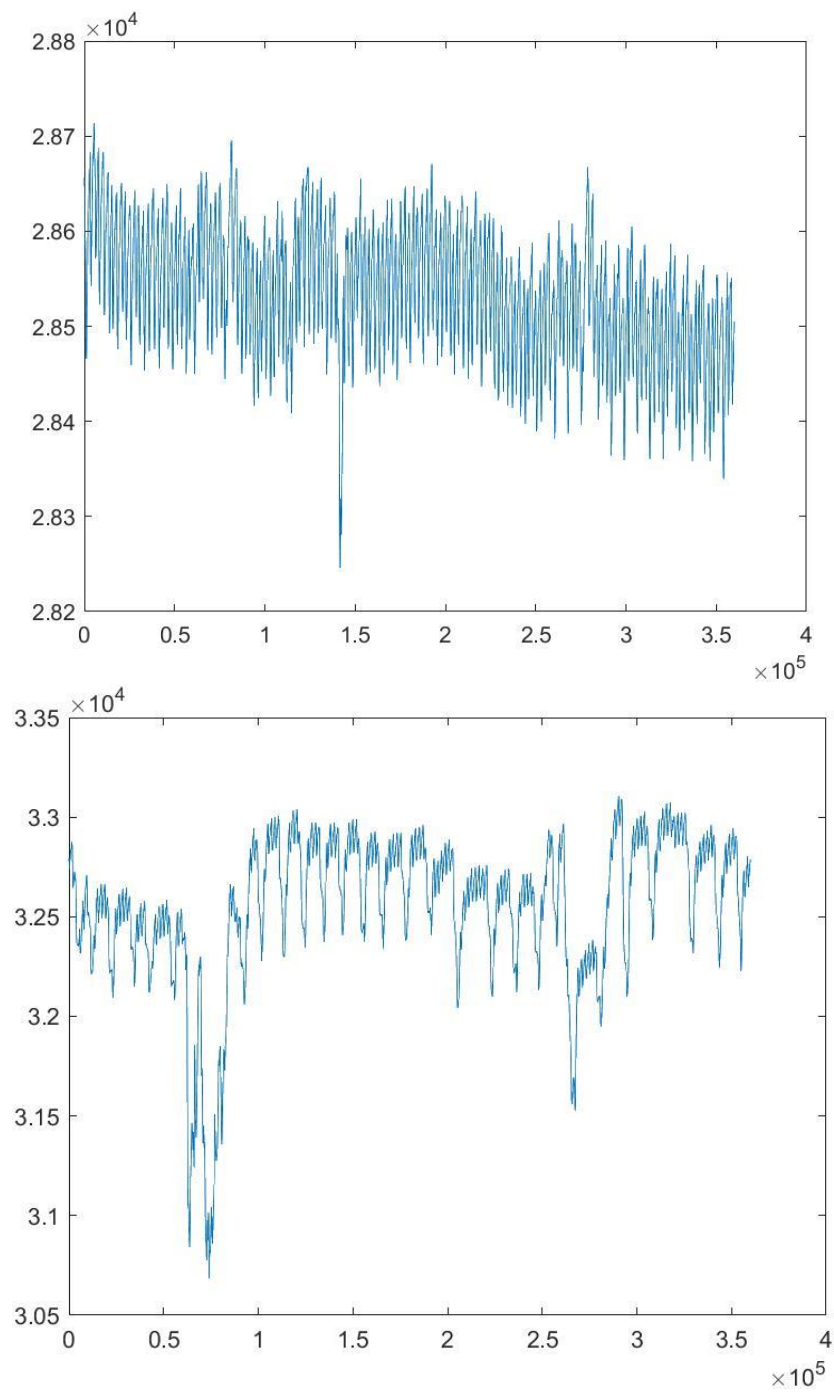
Impedance detected for sample 25 and 26.



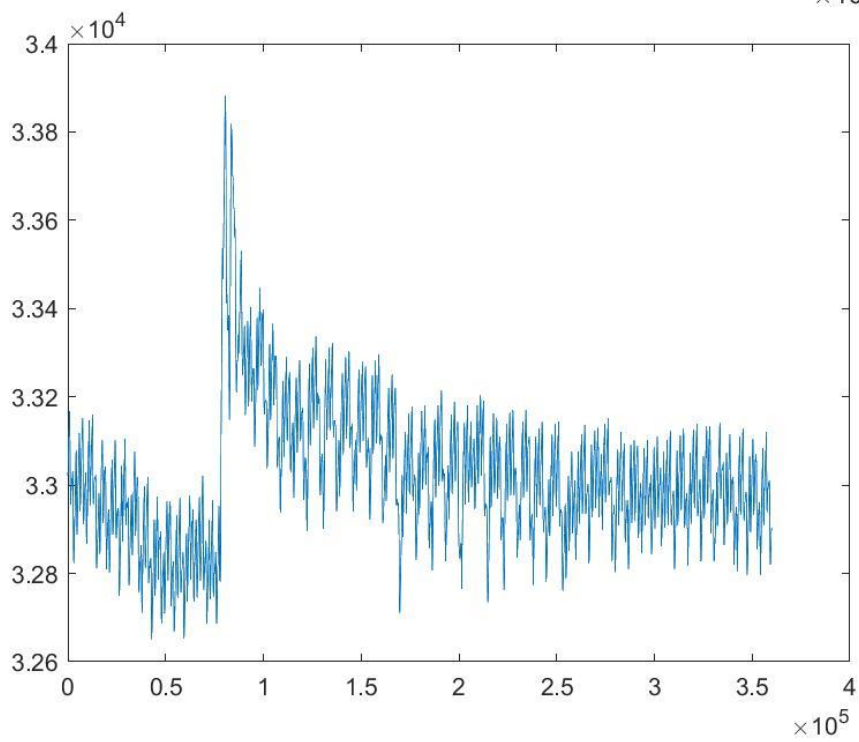
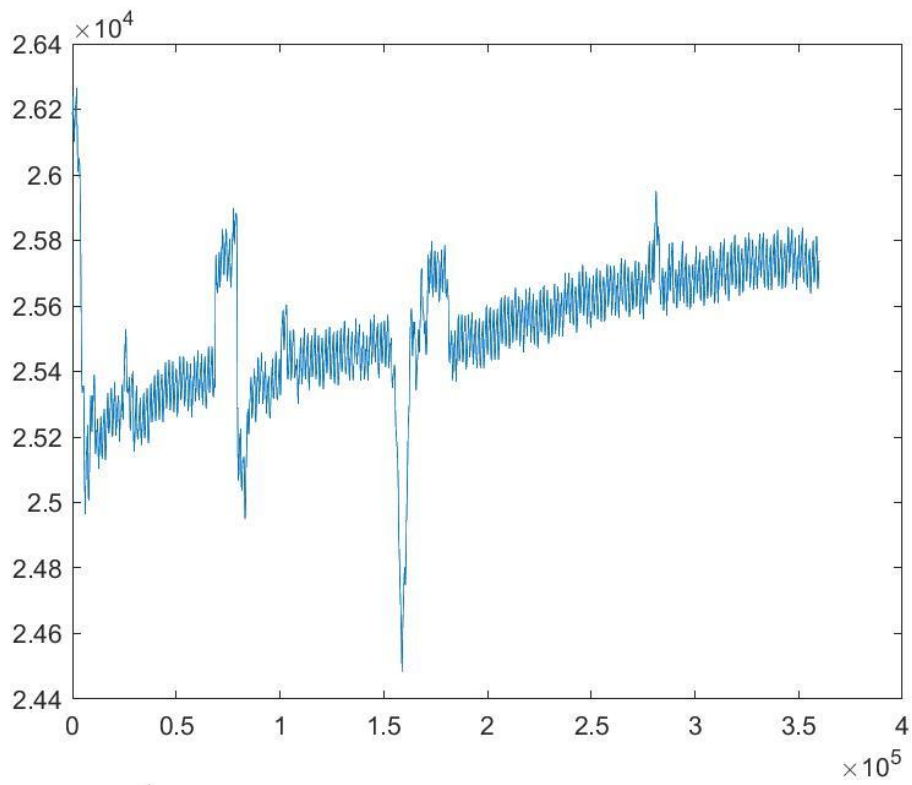
Impedance detected for sample 27 and 28.



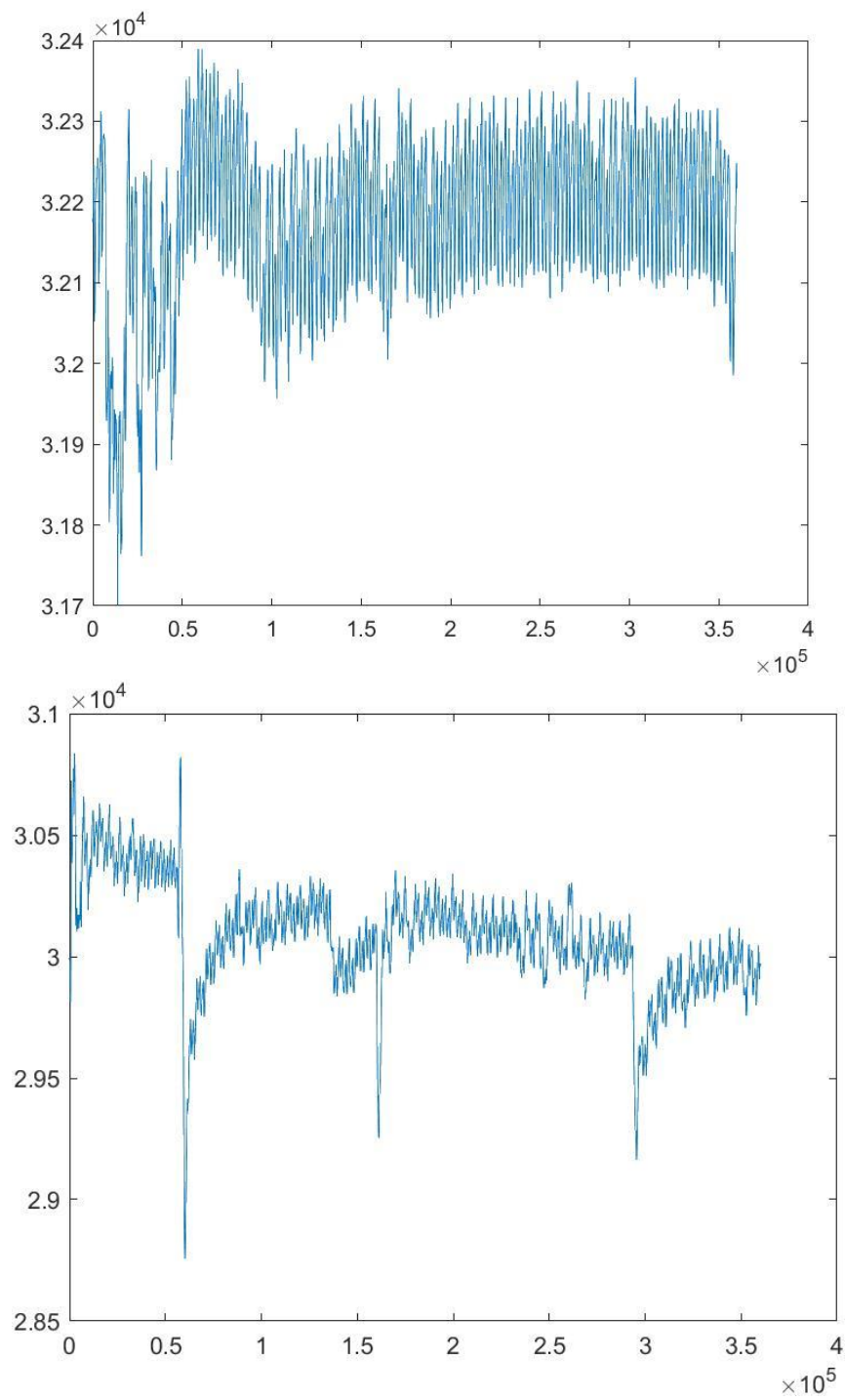
Impedance detected for sample 29 and 30.



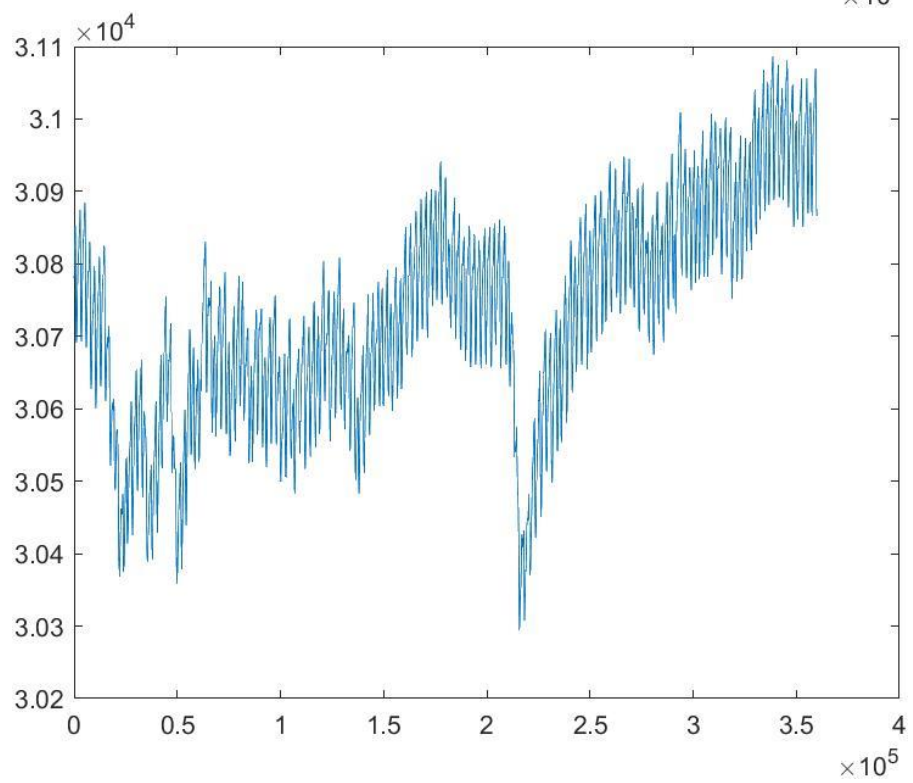
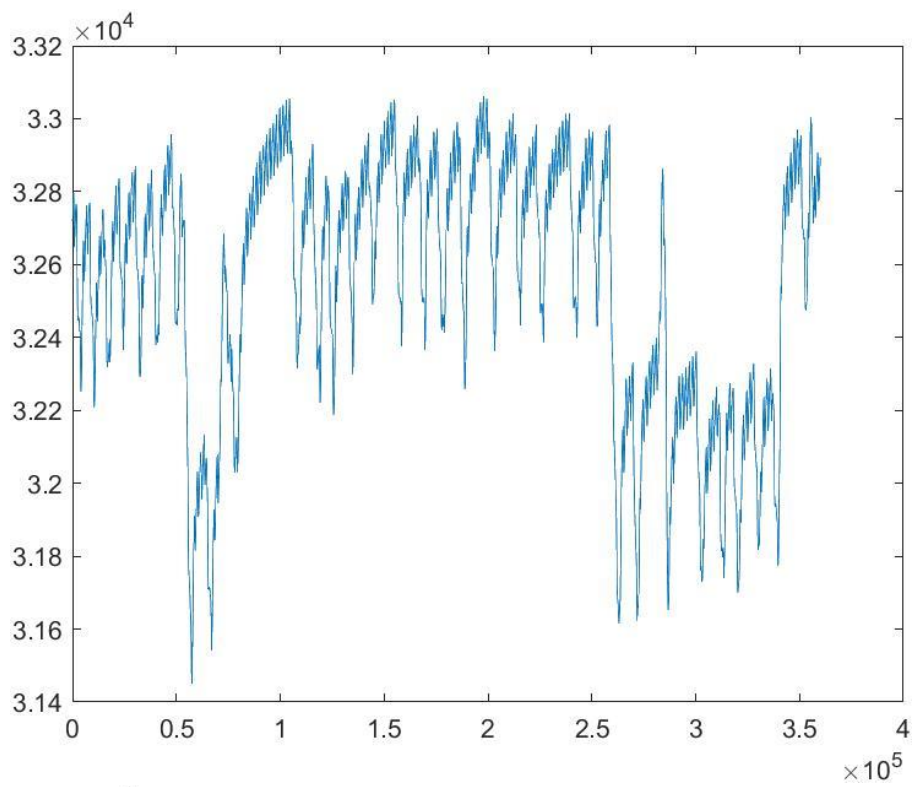
Impedance detected for sample 31 and 32.



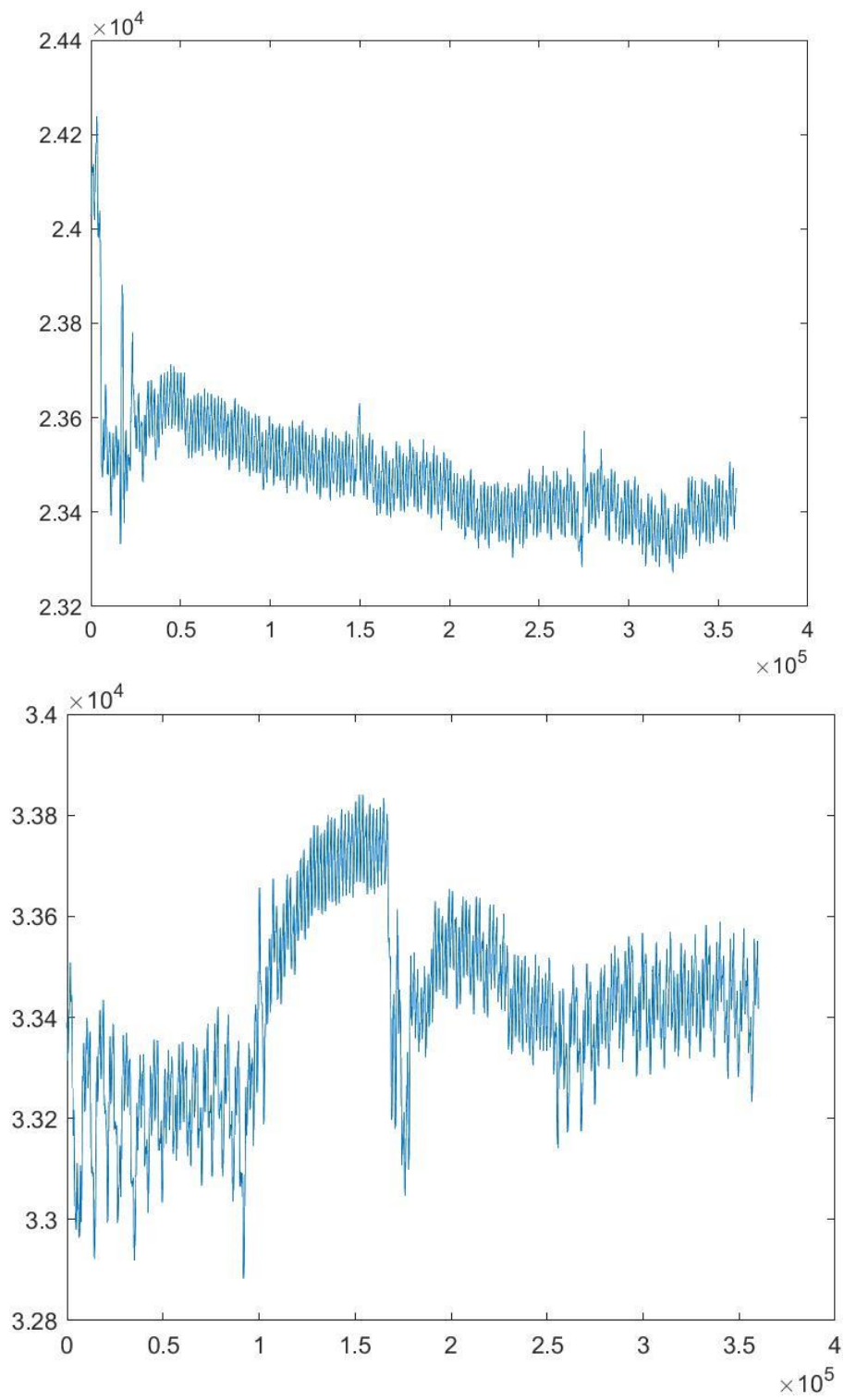
Impedance detected for sample 33 and 34.



Impedance detected for sample 35 and 36.



Impedance detected for sample 37 and 38.



Impedance detected for sample 39 and 40.

Appendix D: regression model concerning the correlation between Stroke Volume and acceleration.

Subject A.

A3 (sample: 230)

2021/06/30 – h 5:46:55

variable	sv	x	y	z
mean	58,49	0,61	-0,145	0,034
DS	7,34	0,017	0,005	0,004
IV%	12,6	2,8	3,6	11,8
median	58,52	0,61	-0,145	0,034

A6 (sample: 179)

2021/06/30 - h 18:41:43

variable	sv	x	y	z
mean	66,46	0,72	-0,107	0,027
DS	7,91	0,043	0,01	0,012
IV%	11,9	6,0	66,4	44,4
median	66,46	0,71	-0,108	0,026

A8 (sample: 97)

2021/07/01 – h 05:49:53

variable	Sv	X	Y	z
mean	60,17	0,62	-0,134	0,035
DS	17,36	0,025	0,01	0,011
IV%	28,85	4	7,46	31,4
median	62,13	0,62	0,134	0,035

A11 (sample: 202)

2021/07/01 – h 07:45:17.000

variable	Sv	x	y	Z
mean	70,79	0,71	-0,130	0,032
DS	7,77	0,032	0,009	0,01
IV%	10,0	4,5	2,76	31,2
median	71,5	0,71	0,131	0,032

A14 (sample: 173)

2021/07/01 – h 17:47:50.000

variable		sv	x	y	Z
mean		52,8	0,66	-0,138	0,031
DS		9,48	0,032	0,009	0,008
IV%		17,9	4,8	6,52	25,8
median		52,99	0,65	0,138	0,03

A17 (sample: 195)

2021/07/02 – h 06:37:41.000

variable	sv	x	y	z
mean	63,41	0,66	0,124	0,032
DS	13,58	0,014	0,005	0,004
IV%	21,4	2,1	4,03	12,5
median	63,27	0,66	0,125	0,033

A20 (sample: 176)

2021/07/02 - h 17:25:14.000

variable	sv	x	y	z
mean	62,32	0,64	-0,108	0,031
DS	8,04	0,041	0,01	0,011
IV%	12,9	6,4	9,3	35,5
median	62,32	0,64	0,108	0,032

A23 (sample: 154)

2021/07/03 h 05:44:42.000

variable	sv	x	y	z
mean	54,05	0,64	-0,13	0,034
DS	9,62	0,025	0,007	0,007
IV%	17,8	3,9	5,4	20,6
median	56,2	0,64	0,129	0,033

A28 (sample: 139)

2021/07/04 - h 06:57:11.000

variable	sv	x	y	z
mean	58,51	0,54	-0,110	0,031
DS	12,05	0,03	0,013	0,016
IV%	20,6	6,5	11,8	51,6
median	58,58	0,54	0,107	0,028

A32 (sample: 161)

2021/07/05 - h 08:08:43.000

variable	sv	x	y	z
mean	51,78	0,58	-0,089	0,033
DS	6,99	0,03	0,007	0,007
IV%	13,5	6,2	7,9	21,2
median	53,17	0,58	-0,09	0,033

A34 (sample: 176)

2021/07/05 - h 17:03:39.000

variable	sv	x	Y	Z
mean	53,36	0,61	-0,079	0,065
DS	6,16	0,06	0,014	0,014
IV%	11,5	9,8	17,7	21,5
median	53,25	0,62	-0,08	0,033

A39 (sample:)

2021/07/06 – h 16:21:58.000

variable	sv	x	y	z
mean	59,28	0,58	-0,1	0,033
DS	6,74	0,02	0,01	0,009
IV%	11,4	3,4	10	28,3
median	59,3	0,58	-0,1	0,034

Subject B

B2 (sample: 112)

2021/06/30 – h 05:05:58.000

variable	sv	x	y	z
mean	72,64	0,61	-0,145	0,034
DS	13,11	0,017	0,005	0,004
IV%	18	2,8	3,6	11,8
median	74,7	0,61	-0,145	0,034

B5 (sample: 142)

2021/06/30 – h 18:20:15.000

variable	sv	x	y	z
mean	52,28	0,71	-0,108	0,028
DS	10,43	0,057	0,016	0,017
IV%	19,9	8	1,5	60,7
median	52,32	0,70	-0,108	0,028

B9 (sample: 121)

2021/07/01 – h 06:12:56.000

variable	sv	x	y	z
mean	61,47	0,66	-0,133	0,033
DS	13,18	0,034	0,009	0,01
IV%	19,5	5,1	6,8	30,3
median	61,6	0,66	-0,132	0,035

B12 (sample: 146)

2021/07/01 – h 17:17:33.000

variable	sv	x	y	z
mean	47,83	0,69	-0,131	0,031
DS	7,89	0,042	0,035	0,026
IV%	16,5	6,1	26,7	83,9
median	47,91	0,69	-0,133	0,034

B16 (sample: 55)

2021/07/02 – h 06:26:50.000

variable	sv	x	y	z
mean	46,85	0,66	-0,125	0,034
DS	13	0,013	0,006	0,006
IV%	27,7	2	4,8	17,6
median	43,7	0,66	-0,126	0,035

B19 (sample: 178)

2021/07/02 – h 17:06:44.000

variable	sv	x	y	z
mean	62,40	0,66	-0,105	0,032
DS	7,24	0,047	0,013	0,014
IV%	11,4	7,1	12,4	43,7
median	62,9	0,61	-0,105	0,032

B22 (sample: 122)

2021/07/03 – h 05:29:21.000

variable	sv	x	y	z
mean	48,07	0,64	-0,13	0,035
DS	11,08	0,017	0,006	0,005
IV%	22,3	2,7	4,6	14,3
median	46,8	0,63	-0,129	0,035

B25 (sample: 141)

202/ 07/03 - h 18:04:07.000

variable	sv	x	y	z
mean	69,28	0,46	-0,144	0,024
DS	12,73	0,250	0,093	0,021
IV%	18,4	54,3	64,6	87,5
median	67,98	0,46	-0,146	0,033

B27 (sample: 156)

2021/07/04 – h 06:46:13.000

variable	sv	x	y	z
mean	51,79	0,55	-0,111	0,029
DS	10,2	0,084	0,009	0,018
IV%	19,7	15,3	8,1	62,1
median	52,55	0,54	-0,11	0,029

B31 (sample: 149)

2021/07/05 – h 07:43:25.000

variable	sv	x	y	z
mean	50,42	0,58	-0,089	0,034
DS	12,28	0,032	0,005	0,006
IV%	24,3	5,5	5,6	17,6
median	49,64	0,58	-0,091	0,033

B35 (sample: 174)

2021/07/05 – h 17:59:27.000

variable	sv	x	y	z
mean	59,87	0,6	-0,074	0,029
DS	10,32	0,033	0,009	0,01
IV%	17,2	5,5	3,4	34,5
median	60,75	0,6	-0,074	0,028

B36 (sample: 174)

2021/07/06 – h 05:41:19.000

variable	sv	x	y	z
mean	46,86	0,67	- 0,074	0,031
DS	7,97	0,009	0,004	0,003
IV%	17	1,5	5,4	9,7
median	46,29	0,58	- 0,067	0,031

Subject C.

C1 (sample: 166)

2021/06/30 - h 04:40:54.000

variable	sv	x	y	z
mean	58,27	0,64	-0,145	0,033
DS	9,45	0,03	0,006	0,006
IV%	16,2	4,7	36,5	18,2
median	59,02	0,63	-0,144	0,033

C4 (sample: 177)

2021/06/30 - h 18:09:25.000

variable	sv	x	y	z
mean	59,11	0,71	-0,107	0,028
DS	10,06	0,038	0,011	0,012
IV%	17	5,3	10,3	42,9
median	59,56	0,71	-0,108	0,027

C7 (sample: 165)

2021/06/30 – h 05:32:29.000

variable	sv	x	y	z
mean	62,99	0,6	-0,144	0,034
DS	9,89	0,01	0,004	0,003
IV%	15,7	1,7	2,8	8,8
median	63,67	0,6	-0,144	0,032

C10 (sample: 211)

2021/07/01/ - h 07:35:57.000

variable	sv	x	y	z
mean	71,96	0,69	-0,13	0,034
DS	10,8	0,048	0,014	0,014
IV%	15	28,7	10,8	41,2
median	73,2	0,69	-0,13	0,033

C13 (sample: 158)

2021/07/01 – h 17:29:13.000

variable	sv	x	y	z
mean	60,97	0,69	-0,14	0,034
DS	19,11	0,028	0,011	0,012
IV%	31,3	4,01	7,9	35,3
median	58,75	0,69	-0,14	0,031

C15 (sample: 158)

2021/07/02 - h 05:38:04.000

variable	sv	x	y	z
mean	56,55	0,67	-0,126	0,036
DS	11,97	0,020	0,006	0,005
IV%	21,2	2,98	4,8	13,9
median	57,05	0,66	-0,125	0,032

C18 (sample: 191)

2021/07/02 – h 16:51:38.000

variable	sv	x	y	z
mean	62,88	0,64	-0,109	0,032
DS	13,61	0,037	0,01	0,009
IV%	21,6	5,78	0,2	28,1
median	64,52	0,65	-0,11	0,033

C21 (sample: 163)

2021/07/03 – h 04:46:29.000

variable	sv	x	y	z
mean	52,70	0,62	-0,13	0,035
DS	9,88	0,015	0,005	0,005
IV%	18,7	2,42	3,8	14,3
median	52,4	0,63	-0,13	0,035

C24 (sample: 198)

2021/07/03 – h 17:53:09.000

variable	sv	x	y	z
mean	70,73	0,35	-0,139	0,031
DS	9,79	0,28	0,096	0,021
IV%	13,8	80	69,1	67,7
median	71,49	0,38	-0,141	0,027

C29 (sample: 173)

2021/07/04 – h 07:12:21.000

variable	sv	x	y	z
mean	60,33	0,55	-0,11	0,029
DS	9,88	0,017	0,006	0,006
IV%	17,2	3,09	5,4	20,7
median	61,58	0,55	-0,11	0,029

C30 (sample: 177)

2021/ 07/05 - h 05:00:26.000

variable	sv	x	y	z
mean	61,67	0,58	-0,079	0,032
DS	7,77	0,033	0,007	0,008
IV%	12,6	5,69	8,9	25
median	61,94	0,58	-0,079	0,033

C33 (sample: 208)

2021/07/05 – h 16:50:28.000

variable	sv	x	y	z
mean	68,91	0,52	-0,071	0,032
DS	9,63	0,047	0,013	0,017
IV%	14	9	18,3	53,1
median	70,27	0,52	-0,071	0,031